Feedback-controlled collective transport in one-dimensional periodic potentials

vorgelegt von

Diplomphysiker
Robert Gernert
geb. in Zossen

Von der Fakultät II - Mathematik und Naturwissenschaften
der Technischen Universität Berlin
zur Erlangung des akademischen Grades

Doktor der Naturwissenschaften
Dr. rer. nat

genehmigte Dissertation

Promotionsausschuss:

Vorsitzender: Prof. Dr. Martin Schoen
Berichterin: Prof. Dr. Sabine H. L. Klapp
Berichter: Prof. Dr. Uwe Thiele

Tag der wissenschaftlichen Aussprache: 16. Oktober 2015

Berlin 2015

Declaration of Authorship

I, Robert Gernert, declare that this thesis titled 'Feedback-controlled collective transport in one-dimensional periodic potentials' and the work presented in it are my own. I confirm that:

- This work was done wholly or mainly while in candidature for a research degree at this university.
- Where any part of this thesis has previously been submitted for a degree or any other qualification at this university or any other institution, this has been clearly stated.
- Where I have consulted the published work of others, this is always clearly attributed.
- Where I have quoted from the work of others, the source is always given. With the exception of such quotations, this thesis is entirely my own work.
- I have acknowledged all main sources of help.
- Where the thesis is based on work done by myself jointly with others, I have made clear exactly what was done by others and what I have contributed myself.

Signed: _____

Date: _____

Acknowledgements

Ich danke meiner Frau, Elisabeth, für ihre endlose Geduld. Sie hielt mir unzählige Abende, Wochenenden, und Nächte den Rücken frei. Sie bestärkte mich in meinem Unterfangen Doktorarbeit *und ermöglichte mir die Gratwanderung zwischen den Rollen Vater und Forscher. Durch ihren Einsatz konnte ich meine Forscherrolle bis zum Abschluss ausführen.*

Weiteren Dank richte ich an meine Betreuerin Sabine Klapp. Sie erklärte mir die Funktionsweise des wissenschaftlichen Arbeitens und führte mir meine Fehler vor Augen, so dass ich gut daraus lernen konnte. Unermüdlich korrigierte sie meine Entwürfe. Ich danke ihr auch für die Erwähnungen, das ein oder andere gelernt und/oder gut umgesetzt zu haben. Es hat mir großen Spaß gemacht, mit ihr zusammen zu arbeiten.

Ich bedanke mich weiterhin bei Nicola Kleppmann für ihre Unterstützung während des Schreibens der Doktorarbeit. Sie motivierte und fokussierte mich, indem sie Termine festsetzte und meine Entwürfe korrigierte. Die Diskussionen mit ihr waren sehr wertvoll für mein Verständnis von Textstrukturierung.

Außerdem denke ich gern an unzählige Gespräche und Diskussionen mit Nicola Kleppmann und Tarlan Vezirov zurück. Ich danke ihnen und Alexander Kraft, Rodrigo Lugo-Frías, Ken Lichtner, Helge Neitsch, Teresa Reinhard, Konstantin Zak, Sascha Gerloff, Arzu Yener, Sarah Loos und den anderen (auch ehemaligen) Mitgliedern der AG Klapp für das freundliche Arbeitsumfeld.

Ich danke Clive Emary, Ken Lichtner, und Sarah Loos für die gute Zusammenarbeit und die vielfältigen Anmerkungen zu meiner Arbeit.

Weiterhin danke ich meiner Familie für die stete Unterstützung.

Abstract

In this thesis, we investigate the transport of colloids in one spatial dimension by numerical computations and theoretical considerations. We consider the Brownian motion of the colloids in the presence of spatially periodic strong external fields, which we model with a tilted washboard potential. We are interested in the time-dependent evolution of non-equilibrium processes in this potential. We focus on the time and length scales which span from the motion inside one valley of the periodic potential to the motion among the valleys.

The theoretical description of the continuous stochastic thermal fluctuations in the particles' positions is achieved via the overdamped Langevin equation and its Fokker-Planck equation, the Smoluchowski equation (SE). Further, we employ the Dynamical density functional theory (DDFT) to predict the motion of interacting colloids on large time and length scales.

In the first two content chapters we consider the transport of a single Brownian particle in a tilted washboard potential. We are interested in the short time diffusion, in particular in the mean squared displacement (MSD). We propose a simple model which yields analytic expressions for the time dependence of diffusional properties such as the MSD. Then we turn to the question: How long does a stochastic process take? To answer this question for our asymmetric continuous system, we propose a generalisation for the waiting time distribution (WTD), which was previously available only for discrete systems. Our definition of the WTD and our recipe to calculate the WTD via a SE facilitates a detailed characterisation of nearly discrete stochastic processes.

In the middle of this thesis we present a time delayed feedback control protocol for the motion of a single Brownian particle in an asymmetric periodic potential. Feedback control means that the systems is steered towards a certain behaviour by using information from the system itself. We show that an ensemble averaged modelling of feedback control via a Fokker-Planck equation makes sense for a dilute colloidal suspension. We apply the modelling to a ratchet system where the time delay in the feedback protocol creates the ratchet effect. By varying the parameters of the control protocol we show that the generated current can be higher than that of a corresponding standard ratchet system. Further, we address stochastic thermodynamics and examine the entropy production entwined with this non-equilibrium process.

In the last two chapters, we consider the effect of particle interactions on diffusion and transport in a tilted washboard potential. We consider ultra-soft particle interaction and attractive hard spheres. We find that ultra-soft repulsive interaction between particles results in a much stronger diffusion compared to the single particle case. We calculate the MSD and the diffusion coefficient and show the influence of particle interaction to the giant diffusion effect. Finally, we propose a feedback control protocol for the collective transport of several particles. We impose a trapping potential onto the colloids which mimics moving optical tweezers. The particles agglomerate to clusters. We show that the combined influence of the feedback controlled trap and the repulsive particle interactions leads to an enhancement of the mobility of the particle cluster of several orders of magnitude.

Zusammenfassung

In dieser Arbeit untersuchen wir den Transport von Kolloiden in einer räumlichen Dimension mit theoretischen und numerischen Methoden. Wir betrachten die Brownsche Bewegung der Kolloide unter dem Einfluss eines starken externen räumlich moduliertes Feldes. Wir modellieren den externen Einfluss mit einem periodischen Potential und einer konstanten treibenden Kraft. Wir interessieren uns für Prozesse außerhalb des thermischen Gleichgewichts. Insbesondere studieren wir die Bewegung auf Längen- und Zeitskalen, die zwischen der Bewegung in den Tälern des Potentials und der Bewegung zwischen den Tälern liegen.

Für die theoretische Beschreibung der Brownschen Bewegung setzen wir die Langevin Gleichung und die zugehörige Fokker-Planck Gleichung, die Smoluchowski Gleichung, ein. Weiterhin benutzen wir die Dynamische Dichtefunktionaltheorie um die Teilchenwechselwirkungen auf großen Längen- und Zeitskalen berechnen zu können.

In den ersten beiden Kapiteln betrachten wir die Bewegung eines einzelnen Brownschen Teilchens im gekippten Waschbrettpotential. Wir betrachten die Kurzzeitdiffusion, die durch die mittlere quadratische Verschiebung des Teilchens quantifiziert ist. Wir präsentieren ein einfaches Modell, das analytische Voraussagen für die zeitabhängigen Diffusionseigenschaften liefert. Weiterhin studieren wir die Zeit, die ein Brownsches Teilchen für die Überquerung einer Energiebarriere benötigt. Dazu schlagen wir eine Verallgemeinerung der Wartezeitverteilung vor, die zuvor nur für diskrete System verfügbar war. Mit dieser Wartezeitverteilung können Systeme, die nahezu diskrete Dynamik besitzen, nun mit hoher Genauigkeit charakterisiert werden.

Nach diesen Grundlagenuntersuchungen wenden wir uns einer Rückkoppelsteuerung zu. Solch eine Steuerung optimiert das Verhalten eines System unter Verwendung von Informationen aus dem System selbst. Unsere Rückkoppelsteuerung steuert ein Brownsches Teilchen in einem asymmetrischen periodischen Potential auf der Basis von zeitverzögerter Bereitstellung der Information aus dem System. Wir zeigen, dass dadurch ein gerichteter Strom in dem System entsteht. Der Vergleich mit dem zugehörigen System ohne rückgekoppelte Steuerung zeigt, dass der Strom durch rückgekoppelte Steuerung verstärkt werden kann.

In den letzten beiden Kapiteln behandeln wir Diffusion und Transport von wechselwirkenden Teilchen. Wir konzentrieren uns wieder auf die mittlere quadratische Verschiebung und zeigen, dass die Diffusion durch repulsive Teilchenwechselwirkung verstärkt wird. Danach schlagen wir eine weitere Rückkoppelsteuerung für den kollektiven Transport vor. Die Steuerung arbeitet wie eine optische Falle, die mit den Teilchen mitbewegt wird. Wir zeigen, dass die Mobilität der Teilchengruppe durch das Zusammenspiel von Falle und Teilchenwechselwirkung um mehrere Größenordnungen erhöht wird.

CONTENTS

Abbreviations

2S/W	two states per well
BD	Brownian dynamics
DDFT	dynamical density functional theory
DFT	density functional theory
FPTD	first passage time distribution
FTCS	forward time centred space
GCM	Gaussian core model
HCAY	hard core, attractive Yukawa
LE	Langevin equation
ME	master equation
MSD	mean squared displacement
SE	Smoluchowski equation
WTD	waiting time distribution

List of publications

[318] C. Emary, R. Gernert, and S. H. L. Klapp: "A minimal model for short-time diffusion in periodic potentials" Phys. Rev. E **86**, 061135 (2012); arxiv:1209.1504 [cond-mat.stat-mech] (2012).

[359] S. A. M. Loos, R. Gernert, and S. H. L. Klapp: "Delay-induced transport in a rocking ratchet under feedback control" Phys. Rev. E **89**, 052136 (2014); arxiv:1403.5905 [cond-mat.stat-mech] (2014).

[331] R. Gernert, C. Emary, and S. H. L. Klapp: "Waiting time distribution for continuous stochastic systems" Phys. Rev. E **90**, 062115 (2014); arxiv:1407.1675 [cond-mat.stat-mech] (2014).

[389] R. Gernert and S. H. L. Klapp: "Enhancement of mobility in an interacting colloidal system under feedback control" Phys. Rev. E **92**, 022132 (2015); arxiv:1506.01846 [cond-mat.soft] (2015).

1. INTRODUCTION

Various challenges in technology can be traced back to effects concerning the transport of colloids in confinement [1–6]. Here, the transport of a single overdamped Brownian particle in a one-dimensional periodic potential (so-called washboard potential) has developed to a paradigm system [7, 8]. Much effort was devoted to the investigation of this stochastic system [9–11] as it provides a lot of fundamental insight into colloidal transport. In this thesis, we provide insight into the short time dynamics of an overdamped Brownian particle driven through a washboard potential by proposing a model for the short time diffusion and by generalising the waiting time distribution (WTD) in order to quantify the duration of valley to valley motion. Building on decades of established research, we now can consider this important paradigm system as well understood.

However, a single Brownian particle is only one step towards fully understanding colloidal transport, where particle interactions are omnipresent. Diffusion and transport of interacting particles in washboard potentials is far from understood. We investigate the short time diffusion of an expanding particle cluster to get an impression of the influence of particle interactions. A further question arises with modern experimental methods which are used to influence colloidal systems based on the motion of the colloids themselves. This so-called feedback control offers a whole new range of possible transport mechanisms. In this work, we propose a feedback control scheme for a single Brownian particle based on the ratchet effect where the generated current is larger than in a corresponding rocking ratchet. Finally, we combine feedback control and collective transport by confining particles in a trap with a feedback-controlled position. This construction, which we call 'dynamic freezing', leads to an enhancement of the mobility of the particle cluster by several orders of magnitude with respect to both, the uncontrolled system and the single particle feedback-controlled system.

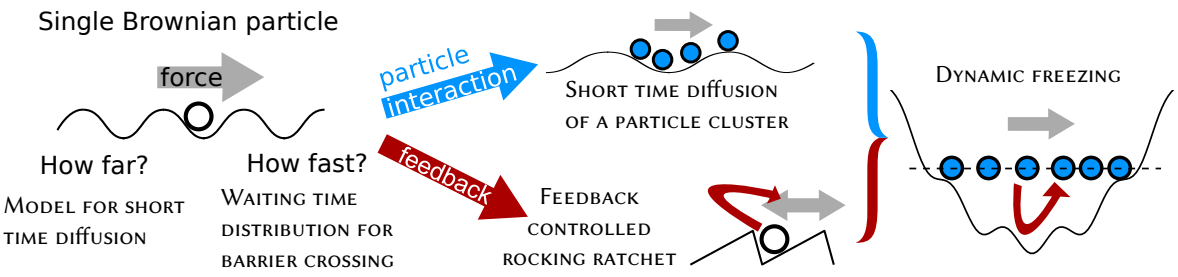

Fig. 1.1: Projects (titles in small capitals). In the field of transport in 1D washboard potentials we combine short time analysis, particle interaction, and feedback control.

The rest of the introduction is held very general. Therefore, every content chapter has an introduction on its own to focus on the specific questions at hand. Colloidal suspensions in general are addressed in section 1.1. Section 1.2 introduces colloids in interaction with external fields. Then, in section 1.3, we introduce the meaning of 'short' and 'long times' and the corresponding effects that we investigate. Our systems are out of thermal equilibrium. Section 1.4 states consequences of non-equilibrium and introduces the standard characterisation. In section 1.5 we review known phenomena concerning transport and diffusion in one-dimensional periodic potentials. Further, our standard form of a sinusoidal washboard potential is discussed. Section 1.6 introduces feedback control. Finally, section 1.7 gives an overview about the contents of the thesis.

1.1 Colloidal suspensions

Many fluids in our everyday life are colloidal suspensions. Colloidal suspensions of natural origin include clay, blood, milk, and many dairy products [12–15]. Additionally, there are numerous household applications which exploit properties of colloidal suspensions, e.g., paints, coatings, lotions, and creams [12, 16–18]. Similarly, colloidal suspensions are relevant for various foods, where their relevance continues to grow [19, 20], and even the production of ceramics is closely interwoven with colloid science [21].

The term *colloidal suspensions* refers to colloids immersed in a solvent, which is mostly a liquid such as water or oil. The colloids are defined through their size, which ranges from 10nm to 10μm [18, 22]. Their material is not restricted, so colloids consist of a variety of materials. Colloids that consist of crystal or glass include SiO_2 and other minerals in clay, putty, and cement [12, 23–26]. Other colloidal suspensions consist of small droplets of a liquid in a different liquid, e.g., oil-in-water suspensions like lotions, milk, and cream, where the colloids themselves are fat droplets [12, 13, 15, 19]. In butter, colloidal water droplets are immersed in a fat solvent. Demixing of the droplets and solvent in liquid colloidal suspensions is often hindered through surfactants – in dairy products, the protein casein acts as such a surfactant [12–14, 19]. A further class of colloids contains a variety of biomolecules where each molecule forms a colloid. Examples for such biomolecules are collagen, the main protein of mammal tissue [27], or mucines, the proteins which form mucus (together with water) [28, 29].

We recognise colloidal suspensions through their mechanical behaviour. An external perturbation can deform a colloidal suspension more easily than a solid, which coined the term *soft matter* for such suspensions [22, 30, 31]. However, the mechanical properties of colloidal suspensions are more complex than those of liquids. One of their typical properties is the formation of gels (in the meaning of shower gel, hair gel, etc.) [12, 21, 32–35]. Further, many colloidal suspensions are non-Newtonian fluids, which means that their shear viscosity changes for increasing shearing. Shear-thinning fluids, such as saliva, ketchup, blood, or paint, show a decreasing viscosity with increasing shear [16, 19, 36, 37]. The opposite behaviour, where the viscosity increases with increasing shear, is called shear-thickening. Shear-thickening colloidal suspensions include clays [25] which are used to enhance the resistance of armour [38–40].

The fundamental property of colloids is their *Brownian motion* [41]. In Brownian motion, the position of a colloid is subject to continuous erratic fluctuations. These fluctuations allow every imbalance in the positions of the particles to decay with time, i.e. Brownian motion results in *diffusion*. The origin of these fluctuations lies in the vast number of collisions

between the colloid and the solvent molecules, which move due to temperature. The colloid is large enough to move only little with every collision, but small enough to still 'feel' the solvent molecules. Dhont used this connection of the colloids' size to the solvent particles' in his book [41] to estimate the range of colloid sizes.

The range of colloid sizes is not sharp. For smaller particles, there is an overlap with the term 'nanoparticles', whose size range is approximately 1nm to 100nm [7, 42–44]. On this very small colloidal length scale, systems, such as fullerenes (size $\approx$ 1nm), exist that display some but not all colloidal properties. Fullerenes gelate, which is typical for colloidal suspensions. However, fullerene gelation does not require a solvent [45]. The attractive interaction, which is necessary for gelation, is provided by van-der-Waals forces, which are important for molecules, but negligible for most colloids.

The upper limit of colloidal sizes is given through particles larger than $\approx 10\mu$m, where Brownian motion becomes irrelevant. Larger particles constitute granular materials, which show complex rheological behaviour [17, 46–48] but sediment in suspension instead of performing Brownian motion. An example at the upper-size limit is quicksand, which consists of clay particles mixed with sand, where only the clay particles have colloidal size [49, 50]. An example of a dispersion with granular matter is the mixture of starch and water, where the size of starch grains is between 20μm and 100μm [48]. This dispersion is very suitable to demonstrate shear-thickening. YouTube gives dozens of examples upon entering the search-term '`starch water`'.

The physical investigation of colloidal suspensions needs both, experimental and theoretical understanding. Larger colloids are easier to measure, while smaller colloids require more involved experimental set-ups. Colloids of μm size and larger can be observed with microscopes operating with visible light [51]. Colloids of this size move rather slowly. The time a colloid needs to move its own diameter due to Brownian motion, the Brownian time τ_B, lies between 10^{-2}s and 10^2s for μm-sized particles (see Table 2.1 on page 31). Exploiting the particle size and their slowness, optical microscopes have been combined with video cameras to create *video microscopy* [51, 52]. Video microscopy enabled access to a large range of experimental data for colloidal systems composed of μm-sized particles.

In theoretical modelling, the first major challenge is the treatment of the thermal molecular motion in the solvent, which causes the Brownian motion of the colloid. This microscopic molecular motion can influence macroscopic properties such as the shear viscosity of the colloidal suspension. Despite a century of research, the understanding is not yet deep enough to thoroughly predict the macroscopic behaviour from the microscopic ingredients [22, 32, 53–58]. This link is desirable, since it would enable us to create (soft) matter with customised mechanical, mixing, thermal, electric, magnetic, and optical properties. To establish this link, theory would have to bridge many orders of magnitude in length and time which is a challenging task. In particular, the computational effort required to treat all effects on a microscopic level is currently simply not feasible. Therefore, a hierarchy of models with different levels of detail is used [41, 59]. The theory chapter, chapter 2, reviews the levels of detail we are going to study.

1.2 Colloidal motion in a structured environment

We are interested in the motion of colloids that are influenced by external forces. External forces stronger than the Brownian motion lead to interesting dynamics, which explain some phenomena in nature and enable the development of new technology. In the following I discuss some examples that serve as inspiration for our work.

In biological cells, there is a group of proteins called 'motor proteins', which convert chemical energy into mechanical energy. One of these proteins, kinesin, is responsible for transport of cargo inside a cell, as depicted in Fig. 1.2(a). Inside the cell there is a network of microtubules [60], where every microtubule has a regular surface structure. The kinesin proteins can dock onto a microtubule, which changes the spatial conformation of the protein and allows adenosine triphosphate (ATP) molecules to bind to it. Using the energy of the chemical reaction of ATP into adenosine diphosphate (ADP), the protein deforms and moves a distance of ≈ 8.2nm along the microtubule, pulling the attached cargo with it [2]. The ADP is then released and the process repeats. Both, deformation and centre of mass motion is Brownian during the whole process. The force fields that work here besides the Brownian motion are the binding between microtubule and protein, and the binding between protein and ATP [61]. Several models have been proposed, with different levels of detail. A very simple one-dimensional model called 'rocking ratchet' is sufficient to explain the basic principle of motion [2, 9, 62]. This model is introduced in section 1.5.2. The Brownian motion does not disturb the motion of the motor, instead it provides (by thermal fluctuations) the necessary energy to release the tubule-protein bound to ignite the process [2].

Similar thermally activated motion is found for colloids diffusing on structured surfaces, see Fig. 1.2(b). If the surface is a crystalline layer of colloids, the places with more neighbours are energetically favoured over places with fewer neighbours [63]. Major influence on the dynamics originates from the ratio of the binding energy to the thermal energy $k_\mathrm{B}T$, where T is the (absolute) temperature and k_B is Boltzmann's constant. In a basic model, the motion of particles can be reduced to thermally activated transitions between binding sites [64] if the binding energy is larger than $k_\mathrm{B}T$. Similar thermally activated processes also occur for particles diffusing across stripes on surfaces with a striped energy landscape [65, 66], and in more complex interface situations [67, 68].

Particle sorting machines discriminate between particles concerning a particular property. Often, particles are separated by size [69–71]. Figure 1.2(c) depicts an example of a size-dependent sorting machine using a structured grid. If the sorted particles are colloids, the process is also called microfiltration [4]. Some sorting machines rely on microfluidics [69, 72–74]. However, we are interested in machines which exploit thermally activated (or hindered) processes [70, 71, 75–77]. Proof of principle experiments [71, 76] were conducted with colloids diffusing in asymmetrically shaped channels. Fig. 1.2(d) depicts a colloid in such a channel.

Intense light fields attract colloids [78]. A laser, focused to a spot in three-dimensional space, constitutes a trap for the colloid [79, 80]. By varying the light intensity in space and time, any potential energy landscape can be created [81–85]. Due to this enormous flexibility the technique of creating a potential using focused lasers is called *optical tweezers*. Motion of colloids in structured light fields is used excessively as a test bed to investigate the behaviour of colloidal suspensions [78, 82, 83, 86–92]. Further approaches to manipulate colloidal motion involve magnetic [6, 65, 77, 80, 93–98] and electric fields [22, 70, 99, 100].

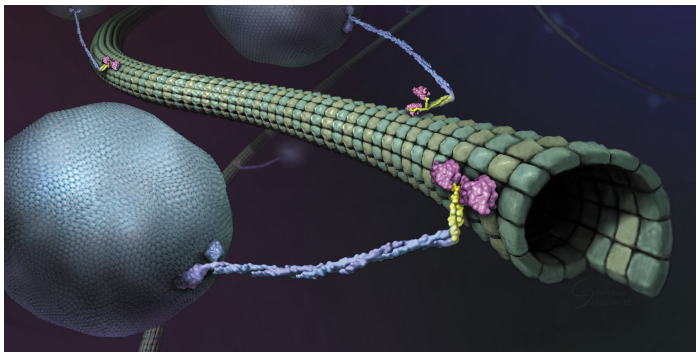

(a) Illustration of kinesin proteins walking on a microtubule carrying vesicles. Vale Lab [101], ©Graham Johnson.

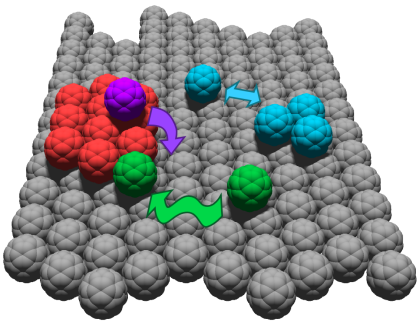

(b) Schematic of diffusion processes of particles on a structured surface. Drawn by N. Kleppmann [102].

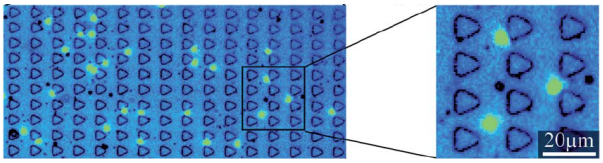

(c) Optical micrograph of a particle sorting device. Reprinted from L. Bogunovic et al. [70].

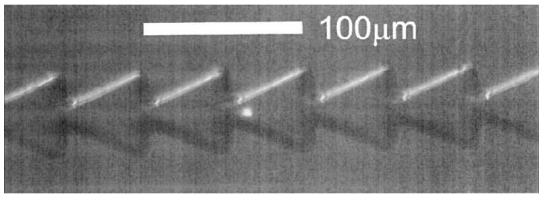

(d) Micrograph of a colloid in an asymmetrically shaped channel. Reprinted from C. Marquet et al. [76].

Fig. 1.2: Examples for systems with a structured environment in which the motion of particles is thermally activated.

Structured confinement, e.g. through solid walls, can have a pronounced influence on the motion of a colloid. As the erratic motion is disturbed by the confinement, an asymmetry in the wall configuration leads to an asymmetry of the motion. This can be used to transport particles, or to create sorting machines or sieves [7, 76, 103]. Channels in cell membranes are natural sieves [104]. It is the energetic and spatial structure of the channel which determines the transport of water molecules [105] or small organic molecules [106] through channels in cell membranes [105, 107].

A porous material constitutes a structured confinement for particles diffusing through it. To diffuse from one pore to another, the particle needs to find an opening that is only a little larger than the particle. Again, the transitions of the particles between the pores can be modelled as thermally activated transition [108–110]. Porous materials are important for battery research, catalysts, and filtration [111–115].

In systems that are densely packed, the motion of every particle is restricted by the neighbouring particles. Already one particle diameter is a large distance to move in these systems. Essentially, the particles are trapped. Such particle trapping occurs in glasses and supercooled liquids (liquids cooled below their melting temperature), where the particles energetically strive towards to a crystal structure. However, they cannot achieve the necessary structural relaxation, but are trapped in cages formed by neighbouring particles [116–118]. The low temperature (with respect to the melting temperature) further decreases the probability of large positional deviations. One interesting aspect of glasses is the dynamics of a particle leaving its cage, which can be studied as an thermally activated escape process. To

this end, the escaping particle is considered to move in an effective energy landscape which models the average influence of the neighbouring particles [119–121].

1.3 Between the time scales

The time scale that studied effects take place on determines the time resolution required in both, theory and experiments. Much faster processes can usually be treated in a time-averaged way, while processes that are much slower are often modelled as static.

The transport over high energy barriers via thermally activated processes is much slower than diffusion without a barrier. We are interested in the transition of the dynamics from the particle level to subsequent thermally activated hopping motion. Further, we are interested in the influence of external time dependent forces on this transition.

First, I want to outline why the *Brownian time* is the fastest time scale we want to consider here. Then, I discuss why *Kramers' rate* sets the longest time scale of our interest. The subsequent sections deal with effects that happen in between these time scales.

1.3.1 Overdamped Brownian motion

The relevant time scales for colloidal motion are well explained in the book of Dhont [41]. I want to repeat the relevant ideas and conclusions here.

The relaxation time of the solvent is about 10^{-14}s. On a time scale much larger than the solvent time scale, the influence of the molecular motion on a colloid can be modelled as Brownian motion. Hence, we model the solvent's molecular motion through time-averaged properties. The vast number of collisions between the molecules and the colloid create an average friction on the motion of the colloid. The friction force acting on a colloid moving with a velocity $\mathbf{v}$ is given by Stokes friction, i.e. $\mathbf{F}_{\text{fric}} = -\gamma\mathbf{v}$, where

$$\gamma = 3\pi\eta\sigma \tag{1.1}$$

is called friction constant. The dynamic viscosity of the solvent is denoted by η, and σ is the particle diameter.

Having averaged molecular motion out, the colloidal motion can be modelled through the *Langevin equation* (LE)

$$M\ddot{\mathbf{r}}(t) = -\gamma\dot{\mathbf{r}}(t) + \mathbf{f}^{\text{deter}}(\mathbf{r}, t) + \mathbf{f}^{\text{stoch}}(t)\,. \tag{1.2}$$

The position of the colloid is denoted with $\mathbf{r}$ and dots denote time derivatives. The Langevin equation for colloidal motion is Newton's equation of motion supplemented with a stochastic force $\mathbf{f}^{\text{stoch}}$, modelling the Brownian motion. The force $\mathbf{f}^{\text{deter}}$ is a deterministic force which results from external influences or colloid-colloid interaction. A derivation of the Langevin equation and the following discussion can be found in Dhont's book [41]. The acceleration term contains the mass M of the colloid. Mass is proportional to volume (for all solid and liquid colloids) which is proportional to σ^3. The friction force, which is connected to the colloid's surface, is much stronger than the inertial force, which is connected to the volume. The Reynolds number is the ratio of initial force to viscous force which is very small for colloids in a solvent [122]. The time scale of the relaxation of accelerations is given by M/γ, where M is the mass of a colloid. For a SiO_2 particle of 1μm diameter in water, $M/\gamma \approx 10^{-7}$s.

We are not interested in these short times because the distance a colloid diffuses in this time is around $10^{-3}\sigma$ [41]. Hence, inertia are irrelevant for transport, where the colloids move distances of 1σ to $10^{3}\sigma$. The resulting motion is called *overdamped Brownian motion*.

Ensemble average: averaging Brownian motion out. The particular trajectory $\mathbf{r}(t)$ of a colloid is unpredictable because of its stochastic nature. It does not matter whether the trajectory was measured in an experiment or calculated as a solution of the Langevin equation, any trajectory is different than all trajectories before and never will there be an identical trajectory again. Therefore, predictions rely on probabilities. An experiment with few colloids can pose a statement only if the experiment is repeated many times and a significant fraction of experiments supports that statement. The evaluation of an observable A is realised by averaging over the values of the observable $A(\mathbf{r}, t)$ for many different realisations of the stochastic force. The more realisations are taken into account the larger the significance of the mean value. In the (theoretical) limit of averaging over all, infinitely many, possible realisations of the random force contained in a given ensemble, the average is called *ensemble average*. Whereas the average over finitely many realisations differs from one experiment to the next, the ensemble average is not of statistical nature any more.

We will mainly work with the canonical ensemble, which contains realisations of the random force with constant temperature and constant number of particles for all positions and particle energies. As position, energy, and time are continuous there are infinitely many realisations. Hence, experiments and numerical solutions of the Langevin equation, so called Brownian dynamics simulations, can only give approximations to the ensemble average. To calculate ensemble averages directly, statistical physics offers the tool of Fokker-Planck equations. The book of Risken [10] gives a comprehensive overview of Fokker-Planck equations. In this thesis, Fokker-Planck equations and similar equations are the central method of investigation.

1.3.2 Diffusion: the Brownian time

With diffusion we denote the phenomenon of a system to have the tendency to equalise every imbalance in the positions of the particles. In colloidal systems, diffusion is a direct consequence of Brownian motion. It can be quantified with the *mean squared displacement* (MSD) of a particle, which for a single particle without external forces, reads

$$\langle (\Delta\mathbf{r}(t))^2 \rangle = 2dD_0 t\,. \tag{1.3}$$

The angle bracket $\langle \dots \rangle$ denotes an ensemble average. The quantity $\Delta\mathbf{r}(t)$ denotes the distance the particle has travelled in the time t, i.e. $\Delta\mathbf{r}(t) = \mathbf{r}(t) - \mathbf{r}(0)$. The mean distance is zero in the absence of external forces, i.e. $\langle \Delta\mathbf{r} \rangle = 0$, because Brownian motion is unbiased. The MSD quantifies the diffusion speed of a particle, given that its position was known for sure at time $t = 0$. Note that a particle which moves with a constant velocity in one direction has a MSD proportional to t^2. The linear growth of the MSD with time is connected to continuous changes of the direction during Brownian motion. The proportionality constant is composed of the number of spatial dimensions d and the diffusion coefficient of free motion D_0 (other names for D_0 are short time diffusion coefficient [123, 124], free diffusion coefficient [7, 125], and self diffusion coefficient [92]). The free diffusion coefficient determines

a characteristic time scale of the system, the *Brownian time*

$$\tau_{\mathrm{B}} = \sigma^2/D_0\,. \tag{1.4}$$

The Brownian time τ_{B} is the time a particle in average needs to diffuse the distance of its own diameter.

Without an external potential, the diffusion coefficient is given by the Einstein relation

$$D_0 = \frac{k_{\mathrm{B}}T}{\gamma} \tag{1.5}$$

where γ is the friction coefficient [41,126]. Evaluating Eqs. (1.1) and (1.5) for a SiO_2 sphere of 1μm diameter in water yields a Brownian time of ≈ 2s at room temperature.

1.3.3 Kramers' rate: thermally activated motion

All systems discussed in section 1.2 can be modelled by particles moving in a potential energy landscape with local minima. Thermal fluctuations provide the energy required to overcome energy barriers and to escape from local energy minima. If an energy barrier ΔV is larger that the thermal energy $k_{\mathrm{B}}T$, then only the strongest fluctuations are sufficient to drive the particle across the barrier. Of course, these fluctuations are rare. The rate r_A at which they occur was first examined in physical chemistry, where this rate is called Arrhenius rate [11]. The important characteristic is its dependency on the temperature: $r_A = \theta_0 \exp(-\Delta V/(k_{\mathrm{B}}T))$. Later, using methods from statistical physics, Kramers could base the rate on properties of the noise in the system and could determine the prefactor θ_0 from the energy landscape [127]. Kramers' rate

$$r_K = \frac{D_0}{2\pi k_{\mathrm{B}}T}\sqrt{-V''(x_{\min})V''(x_{\max})}\,e^{-(V(x_{\max})-V(x_{\min}))/(k_{\mathrm{B}}T)} \tag{1.6}$$

depends on the potential landscape $V(x)$ at the potential minimum $x_{\min}$ and maximum $x_{\max}$. I will sketch the necessary assumptions in section 2.2.1. Kramers' rate defines a time scale $1/r_K$, which corresponds to the mean time that the particle needs to overcome the energy barrier.

On the time scale $1/r_K$, the motion consists of subsequent thermally activated hopping processes between potential minima. The motion can be modelled with a Master equation or continuous time random walk [128,129]. On this time scale, the only effect of the Brownian motion is to set the hopping rates. As we are interested in the effects of noise in more detail, we do not study times much larger than $1/r_K$.

Anomalous diffusion. If the hopping occurs between sites in a regular lattice and there are only finitely many different processes, the resulting motion shows normal diffusive behaviour [129]. Normal diffusion refers to motion where the MSD is linear in time for long times $t > 1/r_K$. Motion with a MSD with other temporal dependency for long times is called anomalous diffusion. Many anomalous diffusion processes [130] approach a long time MSD of the form

$$\langle(\Delta\mathbf{r}(t))^2\rangle = \kappa_E t^E\,. \tag{1.7}$$

If the exponent $E = 1$ the diffusion is called normal, otherwise anomalous. For $E < 1$ the process is called subdiffusive, and superdiffusive for $E > 1$ [130–132].

Subdiffusive processes occur in systems where the potential energy landscape is not completely regular. Examples for such irregularities are random potential energy barriers between traps arranged in a lattice [129, 133], randomly arranged traps [134], or completely random energy landscapes [83]. Anomalous diffusion is present in glasses and supercooled liquids [116, 135, 136].

1.3.4 Short time diffusion

When studying short time diffusion we focus on the influence of Brownian motion for times smaller than $1/r_K$, assuming that $1/r_K \gg \tau_\mathrm{B}$. The main observable on this time scale is the MSD. Further insight can be gained from higher order cumulants of the position of the particles, e.g., the non-Gaussian parameter which is connected to the fourth power of positional deviations [119].

The MSD was recently addressed in experimental and theoretical work for colloidal motion in structured light fields [82, 83], sheared dense suspensions [137], gels [35, 138], and liquid crystals [139]. Further, the investigation of nanoparticle motion on surfaces [66, 140] relies on the MSD. In glassy systems, the MSD is commonly used to describe the escape of a particle from a cage formed by neighbouring particles [116, 119, 136, 141].

In many cases the MSD shows a common three-region structure. A representative example for this structure is the one-dimensional diffusion of a single particle in a periodic potential. The MSD is depicted in Fig. 1.3. In the first regime of very small times the MSD grows proportional with time, which is denoted with 'free diffusion in one well' in Fig. 1.3. From the second regime on, beginning at intermediate times, the MSD grows very slowly. The second regime is called "subdiffusive region", "subdiffusive transient", or "plateau" [82, 142, 143]. The MSD depends linearly on time in this regime which can be seen in the inset of Fig. 1.3. In the last regime, denoted with 'diffusion between potential wells' in Fig. 1.3, the linear time dependence of the MSD can be approximated by a proportional function $\langle \Delta \mathbf{r}^2 \rangle = 2Dt$ (dotted line in Fig. 1.3). For those long times, the type of motion is the thermally activated hopping motion discussed in section 1.3.3. The factor D in the asymptote for the MSD is called effective diffusion coefficient.

The occurrence of a plateau in the MSD is connected to a separation of time scales. The short time scale is the time the particle needs to explore the local minimum of the potential, we call it the inter-well relaxation time τ_iwr (marked with a squared in Fig. 1.3). It is defined as the relaxation time of the exponential relaxation of the MSD in a parabola fitted to the local potential minimum. The longer time scale is $1/r_K$. The duration and the height of the plateau in the MSD quantify the decay of the influence of the local structure of the potential on the motion. Studies show that the end of the plateau is accompanied by a peak in the non-Gaussian parameter mentioned above [82, 144]. The fact that this behaviour is coupled to the separation of time scales is well represented by our model for short diffusion, presented in chapter 3. Our model correctly predicts the time dependence of the MSD and the non-Gaussian parameter for a family of modulated potentials. Moreover, these time dependencies are given analytically in this model.

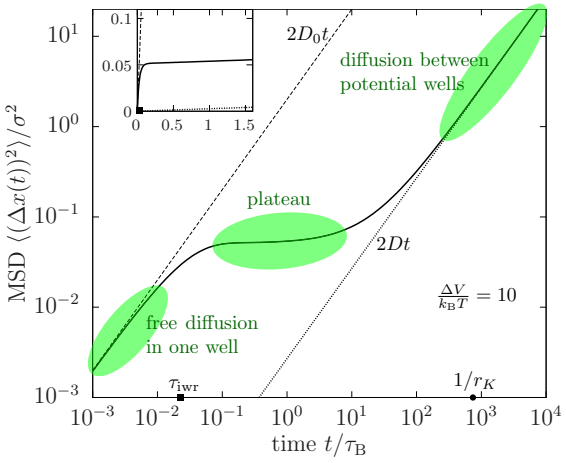

Fig. 1.3: (a) Short time diffusion: double-logarithmic plot of the MSD in dependence on time for a one-dimensional diffusion process in a periodic external potential. The behaviour is categorised into the three regions mentioned in section 1.3.4. The time $1/r_K$ is marked by a filled circle, the inter-well relaxation time τ_{iwr} by a square. The inset shows the MSD, $2D_0t$, and $2Dt$ on linear axes.

Particle interactions. The interplay of Brownian motion, particle interaction, and an external periodic potential is very complex. Additional to the impact of the periodic potential and Brownian motion, the system is influenced by the type and the strength of the particle interaction and the mean density of particles. Further, the behaviour of the system depends on the initial condition and is highly connected to the dimensionality and the geometric constraints of the external periodic potential.

These dependencies are not yet fully understood. One particular type of investigation considers the motion of particles in densely packed systems. Even without an external potential, an interesting motion called single file diffusion sets in if the motion is restricted to one dimension and the particle interaction prevents that particles overtake each other. The particles constitute a chain with fixed order. Each particle's motion is restricted by the left and right neighbour which results in a slow growth of the MSD with $\sqrt{t}$ [145]. This means that single file diffusion is subdiffusive with the exponent $E = 1/2$, in the sense of Eq. (1.7). If the geometrical restriction is gradually loosened the growth behaviour of the MSD gradually returns to normal [146]. Single file diffusion is a consequence of particle interaction and geometrical restriction and similarly occurs in systems with an external periodic potential [147, 148]. However, if the particle interaction allows that particles overtake each other, the diffusion is normal [124].

A different type of investigation considers spatial relaxational processes. The initial condition is a cluster of particles in an otherwise empty system. Of interest is the motion of the particles as they explore the available space. Experimentally this situation can be produced by using a strong external trap potential to force the particles to form a dense cluster. Then, the trap is switched off and the particles move in the periodic potential. For ultra-soft purely repulsively interacting particles the MSD is the larger the stronger the repulsion [124]. Further, the diffusion was found to be normal for these kind of particles [124] and the effective

diffusion coefficient is the larger the stronger the repulsion. For attractive, spring-coupled particles [149] the effective diffusion coefficient is the smaller the stronger the attraction. However, the short time diffusion was not studied in [149].

Particle interactions have a strong impact on the MSD. For example, in conjunction with gels, attractive particle interactions lead to a plateau in the MSD even if no external periodic potential is applied [138]. Hence, the interpretation of the MSD in a system with periodic external potential and particle interactions requires knowledge about the time and length scales of the contributing processes. In the chapter 3 we investigate the plateau in the MSD caused by an external periodic potential. In chapter 6 we study ultra-soft repulsive and attractive particles in an external periodic potential and identify changes in the MSD caused by particle interactions.

1.4 Non-equilibrium

In thermal equilibrium, all particles of a colloidal system, i.e. solvent particles and colloids, move due to thermal motion. This movement is special as it fulfils *detailed balance*, which makes a statement about the probability current $\mathbf{j}(\mathbf{r},t)$. The probability current, which is a ensemble averaged quantity, denotes the probability $|\mathbf{j}|\Delta t$ that a particle located at position $\mathbf{r}$ at time t will move in the direction in which the current vector $\mathbf{j}$ points within the time interval $[t, t+\Delta t]$. A system obeys detailed balance if the (ensemble averaged) probability current $\mathbf{j} = \mathbf{0}$ for all times, directions, and positions. Detailed balance expresses that, on average, every motion of every particle is exactly balanced by the motion of the other particles. An implication is that the probability $p(\mathbf{r})\Delta V(\mathbf{r})$ to find a particle in a small volume $\Delta V(\mathbf{r})$ around $\mathbf{r}$ does not depend on time. The quantity $p(x)$ is called probability density.

We denote a situation where detailed balance is broken as non-equilibrium, i.e. $\exists t \exists \mathbf{r}$: $\mathbf{j}(\mathbf{r},t) \neq 0$. This occurs e.g. through the application of external fields. In general, the probability density and the probability current depend on time and space in non-equilibrium. Probability is a conserved quantity and probability density $p(\mathbf{r},t)$ and current $\mathbf{j}(\mathbf{r},t)$ fulfil the continuity equation

$$\partial_t p(\mathbf{r},t) + \boldsymbol{\nabla} \cdot \mathbf{j}(\mathbf{r},t) = 0\,, \tag{1.8}$$

where $\boldsymbol{\nabla}$ denotes the vector of partial derivatives with respect to the space coordinates. The equation of motion for the probability density $p(\mathbf{r},t)$ corresponding to the overdamped LE is the Smoluchowski equation (SE)

$$\partial_t p(\mathbf{r},t) = D_0 \boldsymbol{\nabla}^2 p(\mathbf{r},t) - \frac{1}{\gamma}\boldsymbol{\nabla} \cdot \left(p(\mathbf{r},t)\, \mathbf{f}^{\mathrm{deter}}(\mathbf{r},t)\right). \tag{1.9}$$

The SE is an extended diffusion equation and a particular Fokker-Planck equation (FPE). A FPE is the equation of motion for the probability density corresponding to a general LE. This correspondence is provided by the Kramers-Moyal expansion [10] which allows to derive a FPE from a LE if the stochastic force in the LE is Gaussian white noise.

1.4.1 Stationary transport

If the ensemble-averaged properties of the systems, i.e. p and $\mathbf{j}$, do not depend on time, the system and the properties are called stationary. A stationary probability density fulfils

$\partial_t p = 0$. From Eq. (1.8) we infer that $\mathbf{j}$ is constant in space, too. We note that equilibrium is a special case of stationarity, as $\mathbf{j} = \mathbf{0} = \text{const}$.

A paradigmatic example for stationary transport is the overdamped Brownian particle which is driven by a constant force. The combination of the Eqs. (1.9) and (1.8) yields $\mathbf{j} = -D_0 \boldsymbol{\nabla} p + p\mathbf{F}/\gamma$. We define the mean velocity as $\mathbf{v}(t) = \langle \dot{\mathbf{r}} \rangle$ which can be calculated from the probability current by [9, 11]

$$\mathbf{v}(t) = \int \mathrm{d}\mathbf{r}\, \mathbf{j}(\mathbf{r}, t)\,, \tag{1.10}$$

where $\int \mathrm{d}\mathbf{r}$ denotes a volume integral. If we, for simplicity, assume that the probability density is constant, then $\mathbf{v} = \mathbf{F}/\gamma$. This result is consistent with result from LE (1.2).

The factor between velocity and force is called *mobility* μ. In the presence of a structured environment, the mobility is a function of the environment and the driving force. For stationary transport in one dimension through a periodic potential, the mobility was found analytically by Stratonovich in 1958 [150, 151]. In a two-dimensional periodic potential, the velocity can have a different direction than the driving force [153]. To represent this direction dependency, the mobility must be a tensor: $\mathbf{v} = \underline{\underline{\mu}} \cdot \mathbf{F}$.

1.4.2 Transients

We denote the influence of the initial condition to the system in the course of time as a 'transient'. If the initial condition does not correspond to a stationary state the system will relax to a stationary state because of the diffusion term in the SE (1.9). This relaxation process is irreversible and produces entropy. If the force field is time-independent the system relaxes to a stationary state. For external oscillatory forces the system relaxes to an oscillatory state whose properties do not depend on the initial condition but only on the external driving (and other external parameters e.g. temperature, friction coefficient, boundary condition).

All systems we consider have a constant temperature, a constant volume, and a constant number of particles. If the system relaxes to equilibrium, a thermodynamic potential, the Helmholtz free energy $F = U - TS$, can be defined, which is minimised during the time evolution of the system. The potential energy of the system is denoted as U and the entropy as S.

The diffusion processes discussed in section 1.3 are examples for transients. Here, a sudden change of the environment, e.g. switching on a driving force, produces a transient reaction of the system.

1.4.3 First passage problems / escape problems

A first passage problem is the task to find the time-dependent probability that an observable of a stochastic system passes a certain threshold value for the first time [10, 11, 154]. First passage problems are inherently transient because they investigate the lifetime of the initial configuration. We consider an example in one dimension. Let a Brownian particle start at $x = 0$ at time $t = 0$. We are interested in the probability $P_{|x|<d}(t)$ that the particle travelled a distance smaller than d in the time t i.e. the probability that it has not escaped the interval $[-d, d]$. The probability $P_{|x|<d}(t)$ is called *survival probability* $S(t)$. In fact, the survival probability is the cumulative distribution function of the stochastic process "the

first passage of the threshold has not happened yet". Usually, the first passage does not happen instantaneously, i.e. $S(0) = 1$, and the threshold is definitely crossed sometime, i.e. $S(\infty) = 0$. The probability density $f(t)$ corresponding to $1 - S(t)$ is called *first passage time distribution* [10,154]. It is a probability density in time which determines the probability $f(t)\Delta t$ that a first passage happens in the time interval $[t, t+\Delta t]$, where Δt is very small. The first moment of the first passage time distribution is the mean first passage time (MFPT) which quantifies the mean time until the observable of the stochastic system crosses the threshold for the first time [10, 11, 154, 155].

First passage times are a common tool for the analysis of stochastic processes in many fields [156,157]. Examples include chemical reactions, where the reaction rate depends on the time the molecules diffuse until they find their reaction partner [11], search algorithms whose applicability depends on the time needing for a finding [158], and information transport through neurons where an emission of information occurs if the input from other neurons follows a certain dynamics for a certain time [159, 160]. The motion of colloids in periodic potentials is subject to a number of first passage investigations whose concern is the time which the colloid needs to escape a local minimum [11, 127, 161–163]. These *escape problems* are first passage problems where the escape is the first passage of a predefined boundary. The first passage distributions of these escape problems represent the dynamics of the colloidal systems on the time scale $1/r_K$. Diffusion of particles in periodic potentials for times larger than $1/r_K$ can be modelled with *continuous time random walk*, which models the motion as hopping between binding sites (which are the local potential minima). To account for asymmetries and inhomogeneities in the nature of the binding sites, continuous time random walk uses several probability densities, called *waiting time distributions* (WTDs), for the time between subsequent jumps between certain types of sites [128,129,164]. In most descriptions, the WTDs split the first passage time distribution into direction-dependent contributions. In general, the relation is more complicated, as the motion of colloids is continuous and the hopping processes are discrete in space. We resolve this discrepancy by providing a definition for a WTD in a continuous system in chapter 4.

1.5 Transport in one-dimensional periodic potentials

Many fundamental insights can be inferred from diffusion in one-dimensional periodic potentials. These include the ratchet effect, a fundamental transport mechanism, or the giant diffusion effect, which shows that a strong periodic potential not always hinders particle motion. Further, the influence of particle interactions on transport and diffusion in periodic potentials is still not completely understood. The solutions of one-dimensional problems can serve as guide for investigations in more spatial dimensions.

We are interested in situations where particles are transported through a one-dimensional structured potential. For transport to occur, there must be some kind of imbalance in the system, i.e. the system must be out of thermodynamic equilibrium. Common ways to drive the system out of equilibrium include imposing external forces or introducing a concentration gradient. Transient phenomena are becoming increasingly relevant for experiments and technology, because these can now measure and operate accurately on a time scale faster than the natural time scale of colloidal motion.

The investigation of overdamped transport in one-dimensional periodic potentials has a

long history [10, 11, 127, 150, 165]. During the years, standard models for transport in one-dimensional periodic potentials have been developed, which we introduce in the following two sections. The standard model to investigate stationary transport is the tilted washboard, whereas ratchet systems serve as the paradigm for directed transport with oscillatory forces.

1.5.1 Tilted washboard

A washboard potential which is not tilted is a spatially periodic potential. Tilting the washboard means exerting a constant force F, i.e. adding a term $-xF$ to the periodic potential. The tilted washboard potential is not periodic, but its force is.

Tilted sinusoidal washboard potential The simplest washboard potential has sine form. As a representative case for the tilted washboard potentials discussed in this section, we introduce the potential

$$u(x) = u_0 \sin^2 \frac{\pi x}{a} - xF. \tag{1.11}$$

This tilted sinusoidal washboard is characterised by the wavelength a, the amplitude u_0, and the constant driving force F. Plots of $u(x)$ for different values of F are shown in Fig. 1.4(a). Due to the symmetry of the system, we consider forces $F > 0$. If F is smaller than $F_c = u_0\pi/a$, which is the critical driving force connected to giant diffusion, the potential has (infinitely many) local extremes. In the domain $x \in [0, a]$ the minimum x^m and the maximum x^M is given by

$$x^m = \frac{a}{2\pi} \arcsin \frac{Fa}{\pi u_0} \qquad \text{and} \qquad x^M = \frac{a}{2} - x^m . \tag{1.12}$$

The difference in potential energy between maximum and minimum, in the direction of the force, reads

$$\Delta u(F) = u(x^M) - u(x^m) = u_0 \left(\sqrt{1 - (F/F_c)^2} - \frac{F}{F_c} \arccos \frac{F}{F_c} \right) . \tag{1.13}$$

The potential difference Δu is the energy barrier height which must be overcome to thermally activate a transport process in this washboard potential. The dependency of the barrier height on the driving force is plotted in the inset of Fig. 1.4(a).

There is no energy barrier in the regime $F > F_c$, where $u(x)$ is strictly monotonic. This case is also shown in Fig. 1.4(a).

Usage General tilted washboard potentials can used to model numerous situations. One example is the overdamped Brownian motion of a single particle in a corrugated channel, see Fig. 1.2(d) for a micrograph of such a channel. By using the Fick-Jacobs approach [166] the two or three dimensional motion of the particles is projected onto motion in one dimension (along the channel), combined with an effective washboard potential to account for the position dependent entropy of the particle. The accuracy of this approximation depends on the type of particles, the size of the corrugation, and the flow of the solvent [167–173].

As mentioned in section 1.2, light fields are very versatile and can be used to create one-dimensional modulated traps for colloids [91, 92], see also Fig. 1.4(b). Again, the motion of

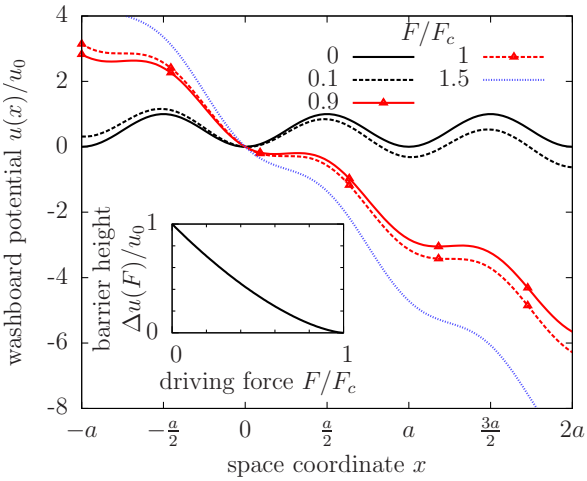

(a) Tilted washboard potential, defined in Eq. (1.11), for different values for the driving force F in units of the critical driving force $F_c = u_0\pi/a$. Inset: barrier height Δu given by Eq. (1.13).

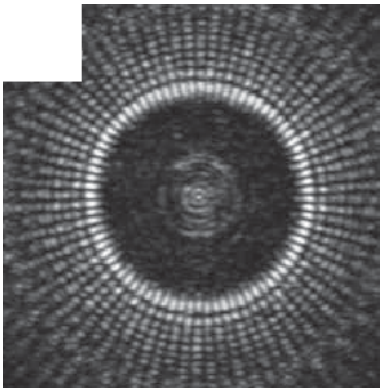

(b) Brightfield image of a structured light field. For colloidal polystyrene spheres the inner ring of the light field forms a corrugated one-dimensional periodic trap. Reprinted from [92].

Fig. 1.4: (a) Tilted one-dimensional sinusoidal washboard potential. (b) Experimental realisation of a one-dimensional tilted washboard potential with laser light [92].

colloids across the stripes in striped light fields can be modelled with overdamped motion a washboard potential [82].

Other systems that can be modelled using tilted washboard potentials include the (not overdamped) motion of cold atoms in standing waves of light [174, 175], and the Frenkel-Kontorova model, which is used to study friction on the nanoscale by examining particles connected through springs that are dragged through a washboard potential [90, 176, 177]. Further, in sheared two-dimensional systems tilted washboard potentials may also be applicable [178, 179].

Finally, quantum systems such as the Thouless motor [180], and the Josephson junction [181–183] can be modelled with a washboard potential.

Velocity. The stationary-state velocity of a single particle in a tilted washboard potential was found analytically in 1958 by Stratonovich [150]. The velocity of interacting colloids in a tilted washboard potential is still an active question [124, 149, 184], and we focus on it in chapter 7.

Giant diffusion effect. The giant diffusion effect or the giant enhancement of diffusion indicates that the motion on the long time scale $1/r_K$ shows an effective diffusion coefficient D which is larger than the diffusion coefficient of free diffusion D_0. This is remarkable because it contradicts the intuitive assumption that a periodic potential always slows down the motion. The effective diffusion coefficient was introduced in section 1.3.4 as half the slope of the MSD for long times, i.e. $D = \lim_{t\to\infty}\langle(\Delta x)^2/(2t)\rangle$.

The motion of a single particle in a tilted washboard potential shows giant diffusion for driving forces near the so-called critical driving force F_c at which the potential minima turn

into saddle points [89,92,125,185–187]. In Fig. 1.4(a) the driving force F is normalised to F_c, i.e., the curve for $F/F_c = 1$ shows the critical case. This enhanced diffusion is the working principle of a group of particle mixing techniques [69, 188]. Further, a particle separation device based on the giant diffusion effect was proposed [88].

Giant diffusion can be understood by considering thermal activated positional transitions of the particle between the valleys of the tilted washboard potential. For small driving forces ($F \ll F_c$) the washboard potential has high energy barriers between neighbouring valleys. Only a small fraction of random fluctuations can drive a colloid over the barrier. This implies a low velocity and a low diffusion coefficient. For very high driving forces ($F \gg F_c$) the tilted washboard potential is merely a linear function with shallow modulations. The modulations become negligible in the limit $F \to \infty$ and the diffusion coefficient D approaches D_0 in that limit.

If the driving force $F \approx F_c$, then the tilted washboard potential consists of alternating regions of steep slope and shallow slope (lines with triangles in Fig. 1.4(a)). The steep slope region is always rapidly traversed. In the shallow slope region, a random fluctuation of the particle's position may transport it to the steep region, which enhances the impact of that particular fluctuation. If the fluctuation leads the particle to another position, no enhancement takes place. Hence, in a short time different random fluctuations may result in very different positions, which is reflected in a high diffusion coefficient.

We now turn to the influence of particle interactions. In a one-dimensional model where particles are tied with springs to a rigid backbone [149] to form a flexible chain, the motion of the backbone through a tilted washboard potential shows giant diffusion. In this model the particles cannot diffuse themselves. We address the motion of ultra-soft repulsive particles through a tilted washboard to investigate the motion of one particle in an interacting system. In chapter 6 we find that the diffusion coefficient is even further enhanced with respect to the single particle case. Note that the fact that ultra-soft particles can permeate each other is crucial to have normal diffusion. Ultra-soft particle interaction is a model for the coarse-grained interaction of fluctuating polymer chains. However, the interaction potential of most types of colloid diverges for small distances. The motion of these non-permeating particles shows single file diffusion, i.e. $\langle \Delta x^2 \rangle = 2\kappa_{0.5}\sqrt{t}$, as we mentioned in section 1.3.4. The so-called mobility factor $\kappa_{0.5}$ shows giant enhancement if the particles are transported through a tilted washboard [147].

So far, we have discussed overdamped Brownian motion in static tilted washboard potentials. Note that giant diffusion can also be achieved through oscillating force fields, as theoretical [169, 189–192] and recent experimental [88, 193] works with single particles show.

1.5.2 Ratchet effect

The ratchet effect states that every combination of spatial asymmetry, noise, and non-equilibrium creates a directed motion. The idea goes back to Smoluchowski [165], was refined by Feynman and is also called the Smoluchowski-Feynman-ratchet [9]. The first application was the thermoelectric effect, found in the 19th century by Seebeck [194], which can be modelled as a ratchet effect [9].

In [9] a thorough review of the different ways of combining asymmetry, noise, and non-equilibrium to obtain a ratchet system is given. Many operate with asymmetric periodic potentials. In the biophysical area these potentials are used to model the above mentioned

motor proteins, e.g., kinesin or myosin [2,9,62]. The ratchet model was adopted for various artificial Brownian motors with physical, chemical, and biological background [7,195,196], where the motion is often one-dimensional. Examples of ratchet systems connected to the development of optical computing include the transport of cold atoms in optical lattices [197,198], and the transport of superconducting electron pairs through Josephson junctions [199–201], where superconducting states are in contact via a grain boundary. For colloidal transport various mechanisms exists [71,76,77,99,202–207]. Based on these mechanisms sorting machines were build [70,71,75–77,208,209], some of them were already mentioned in section 1.2.

From a theoretical point of view terminology exists that distinguishes between different types of ratchets [9]. A periodic asymmetric potential, which is switched on and off, is called a flashing ratchet [210]. A periodic asymmetric potential supplemented with a homogeneous oscillating force, which averages to zero over one period, is called a *rocking ratchet* [211]. The direction and the strength of the current in these ratchets depends on the details of the driving [211,212].

In chapter 5 we show that the oscillatory drive in the rocking ratchet can be replaced with a time delayed feedback control. Feedback control uses information from the system to steer the system. This information is retrieved by continuous measurements. Our feedback controlled rocking ratchet yields a higher current than the standard rocking ratchet and does not rely on external timing any more.

1.6 Feedback control

In order to realise fast and predictable transport of particles, we consider controlling the particle transport using feedback mechanisms. Feedback control or closed-loop control means that the system is steered towards a target behaviour by using information from the system itself, which is retrieved e.g. by continuous measurements. This is different to external control or open-loop control, where system parameters are set externally without reacting to changes within the system.

Open loop control does not need measurements and is the preferred control for systems with predictable dynamics. It is more common to refer to open-loop controlled systems as systems with an external (time-dependent) influence. Examples include systems under the influence of oscillating forces (forming e.g. mixing devices or ratchet systems). Open loop control is present in many ordinary machines, e.g. watches controlled by a quartz crystal or a fluorescent lamp which starts by using a fixed protocol. For complex dynamics or unpredictable dynamics, like the stochastic systems considered in this thesis, feedback control is the most reliable control mechanism.

Application Feedback control has been used in machines since ancient times [213,214]. It has many applications in physics e.g. in reaction diffusion systems to shape moving fronts [215,216], in quantum transport to adjust the number of electrons or photons [217,218], in sheared liquid crystals to stabilise collective orientational states [219], and in laser dynamics to work towards optical (rather than electrical) computing [220]. Further, feedback control is used to investigate the dynamics of the brain on different scales ranging from studies on single neurons [221], over networks of neurons [222], to artificial intelligence [223].

Various feedback strategies exist for colloidal systems. The control mechanisms target effects such as directed transport [91, 224–226], adjustment of structure and viscosity of dense colloidal suspensions [227, 228], the sorting of colloids [97, 229], and their trapping [100, 230, 231].

Experimental prerequisites Recent advances in experimental techniques fostered the development of feedback control of colloids. They include video microscopy and confocal microscopy. Video microscopy yields a fast imaging of a 2D colloidal layer [51,52,82,83,91,92]. Confocal microscopy allows for a three-dimensional time and space dependent measurement, by making 2D measurements in the focal plane and rapidly changing the altitude of the plane [232,233]. The recently demonstrated photothermal microscopy [234] promises a further increase of spatial resolution.

Time delay Time delay is inherent in feedback control, as the measurement of observables and the adjustment of control parameters needs a finite time. Time delay was included in theoretical modelling only recently [226,235–238]. For some transport mechanisms, time delay reduces the effectiveness [235]. However, other feedback controls benefit from time delay and some feedback controls intrinsically rely on time delay, e.g. Pyragas control scheme which stabilises unstable periodic solutions of non-linear systems [239]. In this thesis two feedback protocols are proposed. While transport is generated through time delay in the feedback controlled rocking ratchet in chapter 5, the time delay is found to reduce the effectiveness of the control in chapter 7.

In modern experiments using video microscopy, the overall time delay of measurement and implementation of feedback control of colloids is in the order of 5-50 ms [91, 236, 240]. The Brownian time for colloids of μm size, which is the relevant size for video microscopy, is in the range of 100ms - 10s. This small quotient of time delay to Brownian time means that the particle motion can be controlled very detailed.

Entropy and information In the case of stair-climbing colloids [224] the transport in a tilted washboard potential corresponds to the motion against the ascent. This is achieved by blocking the colloid from moving in the energetically favoured direction. Brownian motion provides the colloid the energy to move to the next valley of the washboard potential against its tilt. The feedback control scheme assures that as soon as the colloid arrives at the next valley, the potential landscape is altered so it cannot go back. This is a prime example for a group of control mechanisms called *information ratchets* [195]. The information ratchet lets the Brownian particle transform heat into mechanical work. This is possible because the restriction of the direction of motion creates a non-equilibrium situation. Entropy increases while the colloids climbs the potential ascent. The amount of work which can be extracted using a certain amount of information is limited and can be calculated using so-called "fluctuation theorems". Fluctuation theorems relate time-reversal and dissipation are the basis of the generalisation of the second law of thermodynamics to non-equilibrium [55, 241]. The search for the correct definition of entropy in non-equilibrium stimulated many theoretical [225, 242–246] and experimental [100, 224, 247] studies.

1.7 Outline of the thesis

This thesis is set in the field of transport of colloids in one-dimensional periodic potentials. We address fundamental questions on the motion of a single Brownian particle in a tilted washboard potential. Based on that knowledge we investigate the role of colloid-colloid interaction on diffusion and transport. Further, we propose two feedback control protocols for colloidal transport.

This thesis is a kind of cumulative PhD thesis. The results of the publications I contributed to are repeated in a cohesive and explanatory way.

In chapter 2, I give an overview of the theory which is important for the motion of colloids for the time scales discussed in section 1.3. Here, I introduce the basic equations that describe colloidal motion, i.e. the overdamped Langevin equation (LE) and the corresponding Fokker-Planck equation (FPE), which is the Smoluchowski equation (SE). Furthermore, I introduce the method that we use to study interacting colloidal systems on large length scales: the dynamical density functional theory (DDFT).

The chapters 3 to 7 each cover a separate question on the frontier of research. However, we focus on non-equilibrium diffusion and transport on the time scales discussed in section 1.3.

The first two content chapters 3 and 4 consider the paradigm of a single Brownian particle in a tilted sinusoidal washboard potential. In chapter 3, we present a simple model for the short time diffusion which emphasises the significant properties of the system much better than the traditional SE-based description. In addition, the model yields analytic results whereas the SE must be solved numerically. We show that the model applies to the regime of "deep wells", where the washboard potential has local minima deeper than $k_{\mathrm{B}}T$. We study the plateau in the MSD and give approximations for duration and height of the plateau.

In chapter 4, we introduce a definition for the waiting time distribution (WTD) for continuous driven systems, which previously was available only for discrete systems. At the same time, we generalise the first passage time distribution (FPTD) by identifying the contributions to the FPTD corresponding to different directions as our WTDs. We use our WTD to characterise the motion of a Brownian particle in a tilted washboard potential which consists of waiting and jumping. Our WTD yields a characterisation of the wide distribution of waiting times in the presence of transport. Further, we find a new time scale which we call "jump duration" which expresses that the crossing of the barrier is of finite duration in a continuous system.

In chapter 5 we propose a time delayed feedback control for the driving of a single particle in an asymmetric periodic potential. We show that the time delay induces a ratchet effect which means that an external timing is not necessary to form a rocking ratchet. Further, we find that our feedback controlled rocking ratchet can be adjusted to a yield a higher current than a corresponding standard rocking ratchet. Our feedback control comprises switchings of the direction of the driving force. These switching events and the following relaxation to a stationary state are particularly visible in the time-dependent entropy production.

In chapter 6 we use theory to predict, for the first time in the literature, the influence of particle interactions on the short time diffusion and the diffusion coefficient of ultra-soft particles in a tilted washboard potential. We find that the plateau in the MSD, which is found for single particles, becomes shorter and transforms to a superdiffusive region as the number

of particles and the interaction strength is increased. Further, we propose a modification to the method to study the motion of hard particles with attractive interactions more easily. We find that chains of these particles dissolve in the presence of a tilted washboard potential.

In chapter 7 we propose a feedback control for the collective transport of repulsively interacting particles through a tilted washboard potential. We focus on the "deep well" case, i.e. the case where the local potential energy minima are deeper than $k_{\mathrm{B}}T$, and where the mobility of uncontrolled transport is very low. The control comprises a strong trapping potential which effectively freezes the particle cluster. This emphasises the role of particle interaction for transport. Finally, this enhances the mobility of the collective transport by several orders of magnitude.

Finally, in chapter 8, we summarise our findings and give a conclusion and an outlook.

2. THEORY

The equations in this chapter are formulated in three dimensions to give a versatile overview for a general class of systems.

2.1 Langevin equation

The Langevin equation (LE) for a single particle was mentioned already in section 1.3.1. However, the LE (1.2) is not completely defined because the stochastic force lacks a proper definition. For most purposes this stochastic force can be modelled as a Gaussian white noise, which obeys

$$\langle \mathbf{f}^{\text{stoch}}(t) \rangle = \mathbf{0} \tag{2.1a}$$

$$\langle f_i^{\text{stoch}}(t) f_j^{\text{stoch}}(t') \rangle = G\delta_{ij}\delta(t-t')\,, \tag{2.1b}$$

where $\langle \dots \rangle$ denotes an ensemble average. The δ-distribution is denoted by $\delta(t)$, and G denotes the so-called noise strength or noise intensity [10, 41, 190]. An differential equation with a noisy ingredient, like Eq. (2.2), is called a stochastic differential equation [154, 248].

For N, possibly interacting, particles the LE reads

$$M\ddot{\mathbf{r}}_i(t) = -\gamma\dot{\mathbf{r}}_i + \mathbf{f}_i(\mathbf{r}_1, \dots, \mathbf{r}_N, t) + \mathbf{f}_i^{\text{stoch}}(t)\,, \tag{2.2}$$

where each $\mathbf{f}_i^{\text{stoch}}$ is a Gaussian white noise on its own, i.e. $\langle \mathbf{f}_i^{\text{stoch}}(t) \otimes \mathbf{f}_j^{\text{stoch}}(t') \rangle = G\delta_{ij}\mathbb{1}\delta(t-t')$ where $\otimes$ is an outer product and $\mathbb{1}$ is the identity matrix.

2.1.1 Fluctuation-dissipation theorem

The order of magnitude of the noise strength G in Eq. (2.1) can be related to the temperature of the solvent. In the case of colloids, this is desirable since it provides a physical background the noise strength. However, the Langevin equation is used in other systems, too, such as superconducting currents through a Josephson junction [201], neuron dynamics [249], population dynamics [250], and for the momentum of cold atoms in optical lattices [251]. Among these systems, the noise strength is related to temperature only for Josephson junctions.

Due to the separation of time scales we assume the solvent to be in equilibrium and having a temperature T. Therefore, it makes sense to introduce a temperature even if Eq. (1.2) is about non-equilibrium dynamics. The relation is established via the equipartition theorem [41]

$$\frac{M}{2} \lim_{t\to\infty} \lim_{t'\to t} \langle \dot{\mathbf{r}}(t) \otimes \dot{\mathbf{r}}(t') \rangle = \mathbb{1}\frac{k_{\text{B}}T}{2}\,. \tag{2.3}$$

Source	$\sigma/\mu m$	τ_B/s	$D_0\,/\,(10^{-12}m^2s^{-1})$
[91]	0.9	1.8	0.44
[92]	1.48	11.5	0.19
[204]	1.53	7.1	0.33
[82]	1.7	0.88	3.3 (from Fig. 5A)
[82]	4	145	0.11 (from Fig. 5C)
[186]	2.8	87	0.09
[89]	3	56	0.16
[252]	1.67	100	0.028

Tab. 2.1: Brownian times and short time diffusion coefficient from experiments of colloids of roughly micrometer size immersed in water [82, 89, 91, 92, 186, 204] or apolar solvent [252].

Following standard textbooks [10, 41], the LE (1.2) is integrated with respect to time, and inserted into Eq. (2.3). Using the noise properties Eq. (2.1) and taking the limits yields

$$G = 2k_BT\gamma\,. \tag{2.4}$$

Equation (2.4) is a *fluctuation-dissipation theorem*, where a quantity describing fluctuations, the noise intensity G, is connected with a quantity describing dissipation, the friction coefficient γ.

2.1.2 Overdamped Brownian motion

For colloidal suspensions accelerations are irrelevant, which becomes clear by comparing the order of magnitude of the inertial force and the friction force the particles experience in the solvent. See the book of Dhont [41] for a rigorous discussion. In section 1.3.1 we introduced the time scale of momentum relaxation $\tau_M = M/\gamma$ and the Brownian time $\tau_B = \sigma^2/D_0$. The diffusion coefficient of free motion, D_0, is connected to the friction constant γ by Eq. (1.5) which can be related to the viscosity of the solvent (cf. Eq. (1.1)). From these relations it can be concluded that $\tau_B \gg \tau_M$. However, we collected values for D_0 from experiments and τ_B from Eq. (1.4) in Table 2.1 to verify that conclusion. Indeed, for micrometre sized particles in water, $\tau_M \approx 10^{-7}$s and $\tau_B \approx 1$s. Because our studies target at times between $10^{-3}\tau_B$ and $10^5\tau_B$, we can treat the inertial degrees of freedom adiabatically.

Inertial degrees of freedom become relevant for cold atoms in optical lattices [253] and a couple of other systems [254, 255].

To express the irrelevance of the inertia in the LE we multiply the LE (2.2) by $1/(\gamma\tau_B)$

$$\frac{M}{\gamma\tau_B}\ddot{\mathbf{r}}_i = \frac{1}{\tau_B}\left(-\dot{\mathbf{r}}_i + \mathbf{f}_i/\gamma + \mathbf{f}_i^{\text{stoch}}/\gamma\right)\,. \tag{2.5}$$

The factor in front of $\ddot{\mathbf{r}}$ is τ_M/τ_B, which is a small quantity. By neglecting this small deviation, i.e. writing Eq. (2.5) in the order $O((\tau_M/\tau_B)^0)$, we arrive at the *overdamped LE*

$$\gamma\dot{\mathbf{r}}_i(t) = \mathbf{f}_i(\mathbf{r}_1, \ldots, \mathbf{r}_N, t) + \mathbf{f}_i^{\text{stoch}}(t)\,. \tag{2.6}$$

The rigorous mathematical characterisation of the solutions of stochastic differential equations, even for the overdamped Langevin equation, is far beyond the scope of the thesis. The

book of Kloeden and Platen [248] discusses existence and uniqueness of solutions and reviews a broad range of numerical methods.

For actual computations, in chapters 4 and 5, we use the one-dimensional reduction of Eq. (2.6) for a single particle

$$\gamma \dot{x}(t) = f(x,t) + \sqrt{2\gamma k_\mathrm{B} T}\xi(t)\,, \tag{2.7}$$

where $\xi(t)$ is a Gaussian white noise with $\langle \xi(t)\xi(t')\rangle = \delta(t-t')$.

2.2 Fokker-Planck equation

The individual trajectories $x(t)$ are often of little interest. Ensemble-averaged quantities like mean particle position, mean squared displacement, (long term) diffusion coefficient or mobility matter. Due to the stochastic term in the LE (Eq. (2.6)) analytic results for those quantities are difficult to obtain.

The Fokker-Planck equation (FPE) fills this gap by providing an equation of motion for the probability density $p(x,t)$ which defines the probability $p(x,t)\,\Delta x$ to find the particle in a interval Δx around position x at time t. In terms of statistical mechanics [59], the probability density can be expressed as an ensemble average

$$p(x,t) = \langle \delta(x - x(t))\rangle\,, \tag{2.8}$$

where x denotes a position variable and $x(t)$ denotes a trajectory.

By using the Kramers-Moyal expansion a FPE can be assigned to every LE with Gaussian white noise [10]. The advantage is that the FPE is a *deterministic* partial differential equation for the time evolution of $p(x,t)$, which makes an analytic treatment possible. The drawback is that the information about the actual particle positions is lost.

The corresponding FPE to the LE (2.6), the *Smoluchowski equation* (SE), reads [10]

$$\partial_t P(\mathbf{r}_1,\ldots,\mathbf{r}_N,t) = \frac{1}{\gamma}\sum_{i=1}^{N} \boldsymbol{\nabla}_i \cdot (k_\mathrm{B}T\boldsymbol{\nabla}_i P \;-\; P\,\mathbf{f}_i)\;, \tag{2.9}$$

The probability density $P(\mathbf{r}_1,\ldots,\mathbf{r}_N,t)$ quantifies the probability $P(\mathbf{r}_1,\ldots,\mathbf{r}_N,t)\Delta\mathbf{r}_1\ldots\Delta\mathbf{r}_N$ to find each particle in its corresponding small cuboidal volume with the corners $\mathbf{r}_i$ and $\mathbf{r}_i+\Delta\mathbf{r}_i$ all at time t. Correspondingly we have

$$P(\mathbf{r}_1,\ldots,\mathbf{r}_N,t) = \left\langle \prod_{i=1}^{N} \delta(\mathbf{r}_i - \mathbf{r}_i(t)) \right\rangle\,. \tag{2.10}$$

Note that the SE is linear in P, whereas the LE, in general, is not linear in $\mathbf{r}$. The SE is a continuity equation

$$\partial_t P(\mathbf{r}_1,\ldots,\mathbf{r}_N,t) + \sum_{i=1}^{N} \boldsymbol{\nabla}_i \cdot \mathbf{j}_i(\mathbf{r}_1,\ldots,\mathbf{r}_N,t) = 0\,, \tag{2.11}$$

where

$$\mathbf{j}_i(\mathbf{r}_1,\ldots,\mathbf{r}_N,t) = -D_0\boldsymbol{\nabla}_i P + \frac{1}{\gamma}\mathbf{f}_i \tag{2.12}$$

is the probability current for the ith particle.

Without any external force, the SE (2.9) reduces to the diffusion equation (or heat equation) $\partial_t P = D_0 \sum_i \boldsymbol{\nabla}_i^2 P$.

In chapters 3, 4, and 5, we investigate one-particle systems in one dimension. The corresponding reduction of Eq. (2.9) reads

$$\partial_t p(x,t) = D_0 \partial_{xx} p(x,t) - \frac{1}{\gamma} \partial_x (p(x,t)\, f(x,t))\,. \tag{2.13}$$

2.2.1 Kramers' escape rate

As mentioned in section 1.3.3, Kramers' escape rate is an important approximation to estimate a time scale for thermally activated processes over a high barrier [11].

The derivation in one dimension from [10] is repeated here to point out the necessary approximations and to distinguish between two forms. The trap is formed by a potential with one local minimum and one local maximum like in the sketch in Fig. 2.1. The rate is defined as the ratio of the outgoing probability current j to the probability P that the particle was in the trap:

$$r := j/P\,. \tag{2.14}$$

The equation of motion for the probability density of one overdamped Brownian particle in one dimension is the SE (2.13). The first approximation is that the outgoing flux is small, so that the probability density in the trap can be treated adiabatically. Hence, stationary is assumed, i.e. $\partial_t p(x,t) = 0$. The SE can be integrated once, yielding

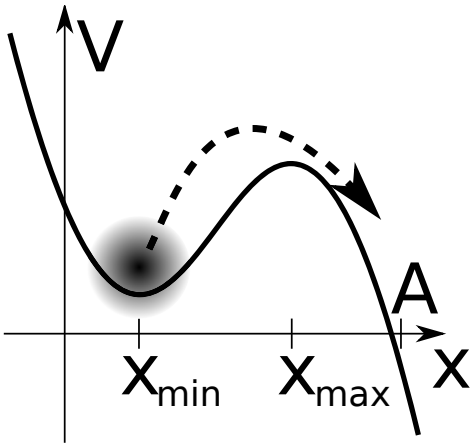

Fig. 2.1: Illustrates a trapping potential (thick line) with a trapped particle (blurred circle) and the small outgoing flux to the right (dashed line).

$$j = -D_0 p'(x) - p(x) V'(x)/\gamma\,, \tag{2.15}$$

where the probability current appears as an integration constant. We solve Eq. (2.15) with variation of constants

$$p(x) = e^{-\beta V(x)} (c - \frac{j}{D_0} I(x)) \quad \text{with} \quad I(x) = \int_{x_{\min}}^{x} \mathrm{d}y\, e^{\beta V(y)}\,, \tag{2.16}$$

where $\beta = 1/(k_\mathrm{B} T)$ and c is another integration constant. We are interested in the outgoing flux. To rule out that the particle can reenter the trap, we assume that the particle disappears at $x = A$. This is equivalent to saying, that we are interested in the probability that the particle leaves the trap *for the first time*. We define that the particle leaves the trap at arriving at $x = A$ and, from then on, the probability to leave the trap for the first time is, of course, zero. Either way, we obtain the boundary condition

$$p(A) = 0\,. \tag{2.17}$$

One integration constant can be eliminated, yielding

$$j = \frac{cD_0}{I(A)} \quad , \quad p(x) = c\, e^{\beta V(x)} \left(1 - \frac{I(x)}{I(A)}\right) . \tag{2.18}$$

The probability to find the particle in the trap reads

$$P = \int_{-\infty}^{x_{\max}} \mathrm{d}x\, p(x) . \tag{2.19}$$

As the process is stationary, P must be constant. The stationarity approximation can hold only for a certain time, as the trap is actually petering out. We investigate this in detail in chap. 4. Equation (2.19) fixes c, yielding

$$\frac{1}{r} = \frac{I(A)}{D_0} \int_{-\infty}^{x_{\max}} \mathrm{d}x\, e^{-\beta V(x)} \left(1 - \frac{I(x)}{I(A)}\right) \tag{2.20}$$

Further, we make approximations about the form of $V(x)$. First, we assume that there is a large energy barrier $V(x_{\max}) - V(x_{\min}) \gg k_{\mathrm{B}}T$. It follows that the $I(x)/I(A)$ term is irrelevant because (a) near the minimum the integral $I(x) = e^{\beta V(x_{\min})}(x - x_{\min}) + O((x - x_{\min})^2)$ is much smaller than $I(A)$ and (b) at the hill $e^{-\beta V}$ is very small while $I(x) < I(A)$.

The result is

$$r_K^{\infty} = D_0 \Big/ \left(\int_{-\infty}^{x_{\max}} \mathrm{d}x\, e^{-\beta V(x)} \int_{x_{\min}}^{A} \mathrm{d}y\, e^{\beta V(y)} \right) . \tag{2.21}$$

The integrals over x and y are measures of the broadness of the valley and the hill, respectively. Usually, they are not elementary. The famous Kramers' rate appears upon expanding the potential $V(x)$ around each extremum to a quadratic function, and expanding the integral bounds to infinity. The resulting integrals can be carried out, yielding Kramers' rate

$$r_K = \frac{D_0}{2\pi k_{\mathrm{B}} T} \sqrt{-V''(x_{\min}) V''(x_{\max})}\, e^{-\beta(V(x_{\max}) - V(x_{\min}))} . \tag{2.22}$$

If the potential is not well approximated by a quadratic curve at the extrema, a fourth order approximation (chapter 5.10.1 in [10]) may be used to still have a rate with elementary integrals.

2.3 Dynamical density functional theory

The applicability of the FPE is limited to a few particles or a few degrees of freedom. A calculation of the motion of many interacting particles with the FPE is almost impossible because the probability density P is a density is depending on every degree of freedom. Hence, the FPE becomes a partial differential equation in many dimensions, which is very difficult to treat. To reduce the number of dimensions, thereby neglecting some information, the n-particle densities are introduced [59]

$$\varrho^{(n)}(\mathbf{r}_1, \ldots, \mathbf{r}_n, t) = \frac{N!}{(N-n)!} \int \mathrm{d}\mathbf{r}_{n+1} \ldots \mathrm{d}\mathbf{r}_N\, P(\mathbf{r}_1, \ldots, \mathbf{r}_N, t) , \tag{2.23}$$

where $\int \mathrm{d}\mathbf{r}_j$ denotes a volume integral over the whole volume that $\mathbf{r}_j$ can address. The n-particle densities describe the expected density of n-tupels of particles at the positions $\mathbf{r}_1, \ldots, \mathbf{r}_n$ at time t, irrespective of the other particles. Highly relevant are the one-particle density $\varrho^{(1)}(\mathbf{r}, t)$ and the two-particle density $\varrho^{(2)}(\mathbf{r}, \mathbf{r}', t)$ because many thermodynamic properties of the many particle system can be derived from these two quantities [59].

With Eq. (2.10) we reformulate the one- and two-particle density as

$$\varrho^{(1)}(\mathbf{r}, t) = \left\langle \sum_{i=1}^{N} \delta(\mathbf{r} - \mathbf{r}_i(t)) \right\rangle \tag{2.24a}$$

$$\varrho^{(2)}(\mathbf{r}, \mathbf{r}', t) = \left\langle \sum_{i=1}^{N} \sum_{j=1, i\neq j}^{N} \delta(\mathbf{r} - \mathbf{r}_i(t))\, \delta(\mathbf{r}' - \mathbf{r}_j(t)) \right\rangle , \tag{2.24b}$$

where the time dependent $\mathbf{r}_i(t)$ are trajectories, i.e. solutions of the LE (2.6). To interpret these densities we first look at the normalisation

$$N = \int \mathrm{d}\mathbf{r}\, \varrho^{(1)}(\mathbf{r}, t) \tag{2.25a}$$

$$N(N-1) = \int \mathrm{d}\mathbf{r}\, \mathrm{d}\mathbf{r}'\, \varrho^{(2)}(\mathbf{r}, \mathbf{r}', t)\,. \tag{2.25b}$$

Clearly, the densities are not strictly probability densities because they are not normalised to one. Nevertheless, their statement is probabilistic. The one-particle density $\varrho^{(1)}$ is the expected density of particles, and the two-particle density $\varrho^{(2)}(\mathbf{r}, \mathbf{r}', t)$ is the expected density of pairs of particles.

The dynamical density functional theory (DDFT) yields a closed equation for the time evolution of the one-particle density $\varrho^{(1)}(\mathbf{r}, t)$. The difficulty lies in the dependence of $\varrho^{(1)}(\mathbf{r}, t)$ on the force $\mathbf{f}$ in the SE (2.9), which can involve interactions between all particles.

The derivation of the DDFT can be done in three different ways. The first was presented by Marconi and Tarazona in 1999 [257] and started with the Langevin equations and used the density operator and Ito calculus. The second was proposed by Archer and Evans 2004 and started with the Smoluchowski equation (2.9). I will briefly present this derivation in the following. Furthermore, an alternative derivation using the projector-operator method [258] was presented by Rex and Löwen in 2008 [259].

In Archers and Evans' approach [260], the Smoluchowski equation is assumed in a form where the force in Eq. (2.9) is a gradient, i.e.

$$\mathbf{f}_i(\mathbf{r}_1, \ldots, \mathbf{r}_N, t) = -\boldsymbol{\nabla}_i V(\mathbf{r}_1, \ldots, \mathbf{r}_N, t)\,. \tag{2.26}$$

It is convenient to assume that the particles only interact via pair interactions through a pair potential v_{int}. The derivation in [260] is not restricted in such a way. The potential in Eq. (2.26) then reads

$$V(\mathbf{r}_1, \ldots, \mathbf{r}_N, t) = \sum_{i=1}^{N} V_{\mathrm{ext}}(\mathbf{r}_i, t) + \frac{1}{2} \sum_{i=1}^{N} \sum_{j\neq i} v_{\mathrm{int}}(\mathbf{r}_i, \mathbf{r}_j)\,. \tag{2.27}$$

By integrating the SE (2.9) for a pairwise additive potential over $N-1$ coordinates one arrives (see appendix 9.1) at a time evolution equation for the one-particle density

$$\gamma\partial_t\varrho^{(1)}(\mathbf{r},t) = k_\mathrm{B}T\Delta\varrho^{(1)}(\mathbf{r},t) + \boldsymbol{\nabla}\cdot(\varrho^{(1)}\boldsymbol{\nabla}V_\mathrm{ext}) + \boldsymbol{\nabla}\cdot\int\mathrm{d}\mathbf{r}'\,\varrho^{(2)}(\mathbf{r},\mathbf{r}',t)\boldsymbol{\nabla}v_\mathrm{int}(\mathbf{r},\mathbf{r}')\,. \tag{2.28}$$

However, Eq. (2.28) is of no direct use because it contains the time dependent two-particle density $\varrho^{(2)}$ which is unknown, too. An integration of Eq. (2.9) over fewer coordinates will yield time evolution equations for the higher order particle densities. A hierarchy similar to the Bogolyubov-Born-Green-Kirkwood-Yvon (BBGKY) [59] hierarchy develops. Therefore, an approximative closure is needed.

2.3.1 Density functional theory

Classical static density functional theory is a very successful method for the description of the equilibrium properties of inhomogeneous fluids [54,56,59,261,262]. It originates [59] from the quantum density functional theory founded by Kohn, Hohenberg and Sham [263,264].

Classical density functional theory operates in the grand canonical ensemble. In equilibrium homogeneous thermodynamics, the independent variables in the grand canonical ensemble are the chemical potential μ, the volume V and the temperature T. In the inhomogeneous case the volume is replaced by an external potential $V_\mathrm{ext}(\mathbf{r})$ which models the confinement. The quantity determining the behaviour is the grand potential Ω and its derivatives. Analogous to Hohenberg and Kohn [263], Hansen and McDonald [59] show that the grand potential is a unique functional $\Omega[\varrho^{(1)}]$ of the grand canonical version of the one-particle density $\varrho^{(1)}$. It follows that the Helmholtz free energy

$$\mathcal{F}[\varrho^{(1)}] = \Omega[\varrho^{(1)}] + \mu\int\mathrm{d}\mathbf{r}\,\varrho^{(1)}(\mathbf{r}) \tag{2.29}$$

is a unique functional of the one-particle density, too. The functional $\mathcal{F}[\varrho]$ can be split into three contributions, the parts concerning entropy, external potential, and the rest. The entropic part (also called ideal gas part) reads

$$\mathcal{F}_\mathrm{ent}[\varrho] = k_\mathrm{B}T\int\mathrm{d}\mathbf{r}\,\varrho(\mathbf{r})[\ln(\Lambda^3\varrho(\mathbf{r})) - 1]\,. \tag{2.30}$$

The quantity Λ is the thermal de-Broglie wavelength which is irrelevant in this study because we are far from the quantum regime. Here, Λ just serves to give the logarithm a dimensionless input. The influence of the external potential is expressed by the external part

$$\mathcal{F}_\mathrm{ext}[\varrho] = \int\mathrm{d}\mathbf{r}\,\varrho(\mathbf{r})\,V_\mathrm{ext}(\mathbf{r})\,. \tag{2.31}$$

Everything else belongs to the *excess* part. Here, the excess part consists of the contributions of the particle interactions. Hence, we call it *interaction* part. We arrive at the decomposition

$$\mathcal{F}[\varrho] = \mathcal{F}_\mathrm{ent}[\varrho] + \mathcal{F}_\mathrm{ext}[\varrho] + \mathcal{F}_\mathrm{int}[\varrho]\,. \tag{2.32}$$

The functional derivatives of the excess part of the Helmholtz free energy, which here is $\mathcal{F}_{\text{int}}$, with respect to ϱ are called *direct correlation functions* [59, 265]

$$c^{(1)}[\varrho](\mathbf{r}) = -\beta \frac{\delta \mathcal{F}_{\text{int}}[\varrho]}{\delta \varrho(\mathbf{r})} \tag{2.33a}$$

$$c^{(2)}[\varrho](\mathbf{r}, \mathbf{r}') = \frac{\delta c^{(1)}(\mathbf{r})}{\delta \varrho(\mathbf{r}')} = -\beta \frac{\delta^2 \mathcal{F}_{\text{int}}[\varrho]}{\delta \varrho(\mathbf{r})\, \delta \varrho(\mathbf{r}')} \,. \tag{2.33b}$$

The notation $c^{(2)}[\varrho](\mathbf{r}, \mathbf{r}')$ indicates that $c^{(2)}$ is an operator mapping a function $\varrho(\mathbf{r})$ to a function taking the two arguments $\mathbf{r}$ and $\mathbf{r}'$. At equilibrium, where Ω is minimal,

$$0 = \frac{\delta \Omega}{\delta \varrho^{(1)}(\mathbf{r})} = -\mu + k_{\text{B}} T \ln(\Lambda^3 \varrho^{(1)}(\mathbf{r})) + V_{\text{ext}}(\mathbf{r}) - k_{\text{B}} T c^{(1)}(\mathbf{r}) \,. \tag{2.34}$$

Equation (2.34) corresponds to an Euler-Lagrange equation. We dropped the functional dependence because $\varrho^{(1)}$ is fixed at equilibrium. We see from Eq. (2.34) that $c^{(1)}$ corresponds to that part of the energy landscape which is caused by the interactions. Knowledge about the structure of the fluid is provided by the *pair distribution function* $g(\mathbf{r}, \mathbf{r}')$ which is defined by

$$\varrho^{(2)}(\mathbf{r}, \mathbf{r}') = \varrho^{(1)}(\mathbf{r}) \varrho^{(1)}(\mathbf{r}') g(\mathbf{r}, \mathbf{r}') \,. \tag{2.35}$$

A further important quantity is the *pair correlation function* $h = g - 1$. These quantities can be related to experimentally measurable quantities, such as the static structure factor [59]

$$S(\mathbf{k}) = 1 + \varrho_0 \tilde{h}(\mathbf{k}) \tag{2.36}$$

where $\tilde{h}(\mathbf{k})$ is the Fourier transform of the pair correlation function in the translational invariant case $h(\mathbf{r}, \mathbf{r}') = h(\mathbf{r} - \mathbf{r}')$. The mean density is denoted by ϱ_0. The pair correlation function is related to $\mathcal{F}_{\text{int}}$ via the Ornstein-Zernike equation [59]

$$h(\mathbf{r}, \mathbf{r}') = c^{(2)}(\mathbf{r}, \mathbf{r}') + \int \mathrm{d}\mathbf{r}''\, c^{(2)}(\mathbf{r}, \mathbf{r}'') \varrho^{(1)}(\mathbf{r}'') h(\mathbf{r}'', \mathbf{r}') \,. \tag{2.37}$$

In principle, the structure of the fluid, i.e. the pair distribution function, could be determined with the Helmholtz free energy functional, its derivatives, and the Ornstein-Zernike equation. But an exact expression for $\mathcal{F}_{\text{int}}$ is known only for very special cases. In fact, approximations for g and/or $c^{(2)}$ are used to integrate Eq. (2.33) to find approximative expressions for $\mathcal{F}_{\text{int}}$ [59, 265]. The achieved approximations for the functional can be used to deal with more complex cases, such as time dependent problems by using DDFT.

Equilibrium sum rule

The so-called "equilibrium sum rule" [260, 265] relates the two-particle density in equilibrium $\varrho^{(2)}$ with the first direct correlation function $c^{(1)}$. To obtain it, we study Eq. (2.28) in equilibrium

$$0 = k_{\text{B}} T \boldsymbol{\nabla} \varrho^{(1)}(\mathbf{r}) + \varrho^{(1)}(\mathbf{r}) \boldsymbol{\nabla} V_{\text{ext}}(\mathbf{r}) + \int \mathrm{d}\mathbf{r}'\, \varrho^{(2)}(\mathbf{r}, \mathbf{r}') \boldsymbol{\nabla} v_{\text{int}}(\mathbf{r}, \mathbf{r}') \,. \tag{2.38}$$

We use the static DFT to calculate the one-particle density $\varrho^{(1)}$ by taking the gradient of Eq. (2.34) and multiplying by $\varrho^{(1)}$. We arrive at a relation between $\varrho^{(2)}(\mathbf{r},\mathbf{r}')$ and $c^{(1)}[\varrho^{(1)}](\mathbf{r})$

$$\begin{aligned}\int \mathrm{d}\mathbf{r}'\varrho^{(2)}(\mathbf{r},\mathbf{r}')\boldsymbol{\nabla}v_{\mathrm{int}}(\mathbf{r},\mathbf{r}') &= -k_{\mathrm{B}}T\varrho^{(1)}(\mathbf{r})\boldsymbol{\nabla}c^{(1)}(\mathbf{r}) \\ &= \varrho^{(1)}(\mathbf{r})\boldsymbol{\nabla}\frac{\delta\mathcal{F}_{\mathrm{int}}[\varrho^{(1)}]}{\delta\varrho^{(1)}(\mathbf{r})}\,. \end{aligned} \tag{2.39}$$

The key point of Eq. (2.39) is that the correlations between particle positions, described by $\varrho^{(2)}$, can be expressed with the one-particle density via the functional $\mathcal{F}_{\mathrm{int}}[\varrho]$.

2.3.2 DDFT equation

In the DDFT we close Eq. (2.28) in a way which incorporates the structure of the fluid. In particular, we approximate the non-equilibrium pair distribution function

$$g(\mathbf{r},\mathbf{r}',t) = \frac{\varrho^{(2)}(\mathbf{r},\mathbf{r}',t)}{\varrho^{(1)}(\mathbf{r})\,\varrho^{(1)}(\mathbf{r}',t)}\,. \tag{2.40}$$

We use the decades of effort that have been invested to construct the approximative functionals $\mathcal{F}_{\mathrm{int}}$ for the static DFT. It is assumed that $g(\mathbf{r},\mathbf{r}',t)$ approaches equilibrium faster than $\varrho^{(1)}(\mathbf{r},t)$. This corresponds to an *adiabatic approximation*. Further, we assume that the equilibrium functional $\mathcal{F}_{\mathrm{int}}$, evaluated at the non-equilibrium density, gives a reasonable approximation for the non-equilibrium correlations, so that we can use the sum rule Eq. (2.39) in non-equilibrium

$$\int \mathrm{d}\mathbf{r}'\varrho^{(1)}(\mathbf{r}',t)g(\mathbf{r},\mathbf{r}',t)\boldsymbol{\nabla}v_{\mathrm{int}}(\mathbf{r},\mathbf{r}') \approx \boldsymbol{\nabla}\frac{\delta\mathcal{F}_{\mathrm{int}}[\varrho^{(1)}]}{\delta\varrho^{(1)}(\mathbf{r},t)}\,. \tag{2.41}$$

With the decomposition of $\mathcal{F}[\varrho]$ in Eq. (2.32) we arrive at a compact equation for the time evolution of the one-particle density, the **DDFT key equation**

$$\partial_t\varrho^{(1)}(\mathbf{r},t) = \frac{D_0}{k_{\mathrm{B}}T}\boldsymbol{\nabla}\cdot\left(\varrho^{(1)}(\mathbf{r},t)\boldsymbol{\nabla}\frac{\delta\mathcal{F}[\varrho^{(1)}]}{\delta\varrho^{(1)}(\mathbf{r},t)}\right)\,. \tag{2.42}$$

The single-particle parts of the Helmholtz free energy functional are straightforward generalisations of Eqs. (2.30) and (2.31)

$$\mathcal{F}_{\mathrm{ent}}[\varrho] = k_{\mathrm{B}}T\int \mathrm{d}\mathbf{r}\;\varrho(\mathbf{r},t)[\ln(\Lambda^3\varrho(\mathbf{r},t)) - 1] \tag{2.43}$$

$$\mathcal{F}_{\mathrm{ext}}[\varrho] = \int \mathrm{d}\mathbf{r}\;\varrho(\mathbf{r},t)\,V_{\mathrm{ext}}(\mathbf{r},t)\,. \tag{2.44}$$

The only change is that the external potential is allowed to depend on time.

Capabilities and limits: The DDFT equation (2.42) is a generalised diffusion equation for the one-particle density $\varrho^{(1)}(\mathbf{r}, t)$. It provides a framework based on microscopic interactions for the theoretical description of many-particle systems. The focus lies on length scales of the size of one colloid to thousandfold that size. For larger systems often coarse-grained is employed to derive effective fluid dynamic continuum theories. An example is the Nernst-Planck-equation for the motion of ions in a solvent under the influence of an electric field [172]. In [266] a connection between static DFT and the macroscopic Frank-Oseen-theory is established. In [267] a continuous line is drawn from Langevin equations over Fokker-Planck equations and DDFT to known equations of fluid dynamics like the Euler equation and the Navier-Stokes equation.

The adiabatic approximation is a severe approximation concerning correlations in the fluid. If the change of positional correlations is dominating the behaviour, e.g. during single file diffusion, the DDFT equation will not be able to predict the motion correctly. This deviation was analysed quantitatively in [268]. However, time varying external fields can be treated as long as the correlations are not affected [269–273].

Reduction to one dimension In chapter 7, we solve the DDFT equation, Eq. (2.42), in one dimension

$$\partial_t \varrho(x,t) = \frac{D_0}{k_\mathrm{B}T}\partial_x \left(\varrho(x,t)\partial_x \frac{\delta \mathcal{F}[\varrho]}{\delta \varrho(x,t)} \right) . \tag{2.45}$$

The one-dimensional reduction of entropic and external part, Eqs. (2.30) and (2.31) respectively, read

$$\mathcal{F}_\mathrm{ent}[\varrho] = k_\mathrm{B}T \int \mathrm{d}x\, \varrho(x,t)[\ln(\Lambda\varrho(x,t)) - 1] \tag{2.46a}$$

$$\mathcal{F}_\mathrm{ext}[\varrho] = \int \mathrm{d}x\, \varrho(x,t)\, V_\mathrm{ext}(x,t)\,. \tag{2.46b}$$

2.3.3 Extensions

In the last decade numerous extensions to the DDFT have been proposed. Principally every shortcoming was addressed. We give a brief overview of the various methods. However, we do not use any of these approaches.

Hydrodynamic interactions In multi-particle systems with high density and high velocities the model of the solvent, which we employ here, i.e. isotropic friction and Gaussian white noise, may be too simple. Hydrodynamics interactions are the interactions between the colloids which are mediated by the solvent. Effects of hydrodynamic interactions on the motion of colloids have been reported [171, 271, 274–277]. Many of them treat the solvent as an incompressible liquid. There have been several proposals to incorporate hydrodynamic interactions into DDFT [259, 271, 278, 279]. Their role is minor in the scope of this thesis, because we discuss single particles in the chapters 3, 4, and 5 and soft particles in chapters 6 and 7. There might be an influence to the dynamics of chains of hard particles in chapters 6 and 7.

Flow and shear In situations where the flow of the solvent is not negligible, i.e. in microfluidic applications [280], extensions of Eq. (2.42) are necessary. A DDFT can then be formulated for a probability density in space and velocity [281]. By making the assumption that the velocities are locally (in space) equilibrated around a mean velocity an equation of motion for the probability density in space and a time and space dependent mean velocity can be derived [267]. In [279] deviations from the mean velocity are studied.

The derivation in [282] addresses the fact that motion with inertia can show waves. A DDFT with a second-order time derivative is developed which allows access to the speed of sound waves.

An important application of flow are sheared systems. There are a lot of dynamical phenomena which arise upon applying shear to a complex liquid, such as shear thinning [137], shear banding [57], structure formation or change [219, 283], and friction in general [284,285]. Understanding shear induced dynamical transitions opens the possibility to control the rheological behaviour of non-Newtonian fluids [22,46,50,228,286], e.g. the friction of thin colloidal films [90, 137, 287]. There are several proposals to incorporate shear into DDFT, reaching from phenomenological approaches to consistent extensions to the above discussed concepts [288–291].

Strongly correlated motion Systems whose dynamics is strongly correlated and where the correlations change with time cannot predict with DDFT. This was one of the first tests of DDFT [257]. Work in this direction [289,292] had to take the time evolution of higher order correlations functions into account. However, correlations are still hard to incorporate into a DDFT because of the lack of suitable non-equilibrium free energy functionals. There are ideas [278,293] how to use such a functional to describe the motion but to my knowledge there are no proposals for actual non-equilibrium free energy functionals. However, the deviations from the adiabatic approximation could be quantified [268].

Canonical vs. grand canonical In all DDFTs mentioned in this thesis, the particle number is conserved, and volume and temperature are fixed. Thus, these DDFTs operate in a canonical ensemble. On the contrary the Helmholtz free energy functionals which are developed in the static DFT are grand canonical functionals. A series expansion of a canonical ensemble average in terms of grand canonical averages is given in [294]. Interestingly, the correction terms decay quite fast with $\langle N\rangle^{-1}, \langle N\rangle^{-2}, \ldots$, such that the use of a grand canonical functional is good approximation.

2.3.4 Interaction functionals

Apart from the adiabatic approximation, often additional approximations are needed because the exact equilibrium interaction Helmholtz free energy functional $\mathcal{F}_{\text{int}}[\varrho]$ is known for very special cases, only. Nevertheless, even simple approximations can yield fairly good predictions in some situations.

Hard spheres in 1D If hard spheres are limited to move on a line, e.g. in a narrow channel [295], every particle corresponds to a segment of the line. For this special case the

equilibrium interaction functional is known [296]

$$\mathcal{F}_{\text{int}}^{\text{hs1D}}[\varrho] = -\frac{1}{2}\int \mathrm{d}x\, \ln(1-n[\varrho](x))\left(\varrho(x+\frac{\sigma}{2})+\varrho(x-\frac{\sigma}{2})\right) \tag{2.47a}$$

$$n[\varrho](x) = \int_{x-\sigma/2}^{x+\sigma/2} \mathrm{d}x'\, \varrho(x')\,. \tag{2.47b}$$

The quantity $n[\varrho](x)$ is called local packing fraction. To use Eq. (2.47) in the DDFT we need to calculate

$$\partial_x \frac{\delta \mathcal{F}_{\text{int}}^{\text{hs1D}}[\varrho]}{\delta\varrho(x)} = \frac{\varrho(x+\sigma)}{1-n[\varrho](x+\sigma/2)} - \frac{\varrho(x-\sigma)}{1-n[\varrho](x-\sigma/2)}\,. \tag{2.48}$$

See [297] for a derivation.

Fundamental measure theory Hard disks in 2D or hard spheres in 3D have a much more complex behaviour. Its description via functionals can be approximated with high quality with the fundamental measure theory [56, 298]. It is based on the fundamental geometric measures of a sphere, which are volume, surface area, mean radius of curvature, and Euler characteristic [56]. Considerable work was invested in the so called dimensional crossover: the reduction of 3D fundamental measure theory to 2D confinement should recover the 2D functional. Further reduction should yield Eq. (2.47) for 1D and a functional for the point cavity (zero dimensions) [56].

Mean-field A common approximation for soft interaction potentials is the mean-field (or random phase approximation) which approximates the direct pair correlation function, defined in Eq. (2.33b), by [299]

$$c^{(2)}(\mathbf{r},\mathbf{r}') = -\beta v_{\text{int}}(\mathbf{r},\mathbf{r}')\,. \tag{2.49}$$

However, colloidal interactions often are strongly repulsive at very short distances and have less strong repulsive or attractive interaction at larger distances [142, 300, 301]. To model the short ranged repulsion the colloids are usually considered as hard spheres, whereas the other interactions are often modelled with a mean-field approach [260, 284, 300, 302–304]. The interaction function incorporating this modelling into the DDFT reads

$$\mathcal{F}_{\text{int}}^{\text{MF}}[\varrho, v_{\text{int}}] = \frac{1}{2}\int \mathrm{d}\mathbf{r}\,\mathrm{d}\mathbf{r}'\, \varrho(\mathbf{r},t)\, v_{\text{int}}(\mathbf{r},\mathbf{r}')\, \varrho(\mathbf{r}',t)\,. \tag{2.50}$$

2.4 Correlations in space and time: The van Hove function

The van Hove correlation function [59, 305]

$$G(\mathbf{d},t) = \left\langle \frac{1}{N}\sum_{i=1}^{N}\sum_{j=1}^{N} \delta(\mathbf{d}-\mathbf{r}_j(t)+\mathbf{r}_i(0)) \right\rangle\,. \tag{2.51}$$

is the density of pairs of positions $(\mathbf{r}_i(t=0), \mathbf{r}_j(t))$ which have the distance $\mathbf{d} = \mathbf{r}_j(t) - \mathbf{r}_i(0)$, averaged over i, j, and the ensemble. The van Hove function is a generalisation of the pair distribution function $g(\mathbf{r})$ (defined by Eq. (2.35)) for time-dependent systems [305].

The sum over j in Eq. (2.51) can be decomposed into a diagonal part ($i = j$) which yields the so-called *self part of the van Hove function*

$$G_\mathrm{s}(\mathbf{r}, t) = \left\langle \frac{1}{N} \sum_{i=1}^{N} \delta(\mathbf{r} - \mathbf{r}_i(t) + \mathbf{r}_i(0)) \right\rangle , \tag{2.52a}$$

and the off-diagonal part ($i \neq j$) which yields the *distinct part of the van Hove function*

$$G_\mathrm{d}(\mathbf{r}, t) = \left\langle \frac{1}{N} \sum_{i=1}^{N} \sum_{j \neq i} \delta(\mathbf{r} - \mathbf{r}_j(t) + \mathbf{r}_i(0)) \right\rangle . \tag{2.52b}$$

The self part of the van Hove function is the probability density for the distance a particle travels on average during the time t. It can be used to calculate the mean squared displacement (MSD) [123] which is a very important quantity to describe diffusion. The standard definition of the MSD in transport is [10]

$$w(t) = \left\langle \frac{1}{N} \sum_{i=1}^{N} (\Delta \mathbf{r}_i(t))^2 \right\rangle \tag{2.53a}$$

$$\Delta \mathbf{r}_i(t) = \mathbf{r}_i(t) - \mathbf{r}_i(0) - \langle \mathbf{r} \rangle(t) + \langle \mathbf{r} \rangle(0) , \tag{2.53b}$$

where $\Delta \mathbf{r}_i(t)$ is the deviation of the distance that particle i travelled to the distance the whole system travelled. The MSD in terms of G_s reads

$$w(t) = \int \mathrm{d}\mathbf{r}\, G_\mathrm{s}(\mathbf{r}, t) \left(\mathbf{r} - \int \mathrm{d}\mathbf{r}'\, \mathbf{r}'\, G_\mathrm{s}(\mathbf{r}', t) \right)^2 , \tag{2.54}$$

where the subtraction of the first moment of G_s, $\int \mathrm{d}\mathbf{r}\, \mathbf{r}\, G_\mathrm{s}(\mathbf{r}, t) = \langle \mathbf{r} \rangle(t) - \langle \mathbf{r} \rangle(0)$, accounts for the mean displacement of the whole system in the time interval $[0, t]$.

A further important derived quantity is the (second) non-Gaussian parameter

$$\alpha(t) = \frac{\langle \Delta \mathbf{r}_i(t)^4 \rangle}{(1 + 2/\mathcal{D}) \langle \Delta \mathbf{r}_i(t)^2 \rangle^2} - 1 = \frac{\int \mathrm{d}\mathbf{r}\, G_\mathrm{s}(\mathbf{r}, t)\, (\mathbf{r} - \int \mathrm{d}\mathbf{r}' \mathbf{r}' G_\mathrm{s}(\mathbf{r}', t))^4}{(1 + 2/\mathcal{D}) w(t)^2} - 1 , \tag{2.55a}$$

where the number of spatial dimensions is denoted by $\mathcal{D}$. Equation (2.55a) is an advection-corrected version of previous definitions [119, 306]. Note that α is closely related to the kurtosis $\kappa = 3\alpha$ of $G_\mathrm{s}(\mathbf{r}, t)$.

Initial values The values of the parts of the van Hove function at $t = 0$ read [59, 307]

$$G_\mathrm{s}(\mathbf{r}, 0) = \delta(\mathbf{r}) \tag{2.56a}$$

$$G_\mathrm{d}(\mathbf{r}, 0) = \frac{1}{N} \int \mathrm{d}\mathbf{r}'\, \varrho^{(2)}(\mathbf{r}', \mathbf{r}' + \mathbf{r}) . \tag{2.56b}$$

The connection to the pair distribution function becomes clear if the system is initially homogeneous, and the correlations only depend on distance, i.e. $\varrho^{(1)}(\mathbf{r}, t = 0) = \text{const}$ and $\varrho^{(2)}(\mathbf{r}, \mathbf{r}', t = 0) = (\varrho^{(1)})^2 g(\mathbf{r}' - \mathbf{r})$. Then, it follows from Eq. (2.56b), that

$$G_\mathrm{d}(\mathbf{r}, 0) = \varrho^{(1)}\, g(\mathbf{r}) . \tag{2.57}$$

2.4.1 Test particle method

The static test particle limit in a homogeneous system means to place a fixed particle, a *test particle*, at a certain position, say $\mathbf{r}_0$, and to calculate the one-particle density of the other particles $\varrho^{(1)}(\mathbf{r}|\mathbf{r}_0)$ [123,307]. The notation $\varrho^{(1)}(\mathbf{r}|\mathbf{r}_0)$ means that we consider the one-particle density under the condition that there is a particle at $\mathbf{r}_0$. The potential landscape of the other particles then consists of interactions among them and the interaction with the test particle. Because the interaction with the test particle is constant, the conditional density $\varrho^{(1)}(\mathbf{r}|\mathbf{r}_0)$ is equal to the non-conditioned density $\varrho^{(1)}_{\text{eff}}(\mathbf{r})$ of $N-1$ particles in an external potential $v_{\text{int}}(\mathbf{r}-\mathbf{r}_0)$ where v_{int} is the pair interaction potential [307]. By expressing the conditional density by the joint probability $\varrho^{(2)}$ a connection between $\varrho^{(1)}_{\text{eff}}$ and the pair distribution function g can be drawn

$$\varrho^{(1)}_{\text{eff}}(\mathbf{r}) = \varrho^{(1)}(\mathbf{r}|\mathbf{r}_0) = \varrho^{(2)}(\mathbf{r},\mathbf{r}_0)/\varrho^{(1)} = g(\mathbf{r},\mathbf{r}_0)/\varrho^{(1)}\,, \tag{2.58}$$

where we used Eq. (2.35).

For the dynamic, inhomogeneous case the method was adapted [123]. A system of N interacting particles is separated in one test particle and the rest. To make a connection with a conditional density, we make a identical transformation of Eq. (2.51)

$$G(\mathbf{d},t) = \int \mathrm{d}\mathbf{r}' \frac{1}{N} \left\langle \sum_{ij} \delta(\mathbf{r}' - \mathbf{r}_i(0))\, \delta(\mathbf{d} + \mathbf{r}' - \mathbf{r}_j(t)) \right\rangle , \tag{2.59}$$

which clearly shows the property of the van Hove function to average over the initial configurations. The quantity enclosed by angle brackets is a correlation function. Due to its similarity to the two-particle density $\varrho^{(2)}$, Eq. (2.24b), we call it *two-particle correlation function*

$$\nu(\mathbf{r},t,\mathbf{r}',t') = \left\langle \sum_{ij} \delta(\mathbf{r} - \mathbf{r}_j(t))\delta(\mathbf{r}' - \mathbf{r}_i(t')) \right\rangle . \tag{2.60}$$

With the test particle method we can calculate the conditional density ϱ^c to find a particle at position $\mathbf{r}$ at time t given that there was a particle at position $\mathbf{r}'$ at time t'

$$\varrho^c(\mathbf{r},t|\mathbf{r}',t') = \left\langle \sum_{i=1}^{N} \delta(\mathbf{r} - \mathbf{r}_i(t)) \right\rangle_{R(\mathbf{r}',t')} . \tag{2.61}$$

The subscript at the angle bracket denotes that this average uses a restricted ensemble. The ensemble contains the configurations that fulfil the restriction $R(\mathbf{r}',t')$ that they had a particle at $\mathbf{r}'$ at time t'. By using $p_R(\mathbf{r}_1(t'),\ldots,\mathbf{r}_N(t'),\mathbf{r}')$ which denotes the probability density to choose a valid configuration from all configurations, we can write Eq. (2.61) with an unrestricted ensemble average

$$\varrho^c(\mathbf{r},t|\mathbf{r}',t') = \langle p_R(\mathbf{r}_1(t'),\ldots,\mathbf{r}_N(t'),\mathbf{r}') \sum_{i=1}^{N} \delta(\mathbf{r} - \mathbf{r}_i(t)) \rangle\,. \tag{2.62}$$

The probability p_R is zero for all $\mathbf{r}' \notin \{\mathbf{r}_1(t), \ldots, \mathbf{r}_N(t)\}$, which are almost all $\mathbf{r}'$. Hence, p_R consists of δ-peaks

$$p_R(\mathbf{r}_1(t'), \ldots, \mathbf{r}_N(t'), \mathbf{r}', t') = c \sum_{i=1}^{N} \delta(\mathbf{r}' - \mathbf{r}_i(t')) \,, \tag{2.63}$$

where a, still unknown, normalisation constant c was inserted. To find the normalisation, we recall that there are N particles in the system

$$\begin{aligned} N &= \int \mathrm{d}\mathbf{r}\, \varrho^c(\mathbf{r}, t|\mathbf{r}', t') = \left\langle \int \mathrm{d}\mathbf{r} \sum_{i=1}^{N} \delta(\mathbf{r} - \mathbf{r}_i(t))\, p_R(\mathbf{r}_1(t'), \ldots, \mathbf{r}_N(t'), \mathbf{r}') \right\rangle \\ &= N \langle p_R(\mathbf{r}_1(t'), \ldots, \mathbf{r}_N(t'), \mathbf{r}') \rangle \,. \end{aligned} \tag{2.64}$$

By comparing with Eq. (2.24a) we recognise the one-particle density in the structure of p_R, yielding $c = 1/\varrho^{(1)}(\mathbf{r}', t')$ and

$$\varrho^c(\mathbf{r}, t|\mathbf{r}', t') = \left\langle \sum_{i=1}^{N} \delta(\mathbf{r} - \mathbf{r}_i(t)) \frac{1}{\varrho^{(1)}(\mathbf{r}', t')} \sum_{j=1}^{N} \delta(\mathbf{r}' - \mathbf{r}_j(t')) \right\rangle \tag{2.65}$$

From Eq. (2.65) we can draw an analogy to the relation between conditional probabilities and their corresponding joint probabilities, i.e. $p_{\mathrm{cond}}(x|y) = p_{\mathrm{joint}}(x, y)/p(y)$. The corresponding joint density to ϱ^c is the two-particle correlation function (defined in Eq. (2.60))

$$\varrho^c(\mathbf{r}, t|\mathbf{r}', t') = \frac{\nu(\mathbf{r}, t, \mathbf{r}', t')}{\varrho^{(1)}(\mathbf{r}', t')} \,. \tag{2.66}$$

The van Hove function can be related to the conditional density through Eq. (2.59)

$$G(\mathbf{d}, t) = \int \mathrm{d}\mathbf{r}' \frac{1}{N} \varrho^c(\mathbf{r}' + \mathbf{d}, t|\mathbf{r}', 0) \varrho^{(1)}(\mathbf{r}', 0) \,. \tag{2.67}$$

The same relation was given in [139]. The self and distinct part read

$$G_{\mathrm{s/d}}(\mathbf{d}, t) = \int \mathrm{d}\mathbf{r}' \frac{1}{N}\, \varrho^c_{\mathrm{s/d}}(\mathbf{r}' + \mathbf{d}, t|\mathbf{r}', 0)\, \varrho^{(1)}(\mathbf{r}', 0) \,, \tag{2.68}$$

where the conditional density ϱ^c_{s} is the probability density to find the test particle and ϱ^c_{d} is the density of the other particles, i.e.

$$\varrho^c_{\mathrm{s}}(\mathbf{r}, t|\mathbf{r}', t') = \left\langle \sum_{i=1}^{N} \delta(\mathbf{r} - \mathbf{r}_i(t)) \frac{1}{\varrho^{(1)}(\mathbf{r}', t')} \delta(\mathbf{r}' - \mathbf{r}_i(t')) \right\rangle \tag{2.69a}$$

$$\varrho^c_{\mathrm{d}}(\mathbf{r}, t|\mathbf{r}', t') = \left\langle \sum_{i=1}^{N} \delta(\mathbf{r} - \mathbf{r}_i(t)) \frac{1}{\varrho^{(1)}(\mathbf{r}', t')} \sum_{j \neq i} \delta(\mathbf{r}' - \mathbf{r}_j(t')) \right\rangle . \tag{2.69b}$$

2.4.2 DDFT-based test particle method

We now concentrate on a equation of motion for the conditional densities $\varrho_{\mathrm{s/d}}(\mathbf{r}, t|\mathbf{r}', t')$. The idea of [123] was to treat the time evolution of the N particles as a mixture of two species. The species s (self) consists of the test particle and the species d (distinct) consists of the other $N-1$ particles. We write down an extended SE for every species

$$\partial_t \varrho_\alpha(\mathbf{r}, t) = D_0 \boldsymbol{\nabla}^2 \varrho_\alpha + \boldsymbol{\nabla} \cdot (\varrho_\alpha \boldsymbol{\nabla}(V_{\mathrm{ext}} + V_{\mathrm{int}}^\alpha))/\gamma \,, \tag{2.70}$$

where $\alpha \in \{\mathrm{s}, \mathrm{d}\}$. The effective interaction potential experienced by species α is denoted by V_{int}^α. The modelling of the interactions (following [123]) is that the test particle interacts with the other particles and the other particles interact with the test particle and with each other. In the framework of DDFT the effective potentials are derived from a Helmholtz free energy functional, i.e.

$$V_{\mathrm{int}}^\alpha(\mathbf{r}, t) = \frac{\delta \mathcal{F}_{\mathrm{int}}^{\mathrm{TPM}}[\varrho_{\mathrm{s}}, \varrho_{\mathrm{d}}]}{\delta \varrho_\alpha(\mathbf{r}, t)} \,. \tag{2.71}$$

Archer et al. [123] propose the functional

$$\mathcal{F}_{\mathrm{int}}^{\mathrm{TPM,2nd}}[\varrho_{\mathrm{s}}, \varrho_{\mathrm{d}}] = \frac{1}{2} \sum_{\alpha,\alpha' \in \{\mathrm{s,d}\}} \int \mathrm{d}\mathbf{r}\, \mathrm{d}\mathbf{r}'\, \varrho_\alpha(\mathbf{r}, t) \varrho_{\alpha'}(\mathbf{r}', t)\, (-k_{\mathrm{B}}T) c_{\alpha\alpha'}^{(2)}(\mathbf{r}, \mathbf{r}') \,. \tag{2.72}$$

The direct correlation functions $c_{\alpha\alpha'}^{(2)}(\mathbf{r}, \mathbf{r}')$ are set to

$$c_{\mathrm{ss}}^{(2)} = 0 \tag{2.73a}$$

$$c_{\mathrm{sd}}^{(2)} = c_{\mathrm{dd}}^{(2)} = c_{\mathrm{ds}}^{(2)} = c^{(2)} \,, \tag{2.73b}$$

where $c^{(2)}(\mathbf{r}, \mathbf{r}')$ is the usual single species direct correlation function. Equation (2.73) means that the test particle does not interact with itself and that all other interactions are identical.

The dynamic test particle method was demonstrated [123] using a mean-field approximation, i.e. $c^{(2)} = -\beta v_{\mathrm{int}}$, whereas later uses [139, 308] employ more elaborate direct correlation functions.

2.4.3 Beyond second order

With Eq. (2.47) an exact free energy functional for hard particles in one dimension exists. It seems crude to use a second order approximation for the test particle method while we use the full functional for normal DDFT calculations. Moreover, the second derivative, in the inhomogeneous case, is quite complex

$$\begin{aligned} c^{(2)}(x, x') = \Theta(x' - x + \sigma)\Theta(x - x' + \sigma) \frac{1}{2} \left(\frac{1}{1 - n[\varrho](x - \sigma/2)} + \frac{1}{1 - n[\varrho](x + \sigma/2)} \right) \\ - \frac{1}{2} \int_{\max(x,x')-\sigma/2}^{\min(x,x')+\sigma/2} \mathrm{d}\tilde{x}\, \frac{\varrho(\tilde{x} + \sigma/2) + \varrho(\tilde{x} - \sigma/2)}{(1 - n[\varrho](\tilde{x}))^2} \,. \end{aligned} \tag{2.74}$$

The Heaviside step function is denoted by $\Theta(x)$.

Instead of the second order approach, Eq. (2.72), we make a generalising subtraction approach

$$\mathcal{F}_{\text{int}}^{\text{TPM,sub}}[\varrho_s, \varrho_d] = \mathcal{F}_{\text{int}}[\varrho_s + \varrho_d] - \mathcal{F}_{\text{int}}[\varrho_s]\,, \tag{2.75}$$

where $\mathcal{F}_{\text{int}}$ is the usual interaction functional, e.g. Eq. (2.47). Note that Eq. (2.75) automatically reduces to the established second order approach if the functionals are expanded to second order. A separate fixing like Eq. (2.73) is not necessary, because of the differentiation property

$$\frac{\delta A[e+f]}{\delta e(\mathbf{r})} = \frac{\delta A[g]}{\delta g(\mathbf{r})}\,, \tag{2.76}$$

where A is a functional and e, f, and $g = e + f$ are functions. The derivatives of $\mathcal{F}_{\text{int}}[\varrho_s + \varrho_d]$ all yield the same correlation functions and the test particle self interaction $\delta\mathcal{F}_{\text{int}}[\varrho_\text{s}]/\delta\varrho_\text{s}$ cancels out. In chapter 6 we use this approach with the functional for hard particles in one dimension.

2.5 Stochastic thermodynamics

The Langevin equation (2.6) contains all information about the motion of the Brownian particles but it does not quantify their interaction with the heat bath. Generalisations of equilibrium thermodynamic relations were worked out in the last decades [53,55,244,310–312]. The first central question is how much work is applied to the Brownian particle and which fraction is dissipated as heat. This is answered by the first law of stochastic thermodynamics.

There is a diversity of Brownian machines [7, 9, 195]. All these machines work in non-equilibrium and hence produce entropy. The second central question is which machine works most efficient. This is tied to the second law.

2.5.1 Trajectory based quantities

We adopt the formulation of stochastic thermodynamics from Seifert [55]. It is instructive to start with the Langevin equation (2.7) for a single particle in one dimension. We stick to the equilibrium thermodynamics rule

$$\underset{\text{work applied to particle}}{\mathrm{d}w} = \underset{\text{change of internal energy}}{\mathrm{d}E} + \underset{\text{dissipated heat}}{\mathrm{d}q}\,. \tag{2.77}$$

In equilibrium no work is applied, i.e. $\mathrm{d}w = 0$. Further, the deterministic force in Eq. (2.7) must have a potential $V(x)$. If the particle changes its position, the internal energy changes by $\mathrm{d}E = \partial_x V \mathrm{d}x$ and a heat $\mathrm{d}q = -\mathrm{d}E = -\partial_x V \mathrm{d}x$ is dissipated ($\mathrm{d}q > 0$) or absorbed ($\mathrm{d}q < 0$). Out of equilibrium there may be an additional external non-conservative force $f_{\text{nc}}(x,t)$ or a time-dependent potential $V(x,t)$ (or both). The internal energy changes if the particle moves in the potential and if the potential itself changes

$$\mathrm{d}E = \partial_x V \mathrm{d}x + \partial_t V \mathrm{d}t\,. \tag{2.78}$$

Heat is dissipated if the particle moves, because friction is the dissipative element in our system

$$\mathrm{d}q = f\mathrm{d}x\,. \tag{2.79}$$

Solving Eq. (2.77) results in an expression for the exerted work

$$\mathrm{d}w = (f + \partial_x V)\mathrm{d}x + \partial_t V\mathrm{d}t = f_{\mathrm{nc}}\mathrm{d}x + \partial_t V\mathrm{d}t\,. \tag{2.80}$$

With the Langevin equation (2.7) the changes can be written time-dependent

$$\mathrm{d}E = \partial_x V\dot{x}\mathrm{d}t + \partial_t V\mathrm{d}t \tag{2.81}$$
$$\mathrm{d}w = f_{\mathrm{nc}}\dot{x}\mathrm{d}t + \partial_t V\mathrm{d}t \tag{2.82}$$
$$\mathrm{d}q = f\dot{x}\mathrm{d}t\,. \tag{2.83}$$

The changes involve products of noisy quantities. We follow [55] and use the Stratonovich interpretation [154]. Integrating Eqs. (2.81)-(2.83) with respect to time yields

$$\begin{aligned} E[x(t)] &= \int_0^t \mathrm{d}t'(\partial_x V(x(t'),t')\dot{x}(t') + \partial_{t'}V(x(t'),t')) = \int_0^t \mathrm{d}V(x(t'),t') \\ &= V(x(t),t) - V(x(0),0) \end{aligned} \tag{2.84}$$
$$w[x(t)] = \int_0^t \mathrm{d}t'(f_{\mathrm{nc}}(x(t'),t')\dot{x}(t') + \partial_{t'}V(x(t'),t')) \tag{2.85}$$
$$q[x(t)] = \int_0^t \mathrm{d}t'\, f(x(t'),t')\,\dot{x}(t')\,. \tag{2.86}$$

This corresponds to a very familiar first law on the level of trajectories

$$w[x(t)] = \Delta V + q[x(t)]\,. \tag{2.87}$$

The definition of entropy is similar. The entropy of the solvent is enlarged if heat is dissipated in it. In Ref. [55], this entropy is called the entropy change of the medium

$$\Delta s^{\mathrm{m}}[x(t)] = q[x(t)]/T\,. \tag{2.88}$$

The system entropy

$$s^{\mathrm{sys}}(t) = -\ln p(x(t),t)\,. \tag{2.89}$$

quantifies to which extent the particle position deviates from the average. This entropy connects trajectory dependent information, the particle position $x(t)$, with ensemble averaged information, the probability density $p(x,t)$.

The deep relation between dissipation and time manifests in the various fluctuation theorems involving time-reversed trajectories $x^\dagger(t) = x(t_e - t)$ [55] where t_e is a chosen end time.

2.5.2 Ensemble averages

The equations for $\dot{q}(x(t))$, $\dot{w}(x(t))$, and $\dot{s}^{\mathrm{m}}(x(t))$ contain products of functions of $x(t)$ and the velocity $\dot{x}(t)$. To calculate their ensemble averages, we first calculate the general average involving an arbitrary function $a(x,t)$

$$\begin{aligned}\langle a(x(t),t)\dot{x}(t)\rangle &= \int \mathrm{d}x \langle \delta(x(t)-x) a(x(t),t)\dot{x}(t) = \int \mathrm{d}x\, a(x,t)\langle \delta(x(t)-x)\dot{x}(t)\rangle \\ &= \int \mathrm{d}x\, a(x,t)\, j(x,t)\,, \end{aligned} \tag{2.90}$$

where we used the common expression for the probability current [9, 59]

$$j(x,t) = \langle \dot{x}(t)\, \delta(x(t)-x)\rangle\,. \tag{2.91}$$

In [55] Seifert insinuates that this reasoning is loose and that the relation (2.90) should be derived via a path integral formulation explicitly evaluating the Stratonovich interpretation. However, using Eq. (2.90) yields

$$W(t) = \langle w[x(t)]\rangle = \int \mathrm{d}t' \left(\int \mathrm{d}x f_{\mathrm{nc}}(x,t') j(x,t) + \int \mathrm{d}x\, p(x,t')\partial_{t'} V(x,t') \right) \tag{2.92a}$$

$$Q(t) = \langle q[x(t)]\rangle = \int \mathrm{d}t'\, \mathrm{d}x\, f(x,t')\, j(x,t') \tag{2.92b}$$

$$\Delta S^{\mathrm{m}}(t) = \langle s^{\mathrm{m}}[x(t)]\rangle = Q(t)/T \tag{2.92c}$$

$$S^{\mathrm{sys}}(t) = \langle s^{\mathrm{sys}}(t)\rangle = -\int \mathrm{d}x\, p(x,t)\, \ln(p(x,t))\,. \tag{2.92d}$$

Of particular interest is the total entropy production

$$\partial_t S^{\mathrm{tot}} = \dot{S}^{\mathrm{m}} + \dot{S}^{\mathrm{sys}}\,. \tag{2.93}$$

The time derivatives $\partial_t p$ appearing in the term $\dot{S}^{\mathrm{sys}}$ are replaced by the continuity equation (2.11). Partial integration is performed where the boundary term vanishes either on natural (p is zero at the boundary) or periodic boundary conditions. The second law then reads

$$\dot{S}^{\mathrm{tot}} = \int \mathrm{d}x \frac{(j(x,t))^2}{D_0\, p(x,t)} \geq 0\,. \tag{2.94}$$

In chapter 5 we compare the entropy production and the applied work for different ratchets.

2.6 Numerical methods

Four different one-dimensional equations are solved in this thesis. Three of them are partial differential equations (PDE), the Smoluchowski equation (2.13), the DDFT equation (2.45), and the test particle method, Eqs. (2.70) and (2.67). Further, the single-particle Langevin equation (2.7) is solved with a Brownian dynamics simulation.

The PDEs are solved with forward-time-centred-space (FTCS), a finite difference method explained in the following section. The DDFT equation and the test particle method are non-local PDE because the interaction term yields an integral term. The efficient calculation of this integrals is essential and described in Sec. 2.6.2.

2.6.1 Finite difference method

All PDEs have the structure

$$\partial_t \varrho(x,t) = \partial_{xx}\varrho(x,t) - \partial_x(\varrho(x,t)\, f(\varrho,x,t))\,, \tag{2.95}$$

where a transformation to dimensionless quantities has already been performed.

Time and space are discretised with constant steps

$$t_n = n\,\Delta t \quad ; \quad x_i = x_{\min} + i\,\Delta x\,. \tag{2.96}$$

Simplest central finite difference derivative discretisation rules [313] lead to the calculation scheme

$$\begin{aligned}\varrho(x_i,t_{n+1}) =& \varrho(x_i,t_n) + \frac{\Delta t}{\Delta x^2}(\varrho(x_{i+1},t_n) - 2\varrho(x_i,t_n) + \varrho(x_{t-1},t_n)) \\ &- \frac{\Delta t}{2\Delta x}(\varrho(x_{i+1},t_n)f(x_{i+1},t_n) - \varrho(x_{i-1},t_n)f(x_{i-1},t_n))\,.\end{aligned} \tag{2.97}$$

Note that the force term is the discretised form of $\partial_x(\varrho f)$ and not of $f\partial_x\varrho + \varrho\partial_x f$. The latter form contains an advective term [1] which cannot be treated with a central space scheme.

To set the discretisation, we employ the Courant criterion [313] $\Delta t\,\Delta x^{-2} \leq 1$ which yields a neutrally stable FTCS scheme. For the non-linear equations the Courant criterion is not exact. We adjust Δt manually if $\Delta t = 0.25\Delta x^{-2}$ fails. The space discretisation must be chosen small enough to sample the spatial variations of the force $f(x,t)$.

Solving via scheme (2.97) was neither a time-critical nor an accuracy issue. Hence, implicit schemes were not taken into account.

2.6.2 Efficient calculation of convolution integrals in Fourier space

The integrals appearing in the interaction parts of Eqs. (2.45) and (2.70) are convolutions. We exploit this special feature by carrying them out in Fourier space to gain speed from the fast Fourier transform. This technique was essential for acquiring numerical results. This is applied to the integrals $n[\varrho](x)$, Eq. (2.47b), and the mean force, $-\partial_x\delta\mathcal{F}^{\mathrm{MF}}[\varrho]/\delta\varrho(x)$, Eq. (2.50). The general form of convolution is

$$a(x,t) = \int \mathrm{d}x'\, b(x',t)\, c(x-x')\,, \tag{2.98}$$

which in Fourier space reads

$$\tilde{a}(k,t) = \sqrt{2\pi}\,\tilde{b}(k,t)\,\tilde{c}(k) \tag{2.99}$$

$$\tilde{a}(k,t) = \frac{1}{\sqrt{2\pi}}\int \mathrm{d}x\, a(x,t)\, e^{-ikx}\,. \tag{2.100}$$

The Fourier transform is defined by Eq. (2.100). By using the fast Fourier transform (in particular the library FFTW [314, 315]), we reduce the computational effort from $O(N_x^2)$ to $O(N_x \log N_x)$ where N_x is the number of spatial discretisation points.

[1] Thanks to Alexander Kraft for pointing this out.

2.6.3 Moving frame

In chapters 3, 6, 7 we simulate transport. The distance the particles travel is in many cases larger than the space they explore through diffusion. The numerical treatment of such a large space was not possible. We therefore adjusted $x_{\min}$ (cf. Eq. (2.96)) to $\langle x\rangle - N_x\Delta x/2$ every $t_{\mathrm{MF}} = 0.1\tau_{\mathrm{B}}$ keeping N_x and Δx constant. The density values $\varrho(x < x_{\min}(t))$ are reinterpreted as $\varrho(x+N_x\Delta x-\Delta x_{\min})$ where $\Delta x_{\min} = x_{\min}(t+t_{\mathrm{MF}})-x_{\min}(t)$. This reinterpretation "moves" a particle which is at $x < x_{\min}$ by a distance $N_x\Delta x - \Delta x_{\min}$ with the probability

$$m_{\mathrm{MF}} = \int_{x_{\min}(t)}^{x_{\min}(t+t_{\mathrm{MF}})} \mathrm{d}x\,\varrho(x,t)\,. \tag{2.101}$$

This spurious particle current must be made negligible whenever the current is the relevant variable. This is assured by choosing N_x large.

2.6.4 Fourier-mode eigendecomposition of the Smoluchowski equation

The Smoluchowski equation (2.13) is linear in $p(x,t)$. Via Fourier transform (2.100) the differential time propagation operator of Eq. (2.13) can be transformed into an integral propagator

$$\partial_t\tilde{p}(k,t) = -D_0k^2\tilde{p}(k,t) - D_0\beta ik\int\frac{\mathrm{d}k'}{\sqrt{2\pi}}\,\tilde{f}(k-k',t)\tilde{p}(k',t) \tag{2.102a}$$

$$= \int \mathrm{d}k'\,a(k,k')\,\tilde{p}(k',t)\,, \tag{2.102b}$$

with the kernel $a(k,k')$. Discretisation into a finite number of modes approximates the integral operator by a matrix-vector product

$$\partial_t\tilde{\mathbf{p}}(t) = A\cdot\tilde{\mathbf{p}}(t)\,, \tag{2.103}$$

where $\tilde{\mathbf{p}}$ is the vector of the chosen Fourier components of $p(k,t)$ and A is the matrix representing the integral in Eq. (2.102b). The solution of Eq. (2.103) can be formulated with the matrix exponential

$$\tilde{\mathbf{p}}(t) = e^{At}\tilde{\mathbf{p}}(0)\,. \tag{2.104}$$

If the matrix A can be diagonalised to $A = S\cdot D\cdot S^{-1}$ the solution can be reduced to simple matrix products

$$\tilde{\mathbf{p}}(t) = S\cdot e^{Dt}\cdot S^{-1}\cdot\tilde{\mathbf{p}}\,, \tag{2.105}$$

where D is a diagonal matrix with the eigenvalues of A on the diagonal and S contains the corresponding eigenvectors column by column. We use this method in chapter 4, where A is diagonalisable.

2.6.5 Brownian dynamics simulation

In chapters 4 and 5, we solve a single-particle overdamped Langevin equation (2.7) with the Euler-Maruyama scheme [248, 316] using a Mersenne Twister random number generator [317].

3. SHORT TIME DIFFUSION OF A SINGLE PARTICLE

Apart from the presentation of the results of the model we worked out with Clive Emary, published in Phys. Rev. E **86**, 061135 (2012) [318], this chapter serves as a introduction into the dynamics of a particle in a one-dimensional periodic potential. The following chapter *Waiting time distribution* provides complementary insights. Together they compose a knowledge base about a single Brownian particle in a washboard potential.

Transport in tilted washboard potentials was first addressed in the long time limit. The mean particle velocity, the most important transport property in a system with constant directed drive, was calculated analytically by Stratonovich [150, 152] already half a century ago. Also for the diffusion coefficient an analytic expression was found a decade ago [125,185]. This completed the research on the long time behaviour for a normally diffusing particle. For a particle which experiences anomalous diffusion where the mean squared displacement growths slower or faster than linear with time (called subdiffusive or superdiffusive, respectively) transport properties became in principle accessible in the past decade [132, 162, 251, 319]. However, the actual equations are much more complicated than for normal diffusion.

In recent years the short-time behaviour of overdamped Brownian particles in a modulated potential became a topic of intense theoretical [119, 147, 254, 277, 320, 321] and experimental [82, 83, 87, 322] investigation. This was driven from research on glasses [120, 323] and, more generally, on systems where the dynamics is hindered by an energetic or entropic barrier. The link between glasses and one-dimensional washboard potentials is drawn by the average view the particle has on its cage formed by neighbouring particles [119]. These hindering, also called kinetic arrest [117], is usually characterised by the mean squared displacement (MSD) in dependence of time which shows a common feature throughout the applications and for the single particle in a washboard potential. In the latter the MSD growths linearly with time initially until the particle reaches a barrier. During the time in which the particle overcomes the barrier the MSD grows slower. If this subdiffusive regime is pronounced it is called plateau. Diffusive behaviour is recovered for long times. These MSD plateaus occur in many-particle systems e.g. in glasses [5, 116, 119, 136, 141, 324], in optical traps [161] and other structured light fields [82, 83], in the formation of a biochemical bond [325], in chains of dipolar particles [138, 142, 326], and in colloidal gels [35].

The analytic accessibility for the long time transport properties had no counterpart for the short time behaviour. This gap was known and phenomenological approaches were given [82, 119]. Albeit the quality of the estimates of these approaches a comprehensive theory which allows analytic results was missing. In [318] we filled this gap with a space discretised model, described by a master equation. Discretisation of diffusion processes is very common in the framework of continuous time random walk models [129, 164, 327]. Note that there is

a deep relation between continuous time random walk and Master equations [328, 329].

Our master equation model is based on assigning two discrete positions per well where the particles may reside. The dynamics is given by prescribing probability rates between the positions based on the knowledge on long time properties and a short time expansions of the Smoluchowski equation. We use numeric solutions of the Smoluchowski equation to check the accuracy of our proposed rate equation model.

The relevant quantities for the investigation of the short-time behaviour are introduced in Sec. 3.1. In Sec. 3.2 the master equation model is introduced on an abstract level. We connect the model to actual predictions in Sec. 3.3, where we specify rates, and in Sec. 3.4, where we address relevant limit cases. The comparison of the predictions of the rate equation model with the numerical solution of the Smoluchowski equation is shown in Sec. 3.5.

Clive Emary developed the Master equation model and carried out the corresponding calculations. My contribution to the rates is the short time expansion of the SE. Further, I carried out the solutions of the SE. Most of the text in our publication [318] was written by Clive Emary. Much of the text in this chapter I literally copied from [318]. Hence, a couple of paragraphs in this chapter are Clive Emary's work. Based on [318], I review the model definition and derivation and give intermediate steps not mentioned in the paper.

3.1 Characterisation of short-time diffusion

We consider the overdamped Brownian motion of a particle in the tilted sinusoidal washboard potential $u(x)$, Eq. (1.11), (see Sec. 1.5.1). We focus on the case where the potential has deep wells which occurs at $\Delta u \gg k_\mathrm{B}T$ and $F < F_c$ (cf. Eq. (1.13)). The time evolution of the probability density $p(x,t)$ is given by the SE

$$\partial_t p(x,t) = D_0 \partial_{xx} p(x,t) + \frac{D_0}{k_\mathrm{B}T} \partial_x (p(x,t) u'(x)) \,, \tag{3.1}$$

which is Eq. (2.13) with the force $f(x,t) = -u'(x)$. We assume that the particle's initial position is known to be x_0, yielding the initial condition

$$p(x,0) = \delta(x - x_0) \,. \tag{3.2}$$

To characterise the transport we use mean particle position $\langle x \rangle$ and mean squared displacement

$$w(t) = \langle (x - \langle x \rangle)^2 \rangle \,, \tag{3.3}$$

which are the first two cumulants of position. Higher order cumulants are important for glassy [116, 119] and gel-forming [144, 326] systems. The (second) non-Gaussian parameter α, which is connected to the fourth cumulant, quantifies the deviation of $p(x,t)$ from a Gaussian distribution. We use the advection-corrected version, Eq. (2.55), because our system is driven. For a single particle whose initial position is known it reads

$$\alpha(t) = \frac{\langle (x - \langle x \rangle)^4 \rangle}{3 w(t)^2} - 1 \,. \tag{3.4}$$

In Eq. (3.4) no correlation function is involved and α is proportional to the kurtosis $\kappa(t) = 3\alpha(t)$ of the probability density.

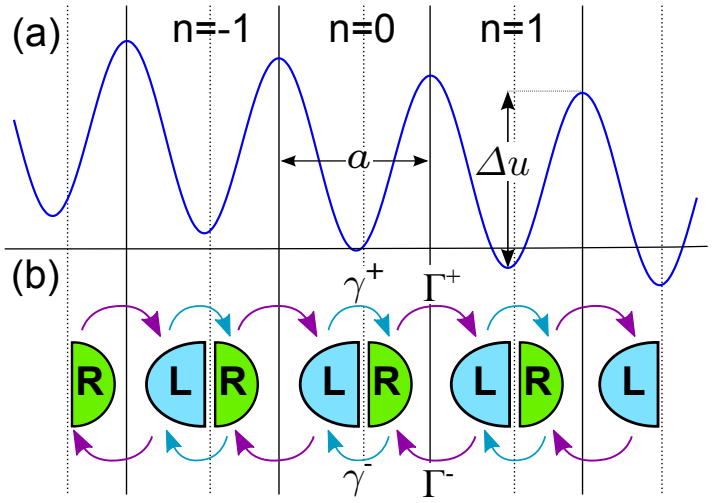

Fig. 3.1: (a) Tilted washboard potential with numbered valleys. (b) Visualisation of the two state per well (2S/W) model with transition rates $\gamma^{\pm}, \Gamma^{\pm}$. The (large) intra-well rates $\gamma^{\pm}$ model transition between the internal states L and R. The (small) inter-well rates $\Gamma^{\pm}$ model barrier crossing. Reprinted from [318].

3.2 Two-state-per-well model

Clive Emary's idea was to model the SE for the probability density defined as a function of continuous variable x with a simpler model involving probabilities for finding the particle in one of a set of discrete states, defined by regions of the x axis. The most obvious approach of this type would be to associate one state with each well of the potential and write down a rate-equation for the probability $p^{(n)}(t)$ of finding the particle in well n at time t. This one-state-per-well approach is discussed in the appendix of our paper [318]. All position cumulants are linear in time for all times. Such a simple rate equation is therefore inadequate to describe the short-time dynamics of interest here.

The model that we shall focus on is the next most simple model in this family. It possesses two states per well (2S/W), which correspond to whether the particle is to be found in the left or right side of the well, see Fig. 3.1. In this model, the location of the particle is described by two discrete indices: the integer well index, n, and the internal index $\alpha = L, R$ and $p_{\alpha}^{(n)}$ is the corresponding probability. For calculating the position cumulants, we take the particles to be localised at positions $x_{\alpha}^{(n)} = na + x_{L/R}$, where x_L and x_R are the offsets of the left and right states respectively.

Let us assume that transitions between these states can be described by rates and define rates γ^{+} and γ^{-} to describe hopping within a single well, and rates Γ^{+} and Γ^{-} to describe hopping between the wells. In both cases, superscript $+$ indicates movement to the right and $-$, movement to the left. The rates are homogeneous due to the periodicity of the force and, since we assume that the barriers are high ($\Delta u \gg k_{\mathrm{B}}T$), the intra-well rates $\gamma^{\pm}$ are significantly larger than the inter-well rates $\Gamma^{\pm}$. The system can then be described by the

rate equation system

$$\frac{\mathrm{d}}{\mathrm{d}t}\begin{pmatrix} p_L^{(n)} \\ p_R^{(n)} \end{pmatrix} = \begin{pmatrix} -\gamma^+ - \Gamma^- & \gamma^- \\ \gamma^+ & -\gamma^- - \Gamma^+ \end{pmatrix}\begin{pmatrix} p_L^{(n)} \\ p_R^{(n)} \end{pmatrix} + \begin{pmatrix} 0 & \Gamma^+ \\ 0 & 0 \end{pmatrix}\begin{pmatrix} p_L^{(n-1)} \\ p_R^{(n-1)} \end{pmatrix} + \begin{pmatrix} 0 & 0 \\ \Gamma^- & 0 \end{pmatrix}\begin{pmatrix} p_L^{(n+1)} \\ p_R^{(n+1)} \end{pmatrix} . \quad (3.5)$$

Denoting the vector of probabilities with the notation $\mathbf{p}^{(n)}(t)$, this master equation can be written in matrix form as

$$\dot{\mathbf{p}}^{(n)} = W_0\mathbf{p}^{(n)} + W_+\mathbf{p}^{(n-1)} + W_-\mathbf{p}^{(n+1)} \quad (3.6)$$

where $W_{0,\pm}$ are two-dimensional matrices defined according to Eq. (3.5). We then define the Fourier-transformed vector $\tilde{\mathbf{p}}(k,t) = \sum_n e^{inak}\mathbf{p}^{(n)}(t)$, such that, by Fourier-transforming Eq. (3.6), we arrive at

$$\partial_t\tilde{\mathbf{p}} = \mathcal{W}(k)\cdot\tilde{\mathbf{p}} \qquad \text{with} \qquad \mathcal{W}(k) = W_0 + e^{ika}W_+ + e^{-ika}W_- . \quad (3.7)$$

Assuming that the particle starts off in the $n = 0$ well, the solution of this equation is

$$\tilde{\mathbf{p}}(k,t) = e^{t\mathcal{W}(k)}\tilde{\mathbf{p}}(k,0) = e^{t\mathcal{W}(k)}\mathbf{p}^{(0)}(0). \quad (3.8)$$

Based on this solution the cumulants of position $\kappa_\ell(t)$ can be calculated via the cumulant generating function $g(k,t)$ [330]

$$\kappa_\ell(t) = \partial_k^\ell g(k,t)|_{k=0} \quad (3.9)$$

$$g(k,t) = \ln\varphi(-ik,t) \quad (3.10)$$

$$\varphi(k,t) = \int \mathrm{d}x\, e^{ikx}p(x,t) = \sum_{n\alpha} e^{ikx_\alpha^{(n)}}p_\alpha^{(n)}(t)\,, \quad (3.11)$$

where $\varphi(k,t)$ is the characteristic function of the position. We break the sum into the n-part which yields $\tilde{\mathbf{p}}(k,t)$ and the α-part which can be written as scalar product involving the internal position matrix Δ

$$\varphi(k,t) = (1,1)\cdot e^{ik\Delta}\cdot\tilde{\mathbf{p}}(k,t) \quad (3.12)$$

$$\Delta = \begin{pmatrix} x_L & 0 \\ 0 & x_R \end{pmatrix} . \quad (3.13)$$

Inserting Eqs. (3.12), (3.8) into Eq. (3.10) yields

$$g(k,t) = \ln\left((1,1)\cdot e^{k\Delta}e^{t\mathcal{W}(-ika)}\cdot\mathbf{p}^{(0)}(0)\right) . \quad (3.14)$$

On applying the derivatives of Eq. (3.9) to Eq. (3.14) we see that the inner derivatives produce the moments of the position and the outer derivatives of the logarithm combine the moments to yield cumulants.

In the following we will always start the particle localised within a single well at either position x_L or x_R.

3.3 Rates

The 2S/W model has six parameters: the four rates, $\gamma^{\pm}$ and $\Gamma^{\pm}$; and the two positions $x_{L/R}$. The inter-well rates we choose as twice Kramers' rates

$$\Gamma^{\pm} = 2r_{K\pm}, \tag{3.15}$$

where $r_{K\pm}$ are Kramers' rates for passage out of the well to the right (+) and left (−). Explicit forms for $r_{K\pm}$ are given in Sec. 2.2.1 where the potential difference is Δu, Eq. (1.13), for r_{K+} and $\Delta u + aF$ for r_{K-}. The factor two arises because, if the particle is localised in the right half of the well, the average time it will take to hit the right edge will be half that as if the particle was distributed over the whole well.

The remaining parameters we fix by comparing the initial behaviour with that of the SE, Eq. (3.1). We expand first and second cumulant to linear order in time t using the SE. If we assume that the particle is initially localised at x_L or x_R we arrive at

$$\langle x\rangle(t) = x_{L/R} - u'(x_{L/R})\frac{D_0}{k_{\mathrm{B}}T}t\,, \quad w(t) = 2D_0 t. \tag{3.16}$$

To compute the initial behaviour of the 2S/W model we set $\Gamma^{\pm} = 0$ which reduces $\mathcal{W}(k)$ to

$$W_{\mathrm{intra}} = (-1, 1)^T \otimes (\gamma^+, -\gamma^-) \tag{3.17}$$

where $\otimes$ denotes an outer product. Expanding Eq. (3.9) in linear order in time for the starting position x_α we arrive at

$$\kappa_1(t) = x_\alpha + s_\alpha t(x_R - x_L)\gamma^{s_\alpha} \tag{3.18a}$$
$$\kappa_2(t) = t(x_R - x_L)^2\gamma^{s_\alpha}\,, \tag{3.18b}$$

where $s_L = +$ and $s_R = -$. Equating these results with Eq. (3.16) and rearranging gives

$$\gamma^+ = \gamma^- = \frac{2D_0}{(x_R - x_L)^2} \tag{3.19a}$$
$$(x_R - x_L)u'(x_L) = -2k_{\mathrm{B}}T \tag{3.19b}$$
$$(x_R - x_L)u'(x_R) = 2k_{\mathrm{B}}T. \tag{3.19c}$$

Equations (3.19) have to be solved numerically for x_L and x_R, which then give the rates $\gamma^{\pm}$.

3.4 Limits

We are interested in an approximation for the plateau regime. The intra- and inter-well rates define time scales of different order of magnitude. We find the plateau between these time scales where the intra-well dynamics has relaxed and the inter-well dynamics has hardly begun. To approximate the plateau regime we use the approximation $\Gamma^{\pm} = 0$, Eq. (3.17), again and calculate the limit for $t \to \infty$. We obtain

$$\langle x\rangle^{\mathrm{plat}} = \frac{1}{2}(x_L + x_R)\,; \quad w^{\mathrm{plat}} = \frac{1}{4}(x_L - x_R)^2\,; \quad \kappa_4^{\mathrm{plat}} = -\frac{1}{8}(x_L - x_R)^4\,. \tag{3.20}$$

For the full 2S/W model we are interested in the asymptotic $t \to \infty$ limit to compare with the already known long time behaviour. We write the diagonalisation of $\mathcal{W}$ in $\partial_t g(k,t)$ as $\partial_t g(k,t) = \partial_t \ln((a,b)\cdot e^{tD}\cdot(y,z)^T)$ where D is the diagonal matrix with the eigenvalues d_1, d_2 on the diagonal. Carrying out the derivative yields $\partial_t g(k,t) = (ayd_1e^{d_1t} + bzd_2e^{d_2t})/(aye^{d_1t} + bze^{d_2t})$ which, in the limit $t \to \infty$ reduces to the largest eigenvalue. We denote this eigenvalue by

$$\lambda_0(k) = -\frac{\Gamma}{2}\left(1 - \sqrt{1 + \frac{4}{\Gamma^2}\sum_{\pm}\gamma^{\pm}\Gamma^{\pm}(e^{\pm ka} - 1)}\right), \tag{3.21}$$

with $\Gamma = \gamma^+ + \Gamma^+ + \gamma^- + \Gamma^-$. The complete cumulant generating function becomes

$$g(k,t) \sim \lambda_0(k)t\,, \tag{3.22}$$

From this expression it is clear that the cumulants are then simply linear in time, as they should be. The first two read

$$\langle x\rangle^{\infty}(t) = a\frac{\gamma^+\Gamma^+ - \gamma^-\Gamma^-}{\Gamma}t; \tag{3.23}$$

$$w^{\infty}(t) = a^2\frac{\Gamma^2(\gamma^+\Gamma^+ + \gamma^-\Gamma^-) - 2(\gamma^+\Gamma^+ - \gamma^-\Gamma^-)^2}{\Gamma^3}t\,, \tag{3.24}$$

where $\Gamma = \Gamma^+ + \gamma^+ + \Gamma^- + \gamma^-$. The latter gives directly the long-time diffusion coefficient

$$D = \frac{1}{2t}w^{\infty}(t). \tag{3.25}$$

3.5 Results

Before discussing the short-time behaviour of the system, we begin by demonstrating that our 2S/W model recovers the known long-time behaviour. In Fig. 3.2(a) we compare the diffusion coefficient D from the 2S/W model, Eq. (3.25), with the exact result of Reimann *et al.* [125]. In accordance with expectations, our model works well provided that the valleys of the potential are sufficiently deep, $\Delta u \ll k_{\mathrm{B}}T$. This condition can be satisfied by ensuring that $u_0 \ll k_{\mathrm{B}}T$ and that the applied force is less than the value of the force $F_c = u_0\pi/a$ at which the minima of the potential disappear.

Turning now to the short-time dynamics, we consider first the MSD $w(t)$ as a function of time in Fig. 3.2(b), where time is measured in units of $\tau = \frac{a^2}{D_0}$. Three distinct behaviours are seen. At the shortest times, the behaviour is essentially free diffusion with the MSD growing linearly. This is the behaviour which was fitted in our 2S/W model to obtain Eqs. (3.19). As the particle begins to feel the influence of the wells, a plateau develops in the MSD. By comparing Figs. 3.3(a) and (b) we see that the MSD shows a well-defined plateau if and only if the two 2S/W results in Fig. 3.3(a) agree.

The duration of this plateau increases the higher the potential barrier between wells. This behaviour is well reproduced by the 2S/W model not just qualitatively, but quantitatively. We note that this behaviour was not explicitly put into the model; rather, it emerges as a

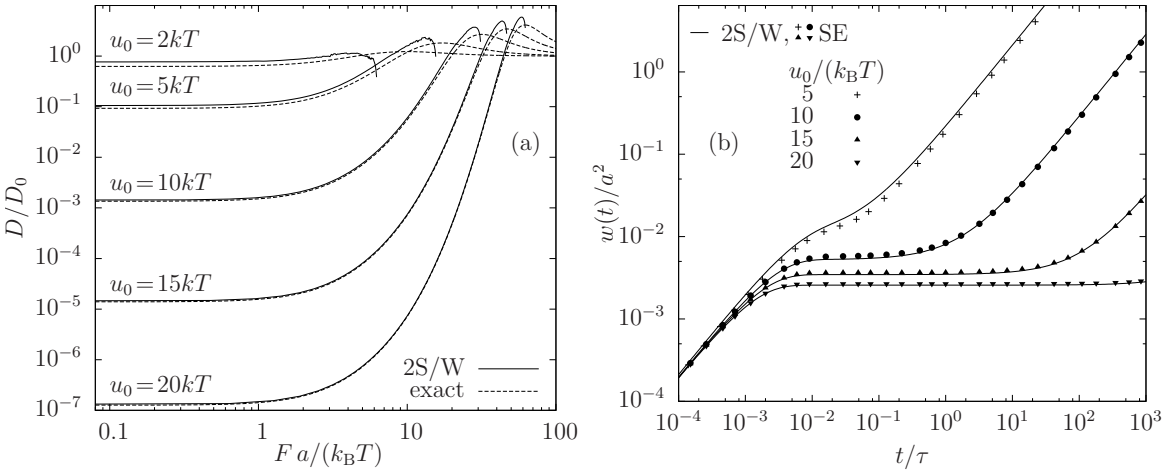

Fig. 3.2: (a) Comparison of diffusion coefficient D, Eq. (3.25), with the exact result of Ref. [125]. The results of the 2S/W model agree well with the exact ones in the regime of deep valleys, i.e. $u_0 \ll k_BT$ and $F < F_c$, with F_c the force for which potential valleys disappear. (b) MSD $w(t) = \langle (x - \langle x \rangle)^2 \rangle$ for different amplitudes u_0 with no applied force ($F = 0$). The lines show the result from the 2S/W model, and the symbols those from numerical integration of the SE. For the parameters shown here, the 2S/W model reproduces the essential features of the short-time dynamics. The agreement increases with increasing well-depth (increasing u_0).

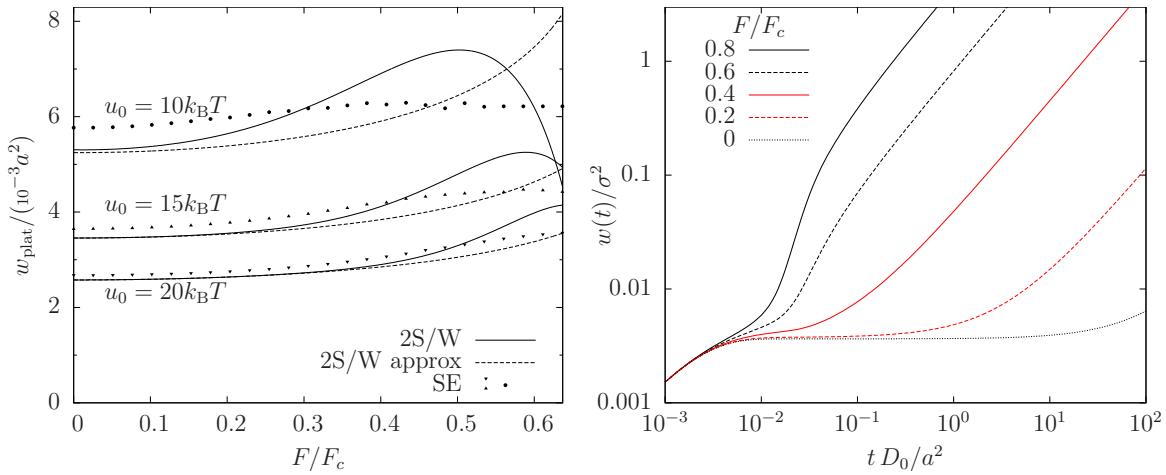

Fig. 3.3: (a) Plateau height w_{plat} as a function of driving force, F, calculated in three different ways. We have defined the plateau height as the value of $w(t)$ at the time for which $\mathrm{d}(\ln w)/\mathrm{d}(\ln t)$ reaches its minimum value. The solid curves show the plateau heights obtained from the 2S/W theory, the symbols from integrating the SE and the dashed lines show the approximation Eq. (3.20). The 2S/W method underestimates the plateau heights slightly, becoming better as u_0/k_BT becomes larger. (b) MSD $w(t)$ as a function of time for different driving forces F for $u_0 = 15k_BT$. The plateau is the less distinctive the larger the force.

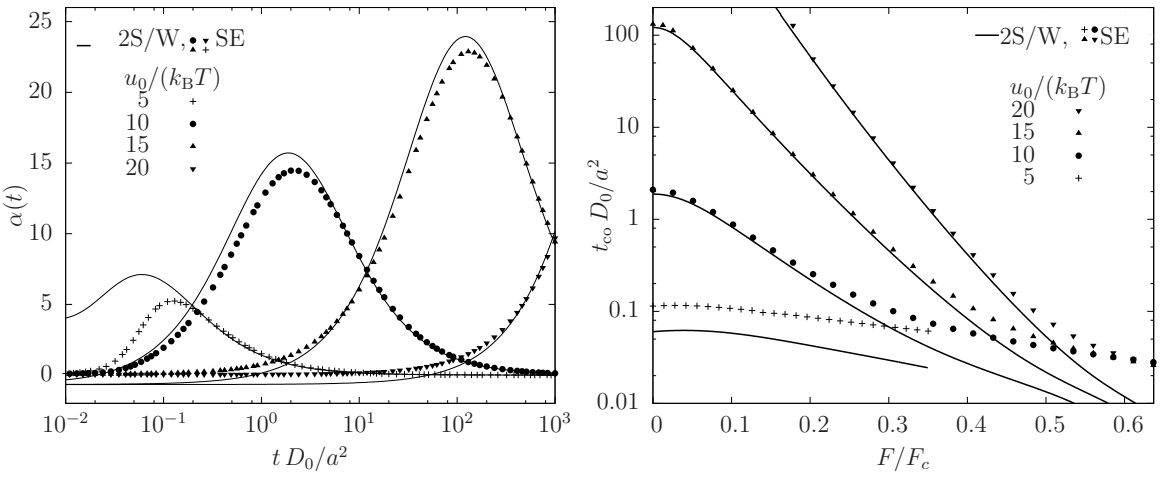

Fig. 3.4: (a) The non-Gaussian parameter $\alpha(t)$, defined in Eq. (3.4), as a function of time for the same parameters as in Fig. 3.2(b). The dominant feature is a peak which occurs around the cross-over time t_{co}. As before, good agreement between 2S/W model and numerics is obtained for $u_0 \gg k_BT$. (b) The cross-over time t_{co} defined as the time of the peak of the non-Gaussian parameter α. Again, the agreement is good for deep valleys.

prediction of it. Figure 3.3(a) shows the height of the plateau as a function of the applied force F. The 2S/W approach works better the more pronounced the potential barriers, but even for $u_0 = 5k_BT$, the 2S/W theory and numerics agree quite well. Figure 3.3(a) shows two different results for the plateau height extracted from the 2S/W model; one based on the full solution and one given by the approximate value of Eq. (3.20). The coincidence of these results is a good indication that the mean-square displacement undergoes a genuine plateau, rather than something more like an inflexion point, see Fig. 3.3(b). Not shown here, but the first cumulant $\langle x \rangle$ shows similar plateau behaviour, the height and duration of which is also well reproduced by the 2S/W model.

At longer times, the particle breaks out of the confinement of its initial well, and starts diffusing through the potential. The second cumulant then starts increasing linearly again, this time with the diffusion constant of Eq. (3.25) and Fig. 3.2(a). The time at which the plateau goes over into diffusive behaviour is the cross-over time t_{co}. During the plateau and through the cross-over, the probability density slowly reshapes. This can be seen in Fig. 3.4(a), which shows the non-Gaussian parameter, Eq. (3.4), as a function of time. By comparing Fig. 3.2(b) and Fig. 3.4(a) one can see that the time of the maximum deviation from Gaussian e.g. the maximum of $\alpha(t)$ can be used as an approximation to the end of the plateau, as proposed in Ref. [119]. It is remarkable that the 2S/W model predicts the dependence of this crossover time on u_0 and F, shown in Fig. 3.4(b), in quantitative agreement with the SE.

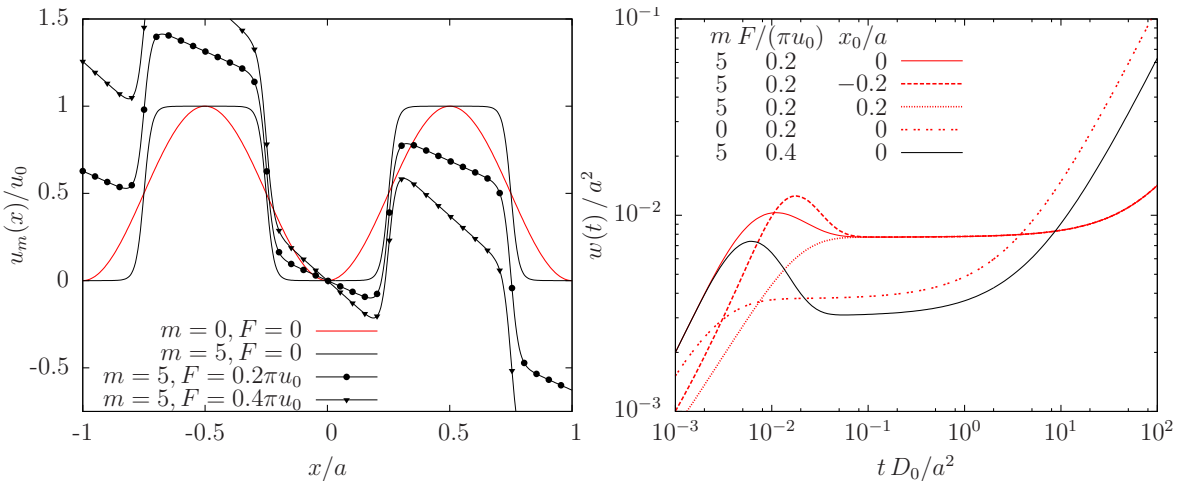

Fig. 3.5: (a) The non-sinusoidal potential $u_m(x)$, Eq. (3.26), for different values of the steepness parameter m and the driving force F. (b) Mean squared displacement $w(t)$ with respect to time for $F/(\pi u_0)$ being 0.2 (red) and 0.4 (black). Depending on the initial condition $p(x,0) = \delta(x - x_0)$ a local maximum forms. In contrast to the plateau height in the $m = 0$ case, the height of the local minimum strongly depends on F.

3.5.1 Non-sinusoidal potential

We briefly consider the short-time diffusion in the potential

$$u_m(x) = \frac{u_0}{2}\left(1 - \frac{\tanh(m\cos(2\pi x/a))}{\tanh m}\right) - xF \tag{3.26}$$

which is sketched in Fig. 3.5(a). Clive Emary proposed this functional form because it has broader wells and hills than the sinusoidal potential and possesses the limit $\lim_{m\to 0} u_m(x) = u(x)$. The larger m the steeper the walls between well and hill. In the limit $m \to \infty$ the shape of u_m becomes rectangular. The mean squared displacement $w(t)$ can become non-monotonous for large m if a driving force is present. As Fig. 3.5(b) shows, this effect is strongly dependent on the initial condition. In fact, also in the sinusoidal potential the effect can be found with the initial condition $p(x,0) = \delta(x + a/4)$, although it is very weak. We find that the local extrema of $w(t)$ are the more pronounced the sharper the minimum of the potential, given that the potential is flat near the initial condition.

To describe the diffusion in the potential $u_m(x)$ with the 2S/W model only modifications for the rates would be necessary. For the inter-well rate for $u(x)$ we used Kramers' rate with polynomial approximations of the potential around the extrema in Eq. (2.21). This will be a rough approximation for $u_m(x)$ since polynomial approximations are of poor accuracy. However Eq. (2.21) may be used directly. Concerning the intra-well rates, the solution of Eq. (3.19) shows that the position x_L and x_R reflect the strong asymmetry of $u_m(x)$. We expect that the 2S/W model can predict the non-monotonous behaviour qualitatively.

3.6 Conclusions

In this chapter we have investigated the short-time dynamics of a particle driven through a modulated potential. We introduced a Markovian master equation approach based on a discretisation of the spatial axis into two states per well. The remaining input into this theory are the transition rates, which we have chosen by using Kramers' rates (inter-well transitions) and by comparison with the true short-time dynamics from the continuous (SE) approach (intra-well transitions).

A major advantage of our discretised two-state model is that relevant transport quantities, such as the mean-squared displacement, can be calculated analytically. In particular, we presented explicit expressions for the heights of the plateaus in the mean-squared displacement at intermediate times, i.e., within the subdiffusive regime, and for the non-Gaussian parameter α, which signals the crossover to the diffusive long-time regime. The results from the two-state model are in excellent agreement with those obtained from numerical solution of the SE with and without external drive, provided that $\Delta u/k_{\mathrm{B}}T \gg 1$ and $F < F_c$. This latter requirement is consistent with the expectation that (only) in this limit, the valleys in our continuous model can be approximated by almost-isolated wells. In the same range of parameters, the diffusion coefficient D, is found to be fully consistent with previous analytical results [125]. It is precisely the high-barrier case, which is relevant in many experimental realisations of colloids in modulated potentials (see e.g. [82]), as well as in the more general context of modeling systems exhibiting cage effects (such as undercooled liquids [233] and dense colloidal suspensions [119]), see also section 1.5.1. For such systems our "minimal" model for short-time dynamics could be particularly useful.

We close this chapter with some remarks on possible extensions of our approach and its relation to other models. To start with, we have found that discrepancies between the master equation and the SE approach arise as $\Delta u/k_{\mathrm{B}}T$ decreases. In this case, quantitative agreement can be improved by modifying the manner in which the rates are calculated. Firstly, expanding the full generating function to linear order in time yields

$$\begin{aligned}\langle x\rangle(t) &\sim x_{L/R} \pm \gamma^{\pm}(x_R - x_L)t \mp \Gamma^{\mp}(a + x_L - x_R)t \\ w(t) &\sim \gamma^{\pm}(x_R - x_L)^2 t + \Gamma^{\mp}(a + x_L - x_R)^2 t.\end{aligned}$$

These values can be equated to Eq. (3.16) to match better with the SE. Secondly, the inter-well rates, Eq. (3.15), can be improved by using higher-order corrections to Kramers' rate (Sec. 2.2.1). These latter corrections are particularly important when the periodic contribution to the potential becomes steeper than a sine function.

A further point concerns the performance of our master equation approach for the prediction of higher-order cumulants. Whereas the complete behaviour of the first two cumulants is well reproduced by our 2S/W model, the agreement for the higher-order cumulants is not as good, and although the broad features of these are reproduced, some fine details at very short times are not captured. To improve these higher cumulants it seems to be promising to augment the model with more states per well, an extension which is conceptually straightforward.

Finally, we note that there is an connection between our model and other models describing subdiffusion. By tracing over the internal degrees of freedom, a non-Markovian master equation for the well-index n alone can be derived, involving a memory kernel which differs

from a delta function (characterizing the Markovian case). It is well established [129] that such non-Markovian kernels are intimately related [328,329] to the waiting-time distribution in continuous-time random walks [128], such that connexion can also be made with these latter methods.

4. WAITING TIME DISTRIBUTION (WTD) FOR BARRIER CROSSING

How long does a complex stochastic process take? The waiting time distribution (WTD) can give the answer, as we presented in our collaboration with Clive Emary, i.e., Phys. Rev. E **90**, 062115 (2014) (Ref. [331]). Parts of the chapter are copied from this publication.

Waiting time distributions (WTDs) are probability densities for the time between subsequent hopping events ("jumps") in a discrete stochastic process. Today's use of WTDs goes back to the beginning of continuous time random walk [128, 129, 332] and renewal theory [157], half a century ago. The corresponding cumulative distribution function to the WTD was used even earlier [333].

WTDs are used to describe transport in systems whose dynamics is discrete or at least approximately discrete, which applies to a wide range of systems, classical as well as quantum. Applications in biophysics include the kinetics of ion receptors [334], of the formation of biochemical bonds [325], and of reaction events of enzyme molecules [335, 336]. In finance, stock market fluctuations were analysed in the context of WTDs [337]. Further important applications concern atoms, molecules, and colloids diffusing on corrugated surfaces [63, 67, 87, 338]. Despite the particles' positions are actually continuous, the effective potential landscape often is characterised by local energy minima whose depth is much larger than the thermal energy. Further examples of approximately discrete stochastic processes are found in protein folding [334, 339, 340] and in the field of glasses and supercooled liquids. In the latter these processes are rearrangements of particle positions or orientations [233, 341, 342] or, more generally, transitions in a coarse-grained configuration space [121, 324, 327]. Recent applications in quantum systems are found in the area of transport in quantum dots [343–345]. The processes studied in the previous chapter are almost discrete, too. Rather than in the cumulants of position we are now interested in time.

For truly discrete systems a WTD can be defined and calculated based on a Master equation (ME). In such systems jumps are *instantaneous*. Simple MEs can even be solved analytically [334, 343, 345, 346]. There is no straightforward route to define a WTD for continuous systems since the definition of a jump is ambiguous for a continuous motion. However, experience-based strategies are used to calculate WTDs from (particle) trajectories. The trajectories can originate from experiments as well as from computer simulations. Recent developments of experimental methods provide time- and particle-resolved measurements of colloids on random and structured surfaces [82, 83, 87, 97, 234, 347], on solid-liquid interfaces [67], or during growth of colloidal crystals [63, 227]. For examples for the calculation of the WTD using trajectory analysis in glassy systems see [121, 341]. The trajectory analysis in systems with quasi-discrete motion reveals that the system spends most time in distinct places (or configurations), the traps, and shows fast motion in between. These traps can be

used to discretise the space and to define jumps. This, naturally ambiguous, process can lead to jumps having *finite* duration. The trajectory analysis procedure yields quite noisy WTDs or requires extensive measurements or simulations. To address this shortcoming we construct a WTD based on a continuous and noise-averaged description. The natural approach is a probability density and a Fokker-Planck equation.

In this chapter we recall the recipe we proposed in our paper [331] to calculate the WTD using a Smoluchowski equation. Our inspiration was the calculation of the first passage time distribution (FPTD) [10]. In fact, our generalisation of the WTD is closely related to FPTDs which themselves have encountered generalisations in the last decades. Both, WTD and FPTD, are probability densities in time. The FPTD is commonly applied to continuous systems, not necessarily quasi-discrete ones, whereas the WTD has its roots in discrete systems. Asymmetric situations are rather common for WTDs [334,339,340,343–345, 348], whereas FPTDs usually are undirected. However, FPTDs with directional resolutions were proposed in mathematics [349, 350], although without a corrugated potential.

We validate our approach by comparing to trajectory analysis based on generated trajectories from a Langevin equation. To this end we choose a specific model system, namely the overdamped Brownian motion of a particle in a one-dimensional washboard potential, which is a generic model with wide applicability (cf. section 1.5.1). As a third method to calculate the WTD we apply the 2S/W model, introduced in the previous chapter. It precisely predicted the short time diffusion in this model in the deep well case and allowed for analytic solutions.

The dynamics of barrier crossing for an overdamped Brownian particle in a washboard potential is approximately determined by Kramers' escape rate (cf. section 2.2.1). The rate-based description of escape problems has a long history [11], and is still an important method of modelling [44, 351]. We will point out how the WTD incorporates the Kramers' escape rate.

In section 4.1 we characterise the quasi-discrete motion in our model system. The three routes to define a WTD, trajectory analysis, Smoluchowski equation, and 2S/W model, and presented in section 4.2 and compared in 4.3.

4.1 Trajectory based characterisation of single particle barrier crossing

We begin with an illustration of the nature of trajectories and jumps in the class of systems we investigate here. We consider the overdamped Brownian motion of a particle in tilted washboard potential $u(x)$, introduced in section 1.5.1. The equation of motion in one dimension is the Langevin equation (2.7). As in chapter 3, we focus on cases where the form of the potential is such that it can be meaningfully divided in a number of wells (defined between subsequent maxima). This occurs if the difference between the potential minima and maxima, $\Delta u(u_0, F)$, is large compared to the thermal energy, i.e., $u_0 \gg k_\mathrm{B}T$ and $F < F_c$ (cf. Eq. (1.13)).

In order to illustrate the motion in such situations we consider representative particle trajectories which we calculate numerically (for details see section 2.6.5).

Exemplary trajectories for two different values of $u_0/k_\mathrm{B}T$ and $F = 0$ are shown in Fig. 4.1(a). The trajectories in Fig. 4.1(a) clearly reflect that the particle is "trapped" for certain times in the regions around the potential minima $x/a \in \mathbb{Z}$. To facilitate the com-

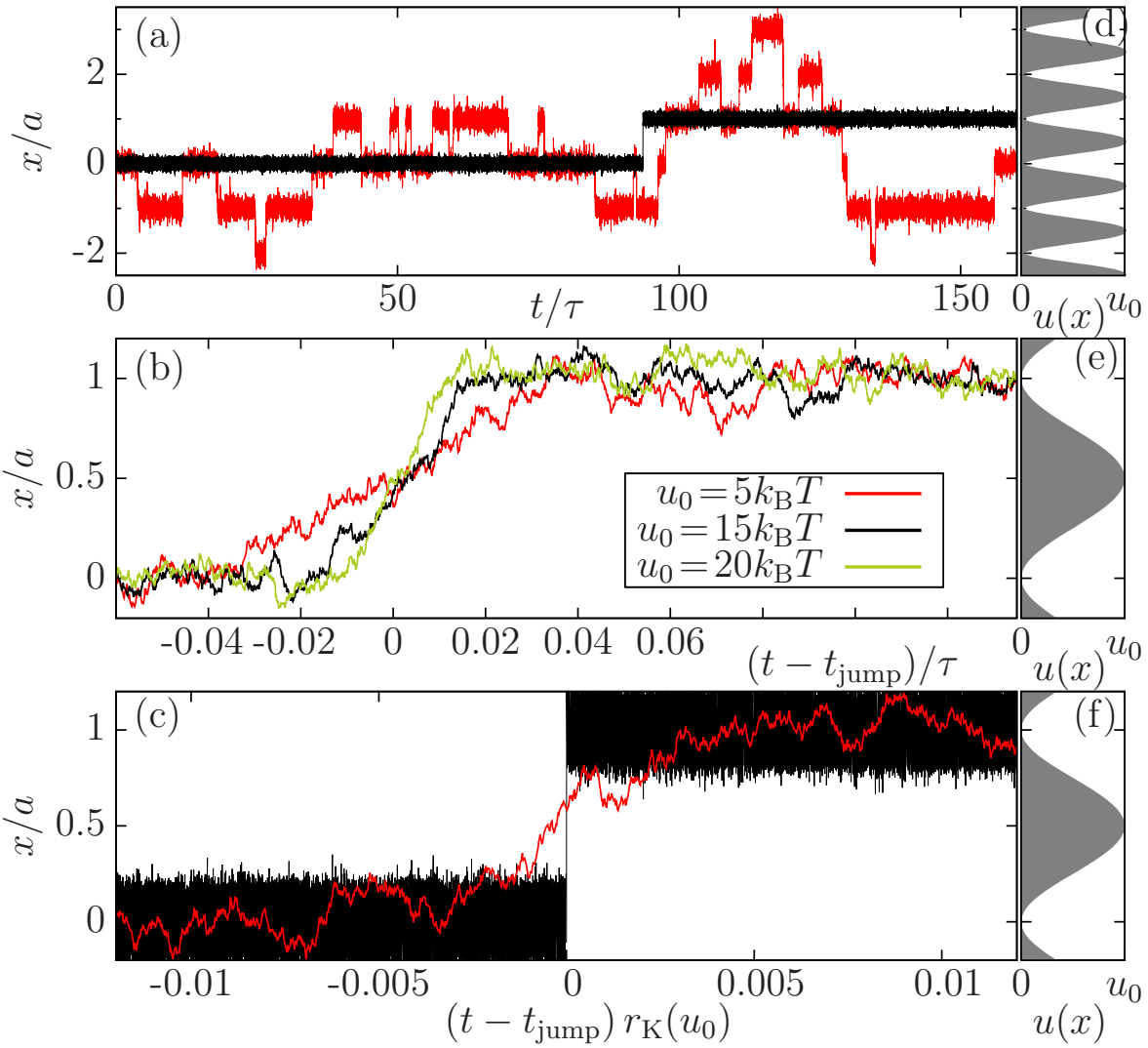

Fig. 4.1: (a) Representative trajectories for $F=0$ for different values of $u_0/k_\mathrm{B}T$. (b) To ease the comparison of the jumps, the trajectories are plotted as functions of the relative time $t-t_\mathrm{jump}$ where t_jump is the arithmetic mean between the times of leaving a potential minimum and arriving at a neighbouring one. We use the time unit $\tau = a^2/D_0$. (c) Comparison of the jumps with the time axis being rescaled by Kramers' rate $r_\mathrm{K}(u_0)$. With this rescaling, the mean time that the particles spend trapped around a minimum is independent of barrier height. Relative to this time scale, the jumps in the $u_0 = 15k_\mathrm{B}T$ case appear instantaneous, whereas those for $u_0 = 5k_\mathrm{B}T$ maintain a continuous character. Parts (d), (e), and (f) are sketches of the potential Eq. (1.11) corresponding to parts (a), (b), and (c), respectively.

parison between the trajectories corresponding to different u_0 they are plotted in Fig. 4.1(b) as functions of the relative time. This latter is defined as the difference between the actual time and the time t_{jump}, which is the arithmetic mean of the times related to the beginning and end of a jump. Here, "beginning" and "end" refer to leaving of a potential minimum (without going back) and arriving at a different minimum (this definition of a jump will later be called minimum-based definition). From Fig. 4.1(b) we see that even for the largest barrier considered, the particle needs a *finite* time to cross the barrier. Thus, the motion is still not perfectly discrete. However, as we may note already here, a different picture on the degree of "discreteness" arises when we rescale the time axis with the corresponding Kramers' rate $r_{\mathrm{K}}(u_0)$, defined in Eq. (2.22), see Fig. 4.1(c). By multiplying the time with this well-known quantity, we take into account that the increase of the potential height alone already leads to an increase of the escape time [155]. As a consequence the intervals between jumps in the rescaled time become independent of u_0 in the long time limit. Indeed, after rescaling, the data for $u_0 = 15k_{\mathrm{B}}T$ reflects an essentially discrete motion. However, at $u_0 = 5k_{\mathrm{B}}T$ we still observe a finite duration of the jump. This clearly demonstrates that the case $u_0 = 5k_{\mathrm{B}}T$ is at the boundary between discrete and continuous motion.

4.2 Routes to calculate the WTD

4.2.1 Direct evaluation via BD simulations

To define the WTD we first need to consider the possible types of jumps. To this end, we note that the stochastic process $x(t)$ (see Eq. (2.7)) is a Markov process. Thus, the jump characteristics are independent of the history. Further, because the motion is one-dimensional, there are only two directions in which the particle can jump. Finally, Eq. (2.7) obeys the translational symmetry $x \to x \pm a$. Because of these three properties the jumps can be grouped into only two types, namely "to the right" and "to the left", independent of when or where the jump began. We label these jump types by the index "J". The WTD $w^J(t)$ is then the probability density for the time between an arbitrary jump and a subsequent jump of type J.

In the context of BD simulations (i.e., direct evaluation of Eq. (2.7)), the WTD $w^J(t)$ is extracted from a histogram of waiting times extracted from the trajectories pertaining to a given realisation of noise. We note that the WTDs $w^J(t)$ must fulfil the normalisation condition

$$1 = \int_0^\infty \mathrm{d}t \sum_J w^J(t), \tag{4.1}$$

which expresses the fact that the particle leaves its minimum for certain. In terms of the survival probability

$$S(t) = \int_t^\infty \mathrm{d}t' \sum_J w^J(t') \tag{4.2}$$

the normalisation is expressed as $S(0) = 1$ and $S(\infty) = 0$. The sum runs over all jumps types that leave a potential minimum, in our case "to the right" and "to the left".

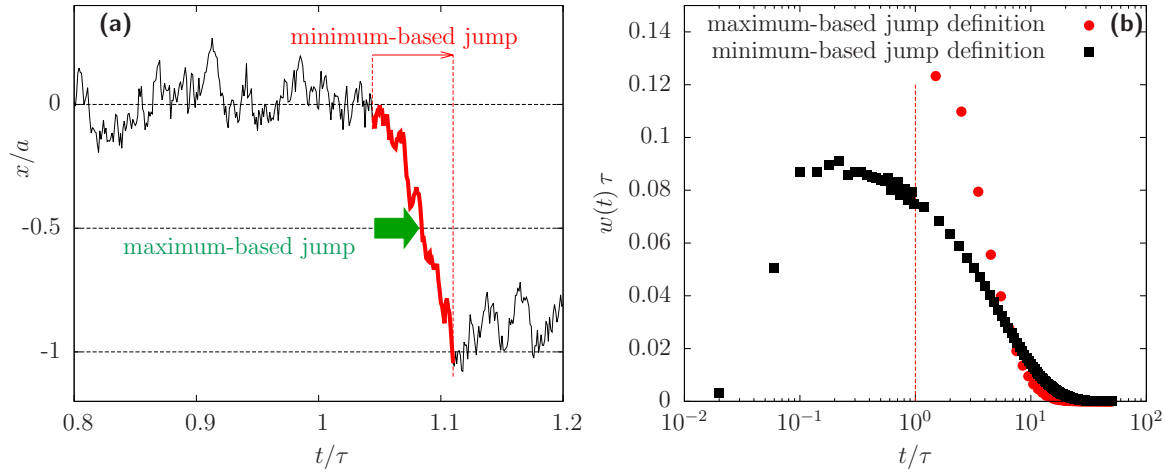

Fig. 4.2: (a) Illustration of different "measurement-based jump" definitions using a typical trajectory. The thick arrow indicates the time at which an instantaneous jump occurs according to the maximum-based definition, i.e. when the particle crosses the potential maximum between the wells. The thick curve indicates the motion during the jump according to the minimum-based definition, where the jump (having a finite duration) begins with the particle's last departure from a potential minimum (in this example $x = 0$) and ends upon arrival at a neighbouring minimum (here $x = -a$). (b) Comparison of the WTDs obtained with the two jump definitions (circles and squares). Time is plotted logarithmically. The maximum-based definition breaks down at short waiting times and we suppress these results by introducing a minimal waiting time ("dead time"), here at $t = \tau$ (dashed vertical line). In both plots is $u_0 = 5k_BT$ and $F = 0$.

In our BD calculations of $w^J(t)$ we consider two definitions of a jump which are illustrated in Fig. 4.2(a). Within the first definition, a jump occurs if the particle crosses a potential maximum (*maximum-based definition*). Note that this automatically defines the jump to be instantaneous.

Within the second definition, a jump involves the entire motion between two neighbouring minima of the potential (*minimum-based definition*). As a consequence, the jump has a finite duration defined as the time between leaving a minimum and arriving at a neighbouring one. We call the corresponding probability distribution the jump duration distribution. Further, we define the waiting time as the time between the end times of two subsequent jumps.

Numerical details of the calculation are given in section 4.4.1.

Discussion of the jump definitions To investigate the role of the two jump definitions we consider the resulting WTDs for the symmetric case $F=0$, $u_0=5k_BT$, plotted in Fig. 4.2(b). Because of the symmetry of the potential at $F=0$, there is only one relevant WTD. Clearly, the choice of the jump definition has a strong impact on the WTD. In particular, we find that only the minimum-based definition yields a smooth shape of $w^J(t)$.

On the contrary, the maximum-based jump definition poses several problems. First, during the analysis of the trajectories we noticed that the particle crosses the maximum many times subsequently which generates a lot of spurious (maximum-based) jumps. We deal with this problem by introducing a "dead time" after recording a jump which must pass until the next jump can be recorded. We set the "dead time" to 1τ (i.e., the time the particle needs to diffuse the distance $\sqrt{\tau/D_0}=a$) to ensure that it leaves the maximum during that time. As a consequence of introducing the dead time, the corresponding WTD is defined to be zero for $t<1\tau$.

Further, we see in Fig. 4.2(b) that by using the maximum-based jump definition, waiting times in the range $1\tau \lesssim t \lesssim 5\tau$ are more likely than by using the minimum-based jump definition. The reason is that the particle, once it has gone uphill, is counted to have made a jump in the maximum-based jump definition. On the contrary, the same particle is only counted in the minimum-based jump definition if it goes downhill *in the same direction* (and not backwards). Thus, the maximum-based jump definition frequently records jumps although the particle does not change the potential well. This contradicts our idea of a jump to cross the potential barrier. In our paper [331] we claimed that this problem could be solved by keeping track of the direction in which the particle crosses the maximum. We did not find a corresponding algorithm in the meantime. Because of these two problems, we choose the minimum-based jump definition for the further investigation.

4.2.2 Definition from the Smoluchowski equation

The Fokker-Planck equation corresponding to Eq. (2.7) is given by the Smoluchowski equation (SE) we used in the previous chapter, i.e., Eq. (3.1), which is Eq. (2.13) with the force $f(x)=-u'(x)$.

Again, we are interested in the distribution of waiting times t. In Sec. 4.2.1 we defined $w^J(t)$ as the WTD for the jump J. Here we associate J with the jumps from an initial position B to a target position C. Typically B and C are neighbouring minima of the potential. In order to realise the requirement that the WTD describes the time between *subsequent* jumps

we need to exclude processes that lead the particle towards the other neighbouring minimum, which we call A. Correspondingly, we describe the WTD by the function $w_A^{B\to C}(t)$ where $B \to C$ stands for J and the subscript A indicates the excluded position. The definition is as follows:

Definition: The quantity $w_A^{B\to C}(t)\,\Delta t$, where Δt is a small time interval, is the probability that

- the particle was *for certain* at position B at $t=0$, (4.3a)
- the particle reaches position C in the interval $[t, t+\Delta t]$, and (4.3b)
- the particle neither arrived at C nor A within the time interval $[0, t]$. (4.3c)

Note that we do not care about what happened at earlier times $t < 0$, that is, whether the particle moved to B via a jump process or whether it was placed there "by hand". This crucial assumption reflects that we are working in a *Markovian* situation, where the motion from B to C is independent of the history.

To formulate a recipe to calculate the WTD, we recall that the SE, Eq. (3.1), can also be written as a continuity equation, that is, the reduction to one-dimension of Eq. (2.11),

$$\partial_t p(x,t) + \partial_x j(x,t) = 0, \tag{4.4}$$

where $j(x,t) = -D_0\left(\partial_x p(x,t) + p(x,t)u'(x)/(k_\mathrm{B}T)\right)$ is the current density. Equation (4.4) and the microscopic interpretations Eqs. (2.8) and (2.91) further show that $j(x,t)\,\Delta t$ (or $-j(x,t)\,\Delta t$, respectively) can be interpreted as the probability that the particle crosses position x into positive (negative) x-direction during the time interval $[t, t+\Delta t]$. Consequently $|j(C,t)\Delta t|$ is the probability that the particle crosses position C in forward or backward direction. This probability is similar in character to that mentioned in condition (4.3b). However, $|j(C,t)\,\Delta t|$ includes the probability that the particle went across C (or A), came back, and crosses C again. Such a process violates condition (4.3c).

Based on these considerations, we propose the following recipe to calculate the WTD $w_A^{B\to C}(t)$: We initialise the probability density as

$$p(x, t=0) = \delta(x - B) \tag{4.5}$$

according to condition (4.3a). Then, we let $p(x,t)$ evolve in time according to Eq. (3.1). However, during this time evolution we exclude processes from the ensemble of realisations (i.e. possible trajectories) where the particle has already reached position C or A [see condition (4.3c)]. Therefore $p(x,t)$, which is an average over this reduced set of realisations, fulfils the boundary conditions

$$p(x,t) = 0,\ x \geq \max(A,C) \quad \forall\, t \tag{4.6a}$$
$$p(x,t) = 0,\ x \leq \min(A,C) \quad \forall\, t\,. \tag{4.6b}$$

Equation (4.6) expresses what is often called "absorbing wall boundary conditions". Clearly, there is some arbitrariness in defining a suitable position A (the boundary "on the other side") for a continuous system in general. However, given that we consider a continuous potential with well-defined wells (as it is the case here) one can give a clear physical meaning to the positions A, B, and C.

To summarise, we calculate the WTD from the relation

$$w_A^{B\to C}(t) = |j_{A,C}^B(C,t)|\,, \tag{4.7}$$

where the notation $j_{A,C}^B$ expresses the dependency of the current density on the initial and boundary conditions given in Eqs. (4.5) and (4.6), respectively. By using the absolute value in Eq. (4.7) we take into account the fact that the sign of j depends on the direction of motion. Indeed, motion into the positive (negative) x-direction implies a positive (negative) sign of j. The numerical calculation of the WTD via the SE route is described in section 4.4.2.

Finally, we note that the WTDs defined according to Eq. (4.7) also fulfil the normalisation condition Eq. (4.1), that is

$$\int_0^\infty \mathrm{d}t \left(w_A^{B\to C}(t) + w_C^{B\to A}(t)\right) = 1. \tag{4.8}$$

Relation to the First passage time distribution By definition [10], the first passage time distribution (FPTD) is the probability distribution for the time t the particle needs to leave a given domain for the first time. In a Markovian situation like ours the FPTD depends on the spatial probability distribution $q(x)$ to find the particle at position x at a starting time $t' \leq t$. We thus consider the FPTD $F_D(t; q(x))$ where the domain D, in an one-dimensional system, is given by an interval, e.g. $D = [A, C]$. Further, if the particle was for certain at a position B at $t = 0$, we can specialise $q(x) = q_B^0(x) := \delta(x - B)$. The relation between the FPTD and the WTDs defined before is then given by

$$F_{[A,C]}(t; q_B^0) = w_A^{B\to C}(t) + w_C^{B\to A}(t). \tag{4.9}$$

Equation (4.9) reflects the fact that the FPTD does not contain information about the direction in which the particle left the domain, whereas the WTD does.

4.2.3 Master equation

In chapter 3, we introduced a simple master equation model of this system. In addition to the definitions of sections 3.2 and 3.3 we define the 'expectation value'

$$\langle\langle \mathcal{A} \rangle\rangle = \mathbf{h}_1^T \cdot \mathcal{A} \cdot \mathbf{h}_0 \tag{4.10}$$

where $\mathbf{h}_1$ and $\mathbf{h}_0$ are defined by

$$\mathbf{h}_1^T \cdot \mathcal{W}(0) = \mathbf{0}^T \tag{4.11a}$$

$$\mathcal{W}(0) \cdot \mathbf{h}_0 = \mathbf{0}\,. \tag{4.11b}$$

The matrix $\mathcal{W}(0)$ is given by Eq. (3.7). Following [343], we then obtain the WTDs as

$$w_{ss'}(t) = \frac{\langle\langle W_s e^{W_0 t} W_{s'} \rangle\rangle}{\langle\langle W_{s'} \rangle\rangle}; \quad s, s' = \pm\,, \tag{4.12}$$

with the matrices $W_{0,\pm}$ defined by Eqs. (3.5) and (3.6). There are four different waiting times defined here, corresponding to the four different combinations of jumps: $s, s' = \pm$. The

parameter s' indicates the position where the jump starts off by determining the jump that led the particle to this well. Hence, for $s' = +$ the particle starts in the left position in the well, and for $s' = -$ it starts in the right position. The parameter s indicates the direction in which the particle leaves the well.

In comparing with the results from BD/SE, we will only consider the diagonal WTDs $w_{ss}(t)$ as these are found to be the closest analogues of the definitions used in the continuous system. The reason for this is that in off-diagonal WTDs, the second jump can occur immediately after the first, and thus $\lim_{t\to 0} w_{ss'}(t)$ for $s' \neq s$ is finite. Clearly, this is not the case in the full dynamics and so we consider only the diagonal WTDs. This difference between on- and off-diagonal WTDs only occurs at very short times and, as we will see in the next section, the ME description is unreliable in this regime, anyway.

4.3 Numerical results

The main new finding obtained in [331] is our definition of the WTD via the continuous SE route. In the following we compare results obtained numerically from this definition with those from BD simulations (using the minimum-based jump definition), as well as with results from the ME approach. Calculations regarding the ME approach were carried out by Clive Emary.

To be specific, we choose the positions A, B, and C to be adjacent minima of the potential $u(x)$ (given explicitly in section 1.5.1). In the following section 4.3.1, we examine the case of zero drive ($F = 0$) for two amplitudes of the periodic potential. Both symmetric and asymmetric initial (and boundary) conditions are considered. In section 4.3.2 we fix u_0 to $15k_BT$ and study driven systems for three values $F < F_c$ where $F_c = u_0\pi/a$ is the "critical" driving force beyond which the minima in $u(x)$ are eliminated.

4.3.1 Zero drive ($F = 0$)

We start by considering fully "symmetric" cases, where the potential is untilted ($F = 0$), and the particle jumps from the centre of a minimum (say, $x = 0$) to the right ($0 \to a$) or to the left ($0 \to -a$). Clearly, these jumps are characterised by the same WTD, i.e., $w_{-a}^{0\to a}(t) = w_a^{0\to -a}(t)$. Moreover, in such fully symmetric situations (with respect to the initial- and boundary conditions, and to $u(x)$), the WTD is proportional to the first passage distribution, i.e., $w_{-a}^{0\to a}(t) = 1/2\, F_{[-a,a]}(t; q_0^0)$ (see Eq. (4.9)). However, as we will demonstrate, the SE approach is more versatile when we deviate from the symmetric case. We thus discuss the symmetric case as a reference.

Results for the corresponding WTD at $u_0 = 5k_BT$ and $u_0 = 15k_BT$ are plotted in Figs. 4.3(a) and (b), respectively. These values of u_0 are representative since, as we recall from our earlier discussion of particle trajectories (see Fig. 4.1), the case $u_0 = 5k_BT$ is at the boundary between continuous and discrete motion while at $u_0 = 15k_BT$, the motion is essentially discrete.

Figures 4.3(a) and (b) contain data from all three approaches (SE, BD, ME). All curves share the same general structure in that the WTD is essentially (but not strictly) zero at very short times ($t \ll \tau$) and then grows with time up to a value which remains nearly constant over a range of intermediate times (note the logarithmic time axis). Finally, at very large times the WTD decays rapidly to zero. The extension of the different regions and the actual

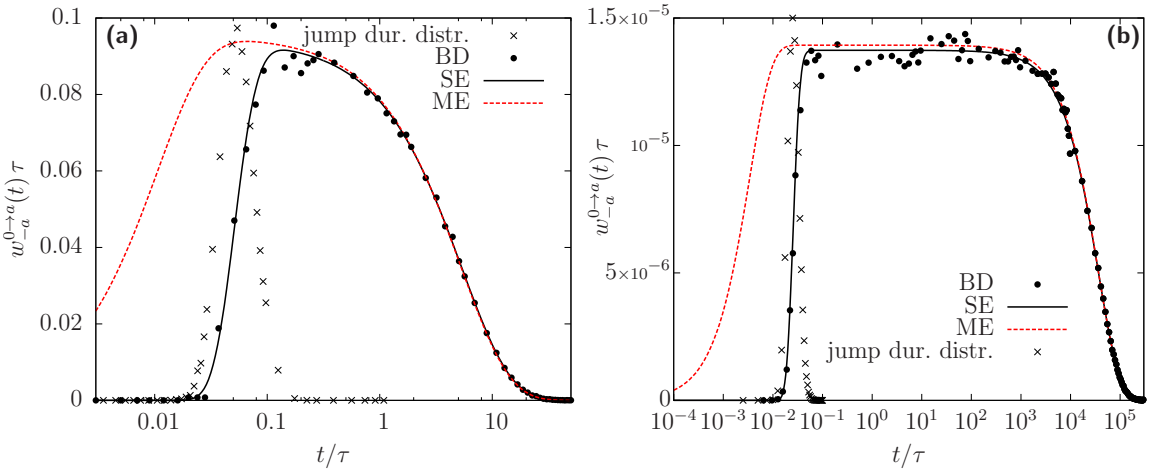

Fig. 4.3: Semilogarithmic plots of the WTD $w_{-a}^{0\to a}(t)$ for the symmetric case $F=0$ for (a) $u_0=5k_BT$ and (b) the deep well case $u_0=15k_BT$ using all three methods BD, SE and ME (in the latter case, we have plotted $w_{++}(t)=w_{--}(t)$). The crosses show the jump duration distribution (from BD) with arbitrary units.

values of the WTD depend on the potential height, as we will analyse in detail below. From a methodological perspective we can state already here that the SE approach represents at all times a very accurate, smooth "fit" of the (somewhat noisy) BD data. The ME approach displays deviations at short times, to which we will come back at the end of this subsection.

The growth region of the WTD can be further analysed by inspection of the jump duration distribution obtained from BD, which is included in Fig. 4.3. At both potential amplitudes this distribution displays a peak located at the (finite) time where the WTD grows most strongly. Moreover, the width of the peak corresponds approximately to that of the entire growth region. We can interpret these findings as follows. First, the fact that the peak occurs at a *finite* time already signals that we are looking at (more or less) continuous stochastic processes where the particles needs a finite time to cross a barrier (see Fig. 4.1(b)). This is also the reason that we find a growth region in the WTD at all. As we have seen from the trajectories in Fig. 4.1, the jump duration tends to decrease with increasing u_0. This explains the shift of the peak of the corresponding distribution towards earlier times in Fig. 4.3(b) with respect to 4.3(a). Second, regarding the width of the jump duration distribution, we note that only realisations of the random force with a strong bias can push the particle against the potential ascent. The larger u_0, the smaller the fraction of appropriate noise realisations and hence the sharper the distribution. This also has a direct influence on the width of the growth region of the WTD: For very short times only very short jumps can contribute to the WTD, hence the WTD rises simultaneously with the jump duration distribution.

Interestingly, it is also possible to calculate the jump duration distribution via the SE approach. To this end we just need to adjust the boundary and initial conditions. During a jump the particle leaves a minimum, say $x=0$, crosses the barrier and arrives at the next minimum, $x=a$. The difference to the jump $0\to a$ we considered above is that the particle actually leaves the minimum at $t=0$, i.e., it does not return. The essential step to the jump duration distribution is to consider an ensemble of realisations without processes where

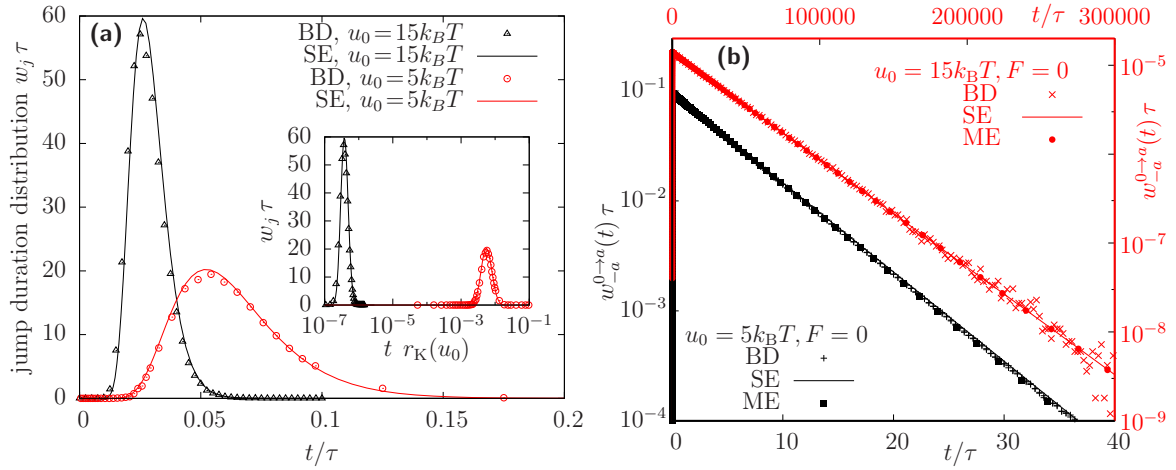

Fig. 4.4: (a) Jump duration distribution $w_j(t)$ for $u_0 = 5k_BT$ and $u_0 = 15k_BT$ calculated with BD and SE (Eq. (4.13)). The starting position is set to $\epsilon = 0.01a$. Inset: Distributions $w_j(t)$ with the time axis being rescaled by Kramers' rate $r_K(u_0)$. (b) Decay of the WTD $w_{-a}^{0\to a}(t)$ at long times for $u_0 = 5k_BT$ (left/bottom-axes) and $u_0 = 15k_BT$ (right/top-axes) for $F = 0$ using all three methods (BD, SE, and ME). In the ME case we have plotted $w_{++}(t) = w_{--}(t)$. The decay constants are listed in Table 4.1.

the particle comes back. Following section 4.2.2 this condition corresponds to an absorbing boundary at $x = 0$. The second absorbing boundary must be located at the point of arrival, $x = a$. This suggests the construction of the WTD $w_0^{\epsilon\to a}(t)$ where the starting position ϵ is close to 0 because the particle just left the minimum. Through the normalisation Eq. (4.8) $w_0^{\epsilon\to a}(t)$ is connected with $w_a^{\epsilon\to 0}(t)$, which states how likely the particle comes back to $x = 0$. We do not have any information about this quantity in the BD simulation, with which we compare. Therefore we need to remove this information. The total probability that the particle returns is given by $\int_0^\infty \mathrm{d}t\, w_a^{\epsilon\to 0}(t)$. This leads us to the following definition of the normalised jump duration distribution.

$$w_j(t) = \frac{w_0^{\epsilon\to a}(t)}{1 - \int_0^\infty \mathrm{d}t'\, w_a^{\epsilon\to 0}(t')} = \frac{w_0^{\epsilon\to a}(t)}{\int_0^\infty \mathrm{d}t'\, w_0^{\epsilon\to a}(t')} \tag{4.13}$$

A comparison between the BD and SE results for the distribution is given in Fig. 4.4(a). Clearly, the SE route yields very good results.

At intermediate times the WTD has a broad maximum which, for deep wells, takes the form of a plateau (see Fig. 4.3(b)). Numerical values for the WTD maxima at the two potential amplitudes are given in Table 4.1, where we have included values of Kramers' escape rate r_K in the most precise form defined in Eq. (2.21), i.e., without the Gaussian approximation of the integrals, in the present case

$$(r_K^\infty)^{-1} = \frac{1}{D_0} \int_{-a/2}^{a/2} \mathrm{d}x\, e^{-\beta u(x)} \int_0^a \mathrm{d}y\, e^{\beta u(y)}\,. \tag{4.14}$$

This close relation can be understood on the basis of our SE approach where we have identified the WTD as a current (i.e., a rate in one dimension). This current has been calculated with

$\frac{u_0}{k_\mathrm{B}T}$	global maximum	Kramers' rate r_K^∞	decay constant
5	$0.0916\tau^{-1}$	$0.0924\tau^{-1}$	$0.1867\tau^{-1}$
15	$1.39059\times10^{-5}\tau^{-1}$	$1.39062\times10^{-5}\tau^{-1}$	$2.7953\times10^{-5}\tau^{-1}$

Tab. 4.1: SE results for the global maximum of the WTD $w_{-a}^{0\to a}(t)$, Kramers' escape rate, given by Eq. (4.14), and the decay constant λ characterising the exponential tail.

absorbing boundary conditions. A very similar calculation, namely by using one absorbing boundary and an infinite soft potential barrier on the other side together with the stationarity approximation, leads to Kramers' rate (cf. section. 2.2.1). Of course, for short and long times the probability distribution is not stationary; therefore the connection between the values of the WTD and Kramers' rate only holds at intermediate times.

At times beyond the maximum (or plateau, respectively), the WTD rapidly decays to zero. In Fig. 4.4(b) we replot the corresponding behaviour with a linear time axis and a logarithmic y-axis. From that it is clearly seen that the decay can be described by a (single) exponential, i.e., $w_{-a}^{0\to a}(t)\sim e^{-\lambda t}$ in this range of times. The corresponding decay constants λ (as obtained from the SE approach) are listed in Table 4.1. We find that, for both values of u_0 considered, λ is approximately twice as large as Kramers' escape rate (or plateau height, respectively). Comparing our situation to the escape out of a similar metastable potential discussed in Risken's book [10], section 5.10, we see that the decay constant is expected to be the sum of Kramers' rates for every barrier, in the symmetric case $\lambda\approx 2r_\mathrm{K}$.

We now turn to the ME approach. As described in section 4.2.3, this approach assumes a discretised two-state-per-well model, that is, the particle can (only) take the positions x_L and x_R within each well. Leaving, e.g., position x_L, the particle performs either an intra-well jump (to x_R) or an inter-well jump to x_R-a or to x_L+a (via x_R). Here we are only interested in processes of the latter type, where the particle actually crosses a barrier. Further, because of translational symmetry and $F=0$ we only need to distinguish between the WTD for a "long" jump $w_\mathrm{long}(t)=w_{x_R-a}^{x_L\to x_L+a}(t)=w_{x_L+a}^{x_R\to x_R-a}(t)$, and the WTD for a "short" jump, $w_\mathrm{short}(t)=w_{x_R-a}^{x_R\to x_L+a}(t)=x_{x_L+a}^{x_L\to x_R-a}(t)$.

The ME results shown in Figs. 4.3(a,b), 4.4(b) pertain to a long jump. It is seen that the ME data become indeed consistent with those from the SE and BD approach, if one considers times *beyond* the growth region of the WTD.

Regarding the short-time behaviour, we find from Figs. 4.3(a,b) that the growth region of the WTD occurs at smaller times in the ME approach as compared to the SE and BD results. In other words, the WTD predicts non-zero waiting times already below the mean jump duration predicted by BD. More precisely, the inflexion point of the WTD occurs at (roughly) the inverse of the transition rate $\gamma=\gamma^+ + \gamma^-$ for *intra-well* transitions. In a linear approximation with respect to x_R and x_L of Eq. (3.19) one has $1/\gamma\approx\tau/(2u_0\pi^2)$, which yields a good estimate of the inflexion point. We conclude that it is the intra-well relaxation (which, in turn, is governed by the potential amplitude) which is the main ingredient determining the short time behaviour of the WTD given by the ME. Indeed, because the ME is based on a discrete model (and thus neglects travel times) we would not expect that the corresponding WTD is connected to the mean jump duration (as it was the case within the continuous SE approach).

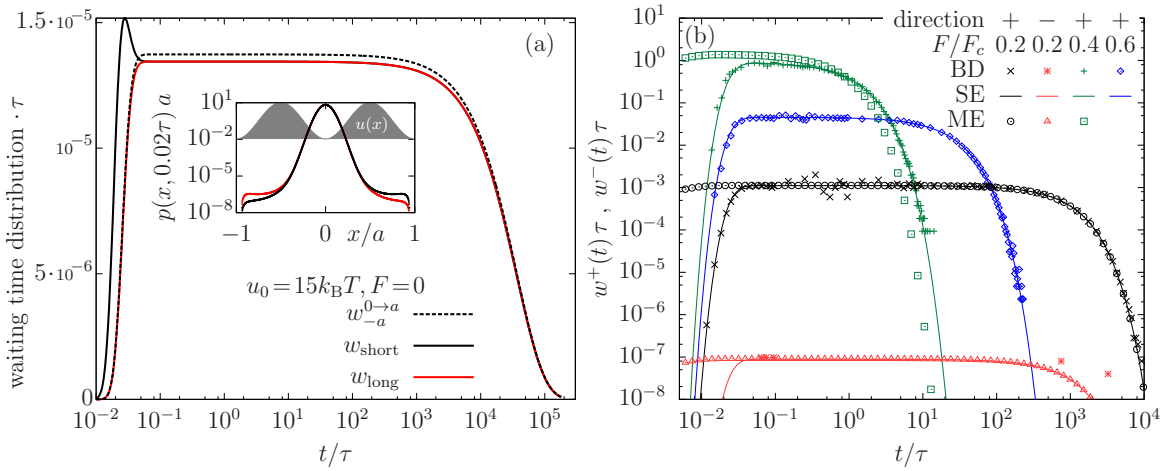

Fig. 4.5: Asymmetric situations. (a) Asymmetric boundary and initial conditions: semilogarithmic plot of the WTDs w_{short}, w_{long} and $w_{-a}^{0\to a}$ calculated with the SE. Inset: Probability density $p(x,t)$ at $t = 0.02\tau$ for the long and short jump. The tiny plateaus at $|x|/a \approx 1$ determine the WTD. (b) Driven system: double-logarithmic plot of the WTD for the jump to the right $w^+(t)$ and to the left $w^-(t)$ (SE and BD) or $w_{++}(t)$ and $w_{--}(t)$ (ME), respectively. A positive force F makes a jump to the left very unlikely which results in very small values for $w^-(t)$. Only for the smallest force $F = 0.2F_c$ the BD recorded such events. Every red star is only a single jump.

We finally note that asymmetric initial conditions such as those used in ME ($x_{L/R} \neq 0$) can also be incorporated into the SE approach. As described before, we can distinguish between the WTD for a "long" jump, $w_{\text{long}}(t)$, and the WTD for a "short" jump $w_{\text{short}}(t)$. In Fig. 4.5(a) we show these two WTDs together with our earlier SE result for $w_{-a}^{0\to a}(t)$. At short times, $w_{\text{short}}(t)$ has a global maximum which exceeds the corresponding values of $w_{\text{long}}(t)$ and the maximum of $w_{-a}^{0\to a}(t)$, that is, Kramers' escape rate. At subsequent time the two WTDs $w_{\text{long/short}}$ then merge at a value slightly below $w_{-a}^{0\to a}$. This is because the blip of w_{short} reduces the survival probability which in turn reduces the escape rate. The inset of Fig. 4.5(a) shows the probability densities $p(x,t)$ corresponding to w_{long} and w_{short} at $t = 0.02\tau$ where the WTDs deviate from each other. At $t = 0.02\tau$ the asymmetrically initialised densities have been broadened by diffusion to reach the boundaries, but yet not strong enough to eliminate the asymmetry.

4.3.2 Driven system ($F > 0$)

We now consider driven systems. Again, minima of the potential occur every a, the first being located at $x = m := a/(2\pi)\arcsin(F/F_c)$. Because of the tilt of the potential, we have to distinguish between jumps to the left, $w^-(t) = w_{m+a}^{m\to m-a}(t)$, and jumps to the right, $w^+(t) = w_{m-a}^{m\to m+a}(t)$. Clearly, these WTDs provide directional information, which cannot be extracted from the first passage time distribution.

Results for the WTDs in the "deep well" case are shown in Fig. 4.5(b). It is seen that the general structure of the WTD (consisting of a growth region, a plateau, and then a rapid decay) is the same as that at $F = 0$ (see Fig. 4.3(b)). One main effect of increasing F from

zero is that the global maximum of w^+ increases, while the time range corresponding to the plateau shortens. In other words, the average waiting time decreases and it occurs with larger probability. This is plausible, since a non-zero driving force leads to a lower *effective* barrier $\Delta u(u_0, F)$ (defined in Eq. (1.13)) in the driving direction. The opposite effects occurs against the driven direction, as reflected by the decreasing maxima in $w^-(t)$. We also note that, for each F, the effects in the two WTDs are coupled via the normalisation condition, i.e., the maximum in one of the WTDs can only grow at the expense of the other one.

Comparing the different methods, we see from Fig. 4.5(b) that the WTDs calculated with the SE agree with the BD results at all times. The WTDs given by the ME are consistent with SE and BD results for intermediate and long times. Again we observe a deviation for short times because, as discussed in the previous section, the short time scale in the two-state-per-well model describes intra-well relaxation and there is no time scale connected to the mean jump duration.

4.4 Numerical solution

4.4.1 WTD from BD simulations

To obtain a reliable WTD the recorded histograms must have a high statistical quality at all times where the WTD is nonzero. Any deviation influences the normalisation and therefore shifts the entire WTD. Typically, the domain of non-zero WTD spans several orders of magnitude. Moreover, for large times the WTD decays exponentially (see Fig. 4.4(b)) which enhances the computational effort due to the need of many long simulations. These considerations imply that the histogram bins must be sufficiently small to capture the time variations of the WTD and sufficiently large to yield a good statistical average. Here we use a piece-wise constant bin size distribution, which we adjust manually.

To achieve the necessary accuracy in the generated trajectories we choose a time step of $\Delta t = 10^{-5}\tau$. This sets the mean size of a fluctuation to $4 \cdot 10^{-3} a$ which is necessary to sample the potential sufficiently accurate.

The simulation starts with the particle at the first minimum $m = a/(2\pi) \arcsin(F/F_c)$. During the simulation the trajectory is analysed to record leavings and arrivals of the particle at other minima $m \pm ka$, $k \in \mathbb{Z}$. Because one simulation alone cannot produce enough jumps in a reasonable computation time, we run several simulations in parallel. The least amount of jumps occur at $u_0 = 15 k_\mathrm{B} T$ and $F = 0$. In this case we run 832 simulations in parallel or successively, each computing 500 jumps, to achieve a reasonable resolution for the long time part of the WTD.

Short waiting times occur even less frequently than large ones. To calculate the WTD at these short times a new set of simulations is started. Contrary to the regular trajectory simulation, the new simulations stop if the jump does not happen in a given time interval u (with $\log_{10}(u/\tau) \in \{-1, \ldots, 2\}$). Each histogram for the Figs. 4.3(a), 4.3(b) and 4.5(b) is made of about 10^4 of those short and 10^5 long waiting times.

4.4.2 WTD from the SE

To calculate the WTD from the SE we mainly use the FTCS (forward-time-centred-space) discretisation scheme (cf. section 2.6.1). Because the whole process is determined by a very

small current j over the barrier and, correspondingly, small values for the probability density (see inset in Fig. 4.5(a)) we need very small discretisation steps Δx, a typical example being $\Delta x = 0.0016a$. Nevertheless, the FTCS method works for all parameter sets except for $u_0 = 15k_BT$, $F = 0$ where the solution of the SE just takes too long. To calculate the long-time part of the WTD in this particular case we use a different method involving a Fourier transform, described in section 2.6.4. We exploit the fact that for the special case $F = 0$ with A, B, C being successive minima of $u(x)$ the set of basis functions of the Fourier transform Eq. (2.100) can be reduced to

$$s_n(x) = \sin\left(\pi n \frac{x+a}{2a}\right), \tag{4.15}$$

which fulfil the absorbing boundary conditions. We can write the Fourier transformation of the probability density as

$$p(x,t) = \sum_{n=1}^{N} p_n(t)\, s_n(x) \tag{4.16a}$$

$$p_n(t) = \frac{1}{a}\int_{-a}^{a} \mathrm{d}x\, s_n(x)\, p(x,t)\,. \tag{4.16b}$$

Applying the Fourier transform (4.16) to Eq. (3.1) yields

$$\dot{p}_n(t) = \frac{\pi^2}{4a^2}\Big(-n^2 p_n + n u_0 (p_{n-4}\Theta(n-4) - p_{n+4} - p_{4-n}\Theta(4-n))\Big), \tag{4.17}$$

where $\Theta(x)$ is the Heaviside-step function. The numerical solution of Eq. (4.17) takes even longer than FTCS. Therefore we use the diagonalisation method, introduced in section 2.6.4, to calculate the vector of Fourier components $\mathbf{p}(t)$. The computation of $\mathbf{p}(t)$ via Eq. (2.105) is fast and reliable. Specifically, for the case $u_0 = 15k_BT$ we find that 100 Fourier modes are sufficient (computations finish in minutes even for 10^4 modes).

A further advantage of the diagonalisation is that it provides a simple access to the long time dynamics. This is because the limit $\lim_{t\to\infty} \partial_t \ln w(t)$ gives the largest eigenvalue d. To see this we first calculate the WTD in terms of $\mathbf{p}(t)$

$$w_a^{0\to -a}(t) = -j(-a,t) = \partial_x p|_{x=-a} = \sum_{i=1}^{N} p_n(t) s_n'(-a)\,, \tag{4.18}$$

where

$$s_n'(x) = \frac{\pi n}{2a}\cos\left(\pi n \frac{x+a}{2a}\right). \tag{4.19}$$

We express Eq. (4.18) as a scalar product

$$w_a^{0\to -a}(t) = \frac{\pi}{2a}\mathbf{n}\cdot\mathbf{p}(t) \tag{4.20}$$

where $\mathbf{n}$ is the vector of the natural numbers from 1 to N. We insert the diagonalisation Eq. (2.105)

$$w_a^{0\to -a}(t) = \frac{\pi}{2a}\mathbf{n}\cdot S\cdot e^{Dt}\cdot S^{-1}\cdot \mathbf{p}(0) \tag{4.21}$$

$$= \mathbf{b}^T\cdot e^{Dt}\cdot \mathbf{c} \tag{4.22}$$

$$= \sum_{i=1}^{N} b_i e^{d_i t} c_i\,, \tag{4.23}$$

where we introduced the vectors $\mathbf{b}$ and $\mathbf{c}$ to group the time-independent parts together. We now can calculate the limit

$$\lim_{t\to\infty}\partial_t \ln w_a^{0\to -a}(t) = \lim_{t\to\infty}\frac{\sum_{i=1}^N b_i d_i e^{td_i} c_i}{\sum_{i=1}^N b_i e^{td_i} c_i} \tag{4.24}$$

$$= d_{\max} = \max_i d_i\,. \tag{4.25}$$

From this result we can verify our claim that the WTD decays exponentially

$$w_a^{0\to -a}(t) \propto e^{td_{\max}}\,. \tag{4.26}$$

Since $d_{\max}$ is negative and close to zero, the decay constant in Table 4.1 is $-d_{\max}$.

4.5 Connection between jump duration distribution and WTD

We begin by analysing the Brownian motion in Fig. 4.1 again. We consider the trajectory as a sequence of *excursions* which are separated by the times at which the trajectory crosses a potential minimum. We have borrowed the term excursion from [352]. For high barriers, most excursions end at the minimum they started. The others are the jumps we considered earlier.

For simplicity we first consider the symmetric case where $F = 0$. The system then is inversion-invariant. So an excursion either returns to its starting point or crosses a barrier. The probability densities for the time that the excursion ends the returning or the crossing way are $w_a^{\epsilon\to 0}(t)$ and $w_0^{\epsilon\to a}(t)$, respectively, where $\epsilon \ll a$. These densities were already introduced in section 4.3.1 above Eq. (4.13) which defines the jump duration distribution. Knowing the statistics of one excursion we begin to assemble the whole motion by concatenating excursions. We are interested in the WTD $w_{-a}^{0\to a}(t) = w_a^{0\to -a}(t)$. Let one jump have ended at t_0. The probability density for the particle to cross a barrier in the first excursion, ending at t_1, is

$$c_1(t_1 - t_0) = w_0^{\epsilon\to a}(t_1 - t_0)\,. \tag{4.27}$$

The probability density to return in the first excursion is

$$r_1(t_1 - t_0) = w_a^{\epsilon\to 0}(t_1 - t_0)\,. \tag{4.28}$$

If the first excursion did not lead to a crossing of the barrier, the particle has subsequent attempts. The probability density to have crossed the barrier at the end of the second

excursion at $t = t_2$ is connected to the joint probability of returning at the first attempt and crossing at the second one. The subsequent excursions are uncorrelated, such that the joint probability is $r_1(t_1 - t_0) w_0^{\epsilon \to a}(t_2 - t_1)$ where t_1 is the time of the end of the first excursion. To include all possible paths we integrate over all possible times t_1 which yields the probability density to cross the barrier at $t = t_2$ at the end of the second excursion

$$c_2(t_2 - t_0) = \int_{t_0}^{t_2} \mathrm{d}t_1 \, r_1(t_1 - t_0) \, w_0^{\epsilon \to a}(t_2 - t_1) \, . \tag{4.29}$$

The probability density to return at the second excursion, too, reads

$$r_2(t_2 - t_0) = \int_{t_0}^{t_2} \mathrm{d}t_1 \, r_1(t_1 - t_0) \, w_a^{\epsilon \to 0}(t_2 - t_1) \, . \tag{4.30}$$

Consequently, the probabilities to cross exactly after the nth excursion and to return n excursions in a row are

$$c_n(t_n - t_0) = \int_{t_0}^{t_n} \mathrm{d}t_{n-1} \, r_{n-1}(t_{n-1} - t_0) \, w_0^{\epsilon \to a}(t_n - t_{n-1}) \tag{4.31}$$

$$r_n(t_n - t_0) = \int_{t_0}^{t_n} \mathrm{d}t_{n-1} \, r_{n-1}(t_{n-1} - t_0) \, w_a^{\epsilon \to 0}(t_n - t_{n-1}) \, . \tag{4.32}$$

The WTD is the probability density to cross at time t at any excursion. Because all excursions are uncorrelated and the c_n describe disjoint events, we can simply add all c_n yielding

$$w_{-a}^{0 \to a}(t) = \sum_{n=1}^{\infty} c_n(t) \, . \tag{4.33}$$

The calculation of the WTD via Eq. (4.33) involves infinitely many nested integrals over $w_a^{\epsilon \to 0}$. A simplification is possible by using the convolution theorem of the Laplace transform. We define the Laplace transform of a function $a(t)$ by

$$\mathcal{L}[a](s) = \int_0^{\infty} \mathrm{d}t \, e^{-st} \, a(t) \, . \tag{4.34}$$

It can be shown that

$$\mathcal{L}\left[\int_0^t \mathrm{d}t' \, b(t - t') \, c(t') \right](s) = \mathcal{L}[b](s) \, \mathcal{L}[c](s) \, . \tag{4.35}$$

The integrals in Eqs. (4.31), (4.32) are of this type. Hence,

$$\begin{aligned} \mathcal{L}[c_n](s) &= \mathcal{L}[r_{n-1}](s) \, \mathcal{L}[w_0^{\epsilon \to a}](s) \\ &= \left(\mathcal{L}[w_a^{\epsilon \to 0}](s) \right)^{n-1} \mathcal{L}[w_0^{\epsilon \to a}](s) \, . \end{aligned} \tag{4.36}$$

We can calculate the Laplace transform of the desired WTD by

$$\mathcal{L}[w_{-a}^{0 \to a}](s) = \mathcal{L}[w_0^{\epsilon \to a}](s) \sum_{n=0}^{\infty} \left(\mathcal{L}[w_a^{\epsilon \to 0}](s) \right)^n \, . \tag{4.37}$$

The Laplace transform can be inverted numerically by using the Gaver-Stehfest algorithm [353].

We now turn to the asymmetric case, discussed in section 4.3.2. The discretisation points are at the local minima. In section 4.3.2 we defined m as the position of the first minimum. There are two types of excursions beginning at m: to the left and to the right. The probability densities to overcome or to return are $w_m^{m-\epsilon\to m-a}$ and $w_{m-a}^{m-\epsilon\to m}$ to the left, respectively, or $w_m^{m+\epsilon\to m+a}$ and $w_{m+a}^{m+\epsilon\to m}$ to the right. We assume the normalisations $1 = \int \mathrm{d}t(w_m^{m-\epsilon\to m-a}(t) + w_{m-a}^{m-\epsilon\to m}(t))$ and $1 = \int \mathrm{d}t(w_m^{m+\epsilon\to m+a}(t) + w_{m+a}^{m+\epsilon\to m}(t))$. We assume that a left excursion follows a right one and vice versa. For simplicity, we assume that the choice of the direction of the first excursion has no bias, i.e. they occur with equal probability 1/2. Then, the probability densities to cross the left, c_1^-, or right, c_1^+, barrier in the first excursion read

$$c_1^+(t_1 - t_0) = \frac{1}{2} w_m^{m+\epsilon\to m+a}(t_1 - t_0) \tag{4.38a}$$

$$c_1^-(t_1 - t_0) = \frac{1}{2} w_m^{m-\epsilon\to m-a}(t_1 - t_0)\,. \tag{4.38b}$$

The corresponding return densities read

$$r_1^+(t_1 - t_0) = \frac{1}{2} w_{m+a}^{m+\epsilon\to m}(t_1 - t_0) \tag{4.39a}$$

$$r_1^-(t_1 - t_0) = \frac{1}{2} w_{m-a}^{m-\epsilon\to m}(t_1 - t_0)\,. \tag{4.39b}$$

In the same manner as above we define the probability densities for the nth excursion recursively, yielding

$$c_n^\pm(t_n - t_0) = \int_{t_0}^{t_n} \mathrm{d}t_{n-1}\, r_{n-1}^\mp(t_{n-1} - t_0)\, w_m^{m\pm\epsilon\to m\pm a}(t_n - t_{n-1}) \tag{4.40a}$$

$$r_n^\pm(t_n - t_0) = \int_{t_0}^{t_n} \mathrm{d}t_{n-1}\, r_{n-1}^\mp(t_{n-1} - t_0)\, w_{m\pm a}^{m\pm\epsilon\to m}(t_n - t_{n-1})\,. \tag{4.40b}$$

We define the WTDs $w_+(t)$ and $w_-(t)$ discussed in section 4.3.2 by

$$w^+(t) = \sum_{n=1}^{\infty} c_n^+(t) \quad , \quad w^-(t) = \sum_{n=1}^{\infty} c_n^-(t)\,. \tag{4.41}$$

Again, Laplace transforms can be used to circumvent the integrals

$$\mathcal{L}[c_n^\pm](s) = \mathcal{L}[r_{n-1}^\mp](s)\, \mathcal{L}[w_m^{m\pm\epsilon\to m\pm a}](s) \tag{4.42a}$$

$$\mathcal{L}[r_n^\pm](s) = \mathcal{L}[r_{n-1}^\mp](s)\, \mathcal{L}[w_{m\pm a}^{m\pm\epsilon\to m}](s)\,. \tag{4.42b}$$

4.6 Conclusion

In this chapter we have introduced and compared several routes to calculate the WTD in a system with continuous, Markovian dynamics. Specifically, we have considered the example

of a Brownian particle in an one-dimensional tilted washboard potential, and focused on cases where the potential barriers are large against the thermal energy. The same example was used in chapter 3 where we find complementary insights about the motion in terms of the cumulants of position.

Traditionally, the WTD in such a situation is calculated by analysing trajectories, e.g. obtained from BD simulations of the Langevin equation. Here we define the WTD on the basis of the corresponding Smoluchowski equation (SE); i.e., we identify the WTD with one of the outgoing currents calculated from the SE with absorbing boundaries. The resulting WTD is closely related to the first passage time distribution; however, the WTD contains directional information which is usually not present in the FPTD. This becomes particularly important in spatially asymmetric situations. Moreover, our definition of the WTD is more versatile than the FPTD in that the usage of WTDs naturally involves a dependence on special initial and/or boundary conditions. Although our result can be formulated in terms of FPTDs, we chose the term WTD due to its broader usage in the field of quasi-discrete and direction-dependent stochastic processes.

Analysing a variety of systems with different initial conditions, as well as with and without external drive, we find in all cases full quantitative agreement between the SE and BD results for the WTD. We also stress that, due to our rather general definition of the WTD in the SE approach, we are able to calculate additional quantities such as the jump duration distribution. The latter is crucial for understanding the growth behaviour of the WTD at short times.

In addition to the SE (and BD) method, we have also presented a fully analytic master equation approach to the WTD. The ME approach is based on the discrete, two-state-per well model introduced in chapter 3. Comparing the results with those from SE and BD it turns out that the ME yields a very accurate WTD at intermediate times, where it exhibits a plateau, as well as at long times, where it has an exponential tail. Only the short-time behaviour differs due to the fact that the ME model's (only) short time scale is the "intra-well" relaxation time, which precisely determines the short-time behaviour of the cumulants of position in chapter 3. In the continuous approaches a third time scale between intra-well relaxation and inter-well relaxation can be identified, which is the mean jump duration.

From a computational point of view the BD route to the WTD seems, at first glance, to be the most straightforward one. However, closer inspection shows that the results are quite dependent on the definition of "jumps". Furthermore, the results are often quite noisy. Here, the SE approach where noise is averaged out *a priori*, is clearly superior. We stress, however, the solution is computationally expensive and "fragile" when using a standard solver. In section 4.4.2 we have therefore sketched an alternative route to obtain the WTD from the SE based on a Fourier transform.

Finally, our SE approach to the WTD can be easily generalised to systems characterised by a different potential, to interacting systems, and to systems with higher dimensionality. For example, for processes involving more than one spatial dimension, one would simply replace the absorbing boundary value by an absorbing surface and calculate the WTD as an integral over the probability current over a part of the surface [339]. Another generalisation concerns the character of the dynamics, which we here assumed to be Markovian. For a non-Markovian SE (for examples see [132,354,355] or the system studied in chapter 5) which involves memory kernels and thus has higher dimension in time, the FPTD can be applied straightforwardly

[132, 356, 357]. Therefore, and due to the similarity between WTD and FPTD we expect that the identification of the WTD with the probability current remains intact. Finally, our generalisation of the WTD for continuous systems opens the route to calculate other quantities typically reserved for discrete (Markovian or non-Markovian) systems, such as the idle-time distribution [358].

5. TIME DELAYED FEEDBACK CONTROLLED ROCKING RATCHET

In this chapter we present the results from our collaboration [359] with Sarah A. M. Loos, Phys. Rev. E **89**, 052136 (2014). We investigate the transport of a single colloidal particle in a static asymmetric periodic potential supplemented by a homogeneous force which is controlled by time delayed feedback. Feedback control (introduced in section 1.6) means that the time-dependent evolution of the system is influenced based on information from the system itself. For a nonzero delay time the feedback control force develops regular oscillations. Due to the ratchet effect, introduced in section 1.5.2, a net transport of the particle emerges.

As already mentioned in section 1.6, feedback control is an established method to manipulate the dynamics of various sorts of systems, including colloidal transport. A prime example for the generation of transport in ratchet systems by using feedback control is the feedback controlled flashing ratchet demonstrated in [91]. The effectiveness of ratchet-like feedback controls is measured against corresponding open-loop controls [360, 361], which are the Brownian ratchets introduced in section 1.5.2.

Time delay is inherent in the feedback process. In the feedback controlled flashing ratchets time delay decreases the net current [226, 235, 236]. However, other systems benefit from time delay. Pyragas' control is a time delayed feedback control which can stabilise desired states in a dynamical system [239, 362]. It is applied to sheared liquid crystals [219] and in nonlinear optics to study all-optical calculation [220, 363]. Time delay is an essential ingredient in models for population dynamics [250, 364] and brain dynamics [221, 365]. Moreover, it generates new effects such as the reversal of the current in one-dimensional transport [124, 366], spatio-temporal oscillations in extended systems [355, 367], and, in general, oscillations in numerous systems [368].

The development of non-equilibrium stochastic thermodynamics [55, 242, 312] is connected to feedback control twofold. On the one hand, feedback control is more versatile than open-loop control so that it enables the direct test of principles of non-equilibrium statistical mechanics [100, 195, 224, 245, 247]. On the other hand, stochastic thermodynamics had to be extended to incorporate feedback control and time delay [238, 243, 245].

Feedback controls optimise. Our control enhances the net current of a single Brownian particle in a one-dimensional asymmetric potential under the influence of a time-dependent homogeneous force. In contrast to the classical rocking ratchet [211, 369] where the homogeneous force is an externally given oscillating function, our force switches, i.e. reverses its sign, if the mean particle displacement at a previous time $t - \tau_D$, where τ_D is the time delay, crosses a "switching position". The control target in our model, the mean displacement, is an ensemble averaged quantity. This is different from previous studies where the control target itself is stochastic [91, 226, 243, 360]. From the point of view of these latter controls, our

control represents the limit case of controlling infinitely many non-interacting particles. This limit is a good approximation for dilute colloidal suspensions [70, 82]. We model the motion with the SE (2.13) where the delayed feedback force enters directly. We note that the connection between LE and SE is not straightforward in the presence of time delay [354, 370, 371]. However, the usual connection, i.e. Eq. (2.9), holds for a control target which is an ensemble average. We discuss this issue in section 5.5. Through numerical solution of a SE, we show that it is the time delay which generates current in our system. Moreover, by varying the switching position we achieve a net current which is higher than in the corresponding open-loop control.

The model was developed by Sarah. A. M. Loos and Sabine H. L. Klapp. The numerical solution is based on Sarah's work during her Bachelor thesis which I supervised. I later joined the project and made significant contributions to the interpretation of the findings, to numerical calculations, figures, and writing.

5.1 Definition of the model

We consider the motion of a single particle (as in the previous chapters) in a one-dimensional, "sawtooth" potential [76, 91, 372], defined by $u_R(x+a) = u_R(x)$ and

$$u_R(x) = \begin{cases} \frac{u_0 x}{\psi a}, & 0 < x \leq \psi a, \\ \frac{u_0 x}{(\psi-1)a}, & (\psi-1)a < x \leq 0\,, \end{cases} \tag{5.1}$$

where u_0 is the potential height, a is the period, and $\psi \in [0,1]$ is the asymmetry parameter. In contrast to the tilted washboard used in the other chapters, u_R is asymmetric already without tilt. An illustration of $u_R(x)$ is given in Fig. 5.1(a). Here we choose $a = 8\sigma$, and $\psi = 0.8$. The potential minimum is at $x = x_{\min} = 0$.

We model the motion via the SE (2.13) for the probability density $p(x,t)$ where we set the force $f(x,t)$ in Eq. (2.13) to $f(x,t) = -u_R'(x) + F(t)$ which yields the SE

$$\partial_t p(x,t) = -\partial_x j = D_0 \partial_{xx} p(x,t) + \frac{D_0}{k_\mathrm{B}T} \partial_x \left((u_R'(x) - F(t)) p(x,t) \right) . \tag{5.2}$$

In the absence of any further force beyond that arising from $u_R(x)$, i.e. $F(t) = 0$, the system approaches for $t \to \infty$ an equilibrium state and thus there is no transport (i.e., no net particle current). It is well established, however, that by supplementing $u_R(x)$ by a time-dependent oscillatory force (yielding a rocking ratchet), the system is permanently out of equilibrium and macroscopic transport can be achieved [9, 211, 369]. This occurs even when the time-average of the oscillatory force is zero, a characteristic feature of a true thermal ratchet.

Here we propose an alternative driving force, where the time dependency arises only through the *internal state* of the system. Thus, the force applies feedback control onto the system. As control target we consider the mean particle position

$$\bar{x}(t) = \int_S \mathrm{d}x\, p(x,t)\, x \tag{5.3}$$

within the central interval $S = [(\psi-1)a, \psi a[$ where $p(x,t)$ is the probability density calculated with periodic boundary conditions on Eq. (5.2), that is, $p(x+a,t) = p(x,t)$.

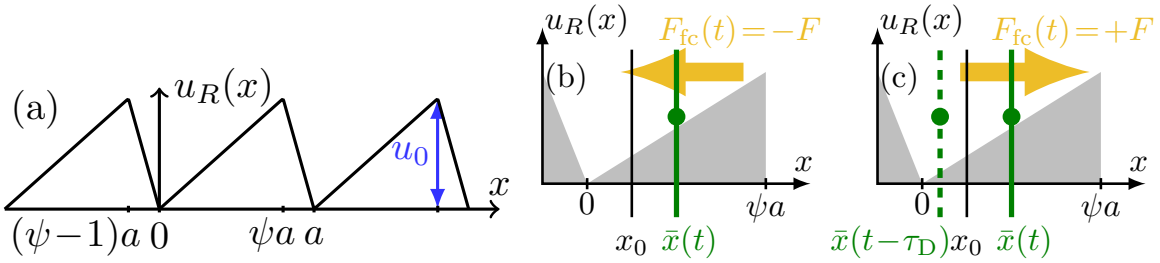

Fig. 5.1: (a) Sketch of the static "sawtooth" potential, defined in Eq. (5.1). The central interval S is defined by $(\psi-1)a \le x \le \psi a$. (b,c) Sketch of the static potential and the direction of the force $F_{\rm fc}(t)$ (b) in the absence of time delay ($\tau_{\rm D}=0$) and (c) with time delay. The vertical lines indicate the switching position x_0, as well as the non-delayed [i.e. $\bar{x}(t)$] and delayed control target [i.e. $\bar{x}(t-\tau_{\rm D})$].

Our reasoning behind choosing the *mean* rather than the true position as control target is twofold: First, within the SE treatment we have no access to the particle's position for a given realisation of noise, because the latter has already been averaged out. This is in contrast to previous studies using Langevin equations [91, 226, 235] where the dynamical variable is the particle position itself. Second, the mean position is an experimentally accessible quantity, which can be monitored, e.g., by video microscopy [77, 226, 252].

Our ansatz for the force reads

$$F_{\rm fc}(t) = -F\ \mathrm{sign}(\bar{x}(t-\tau_{\rm D}) - x_0)\,, \tag{5.4}$$

where F is the amplitude (chosen to be positive), x_0 is a fixed position within the range $[0, \psi a]$ (where u_R increases with x), and the sign function is defined by $\mathrm{sign}(y) = +1$ (-1) for $y > 0$ $(y < 0)$. From Eq. (5.4) one sees that the feedback force changes its sign whenever the delayed mean particle position $\bar{x}(t-\tau_{\rm D})$ becomes smaller or larger than x_0; we therefore call x_0 the "switching" position.

Our ansatz is partially motivated by an earlier (Langevin equation based) study of Craig *et al.* [226] on feedback control of a flashing ratchet via the so-called "maximum-displacement strategy". In that study, the fixed position x_0 was identified with the mean particle position of the *uncontrolled system* (i.e., $F_{\rm fc}(t) = 0$) at $t \to \infty$, that is, the equilibrium position $\bar{x}_{\rm eq} = \int \mathrm{d}x x p_{\rm eq}(x)$, where $p_{\rm eq}(x) \propto \exp\left(-u_R(x)/k_{\rm B}T\right)$. Here we rather regard x_0 as a free parameter.

Another main feature of our driving mechanism is the presence of a time delay, $\tau_{\rm D}$. As discussed in several studies [226, 235–238, 363, 368, 373], time delay is a rather natural phenomenon which may arise, e.g., through the finite time required for measuring or processing information from a measurement. In the present case, as we will demonstrate below, the time delay is indeed *crucial* for generating particle transport.

5.2 Transport mechanism

To better understand the impact of the force, defined in Eq. (5.4), let us briefly consider the case $\tau_{\rm D} = 0$. For simplicity, we set $x_0 = \bar{x}_{\rm eq} \approx 0.32\sigma$. In Fig. 5.1(b) we illustrate a

situation, where the mean particle position at time t is on the right hand side of x_0. In this case $F_{\rm fc} = -F$, meaning that the force tends to push the particle towards x_0. In analogous manner we find that $F_{\rm fc} = +F$ if the particle is left from x_0. As time is progressing the mean particle position thus becomes "trapped" at x_0. Clearly, this excludes any net transport.

However, transport can be generated in the presence of a non-zero time delay, $\tau_{\rm D} > 0$. Figure 5.1(c) shows as an example a situation where the mean particle position at time t is at the right side of x_0, while it has been on the left side at time $t - \tau_{\rm D}$. In this situation the force $F_{\rm fc}(t)$ points *away* from x_0 (i.e., $F_{\rm fc} > 0$), contrary to the case $\tau_{\rm D} = 0$ considered in Fig. 5.1(b). Thus, the particle experiences a driving force towards the next potential valley, which changes only when the delayed position becomes larger than x_0. The force then points to the left until the delayed position crosses x_0 again. This oscillation of the force (see also Sec. 5.3.1), together with the asymmetry of $u_R(x)$, creates a ratchet effect.

We note that the feedback-controlled ratchet introduced here strongly differs from previous models of such systems. In particular, Feito *et al.* [374] have considered a rocking ratchet composed of a static potential similar to ours plus an oscillatory drive. Feedback-control (based on the average particle force) is then introduced as a prefactor in front of the static potential; i.e., the latter is switched on only if the force satisfies certain requirements. In the present model, the control force acts in addition to the static potential, and there is no additional oscillating force.

Another, somewhat subtle aspect of the present model is that we introduce feedback on the level of the Fokker-Planck equation describing the evolution of the probability density. This is different from earlier studies based on the Langevin equation (see, e.g., [91,226,235]), where the feedback is applied directly to the position of one particle, $\chi_i(t)$, or to the average of N particle positions $N^{-1}\sum_{i=1}^{N}\chi_i(t)$. Introducing feedback control in such systems implies to introduce effective *interactions* between the particles [360]. As a consequence, the transport properties in these particle-based models depend explicitly on the number of particles, N. Typically, it turns out that the current becomes small or even vanishes when the particle number increases, the reason being that fluctuations (which are essential for the ratchet effect) disappear [360]. From the perspective of these Langevin-based models, the present model corresponds to the "mean-field" limit $N \to \infty$. This connection to a Langevin model is further discussed in section 5.5. Given that we are in the "mean-field" limit, it is even more interesting that we do observe a non-vanishing current which can be even larger than in an open-loop system [360]. This is because our model involves a time delay.

5.3 Numerical results

5.3.1 Dynamics of the control target

In this section we present numerical results for the feedback-controlled transport based on numerical solution of the SE (5.2). The height of the static potential is set to $u_0 = 15k_{\rm B}T$. In fact, similar values are found in experiments of colloids in structured light fields [82, 89, 91]. Time is measured in units of the Brownian timescale, $\tau_{\rm B} = \sigma^2/D_0$, which is of the order of $10^0 s$ to $10^2 s$ for typical colloids [82,89,91,186,204] (see also Table 2.1 in section 2.1.2). In all calculations, the initial condition for the probability density is a δ-function localised at the minimum of $u_R(x)$, $x_{\rm min} = 0$. Further, to initialise the control force, we set a history function, i.e. $\bar{x}(t) = x_{\rm min} = 0$ for $t \in [-\tau_{\rm B}, 0]$. In fact, we have performed various test calculations

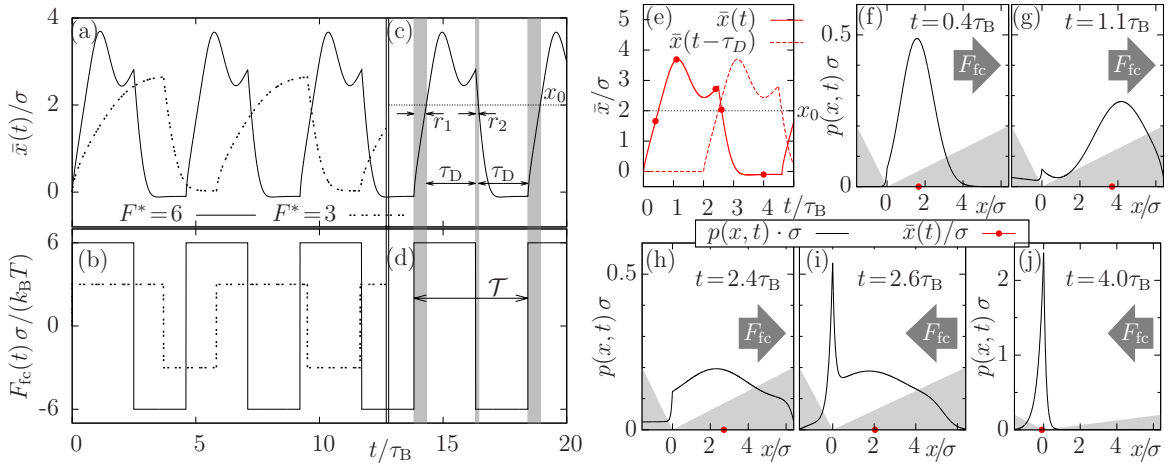

Fig. 5.2: (a) Mean particle position and (b) control force as functions of time for $\tau_D = 2\tau_B$, $x_0 = 2\sigma$ and $F^* \in \{3, 6\}$. In (c) and (d) the oscillation is divided into segments by the times at which F_{fc} changes (left border of the shaded regions) and the times the mean particle position crosses x_0 (right border). (e) One cycle of the function $\bar{x}(t)$ at $\tau_D = 2\tau_B$ and $F^* = 6$, with the filled circles indicating specific times. The switching position is set to $x_0 = 2\sigma$. Also shown is the corresponding function $\bar{x}(t - \tau_D)$. (f)-(j) Density distribution as function of space at the times indicated in (e). The thick arrows show the direction of the control force. The filled (red) circles indicate the values of $\bar{x}(t)$.

involving other (than delta-like) initial densities and other history functions. However, the effect of the initial conditions was found to be only of transient character. The data presented in the following correspond to time ranges after an initial (yet very short) "equilibration" period, after which the dynamic quantities considered display a regular dynamical behaviour, i.e. the system is not in a transient state.

We start by considering the time evolution of the mean particle position, $\bar{x}(t)$, which determines the control force. Exemplary data for two amplitudes $F^* = F\sigma/k_BT$ are shown in Fig. 5.2(a), where the parameter x_0 has been set to 2σ, and $\tau_D = 2\tau_B$. It is seen that $\bar{x}(t)$ displays regular oscillations between values above and below x_0 for both force amplitudes considered. The period of these oscillations, $\mathcal{T}$, is roughly twice the delay time. We will come back to this point later in this section. We also note that the *precise* value of the period as well as the shape of the oscillations depend on the values of F^* and x_0 (see also Sec. 5.3.2).

Due to the oscillatory behaviour of $\bar{x}(t)$, the delayed position $\bar{x}(t - \tau_D)$ oscillates around x_0 as well. It follows from our definition of the feedback force [see Eq. (5.4)], that the latter switches periodically between $+F$ and $-F$ with the same period as that observed in $\bar{x}(t)$. This is clearly seen in Fig. 5.2(b) where we plotted $F_{fc}(t)$.

A closer view on the dynamic behaviour within one cycle is given in Fig. 5.2(e-j), where we focus on the case $\tau_D = 2\tau_B$ and $x_0 = 2\sigma$. Figure 5.2(e) depicts one cycle of the function $\bar{x}(t)$ together with its time-delayed counterpart, $\bar{x}(t - \tau_D)$. The parts (f-j) of Fig. 5.2 then plot the probability density p as function of x for specific times indicated by filled circles in Fig. 5.2(e).

The mean particle position starts from $\bar{x} = 0$ (i.e., localisation in the potential minimum) at $t_0 = 0$. The value $F^* = 6$ of the amplitude F^* is that large that the total systematic force $-u_R'(x) + F_{\rm fc}$ at $t = 0$ is positive for every x. Hence, at $t = 0.4\tau_{\rm B}$ [part (f)], the density distribution has broadened by diffusion and $\bar{x}(t)$ has moved to the right. We also see from Fig. 5.2(f) that the probability density is still very small at the boundary $x = \psi a$. This changes at $t = 1.1\tau_{\rm B}$ when probability "flows" over the boundary, indicating transport [see part (g)]. The function $\bar{x}(t)$ is now in its maximum. At $t = 1.1\tau_{\rm B}$ the mean particle position has already crossed x_0; however, the time delayed mean particle position is still below x_0, and thus, $F_{\rm fc}(t) > 0$. Note that due to the periodicity of the system an inward probability flow occurs at the lower boundary $x = (\psi-1)a$. With progressing time this eventually leads to a shift of the mean particle position towards smaller values, as seen in Fig. 5.2(h) for the case $t = 2.4\tau_{\rm B}$. When $\bar{x}(t - \tau_{\rm D})$ crosses x_0 the feedback control force is reversed. The total systematic force is now positive for $x < 0$ and negative for $x > 0$. The confining effect of this force to the particle can be seen in Fig. 5.2(i) where a peak in the probability density evolves. As a consequence, the mean particle position moves towards values around the potential minimum. When the same happens to the delayed position $\bar{x}(t - \tau_{\rm D})$, the cycle starts again.

From the above considerations it follows that [as illustrated in Figs. 5.2(c) and (d)], each cycle consists of two intervals of duration $\tau_{\rm D}$ which are separated by smaller time intervals r_1 and r_2. The latter correspond to the times which the control target needs to reach x_0 after the control force has switched. Thus the duration of the total period is $\mathcal{T} = 2\tau_{\rm D} + r_1 + r_2$. We note that this finding is independent of the chosen initial conditions.

We also remark that in order to see *persistent* oscillations of the control target and thus, the control force, it is crucial that the function contained in $F_{\rm fc}$ is very sensitive to even tiny differences between $\bar{x}(t - \tau_{\rm D})$ and x_0. Indeed, besides the sign-function we have also tested continuous functions such as $\sin(y)$ [or $\cos(y)$], which tend to zero when $\bar{x}(t - \tau_{\rm D}) - x_0 \to 0$ [or $\pi/2$]. In these cases, the oscillations just dampen out and thus, there is no ratchet effect.

5.3.2 Effective current

So far we have focused on the mean particle position $\bar{x}(t)$ within one interval, defined in Eq. (5.3), i.e., the quantity determining our feedback force. However, to visualise the particle transport, it is more convenient to consider the distance $\tilde{x}(t)$ the particle has actually travelled at time t (in the ensemble average) relative to its value at $t = t_0$. Contrary to $\bar{x}(t)$, the travelled distance $\tilde{x}(t)$ takes into account that the particle actually moves from one potential valley to the next.

To this end we first introduce the particle current

$$\bar{j}(t) = \int_S \mathrm{d}x\, j(x,t)\,, \tag{5.5}$$

with the probability current $j(x,t) = -D_0\partial_x p + D_0(F(t) - u_R')p/k_{\rm B}T$ given by the SE (5.2). As shown in Ref. [9], by using the periodic boundary conditions which p obeys, this current can also be expressed as

$$\begin{aligned}\bar{j}(t) &= \frac{\mathrm{d}}{\mathrm{d}t}\left[\int_{x_{\rm ref}}^{x_{\rm ref}+a} \mathrm{d}x\, x\, p(x,t)\right] + a\, j(x_{\rm ref},t) \\ &= \frac{\mathrm{d}}{\mathrm{d}t}\bar{x}(t) + a\, j(x_{\rm ref},t)\,,\end{aligned} \tag{5.6}$$

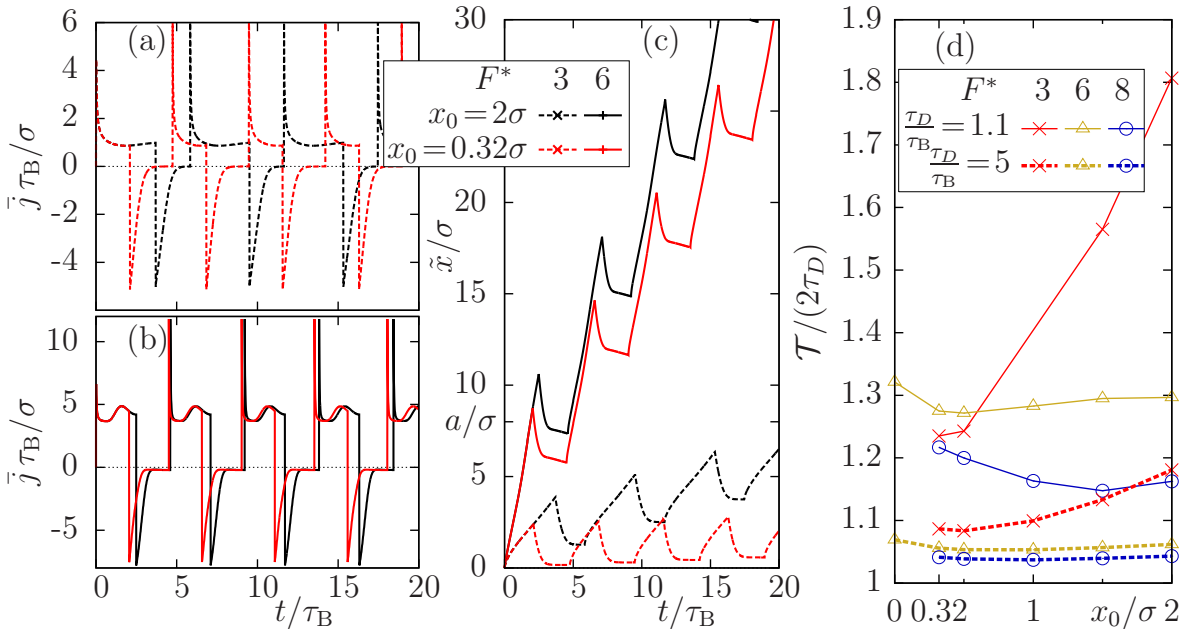

Fig. 5.3: (a), (b) Space-averaged current density $\bar{j}$ as function of time for (a) $F^* = 6$ and (b) $F^* = 3$ (and different switching positions). (c) Travelled distance $\tilde{x}$ as function of time. In all parts the delay time is set to $\tau_D = 2\tau_B$. (d) Mean period of the oscillations of the control target in dependence of x_0 and F^* (for $\tau_D \in \{1.1\tau_B, 5\tau_B\}$).

where x_{ref} is an arbitrary reference position within the central interval. Here we choose x_{ref} equal to $(\psi-1)a$, that is, the lower boundary of the central interval. Equation (5.6) expresses the fact that the particle current is composed of the motion of the "centre of mass" plus a times the probability current (evaluated for the periodic system) at the reference point. We now define $\tilde{x}(t)$ as the time integral of $\bar{j}(t)$, yielding

$$\tilde{x}(t) = \int_{t_0}^{t} \mathrm{d}t'\, \bar{j}(t') = \bar{x}(t) + a \int_{t_0}^{t} \mathrm{d}t'\, j(x_{\mathrm{ref}}, t')\,, \tag{5.7}$$

where we have used that $\tilde{x}(t_0) = \bar{x}(t_0)$. Through relation (5.7) and interpreting $\tilde{x}(t)$ as mean travelled distance, we give $\bar{j}(t)$ the interpretation of the mean velocity of the particle.

Numerical results for $\tilde{x}(t)$ and $\bar{j}(t)$ are plotted in Fig. 5.3(a-c) for different values of the control force parameters F^* and x_0. The delay time is kept fixed. In all cases considered, $\tilde{x}(t)$ displays a regular "back-forth" rocking motion, but with a net drift to the right – indicating particle transport. Also shown in Fig. 5.3 is the mean velocity $\bar{j}$ defined in Eq. (5.5). It is seen that $\bar{j}(t)$ reflects the rocking-like behaviour of $\tilde{x}(t)$ by oscillations around zero. The fact that positive values dominate signals the presence of net transport.

Not surprisingly, both the current and the strength of the drift visible in $\tilde{x}(t)$ depend on the amplitude of the control force, as one can clearly see by comparing the dashed and solid curves in Fig. 5.3(a-c). However, we also observe a significant influence of the position x_0: The larger x_0, the longer are the times in which the travelled distance increases in each cycle and in which the current is positive. We understand this behaviour such that, the larger x_0, the longer the time in which the mean particle position in the central interval S is below x_0

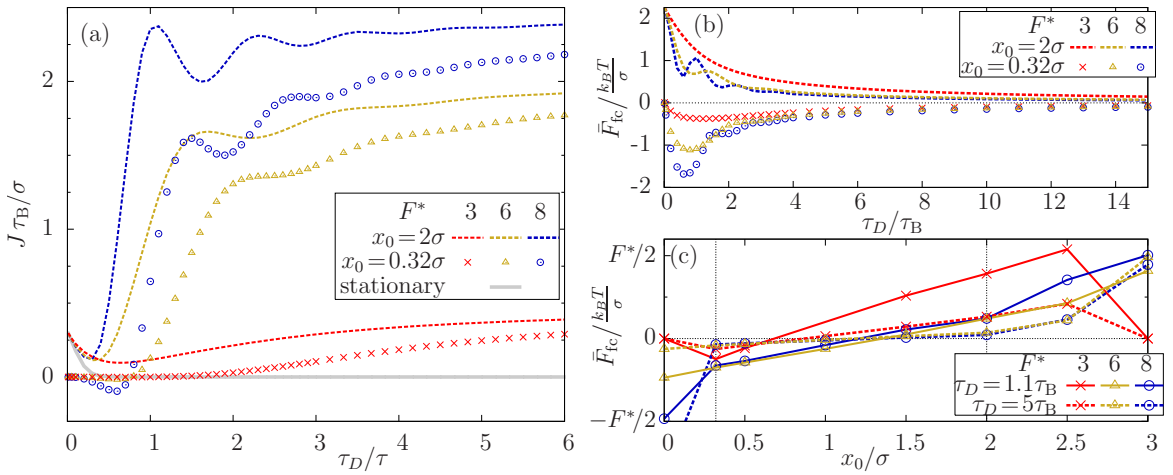

Fig. 5.4: (a) Net particle current J as function of the delay time for several values of F^* and x_0. The curve termed "stationary" is discussed below Eq. (5.9). (b,c) Time-averaged control force $\bar{F}_{\rm fc}(t)$ as function of (b) the delay time and (c) the switching position x_0. In (c), the dotted lines indicate the boundaries of the range of switching positions where we consider the transport being essentially delay-induced.

(yielding $F_{\rm fc} > 0$). The period $\mathcal{T}$ of the oscillations of $\tilde{x}(t)$ and $\bar{j}(t)$ slightly increases with x_0 as well. An overview of the dependence of $\mathcal{T}$ on x_0 and F^* is given in Fig. 5.3(d). In all cases, $\mathcal{T}$ is *roughly* given by twice the delay time, however, its actual value depends on the precise choice of the control force parameters.

Having understood the time-dependence of the control target and the current density we now turn to the overall (time-averaged) transport. The latter is measured by the net particle current defined as

$$J = \mathcal{T}^{-1} \int_{t_1}^{t_1+\mathcal{T}} \mathrm{d}t'\, \bar{j}(t')\,, \tag{5.8}$$

where $\bar{j}(t)$ is defined in Eq. (5.5), and t_1 is a time after the transients. Numerical results for J in dependence of the delay time $\tau_{\rm D}$ and force amplitude F^* are plotted in Fig. 5.4(a), where we consider two switching positions.

We first discuss the behaviour at finite delay times in the range $\tau_{\rm D} \approx 5\tau_{\rm B}$. In this range the current generally increases with $\tau_{\rm D}$, with the values being the larger the larger the force amplitude and the switching position are. This is consistent with our earlier findings regarding the particle's travelled distance and the time-dependent current (see Fig. 5.3). We also see from Fig. 5.4(a) that all curves saturate in the limit of large $\tau_{\rm D}$ at some finite value of J. This limit value solely depends on F^* which we discuss later with the adiabatic approximation Eq. (5.11), shows as dashed horizontal lines in Fig. 5.5(a) which shows $J(\mathcal{T})$.

At small delay times ($\tau_{\rm D} < 5\tau_{\rm B}$) the behaviour of the function $J(\tau_{\rm D})$ strongly depends on both, F^* and x_0. For $x_0 = 0.32\sigma$, the net current vanishes at $\tau_{\rm D} \to 0$ regardless of the strength of the drive, consistent with our previous considerations that the ratchet effect in our model is essentially driven by the time delay. Upon increasing $\tau_{\rm D}$ the current then deviates from zero. Interestingly, for large force amplitudes ($F^* = 6$, 8), J may even become *negative*

before finally increasing towards positive values. Note that negative values imply transport *opposite* to the direction supported by the asymmetric potential.

Considering now the larger switching position $x_0 = 2\sigma$, we observe again a strong decrease of the current when we decrease the time delay from large values. However, contrary to the situation at $x_0 = 0.32\sigma$, $J(\tau_D)$ stays *finite* in the limit $\tau_D \to 0$. We can understand this behaviour, as well as the negative currents arising at $x_0 = 0.32\sigma$ and $F^* = 8$, by considering the time average of the control force,

$$\bar{F}_{fc} = \mathcal{T}^{-1} \int_{t_1}^{t_1+\mathcal{T}} dt' \, F_{fc}(t') \, . \tag{5.9}$$

Figure 5.4(b) plots the averaged control force as function of τ_D. Considering first the case $x_0 = 0.32\sigma$, we see that $\bar{F}_{fc}(\tau_D)$ approaches zero in the limit of vanishing delay time. In other words, there is no *average* drive, which justifies to consider the present transport mechanism as a true (delay-induced) ratchet effect. For small τ_D, however, there is a minimum in the function, which becomes the more pronounced the larger F is. The negative values of $\bar{F}_{fc}(\tau_D)$ are responsible for the negative net current J arising in the same range of delay times (see Fig. 5.4(a)). Therefore, the appearance of negative J here has a different origin than in the open-loop controlled case [211].

At $x_0 = 2\sigma$ the average force is non-zero and positive throughout the entire range of delay times, becoming largest in the limit $\tau_D \to 0$. We note, however, that at any finite delay time the absolute value of $\bar{F}_{fc}$ is quite small. To check the influence of this remaining force we have calculated the current $\bar{j}$ defined in Eq. (5.5) for a system under the time-constant force $F(t) = \bar{F}_{fc}(\tau_D)$, taking the case $F^* = 6$, $x_0 = 2\sigma$ as an example. It turns out that this current, which is shown in Fig. 5.4(a) by the curve termed "stationary", is indeed negligible except at $\tau_D \to 0$. Thus, we can conclude that even with this larger switching position the ratchet effect is essentially delay-induced. A more systematic view of the dependence of $\bar{F}_{fc}$ on x_0 is given in Fig. 5.4(c), where we focus on specific, finite values of τ_D. It is seen that, outside the range $0.32\sigma \leq x_0 \leq 2\sigma$ (see vertical dotted lines in Fig. 5.4(c)), the average force deviates significantly from zero. In these cases, it becomes questionable to which extent the current is really induced by time delay. Therefore we have restricted x_0 to values inside the interval defined above.

At this point it is worth to compare the current generated by our feedback-controlled ratchet with that of an ordinary, "open-loop" rocking ratchet. To this end we supplement the static periodic potential given in Eq. (5.1) by a time-periodic drive characterised by a fixed period $\mathcal{T}_{ol}$ with vanishing time average. To be as close as possible to our feedback model [see Eq. (5.4)], we choose a *rectangular* oscillatory drive

$$F_{osc}(t) = -F \, \text{sign} \left[\cos\left(\frac{2\pi}{\mathcal{T}_{ol}} t \right) \right] \, . \tag{5.10}$$

For a discussion of the *deterministic* version of this model we refer to [375]. In the present, noisy system we calculate the resulting net current via Eq. (5.8) after replacing $\mathcal{T}$ by $\mathcal{T}_{ol}$. In Fig. 5.5(a) we show numerical results for J as function of the oscillation period, together with the corresponding functions $J(\mathcal{T})$ for a feedback-controlled ratchet with two values of x_0.

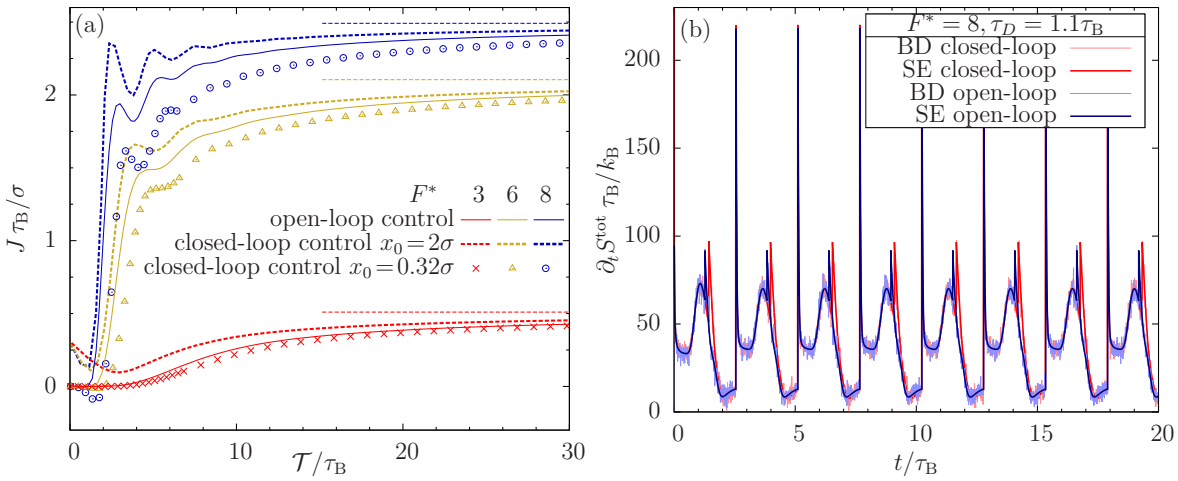

Fig. 5.5: (a) Net particle current J for the open-loop rocking ratchet, given by Eq. (5.10), and the feedback-controlled ratchet in dependency of the (mean) oscillation period of the driving force. The horizontal lines pertain to the adiabatic limit [see Eq. (5.11)]. (b) Total entropy production as function of time for $F^* = 8$, $\tau_D = 1.1\tau_B$, and $x_0 = 2\sigma$, and for the corresponding open-loop-controlled ratchet with $F^* = 8$ and $\mathcal{T}_{ol} = 2.558\tau_B$. Included are results based on BD simulations of the Langevin equation (see section 5.5).

While the general behaviour of the current (that is, small values of J for small periods, saturation at large values for large periods) is similar for both, open-loop and closed-loop systems, the actual values of J for a given period strongly depend on the type of control. This is seen already at very small periods where, e.g., the current of the closed-loop system with $x_0 = 0.32\sigma$ can become negative, while that of the open-loop system is still zero. The most interesting differences, however, occur at finite periods which are still below those corresponding to the saturation regime.

Comparing curves with the same value of F^* we find that the net current in the open-loop system is larger than in the closed-loop system with small switching position ($x_0 = 0.32\sigma$), but *smaller* than in the closed-loop system with $x_0 = 2\sigma$. In other words, the net current, which is the measure for transport, can be larger in the feedback-controlled system than that in the open-loop case, provided that the switching position is sufficiently large. At very large periods, however, the currents corresponding to a given value of F approach the same values. The latter correspond to the "adiabatic limit" ($\mathcal{T} \to \infty$), where the drive changes so slowly so that the system can be assumed to be in a stationary state at every time t [9]. This allows to calculate the current analytically, yielding

$$J = \frac{D_0 a}{\mathcal{T}} \int_0^{\mathcal{T}} \mathrm{d}t \left(1 - e^{-\frac{aF(t)}{k_B T}}\right) / \mathcal{N}(t) \tag{5.11}$$

$$\mathcal{N}(t) = \int_S \mathrm{d}x\, e^{-\frac{u_R(x) - xF(t)}{k_B T}} \int_x^{x+a} \mathrm{d}x'\, e^{\frac{u_R(x') - x'F(t)}{k_B T}} ,$$

where $F(t) = F_{\mathrm{osc}}(t)$ and $F(t) = F_{\mathrm{fc}}(t)$ for the open- and closed-loop case, respectively.

5.4 Entropy production and work

In view of our results for the net current in the feedback-controlled ratchet, on the one hand, and the open-loop controlled rocking ratchet, on the other hand (see Fig. 5.5(a)), it is interesting to further explore the impact of the control scheme in terms of (non-equilibrium) thermodynamics introduced in section 2.5. In particular, we are interested in the *total entropy production*, which measures how far the system is away from equilibrium, and in the *work* that is performed on the particle. We calculate these quantities on the basis of stochastic thermodynamics. For systems with *instantaneous* feedback control this is a well-established field [55, 312]. This is generally not the case for systems with time delay, in which the underlying (Langevin or Master) equations of motion become *non-Markovian* such that concepts of standard stochastic thermodynamics (which assumes Markovian dynamics) are not immediately applicable [238, 243].

In the present case the situation is somewhat easier because we are working in a mean-field limit. As discussed in section 5.5, this limit allows us to establish a connection between our SE and an underlying Langevin equation; it also allows us to consider our delayed feedback control force just as a special type of time-dependent force. In the following we stress this argument further and use various SE-based standard formula for thermodynamic quantities. To test the SE results we compare with those obtained from trajectory-based expressions via Brownian Dynamics (BD) simulations.

We start by considering the *ensemble-averaged* total entropy production, $\dot{S}^{\mathrm{tot}}$. Within stochastic thermodynamics, the total entropy $s^{\mathrm{tot}}(t)$, for a single trajectory $\chi(t)$, consists of two contributions [55], i.e., $s^{\mathrm{tot}}(t) = s(t) + s^{\mathrm{m}}(t)$. Here, $s(t) = -k_{\mathrm{B}} \ln p(\chi(t), t)\sigma$ is the trajectory-dependent entropy of the "system" (i.e., the particle), and $s^{\mathrm{m}}(t) = q[\chi(t)]/T$ is the medium entropy related to the heat $q[\chi(t)]$ dissipated into the medium. Upon averaging over the ensemble of trajectories [55], one finds the following compact expression for the time-derivative (production rate) of the total entropy

$$\dot{S}^{\mathrm{tot}}(t) = k_{\mathrm{B}} \int_S \mathrm{d}x \, \frac{j(x,t)^2}{D_0 \, p(x,t)} \,, \tag{5.12}$$

where $j(x,t)$ is the probability current [see Eq. (5.2)].

Numerical results for $\dot{S}^{\mathrm{tot}}$ are shown in Fig. 5.5(b) where we focus on a situation where the net current in our closed-loop scheme is larger than in the open-loop system. Included are results for the corresponding open-loop system (in which $\mathcal{T}_{ol} := \mathcal{T}$). For both the closed-loop and the open-loop system, $\dot{S}^{\mathrm{tot}}(t)$ displays periodic behaviour with similar features. First, the beginning of a new cycle is indicated by a very large and narrow peak. After the peak, $\dot{S}^{\mathrm{tot}}(t)$ decreases to a small, yet non-zero value and then rises towards a second, broader maximum, followed by a further sharp peak. The latter is related to the change of the feedback force from positive to negative values. For the open-loop system this happens exactly in the middle of the cycle [see Eq. (5.10)]. In the closed-loop system, the change is somewhat shifted. This deviation is indeed the main difference between the closed-loop- and the open-loop-controlled system.

We have also calculated the total entropy production by BD simulations based on the LE (5.16). On that level, the rate of change of the system entropy is given as $\dot{S}(t) = -k_{\mathrm{B}}\mathrm{d}/\mathrm{d}t\langle \ln p(\chi(t), t)\sigma\rangle$, with $\langle \ldots \rangle$ being a noise average. In practice, we have evaluated

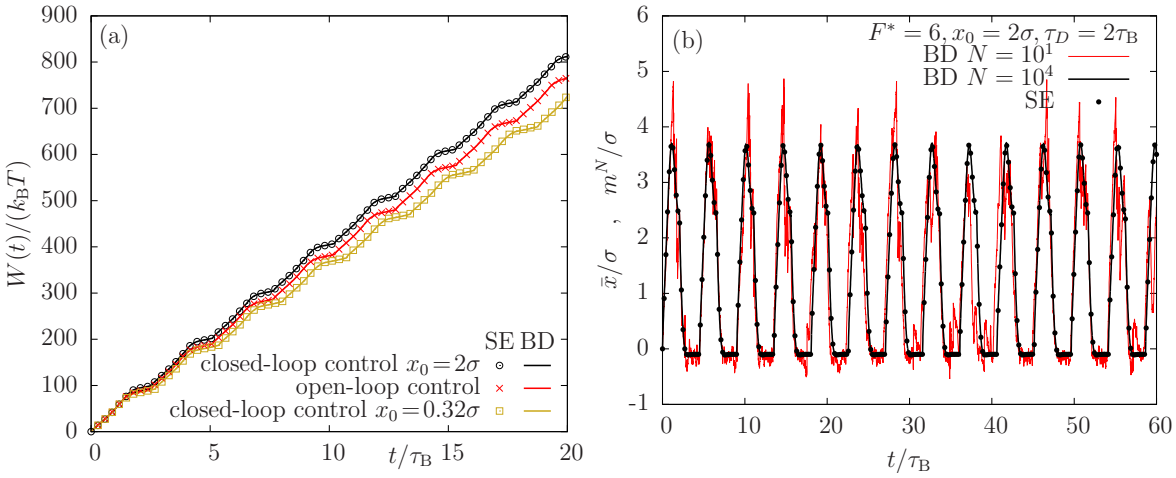

Fig. 5.6: (a) Work performed on the particle as function of time for $F^* = 8$, $\tau_D = 1.1\tau_B$, and two switching positions x_0. Included are results for the corresponding system under open-loop control. (b) BD simulation results for the mean particle position as function of time and particle number N. Indeed, the solution of the LE for many particles ($N = 10^4$) coincides with the results from the SE.

$\dot{S}$ using the relation $\langle \ln p(\chi(t),t)\sigma\rangle = \int_S \mathrm{d}x\, p(x,t) \ln p(x,t)\sigma$ where we use the microscopic definition of the probability density Eq. (2.8), i.e. $p(x,t) = \langle \delta(x-\chi(t))\rangle$. Further, the medium entropy [55] is given by

$$\dot{S}^{\mathrm{m}}(t) = \langle (-u_R'(\chi(t)) + F_{\mathrm{fc}}^N(t))\dot{\chi}(t)/T\rangle\,. \tag{5.13}$$

To evaluate this expression we have used the Stratonovich interpretation. It is seen in Fig. 5.5(b) that the BD data (which have been obtained with $N = 10^5$) are fully consistent with those from the SE approach.

To calculate the work performed on the particle we note that, contrary to the dissipated heat, the work involves only changes of the total systematic force at fixed particle position [55] which is, in our case, $F_{\mathrm{fc}}(t)$. On the level of a single trajectory $\chi(t)$ the work therefore reads

$$w[\chi(t)] = \int_0^t \mathrm{d}t'\, F_{\mathrm{fc}}(t')\,\dot{\chi}(t')\,. \tag{5.14}$$

To achieve a description in terms of the SE we make use Eq. (2.90) (implicitly assuming again that the time delayed feedback control force enters the SE just like a special time-dependent force). The noise-averaged work is then given by

$$W(t) = \int_0^t \mathrm{d}t'\, F_{\mathrm{fc}}(t') \int_S \mathrm{d}x\, j(x,t')\,. \tag{5.15}$$

In Fig. 5.6(a) we compare the time-dependence of the work for the closed-loop system with two different switching positions with the corresponding open-loop system. It is seen that the work increases in each cycle, with the strongest ascent taking place in those portions of the cycle where the force is positive. Furthermore, comparing the two systems with feedback

control, we find that the amount of work needed to transport the particle is larger for the system with $x_0 = 2\sigma$, than for the one at $x_0 = 0.32\sigma$. We recall that the net current is larger at $x_0 = 2\sigma$, too (see Fig. 5.5(a)). Figure 5.6(a) also shows that the work pertaining to the system under open-loop control has qualitatively a similar time dependence, with the numerical values being in between those of the two feedback-control ratchets. In other words, in our system feedback control does not necessarily imply that the energy input is smaller than that in a comparable open-loop device.

5.5 Connection between Langevin and Smoluchowski equation in the presence of delayed feedback

In this section we discuss the connection of the SE (5.2) and the Langevin equation

$$\gamma\dot{\chi}_i(t) = -u_R'(\chi_i) + F_{\rm fc}^N(m^N(t-\tau_{\rm D})) + \sqrt{2\gamma k_{\rm B}T}\xi_i(t)\,, \tag{5.16}$$

where $u_R(\chi_i)$ is given by Eq. (5.1), $\xi_i(t)$ represents Gaussian white noise, $i \in \{1,\ldots,N\}$, and

$$F_{\rm fc}^N(t) = -F\mathrm{sign}\left[m^N(t-\tau_{\rm D}) - x_0\right] \tag{5.17}$$

with

$$m^N(t) = \frac{1}{N}\sum_{i=1}^{N}\chi_i(t)\,. \tag{5.18}$$

Thus, m^N is the average of the positions of the N particles.

For the special case $N = 1$, one has obviously $m^1(t) = \chi_1(t)$ and thus, $F_{\rm fc}^{N=1}(t) = -F\mathrm{sign}\left[\chi_1(t-\tau_{\rm D}) - x_0\right]$. Then, Eq. (5.16) has the form discussed in earlier studies on delayed Langevin equations [354, 370, 371]. For such systems, the problem in going from the LE to the SE is that the feedback control force depends on the *full* microscopic (stochastic) trajectory of the particle in phase space up to time t. Therefore, the resulting SE involves the conditional probability that the particle was at position x' at time $t-\tau_{\rm D}$ *given* that it is at position x at time t. An SE which is formally similar to the usual one [involving only $p(x,t)$] can then be obtained by introducing a "delay-averaged force", that is, the integral over space of $F_{\rm fc}^{N=1}(t)$ times the conditional probability [243, 354].

Now we consider the "mean-field" limit $N \to \infty$. For each time t, averaging over an infinite number of particles is equivalent to averaging over the infinite number of realisations of the stochastic force. Therefore, the quantity m^N in Eq. (5.18) becomes identical to the ensemble-averaged particle position, i.e., $\lim_{N\to\infty} m^N(t) = \bar{x}(t)$. As a consequence, the force $F_{\rm fc}^N(t)$ does not depend any more on a stochastic quantity, in other words, the information about the individual stochastic trajectories at time $t-\tau_{\rm B}$ is no longer required. In the "mean-field" limit, we can thus consider the feedback force as a conventional time-dependent force entering the "mean-field" version of Eq. (5.16), that is,

$$\gamma\dot{\chi}(t) = -u_R'(\chi) + F_{\rm fc}(\bar{x}(t-\tau_{\rm D})) + \sqrt{2\gamma k_{\rm B}\mathcal{T}}\xi(t)\,. \tag{5.19}$$

From Eq. (5.19), we can derive the SE in the standard way, i.e., by using the Kramers-Moyal (KM) expansion [10]. The calculations are, in principle, straightforward; in particular,

there is no problem with multiplicative noise in the mean-field limit. The only uncommon issue arises through the fact that our feedback force changes its sign *abruptly* when $\bar{x}(t-\tau_\mathrm{D})$ crosses x_0. We thus consider in more detail the first ("drift") KM coefficient

$$D^{(1)}(x,t) = \lim_{\tau\to 0}\frac{1}{\tau}\langle(\chi(t+\tau)-x)_{\chi(t)=x}\rangle\,. \tag{5.20}$$

The expression in brackets is evaluated through

$$\chi(t+\tau)-\chi(t) = \int_t^{t+\tau}\mathrm{d}t'\,\dot{\chi}(t') \tag{5.21}$$

which can be treated by inserting Eq. (5.19) for $\dot{\chi}$ into Eq. (5.21), iteratively (see [10]). Due to the limit $\tau\to 0$ and the noise average incorporated in $D^{(1)}$ [see Eq. (5.20)] all terms $\mathcal{O}(\tau^2)$ as well as terms involving $\langle\xi(t)\rangle$ vanish. The remaining task is to evaluate the term

$$I(t) = \lim_{\tau\to 0}\frac{1}{\tau}\int_t^{t+\tau}\mathrm{d}t'\,F_\mathrm{fc}(\bar{x}(t'-\tau_\mathrm{D}))\,. \tag{5.22}$$

The problem with Eq. (5.22) is that, if $F_\mathrm{fc}(\bar{x}(t'-\tau_\mathrm{D}))$ changes its sign in the interval $[t,t+\tau]$, the limit $\tau\to 0$ of $I(t)$ does not exist. Therefore, we make the *assumption* that the time between two switching events has a lower bound, t^*. Further, we define that at the switching times t_s (when $\bar{x}(t_\mathrm{s}-\tau_\mathrm{D})=x_0$) the force $F_\mathrm{fc}(t_\mathrm{s})$ is already set to the new value. For all τ in the interval $[0,t^*[$ we then have $F_\mathrm{fc}(t+\tau_\mathrm{fc}(t)$. As a consequence, Eq. (5.22) yields $I(t)=F_\mathrm{fc}(\bar{x}(t-\tau_\mathrm{D}))$ and the first KM coefficient becomes

$$D^{(1)}(x,t) = \frac{1}{\gamma}(-u_R'(x)+F_\mathrm{fc}(\bar{x}(t-\tau_\mathrm{D})))\,. \tag{5.23}$$

With this expression (and the usual result $D^{(2)}=k_\mathrm{B}T/\gamma$), one arrives directly at the SE (5.2).

In order to check our argumentation, we have performed Brownian Dynamics simulations of Eq. (5.16) for different values of N. Representative results for the quantity $m^N(t)$ are plotted in Fig. 5.6(b), where we have included corresponding results for $\bar{x}(t)$ from the SE. We see that the results become fully consistent if N is sufficiently large.

5.6 Conclusion

In this chapter we have presented a novel type of a rocking ratchet system, where the particle is subject to a space-dependent, asymmetric potential and a time-dependent, homogeneous feedback control force. The control target is the time-delayed mean particle position relative to a switching position, x_0. The dynamical properties are mainly studied with a Fokker-Planck equation, where the time-delayed feedback force is introduced *ad hoc*. We have established a connection to a corresponding Langevin equation with mean-field coupling.

To explore the transport properties of our system we have investigated the net current in dependence of the parameters of the control force, that is, delay time, amplitude and switching position. Our results clearly show that the time delay involved in the feedback protocol is *essential* for the creation of a ratchet effect and, thus, for a nonzero net current.

A further important ingredient is the discontinuous dependence of the feedback force on the control target.

An important question for every feedback-controlled system is its efficiency relative to a comparable system under open-loop control. We have found, indeed, that for a certain range of switching positions (and not too large delay times), the net current is *enhanced* relative to the open-loop system. At the same time, however, the work performed on the particle is larger in the feedback-controlled system. This finding is somehow in contrast to a recent result for another ratchet system [312] where, at the same time, the current was enhanced and the work was *reduced* by feedback control. Another interesting question is to which extent the present feedback scheme, which relies on the (time-delayed) mean particle position as a control target, could be improved, e.g., to realise an even larger net current. In fact, as indicated in Fig. 5.5(a), the current J does not exceed its value pertaining to the adiabatic limit, at least not for the range of switching positions considered here (recall that this range has been chosen such that the time-averaged force is close to zero). Therefore, it would be interesting to see whether larger values of J are achievable by choosing a different control target or by an otherwise modified control protocol.

So far, there exists no direct experimental realisation of the system proposed here, but the main ingredients are already well established. As mentioned in the introductory sections 1.5.2 and 1.6 ratchet potentials acting on colloids can be easily realised by using laser beams [87,91,204] (creating an optical line trap), and the position of a colloidal particle (or the mean position of many particles) is accessible, e.g., by video microscopy. Moreover, feedback control based on the particle position (or mean position) has already been realised experimentally, e.g. in the context of a feedback-controlled *flashing* ratchet [91] and a Maxwell demon [224]. Another ingredient, which is indeed crucial in our system, is the presence of a time delay. Experimentally, delay arises from various factors [236], including the time for numerical determination of particle positions via the camera and the time for the decision whether to switch the force. In section 1.6 we discussed the speed of modern experimental feedback controls with the conclusion that the time delay can be made small with respect to the Brownian time. This includes the regime of ratios τ_D/τ_B, where, according to the results presented in Fig. 5.4(a), the current strongly deviates from the adiabatic limit and, in particular, can be larger than in the open-loop protocol.

The mean-field limit we employed holds in the limit of a large number of particles in the system, as we discussed in section 5.5. In is an open question whether a feedback control, similar to ours, but operating with a finite number of particles can enhance the net current further. An ensemble averaged modelling of this motion, maybe in the spirit of the DDFT, would be very useful for further investigations.

6. SHORT TIME DIFFUSION OF SEVERAL PARTICLES

The results presented in this chapter are not published, yet.

We focus on the short time diffusion of interacting colloids in a tilted washboard potential in one dimension. Further, we address the long-time limit to discuss the diffusion coefficient. This is a sequel to chapter 3 where we studied the diffusion of a single particle. Interactions between particles have a pronounced influence on the diffusion, for short and long times. A slowing down of diffusion by repulsive particle interactions appears in dense suspensions, e.g. liquid crystals [139] or colloidal glasses [116, 141]. Attractive interactions slow diffusion down, too, which can result in the formation of gels [138, 144, 233]. Further, the interplay between attractive interactions and diffusion can create fractal structures [140].

Short time diffusion is actively studied for glasses [123, 136], gels [35, 326], liquid crystals [139], for colloids in light fields [82, 83, 87, 92], and in the development of feedback controls [376]. As we discussed in chapter 3, the MSD is an important quantity to describe short time diffusion. We have seen that a slow down of the diffusion from short to long times manifests as plateau in the MSD (cf. chapter 3 and section 1.3.4). If diffusion is enhanced we find a superdiffusive transient regime instead of a plateau in the MSD.

The analysis of long-time diffusion in periodic potentials has a long history. Much effort invested in the continuous time random walk models was targeted to diffusion coefficients for diffusion in three dimensions [128, 129]. The diffusion coefficient of a single Brownian particle in a tilted washboard potential is available analytically [125, 185]. Interestingly, the driving force (i.e. the tilt) has a strong influence on the diffusion coefficient D. For small driving forces D is several orders of magnitude smaller than D_0, the diffusion coefficient of free diffusion. In contrast, for driving forces F near the so-called *critical driving force* F_c [125] the ratio D/D_0 is much larger than 1. This effect is called giant enhancement of diffusion or, short, giant diffusion. It it seen in many other systems including ratchet systems [169, 186, 189], single file diffusion in tilted washboard potentials [147], and periodic potentials with oscillating components [190,377]. Giant diffusion is mainly studied with single particles and the effects of particle interaction are still not entirely clear. Studies of the giant diffusion effects considering particle interactions include a single particle with inner degrees of deformational freedom [149] and single file diffusion [147].

We focus on short time diffusion and giant diffusion of ultra-soft particles modelled by the Gaussian core model (GCM). These particles can overlap and do not show single file diffusion. Ultra-soft particle interaction is a model for the interaction of fluctuating polymer chains [299,378,379]. We find that the purely repulsive particle interaction enhances diffusion which leads to a shorter plateau in the MSD and emphasises the giant diffusion effect. Further, we study the short time diffusion of attractive hard particles.

We employ the dynamic test particle method to calculate the MSD via the van Hove correlation function [123] (see also section 2.4). We model the particle interactions with DDFT, introduced in section 2.3.1. The DDFT provides an effective potential landscape for the motion of the one-particle density by approximating the positional correlations by the equilibrium correlations. For our second system, the attractive hard spheres, this equilibrium assumption fails to predict single file diffusion [257,292,294]. However, the motion of a cluster formed by those particles can be correctly modelled with DDFT [272, 380]. Therefore, we restrict our analysis of the hard-sphere system to the dissociation of the cluster in dependence on interaction strength and driving force.

In the next section 6.1 we define the models for the two interacting systems and specialise the test particle method for our usage. In the results section 6.2 we first address the short time diffusion of ultra-soft particles, then giant diffusion of ultra-soft particles, and attractive hard spheres at the end. The chapter ends with the conclusion in 6.3.

6.1 Model

We consider the overdamped motion of N Brownian particles in one dimension under the influence of the tilted washboard potential $u(x)$, given by Eq. (1.11). On the particle level, the motion can be described by the N coupled LE (2.6).

We consider two types of interacting systems, that is, ultra-soft particles described by the GCM and attractive hard particles, where the attraction is modelled by a Yukawa potential.

The pair interaction potential according to the GCM reads

$$v_{\mathrm{GCM}}(d{=}|x_i - x_j|) = \varepsilon\, e^{-d^2/\sigma^2}\,. \tag{6.1}$$

This potential is a coarse-grained potential modelling the interaction of two fluctuating polymer chains, where the particle diameter σ is proportional to the polymers' radius of gyration [299, 378, 381].

The pair interaction potential of the hard-core-attractive-Yukawa (HCAY) system reads

$$v_{\mathrm{HCAY}}(d{=}|x_i - x_j|) = \begin{cases} \infty & d < \sigma \\ -Y \frac{\exp(K\sigma(1-r/\sigma))}{r/\sigma} & d \geq \sigma \end{cases}. \tag{6.2}$$

This potential is used to model attractive depletion interactions for the investigation of phase coexistence in colloidal suspensions [304, 382–384], but it is also used to model the attraction between oppositely charged colloids [385].

We are interested in the short time diffusion described by the MSD and the non-Gaussian parameter α. Further, we consider the long time diffusion where we extract an effective diffusion coefficient, if appropriate, from the MSD. Using the relations Eqs. (2.54) and (2.55) we express the MSD and α through the van-Hove function, introduced in section 2.4.

We employ the test particle method (see section 2.4.1) to compute an approximation to the van-Hove function by using conditional densities. The test particle method is a commonly used method to calculate correlation functions from conditional (one-particle) densities [123, 124, 139, 308, 386]. We employ the DDFT based test particle method (cf. section 2.4.2) in 1D,

governed by the extended Smoluchowski equations

$$\partial_t \varrho_\mathrm{s}(x,t;x_0) = D_0 \partial_{xx} \varrho_\mathrm{s} + \partial_x(\varrho_\mathrm{s} \partial_x (V_\mathrm{ext} + V_\mathrm{int}^\mathrm{s}))/\gamma \tag{6.3a}$$

$$\partial_t \varrho_\mathrm{d}(x,t;x_0) = D_0 \partial_{xx} \varrho_\mathrm{d} + \partial_x(\varrho_\mathrm{d} \partial_x (V_\mathrm{ext} + V_\mathrm{int}^\mathrm{d}))/\gamma \,. \tag{6.3b}$$

In Eq. (6.3) $\varrho_\mathrm{s}(x,t;x_0)$ is the one-particle density of the test particle which, according to Eq. (2.68), yields the self part G_s of the van-Hove function by averaging over the initial positions x_0. Analogously, the distinct part G_d can be inferred from $\varrho_\mathrm{d}(x,t;x_0)$. In Eq. (6.3), the effective interaction potential that one particle exhibits due to particle interaction with the other particles is denoted with $V_\mathrm{int}^{s/d}$. The effective interaction potentials are modelled with the DDFT, i.e.

$$V_\mathrm{int}^n(x,t) = \frac{\delta \mathcal{F}_\mathrm{int}^\mathrm{TPM,sub}[\varrho_\mathrm{s}, \varrho_\mathrm{d}]}{\delta \varrho_\mathrm{n}(x,t)} \quad \text{for } n \in \{\mathrm{s}, \mathrm{d}\} \,. \tag{6.4}$$

The functional $\mathcal{F}_\mathrm{int}^\mathrm{TPM,sub}$ is given by Eq. (2.75) which depends on the interaction part of Helmholtz free energy functional $\mathcal{F}_\mathrm{int}[\varrho]$.

For the GCM interaction we employ the mean-field free energy functional, defined in Eq. (2.50)

$$\mathcal{F}_\mathrm{int}^\mathrm{GCM}[\varrho] = \mathcal{F}_\mathrm{int}^\mathrm{MF}[\varrho, v_\mathrm{int}^\mathrm{GCM}] \,. \tag{6.5}$$

The mean-field approximation is reliable for ultra-soft particles in and outside equilibrium at intermediate and high density [54, 270, 387].

For the HCAY interaction we employ a common composition approach [260, 272, 284, 380]

$$\mathcal{F}_\mathrm{int}^\mathrm{HCAY}[\varrho] = \mathcal{F}_\mathrm{int}^\mathrm{hs1D}[\varrho] + \mathcal{F}_\mathrm{int}^\mathrm{MF}[\varrho, v_\mathrm{int}^\mathrm{HCAY}] \,, \tag{6.6}$$

where $\mathcal{F}_\mathrm{int}^\mathrm{hs1D}$, defined in Eq. (2.47), is the exact grand canonical equilibrium Helmholtz free energy functional for the interaction of hard spheres in one dimension.

6.2 Results

We solve Eqs. (6.3) numerically (see section 2.6 for details) under periodic boundary conditions in a system of size $L = 100a$. The initial condition for the test particle being located at $x = x_0$ reads

$$\varrho_\mathrm{s}(x,0;x_0) = \delta(x - x_0) \,. \tag{6.7}$$

For the other particles we compute the equilibrium density profile in a harmonic trap $u_Q(x) = 2u_0\pi^2 a^{-2} x^2$ in the presence of the test particle being fixed at x_0. The trap $u_Q(x)$ is the lowest order approximation to $u(x)$ for $F = 0$ around a minimum.

We set $u_0 = 15 k_\mathrm{B} T$ and $a = 8\sigma$. Due to symmetry, we only consider forces $F > 0$.

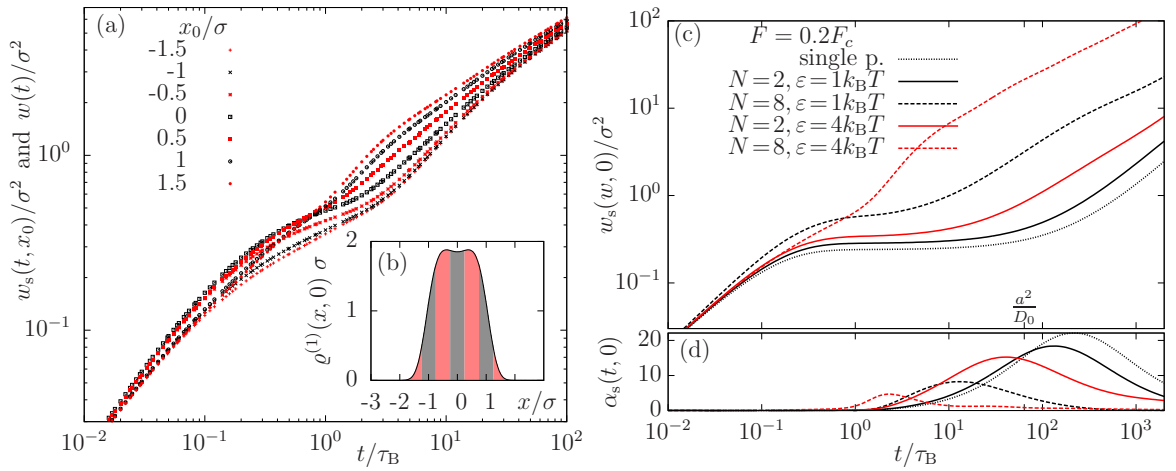

Fig. 6.1: (a) Width of ϱ_s, given by Eq. (6.8), for various initial positions of the test particle x_0 and the MSD $w(t)$, given by Eq. (2.54). The other parameters are $F = 0.2F_c, N = 4, \varepsilon = 4k_BT$. All $w_s(t,x_0)$ differ less than a factor 2 from $w(t)$. We use $w_s(t,0)$ for further investigations. (b) One-particle density $\varrho^{(1)}(x)$ corresponding to the initial condition (the particles are trapped in a harmonic potential). The vertical bars indicate the discretisation of the integral Eq. (2.68). (c) Double-logarithmic plot of $w_s(t,0)$ for different N and ε at $F = 0.2F_c$. Depending on the values of N and ε a subdiffusive region (a plateau) or a superdiffusive region establishes. (d) Non-Gaussian parameter $\alpha_s(t,0)$ which shows a pronounced peak at a time when the plateau (if any) ends.

6.2.1 Short time diffusion of ultra-soft particles

We first discuss the importance of Eq. (2.68) for our problem. In Fig. 6.1(a) we plot the width of ϱ_s, i.e.

$$w_s(t,x_0) = \int \mathrm{d}x\,(x - \int \mathrm{d}y\, y\, \varrho_s(y,t;x_0))^2 \varrho_s(x,t;x_0)\,, \tag{6.8}$$

which is the second cumulant of the position of the test particle. Further, Fig. 6.1(a) shows $w(t)$ calculated from Eq. (2.54) with $G_s(\Delta x,t)$ given by Eq. (2.68). The integral over x_0 is approximated by a sum over 7 intervals which are indicated in Fig. 6.1(b). Clearly, $w(t)$ does not coincide with any $w_s(t,x_0)$. However, each $w_s(t,x_0)$ displays roughly the same behaviour than $w(t)$. In particular, for times $t > 10^1\tau_B$ the $w_s(t,x_0)$ and $w(t)$ approach each other. Therefore, and to reduce the computational effort, we use $w_s(t,0)$ instead of $w(t)$ to analyse the particles' behaviour.

In Fig. 6.1(c,d) and 6.2(a,b), we plot $w_s(t,0)$ and

$$\alpha_s(t,x_0) = 3\kappa(\varrho_s(x,t;x_0))\,, \tag{6.9}$$

where $\kappa(f(x))$ denotes the kurtosis of the distribution $f(x)$. We use $\alpha_s(t,0)$ as an approximation for the non-Gaussian parameter $\alpha = 3\kappa(G_s)$.

For small times $w_s(t,0)$ growths proportionally with time. The slope is $w_s(t,0)/t = 2D_0$ which corresponds to free diffusion.

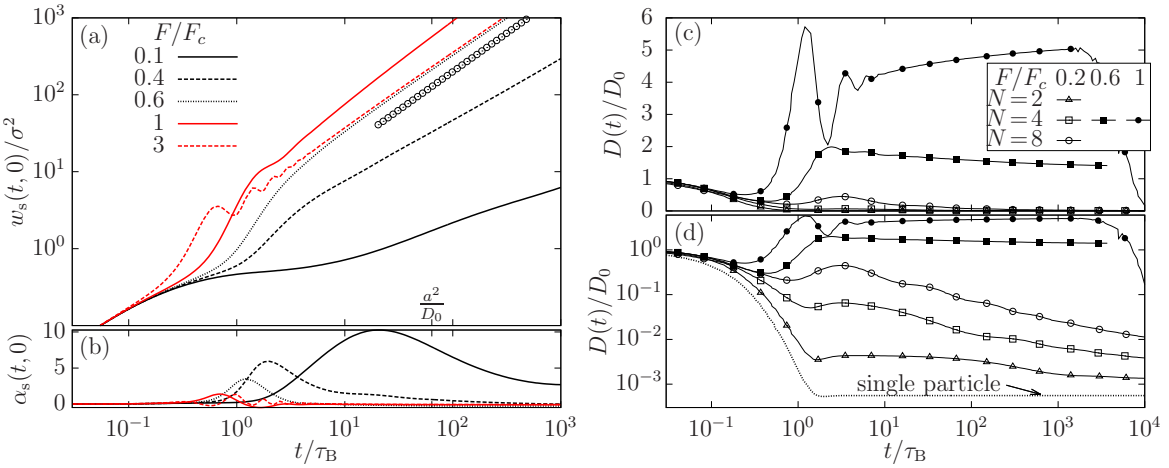

Fig. 6.2: (a) Double-logarithmic plot of $w_s(t,0)$ for different F at $N=4, \varepsilon/k_BT=4$. For $F<0.4F_c$ a subdiffusive region (a plateau), for $F\geq 0.4F_c$ a superdiffusive region emerges. The circles indicate the function $2D_0t$. (b) Non-Gaussian parameter $\alpha_s(t,0)$. (c,d) Rate of change of the MSD, i.e. $D(t)$, defined in Eq. (6.10), in dependence of time, plotted semilogarithmically (c) and double-logarithmically (d). For $F/F_c\in\{0.6,1\}$, $D(t)$ approaches a constant for large t which means that the behaviour is diffusive. For $F=0.2F_c$ we observe a long lasting subdiffusive regime.

For $F=0.2F_c$ and $N<8$ or $\varepsilon/k_BT<4$ in Fig. 6.1(b) and $F<0.4F_c, N=4, \varepsilon=4k_BT$ in Fig. 6.2(a) we observe a more or less pronounced plateau. For $F\geq 0.4F_c$ (Fig. 6.2) or $N\geq 8$ and $\varepsilon\geq 4k_BT$ (Fig. 6.1(c)) a superdiffusive region appears. Based on our investigations in the single-particle case (chapter 3) we interpret the occurrence of a plateau as there is a energy barrier in the effective potential energy landscape $u(x)+V_{\text{int}}^{\text{s}}$ the test particle exhibits. Further, we interpret that the energy barrier becomes small and finally disappears for values for F, ε, and N where we observe a weakly pronounced plateau and a superdiffusive region, respectively.

An important characterisation of plateaus of MSDs is given by the height and the duration of the plateau [119]. As suggested by [119, 144] we define the end of the plateau as the time at which α peaks. It is clearly seen in Figs. 6.1(d) and 6.2(b) that α_s peaks at the time of the end of the plateau. It should be noted, that the crossover from sub/superdiffusive behaviour for intermediate times to diffusive behaviour for long times is the crossover from a linear function, $w_s(t,0)$, to a proportional function, $2Dt$, where the offset is the less important the larger t. This fact was sketched in Fig. 1.3 on page 19.

We analyse $w_s(t,0)$ in more detail by plotting

$$D(t)=\frac{1}{2}\partial_t w_s(t,0) \tag{6.10}$$

in Figs. 6.2(c,d). For strong forces $F/F_c\geq 0.6$, we see $D(t)$ approaching a constant value for long times, indicating diffusive long-time behaviour. For a weak force $F/F_c=0.2$ we observe a long lasting subdiffusive behaviour. Our interpretation is that the subdiffusive behaviour is produced by the interaction between the particles by the following reasoning. The interaction term in the equations of motion is quadratic in the densities. As time elapses the particles

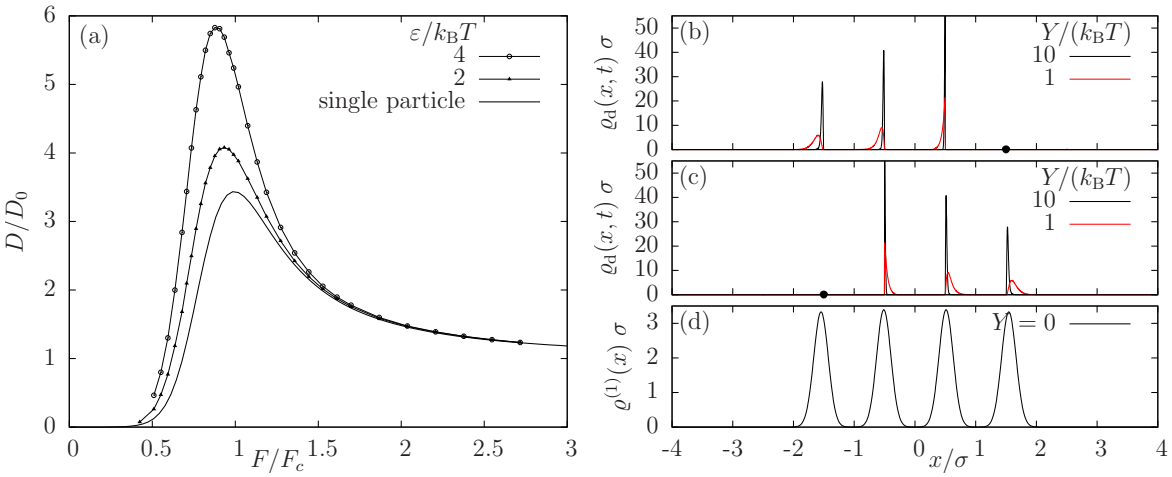

Fig. 6.3: (a) Effective diffusion coefficient in dependence on the driving force F for $N = 4$ and two values of ε. The solid line shows the diffusion coefficient in the single particle case, given by [185]. (b,c) Initial conditional densities $\varrho_d(x, 0)$ for (b) $x_0 = 1.5\sigma$ and (c) $x_0 = -1.5\sigma$. The black dot indicates the position of the test particle. (d) Equilibrium one-particle density for 4 hard particles without attraction.

diffuse away from each other which reduces the density. With time interaction effects are weakened and $D(t)$ is reduced. However, the system is of finite size, so that the growth of the MSD is limited. We observe that w_s saturates at approximately $5 \cdot 10^4\sigma^2$. Consequently, $D(t)$ approaches zero for very large times (see 6.2(c)). Further, we expect that MSD and $D(t)$ in the interacting system are always larger than in the single-particle system because the particle interaction is purely repulsive.

6.2.2 Giant diffusion

For strong forces $F \geq 0.5F_c$ we observe that $w_s(t, 0)$ is linear with time for long times and, hence, becomes proportional for even longer times. According to Eq. (1.7), this is normal diffusive behaviour. The effective diffusion coefficient is defined by Eq. (3.25), i.e. $D = \lim_{t\to\infty} w(t)/(2t)$. However, the approach of $w(t)$ to $2Dt$ is slow and easily predictable because the slope is constant. To ease the computation we use

$$D = D(t_{\text{lin}})\,, \tag{6.11}$$

where t_{lin} is a large time where $D(t)$ is at least almost constant.

We plot D in dependence of F for two values of ε in Fig. 6.3. The function $D(F)$ for a single particle is known analytically [125] (shown as solid line in Fig. 6.3(a)). The structure of $D(F)$ is similar for all cases shown: For small $F < F_c$ the diffusion coefficient is nearly zero, for $F \approx F_c$ it has a global maximum, and for $F \gg F_c$ it is almost equal to D_0, the diffusion coefficient of free diffusion. The appearance of a global maximum $D_{\text{max}} > D_0$ is called giant diffusion. It contrasts the intuitive assumption that a rough potential slows the motion down.

We first explain the giant diffusion effect for a single particle in terms of the potential landscape $u(x)$ ($u(x)$ is plotted in Fig. 1.4(a) on page 24). For small F, there are local

minima in $u(x)$. Thermal fluctuations can drive the particle out of a minimum at a small rate (we discussed this in detail in chapter 4). The diffusion coefficient measures the spread of the particle position under the influence of different realisations of the random force. In the case of small F, where the rate of escape is small, D is small, i.e. $D \ll D_0$. For very large F, the structure of $u(x)$ is that of a linear function with shallow modulations. The system is similar to the free motion of a single particle under the constant force F where the diffusion coefficient is D_0. Thus, we expect $\lim_{F\to\infty} D(F) = D_0$. The interesting region is at $F \approx F_c$ where the form of $u(x)$ is similar to that of a staircase, i.e. a sequence of steep slope and gentle slope intervals. The steep slope is quickly traversed downhill, whereas the particle almost freely diffuses in the gentle slope interval. Most of the time the particle is located in one of the gentle slope intervals. To explain the effect, we consider two realisations of the random force. One pushes the particle to the right down the steep slope, the other to the left where it continues to diffuse. In a short time, the two realisations have led the particle to very different positions which is a fast spread in particle position and, thus, corresponds to a large diffusion coefficient. From this picture we can also infer that $D > D_0$. During the traversal of the steep region the particle departs much faster from the mean position than it would do without a force field.

With this picture in mind we investigate the influence of particle interactions to $D(F)$. There are two main influences: a shift of the peak to lower F and higher values of D in general. The relevant potential landscape is $u(x) + V_{\text{int}}^{\text{s}}$, where $V_{\text{int}}^{\text{s}} > 0$ because the GCM interaction is purely repulsive. In the proximity of x where $\varrho_{\text{d}}(x,t)$ is large, $V_{\text{int}}^{\text{s}}$ assumes large values. For $F < F_c$ the particles are mainly located in the valleys of $u(x)$ which produces a hill in $V_{\text{int}}^{\text{s}}$ which, in the end, leads to a shallower valley of $u + V_{\text{int}}^{\text{s}}$. Therefore, the force at which local minima in $u + V_{\text{int}}^{\text{s}}$ disappear is smaller than F_c. In analogy to the single-particle case where the peak of $D(F)$ is located at F_c, we find it plausible to find the peaks in Fig. 6.3(a) shifted to lower F for larger ε. Concerning the second interaction effect, namely larger values for D in general, we again consider the particle based viewpoint. Whenever a particle finds itself being driven by the steep part of u it additionally is repelled by the other particles which leads to an even faster transport of that particle. This implies a higher separation rate of the particles from each other which corresponds to a higher diffusion coefficient.

6.2.3 Hard attractive particles

We set the screening length of the Yukawa part of the pair interaction potential, defined in Eq. (6.2), to $K^{-1} = \sigma/7$. This value for the attraction range is commonly used to model depletion interactions [382–384].

Particles which cannot pass each other show single file diffusion for long times [145, 147]. The DDFT predicts normal diffusion for long times [294, 388], which is a known shortcoming and originates in the equilibrium approximation of the pair distribution function. However, attractive hard spheres form a chain whose motion is correctly predicted by DDFT [272, 380].

The numerical solution of Eq. (6.3) for the initial condition of ϱ_{d} comprises a numerical difficulty. The test particle is fixed at x_0 which assigns the value 1 to the local packing fraction $n[\varrho_{\text{s}} + \varrho_{\text{d}}](x)$ for $x_0 - \sigma \le x \le x_0 + \sigma$. At these x the force term of the hard sphere

repulsion

$$-\partial_x \frac{\delta \mathcal{F}_{\mathrm{int}}^{\mathrm{hs1D}}[\varrho_\mathrm{s}+\varrho_\mathrm{d}]}{\delta \varrho_\mathrm{d}(x,t)} = -\frac{\varrho_\mathrm{d}(x+\sigma,t)}{1-n[\varrho_\mathrm{s}+\varrho_\mathrm{d}](x+\sigma/2)} + \frac{\varrho_\mathrm{d}(x-\sigma,t)}{1-n[\varrho_\mathrm{s}+\varrho_\mathrm{d}](x-\sigma/2)} \tag{6.12}$$

diverges. A usual approach to solve an diffusion equation in the presence of hard walls is to set reflective boundary conditions, i.e. Neumann boundary conditions with zero flux. It turns out that one needs a very high numerical accuracy to solve Eq. (6.3) with reflective boundaries at $x_0 \pm \sigma$. Therefore, we employ a workaround. For the initial condition we replace $V_{\mathrm{int}}^{\mathrm{d}}(x,t)$ by

$$\int \mathrm{d}x'(\varrho_\mathrm{d}(x',t)+\varrho_\mathrm{s}(x',t))v_{\mathrm{int}}^{\mathrm{HCAY}}(x-x') + \frac{\delta \mathcal{F}_{\mathrm{int}}^{\mathrm{hs1D}}[\varrho_\mathrm{d}]}{\delta \varrho_\mathrm{d}(x,t)} + \Theta(\sigma-|x-x_0|)\cdot 100 k_\mathrm{B}T(2-(x-x_0)^2\sigma^{-2})\,. \tag{6.13}$$

Further, we replaced $1-n[\dots]$ in Eq. (6.12) by $\max(\epsilon_n, 1-n[\dots])$ where $\epsilon_n = 10^{-2}$. Exemplary density profiles obtained by this technique are shown in Figs. 6.3(b,c). We tested our method successfully against Monte-Carlo simulations for the simpler case of $u_0 = 0, Y = 0$ (not shown).

We solve Eqs. (6.3) numerically for two values of x_0, i.e. $x_0 = 1.5\sigma$ and $x_0 = -1.5\sigma$. Figure 6.4(a) shows the MSD where the integration over the initial positions is replaced by the sum over these two values for x_0. Clearly, the MSD for the weaker attraction, i.e. $Y = 1$, growths much faster than the MSD for the strong attraction, i.e. $Y = 10$. We further see from Fig. 6.4(a) that the larger F the larger the MSD. Our interpretation of this finding is that the particle cluster is destabilised by being driven through the washboard potential. It should be noted that diffusive behaviour is established for $Y = k_\mathrm{B}T$, $F = F_c$. As mentioned earlier, hard particles in 1D show single file diffusion. Hence, our results can be interpreted only in a qualitative way.

In Fig. 6.4(b,c) we plot G_s for $t = 3\tau_\mathrm{B}$, where the MSDs in Fig. 6.4(a) differ. We see that the cluster of strongly attractive particles ($Y = 10k_\mathrm{B}T$) is transported almost without distortion. Further, we see that the van Hove functions for the weakly attractive particles ($Y = k_\mathrm{B}T$) are spread over several particle diameters. Thus, the cluster dissociates where the rate of dissociation depends on F.

6.3 Conclusion

We investigated the dynamics of interacting colloids in a one-dimensional washboard potential. We focused on the influence of particle interaction on the diffusion, particularly on the MSD. We take two complementary interacting systems into account, ultra-soft particles, described by the Gaussian core model, and attractive hard particles, where the attractive part is modelled via a Yukawa potential. Our target quantities are the MSD and the non-Gaussian parameter α which we extract from the van Hove correlation function.

For the short time diffusion of the purely repulsive ultra-soft particles we find that the particle interaction enhances the diffusion in comparison to the single particle case, which we investigated in chapter 3. For $N \leq 4$ and $\varepsilon \leq k_\mathrm{B}T$ we find a plateau in the MSD in the regime of small driving forces. For a larger number of particles and a stronger particle interaction, the plateau in the MSD gradually becomes shorter and is replaced by a superdiffusive

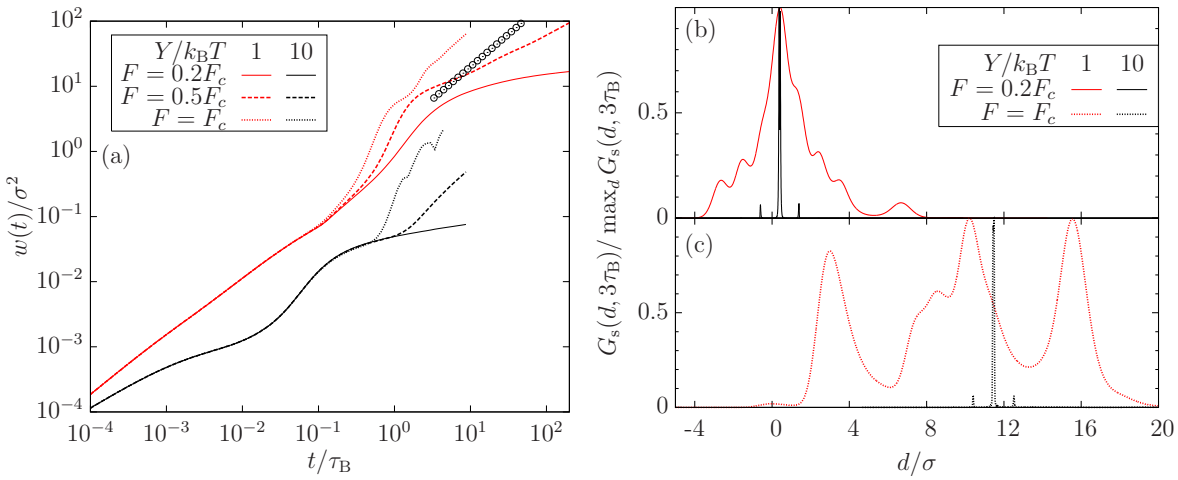

Fig. 6.4: (a) MSD $w(t)$ with respect to time for $N = 4$ particles for different driving forces F and attraction strengths Y. The circles show $2D_0t$. (b,c) Self part of the van Hove function, G_s, at $t = 3\tau_B$ with respect to travelled distance $d = x - x_0$. The y axis is normalised to the maximum for each F and Y separately.

transient region. For times beyond the sub- or superdiffusive region we find normal diffusive behaviour if the driving force is rather strong ($F \geq 0.5F_c$). For these cases we compute the diffusion coefficient and find that the giant diffusion effect is enhanced by the repulsive particle interaction. For smaller values of F we find subdiffusive motion.

The giant diffusion effect is also observed for oscillating washboard potentials [190]. Ultrasoft particle interaction enhances the diffusion coefficient in such systems, too. We presented this result on the conference "Delayed complex systems" in 2012.

Our numerical investigation is based on the dynamic test particle method [123] which uses conditional densities. Averaging the conditional densities over all initial conditions then yields the van Hove correlation function. The procedure is numerically challenging because the computation of the conditional densities comprises the solution of a nonlinear non-local integro-differential equation in a large system. We use a large system of size $L = 100a$ to be able to study even the long-time diffusion in our interacting systems. To reduce the computational effort we mainly restrict ourselves to the diffusion of the test particle starting from only one position, i.e. not averaging over the initial conditions. We analyse the error of this simplification and find that the short time diffusion is not affected qualitatively and the long time diffusion is not affected at all.

We considered a chain of attractive hard particles moving in a tilted washboard potential. For strong attraction we found that the cluster moves undistorted whereas the cluster dissociates for weak attraction. We observed that the dissociation is faster if the driving F is near F_c, the force connected to giant diffusion. To cope with the system with attractive hard particles we modified the DDFT approach for the test particle method from the second direct correlation function approach [123, 308] to the subtraction approach (cf. 2.4.3). This modification allows us to use the full Helmholtz free energy functional, which yields a much easier formula than the second order approach. Nevertheless, we use the standard equilibrium correlation approximation. It is known that this erroneously predicts diffusive

motion instead of single file diffusion [294, 388]. However, our focus is more qualitatively. A more detailed analysis must take dynamic correlations into account, for example by using an equation of motion for the two-particle density $\varrho^{(2)}$ [292].

The short and long time diffusion of interacting colloids in washboard potentials was not studied previously. Based on our findings we conclude that the influence of particle interactions can be very strong and should not be neglected. We presented a technique which makes the theoretical investigation of the dynamics of interacting colloids feasible.

7. DYNAMIC FREEZING: MOBILITY ENHANCING FEEDBACK CONTROL

In this chapter we present our publication [389]. We propose a feedback control scheme to enhance the *collective* transport of colloidal particles with repulsive interactions through a one-dimensional tilted washboard potential. Large parts of this chapter are taken from [389].

As introduced in section 1.6, feedback control is an important concept for the modification of the dynamic properties of all sorts of systems. We focus on colloidal transport which was already our concern in chapter 5 where we improved the net current of a one-dimensional ratchet system. Feedback controlled colloidal transport has more facets than ratchet systems. Examples include the transport of interacting particles in a tilted washboard under Pyragas control [124, 355], the sorting of colloids in a micro-fluidic channel [229], and the adjustment of viscosity of a sheared colloidal suspension [228]. Further, feedback control has become an important concept in particle trapping [100, 230, 231, 376, 390, 391], reaction-diffusion systems [215], quantum transport [218, 237, 392], laser dynamics [220], and brain dynamics [221, 222]. As outlined in section 1.6 new experimental methods foster the development of feedback control strategies.

Within colloidal transport, most of the feedback studies so far involve single particles [225, 246, 390] or dilute suspensions [91, 236], i.e., systems of non-interacting particles. That includes our study in chapter 5. For many colloidal systems, especially in transport, particle interactions are very important and should not be neglected. First studies of feedback control in presence of colloidal interactions showed complex spatio-temporal dynamics [124, 355], where a Pyragas-type control of colloidal transport in one dimension resulted in current reversal and oscillatory states.

Here, we consider the transport of interacting (repulsive) colloids in presence of a feedback-controlled harmonic "trap". Indeed, trap-like devices appear as a standard tool to implement feedback, both in experiments (see, e.g., [91, 97, 230, 231, 376, 391]) and in theory [225]. A prominent example are optical laser tweezers acting on polarisable colloids. The corresponding trap potential can be modelled as a quadratic function in space [80, 391, 393].

In conventional applications, the position of the centre of the trap acting on the colloids is either constant in space, or it moves in an externally prescribed manner [84, 393, 394]. In contrast to these open-loop controls, we here consider a feedback controlled harmonic trap whose centre is set to the mean position of the particles. Our control target, the mean particle position, is an ensemble averaged quantity. Based on our considerations in chapter 5, we do not expect that our feedback induces effective particle interactions [360].

We demonstrate the principle of our feedback control by considering the model system of interacting colloids in a one-dimensional tilted washboard potential with energy barriers much larger than $k_{\mathrm{B}}T$. Already without feedback or any trap potential these systems show

interesting effects such as absolute negative mobility [395] or various changes in the giant enhancement of diffusion, see [147, 149] or chapter 6. Further, recent numerical studies indicate interesting interaction-induced transport phenomena, examples being coherent motion of attractively interacting particles [149, 272, 395], density excitations in Frenkel-Kontorova models [177], or single file diffusion [147]. Given this background, one may expect that the interplay of external potentials, particle interactions, and feedback yields exciting additional effects. Our study shows that this is indeed the case.

Specifically, we consider two interacting systems with repulsive particle interaction: hard repulsion and ultra-soft (Gaussian) repulsion. The latter describes polymeric particles in a coarse-grained fashion [299, 378]. The feedback control is implemented on the level of the SE, in which the particle interactions are treated via DDFT. Our numerical results demonstrate that the feedback-controlled trap in conjunction with particle interactions can lead to a drastic increase of the mobility by orders of magnitude. This phenomenon is related to the fact that the particles, loosely speaking, "push each other over the energy barrier". The same mechanism resulted in an enhancement of diffusion in chapter 6. Here, diffusion is 'frozen' because the particles are trapped. The trap establishes an upper bound to the width of the density distribution. Further, we observe time-periodic oscillations of the mean velocity, which are not seen in the uncontrolled case.

In the major part of our study we assume instantaneous feedback. This is clearly an idealisation because feedback control always entails a time delay due to measurement, information processing, and implementation of the forcing [226]. However, the time delay of modern experimental feedback techniques for colloids [91, 100, 231, 240] is much smaller than the time scale of particle motion, justifying the approximation of instantaneous feedback. Still, to estimate the effects we also consider briefly the impact of time delay.

In the following section 7.1 we introduce the model. To familiarise with the feedback control, we discuss the effect of our feedback control on a single particle in section 7.2. The full problem is discussed in section 7.3, where we present the main results. A conclusion is given in section 7.4.

7.1 Model

We consider the motion of N interacting Brownian particles in one dimension under the influence of the externally imposed, tilted washboard potential $u(x)$, defined in Eq. (1.11). We denote the periodic part of $u(x)$ by

$$u_{\mathrm{per}}(x) = u_0 \sin^2 \frac{\pi x}{a} \,. \tag{7.1}$$

We describe the motion in terms of the one-particle density defined in Eq. (2.24a), which we here call just $\varrho(x,t)$. The time evolution is governed by the extended Smoluchowski equation

$$\partial_t \varrho(x,t) = \frac{k_{\mathrm{B}}T}{\gamma} \partial_{xx} \varrho(x,t) + \frac{1}{\gamma} \partial_x \left(\varrho(x,t) \partial_x (V_{\mathrm{ext}}(x) + V_{\mathrm{DF}}(x,\varrho) + V_{\mathrm{int}}(x,\varrho)) \right) \,, \tag{7.2}$$

where the impact of particle interactions and of feedback control enters via the potentials V_{int} and V_{DF}, respectively. Specifically, to treat the particle interactions we employ the DDFT

which was introduced in section 2.3.1. In this framework,

$$V_{\text{int}}(x,\varrho) = \frac{\delta \mathcal{F}_{\text{int}}[\varrho]}{\delta \varrho(x,t)}\,, \tag{7.3}$$

where $\mathcal{F}_{\text{int}}[\varrho]$ is the interaction part of an *equilibrium* free energy functional.

We consider two types of interacting systems, that is, ultra-soft particles described by the Gaussian core model (GCM) and hard particles. The GCM is a model for the interaction of polymer chains and we introduced it in chapter 6. The pair interaction potential is defined by Eq. (6.1) and the interaction part of the Helmholtz free energy is well approximated in a mean-field way, i.e. using Eq. (2.50). We obtain

$$V_{\text{int}}^{\text{GCM}}(x,\varrho) = \int \mathrm{d}x'\, \varrho(x',t)\, v_{\text{GCM}}(x-x')\,. \tag{7.4}$$

Hard particles with diameter σ are described by the interaction potential

$$v_{\text{hard}}(x_i,x_j) = \begin{cases} 0 & \text{, for } |x_i - x_j| \geq \sigma \\ \infty & \text{, for } |x_i - x_j| < \sigma \end{cases}\,. \tag{7.5}$$

For one-dimensional systems of hard spheres there exists an exact free energy functional [296], given by Eq. (2.47a).

We now turn to the modelling of feedback control. To this end we use the potential

$$V_{\text{DF}}(x,\varrho) = \eta(x - \langle x\rangle)^2\,, \tag{7.6}$$

where

$$\langle x\rangle(t) = \frac{1}{N}\int \mathrm{d}x\, x\, \varrho(x,t) \tag{7.7}$$

is the time-dependent mean particle position. Thus, Eq. (7.6) describes a moving harmonic trap centred around the mean position, resembling the potential seen by particles in moving optical traps [391, 393]. The strength of the harmonic confinement, η, is set to constant. Since V_{DF} depends on $\langle x\rangle(t)$ and, thus, on the dynamical state of the system, it corresponds to a feedback control. This is different from an "open-loop controlled" moving trap, where $\langle x\rangle$ in Eq. (7.6) would be replaced by a position moving with fixed velocity v_0.

We also note that the fact that our feedback control is coupled to an ensemble averaged quantity is in contrast to other feedback mechanisms which are based on individual particle positions [226]. On the particle level, the motion is described by the N coupled LEs (2.6) in one dimension where the ith particle experiences the force

$$f_i(x_i,t) = -u'(x_i) + f_i^{\text{int}}(x_1,\ldots,x_N) + f_i^{\text{DF}}\,. \tag{7.8}$$

The forces due to interaction and feedback control read $f_i^{\text{int}} = -\sum_{j\neq i}\partial_i v_{\text{int}}(x_i,x_j)$ and

$$f_i^{\text{DF}}(x_i,\langle x\rangle) = 2\eta(x_i - \langle x\rangle(t))\,. \tag{7.9}$$

Thus, f_i^{DF} only depends on a single coordinate, x_i, and on $\langle x\rangle$. This differs from other feedback control approaches where the feedback force itself depends on the number of particles [226, 236, 360].

7.2 Single-particle transport

To understand the basic properties of the effect of the feedback control Eq. (7.6) we first discuss the single-particle case ($N=1, \mathcal{F}_{\text{int}} = 0$) without the periodic potential ($u_0 = 0$). In this case Eq. (7.2) reduces to the one-dimensional SE

$$\gamma \partial_t \varrho = k_{\text{B}} T \partial_{xx} \varrho + \partial_x (\varrho (V'_{\text{DF}} - F)) \,. \tag{7.10}$$

A main quantity characterising the transport is the mean particle position $\langle x \rangle$, defined in Eq. (7.7), as function of time. Solving Eq. (7.10) analytically with the initial condition $\varrho(x, t=0) = \delta(x - x_0)$ yields

$$\langle x \rangle (t) = \frac{F}{\gamma} t + x_0 \,. \tag{7.11}$$

Equation (7.11) shows that the mean particle position does not depend on the confinement strength η. This can also be seen by applying the coordinate transformation $x' = x - vt$ to the SE (7.10), setting $v = F/\gamma$. With this transformation the term $\partial_x(\varrho F)$ vanishes. Further, the force related to V_{DF} is invariant with respect to this transformation. Hence, the influences of F and η decouple. From Eq. (7.11) we calculate the mobility

$$\mu := \lim_{t \to \infty} \frac{\partial_t \langle x \rangle}{F} \tag{7.12}$$

$$= \frac{1}{\gamma} \,, \tag{7.13}$$

which only depends on the friction constant γ. We will refer to this value of μ as the mobility of free motion.

A further quantity of interest is the width of the density distribution (which is equal to the MSD in the single-particle case)

$$W(t) = \langle (x - \langle x \rangle)^2 \rangle \,. \tag{7.14}$$

To calculate $W(t)$ we use $\langle V_{\text{DF}} \rangle = \eta W$ (cf. Eqs. (7.6) and (7.10)) which yields

$$W(t) = \frac{k_{\text{B}} T}{2\eta} \left(1 - e^{-4\eta t/\gamma} \right) \,. \tag{7.15}$$

For short times $W(t)$ growths linearly with time, corresponding to diffusive behaviour. For long times diffusion is suppressed: $W(t)$ approaches a limiting value determined by η. Interestingly, a similar behaviour of $W(t)$ occurs in a model of feedback control of quantum transport [218]. There, the fluctuations of the number of electrons tunnelling through a quantum junction are suppressed with a feedback control force, which is linear in the fluctuation of the number of electrons. This corresponds to our harmonic confinement of the density fluctuation, and indeed, the two physically different situations are describable by a formally identical SE [245].

We now turn to the system in presence of the potential $u(x)$. In the single particle case ($N=1, \mathcal{F}_{\text{int}}=0$) Eq. (7.2) then reduces to the SE

$$\gamma \partial_t \varrho = k_{\text{B}} T \partial_{xx} \varrho + \partial_x (\varrho (V'_{\text{DF}} + u'(x))) \,. \tag{7.16}$$

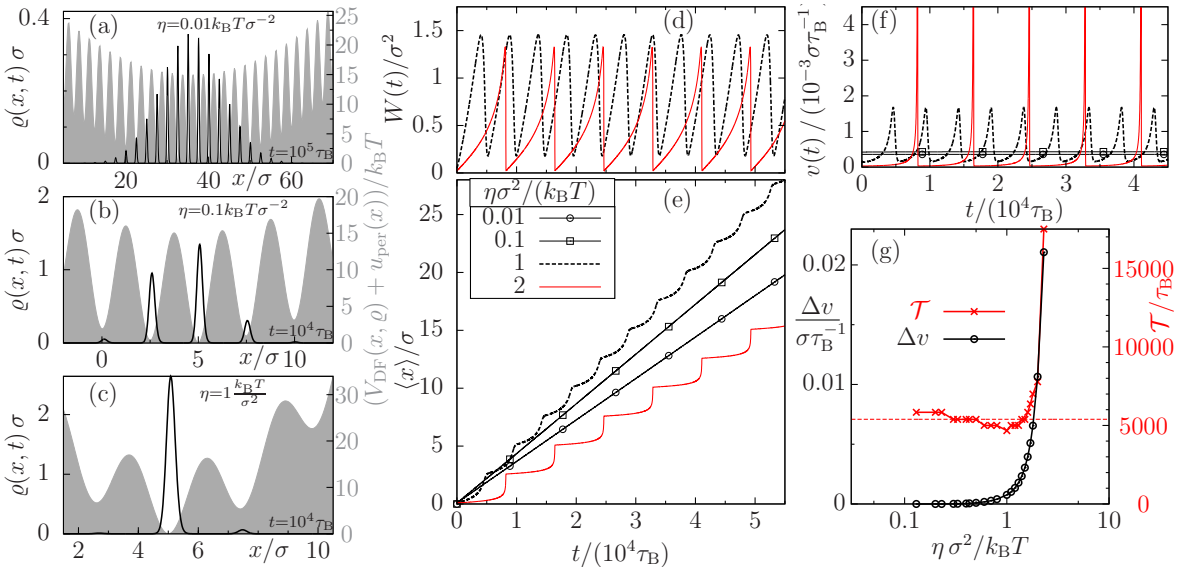

Fig. 7.1: Single particle transport: (a-c) Density plots (black, left axis) and potential $V_{\mathrm{DF}} + u_{\mathrm{per}}$ (grey, right axis). (d) Width $W(t)$, (e) mean particle position, and (f) velocity with respect to time for different η. (g) Amplitude Δv and period $\mathcal{T}$ of the velocity as function of η. The dashed line indicates the time $1/r_K$ where r_K is Kramers' rate. $a = 2.5\sigma$.

Without control ($\eta = 0$) Eq. (7.16) describes the thoroughly studied case of a Brownian particle in a washboard potential which we considered in chapter 3. The mobility and the long-time diffusion constant are accessible analytically [10, 150, 185]. The mobility is very small in the "deep well" case, that is if the barrier height $\Delta u \gg k_{\mathrm{B}}T$ (cf. Eq. (1.13)). Otherwise the mobility is large, in particular it approaches $1/\gamma$ for $u_0/F \to 0$. The goal of our study is to enhance the mobility in the regime of deep wells.

7.2.1 Numerical Results

To explore the single particle transport for finite η and $u \neq 0$ we solve Eq. (7.16) numerically, choosing $u_0 = 15k_{\mathrm{B}}T$ and $F = 0.2F_c$. As initial condition we choose the equilibrium (Boltzmann) distribution corresponding to the case $F = 0$

$$\varrho(x,0) = \exp\left(-(\eta\, x^2 + u_{\mathrm{per}}(x))/k_{\mathrm{B}}T\right)/Z\,, \tag{7.17}$$

where Z is a normalisation constant.

Figures 7.1(a-c) show plots of the one-particle density $\varrho(x,t)$ for three values of η. As expected for a trap, the width of the density distribution becomes the smaller the larger η. Figure 7.1(e) shows additionally the mean particle position with respect to time. Interestingly, we find that at large values of η, oscillatory solutions emerge. At the corresponding values of η the confinement is so strong that the particle is confined to a single well of the periodic potential, cf. Fig. 7.1(c).

We explain the occurrence of oscillations as follows. We take a view on the beginning of one step of an oscillation at time $t = 10^4\tau_{\mathrm{B}}$ for $\eta = 1k_{\mathrm{B}}T\sigma^{-2}$ (cf. Fig. 7.1(e)). The potential $V_{\mathrm{DF}} + u_{\mathrm{per}}$ at this time, shown in Fig. 7.1(c) as grey shade, shows that the particle

is localised at a minimum of $V_{\mathrm{DF}} + u_{\mathrm{per}}$. As time progresses, the constant driving force causes the diffusion of the particle to the next minimum. This leads to a slow increase of the mean particle position $\langle x \rangle$. Then, the feedback control which moves with $\langle x \rangle$, lowers the energy barrier, and steadily accelerates the diffusion through the barrier. This leads to a fast motion until the particle arrives in the next well. The next oscillation then starts again with slow diffusion over the next barrier. The repeated cycle of motion consisting of slow and fast portions is particularly visible in the velocity

$$v(t) = \frac{d}{dt}\langle x \rangle(t)\,, \tag{7.18}$$

and the width $W(t)$ which are plotted in Figs. 7.1(f) and (d), respectively. Notice that $W(t)$ oscillates around a *constant* value, reflecting that the width of the distribution stays finite even at large times ("dynamic freezing").

We analyse the occurrence of these oscillations numerically in terms of period $\mathcal{T}$ and amplitude $\Delta v = (v_{\max} - v_{\min})/2$ of velocity, shown in Fig. 7.1(g). The values $v_{\max}$ and $v_{\min}$ are the global maximum and minimum of $v(t)|_{t>t_1}$, respectively, where t_1 is a time after the disappearance of transients. From Fig. 7.1(g) we find that oscillatory solutions occur in a range of intermediate η. In that range the amplitude Δv increases with η from nearly zero to large values. Furthermore, the period $\mathcal{T}$ of oscillations roughly coincides with the inverse Kramers rate, which is the relevant time scale for the slow barrier-crossing mentioned before. As we see in Fig. 7.1(e), the regime of pronounced oscillations partly coincides with a "speed up" of the motion. We quantify this "speed up" via an average mobility based on the time-averaged velocity

$$\bar{v} = \frac{1}{\mathcal{T}} \int_{t_1}^{t_1+\mathcal{T}} \mathrm{d}t\, v(t) \tag{7.19}$$

such that

$$\mu = \frac{\bar{v}}{F}\,. \tag{7.20}$$

Figure 7.2(a) shows μ/μ_0 depending on η, where $\mu_0 \approx 1.2 \cdot 10^{-4}/\gamma$ is the mobility of the uncontrolled system ($\eta = 0$) with the same external potential [10, 150]. For small η, we find $\mu \approx \mu_0$. The remaining deviation is presumably a numerical issue because, by definition, $\lim_{\eta\to 0} \mu = \mu_0$. At intermediate values of η the mobility shows a global maximum which lies above μ_0. From comparison with Fig. 7.1(g) we see that the maximum of $\mu(\eta)$ lies in the range of η where the oscillation periods of $v(t)$ are about (in fact, somewhat smaller) than the inverse Kramers rate [10, 331]. Quantitatively, the maximal enhancement of mobility of $\approx 20.4\%$ is reached at $\eta \approx 0.96 k_{\mathrm{B}} T \sigma^{-2}$. For even larger values of η a sharp decrease of the mobility to zero is observed – the motion comes to a halt. To investigate this phenomenon we first note that the motion is always oscillatory (for these large η) as long as there is transport at all (compare Figs. 7.2(a) and 7.1(g)). From the explanation of the oscillations above, we recall that the oscillation period is determined by the slow diffusion process over the energy barrier. Figure 7.2(b) shows the potential $V_{\mathrm{DF}}(x, t=0) + u_{\mathrm{per}}(x)$ for three values of η. To ignite transport the particle must diffuse from the central valley at $x = 0$ to the next valley at $x \approx 2.5\sigma$. The larger η the larger the energy barrier. Thus, the larger η the

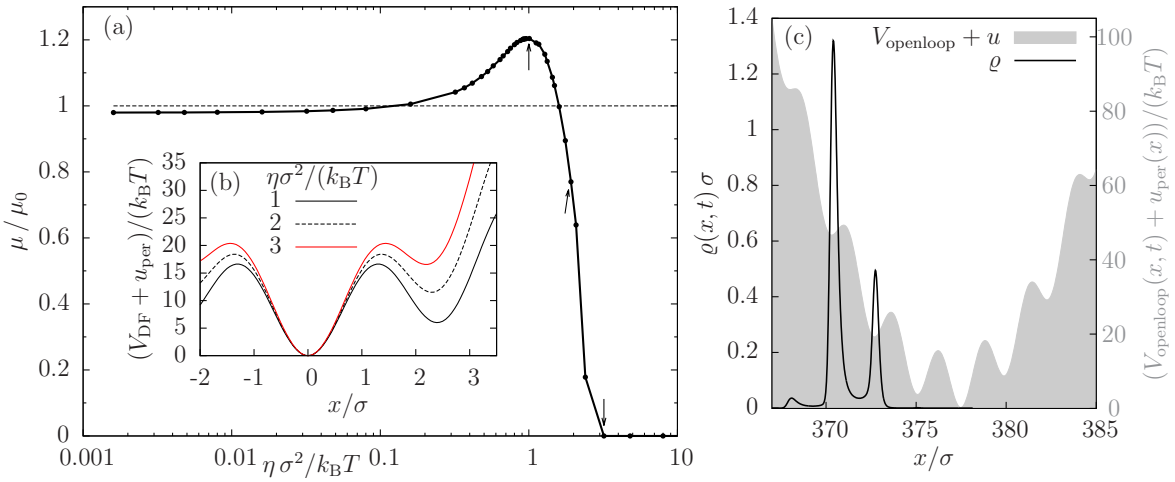

Fig. 7.2: Single particle transport: (a) Mobility μ in dependence on η for $a = 2.5\sigma$. The mobility is scaled by the mobility μ_0 of uncontrolled diffusion in a washboard potential. The feedback control can enhance the mobility by up to $\approx 20\%$. (b) Potential $V_{\mathrm{DF}}(x, t = 0) + u_{\mathrm{per}}(x)$ for the three values of η which are indicated by arrows in $\mu(\eta)$. Single-particle transport in presence of the open-loop potential V_{openloop} (see Eq. (7.21)) with $\eta = 1 k_{\mathrm{B}}T\sigma^{-2}$ and $v_0 = F/\gamma$ at $t = 100\tau_{\mathrm{B}}$ and $a = 2.5\sigma$. Black line: one-particle density $\varrho(x, t)$. Grey shade: potential $V_{\mathrm{openloop}} + u_{\mathrm{per}}$.

smaller the probability that the particle diffuses to the next valley, the longer the period of the oscillations, and the lower the mobility. For $\eta = 3k_{\mathrm{B}}T/\sigma^2$ there is no motion at all in the time range of our calculations ($t \leq 10^5\tau_{\mathrm{B}}$).

Finally, we note that for single-particle transport the actual value of a is essentially arbitrary because a only determines the scales of time, density, and confinement strength, not the qualitative behaviour.

7.2.2 Comparison with open-loop control

To estimate the benefit of the feedback control scheme over the more established open-loop control, we briefly discuss the motion of a single particle under the potential

$$V_{\mathrm{openloop}}(x, t) = \eta\,(x - v_0 t)^2\,, \tag{7.21}$$

where v_0 is a constant velocity of the trap. Choosing v_0 equal to the mean velocity $\bar{v}$ of the feedback controlled system, one observes the same general behaviour, but slight variations of oscillation frequency and amplitude. Large values $v_0 > \bar{v}$ lead, by construction, to a fast transport, but the particle is no longer located in the centre of the trap. We can see this from Fig. 7.2(c) which shows the one-particle density for the velocity $v_0 = F/\gamma$ [corresponding to free motion, see Eq. (7.11)] and the effective trap generated by the potential $V_{\mathrm{openloop}} + u_{\mathrm{per}}$. In a real optical trap a large distance of the particle position to the centre of the trap implies a large probability to escape [230,391]. Hence, driving the particle too fast implies the risk of losing the particle completely. On the other hand, being too cautious and driving the particle too slowly is inefficient. Thus, the optimal velocity is difficult to predict in open-loop control.

The feedback control automatically finds the optimal driving speed without taking the risk of losing the particle. Furthermore, the feedback control does not influence the direction of motion, it only enhances the absolute value of the mobility.

7.3 Many-particle transport

We now turn to interacting systems, as described by the SE (7.2) with Eq. (7.4) for ultra-soft particles and Eq. (2.48) for hard particles. There are now two relevant length scales, the wavelength of the periodic potential, a, *and* the particle diameter σ. Hence, the wavelength a is not just a scaling factor, as it was the case in single-particle transport. In addition, the number of particles N will play a role because the equations are now non-linear in ϱ. In our numerical calculations, we set the ultra-soft particles' interaction strength ε appearing in Eq. (7.4) to $\varepsilon = 4k_\mathrm{B}T$. The hard-particle interaction has no parameter besides σ. The initial condition is set to the equilibrium density resulting at $F = 0$.

In the following we study motion of clusters of interacting particles for various trap strengths η, numbers of particles N, and dimensionless wavelengths a/σ.

7.3.1 General behaviour

The overall goal is to explore whether particle interactions enhance the efficiency of our feedback control in terms of the mobility. Before we start with the analysis of the mobility we want to give an impression of the general behaviour of our interacting systems.

We begin our study of the three-dimensional parameter space (N, η, a) with small N and small η. In Fig. 7.3(c) we present a plot of the density profile and the potential $V_\mathrm{DF} + u_\mathrm{per}$ at $\eta = 0.01 k_\mathrm{B}T\sigma^{-2}, N = 4$. In fact, the density profiles shown in Fig. 7.3(c) and Fig. 7.1(a) are very similar. Similarities to the single-particle case vanish gradually if N or η (or both) are increased (at constant a), yielding larger values of the density in the trap. To describe the effect of these changes in density, we consider the effective potential V_int that one particle experiences due to the interaction with the other particles. The value of V_int at a position x increases with the corresponding densities $\varrho(x'), x' \approx x$. Particularly large values of both, $\varrho(x)$ and $V_\mathrm{int}(x)$, occur at the minima of $V_\mathrm{DF} + u_\mathrm{per}$. As a consequence, the potential $V_\mathrm{DF} + u_\mathrm{per} + V_\mathrm{int}$, which governs the motion (together with the constant driving force), is characterised by smaller energy barriers than $V_\mathrm{DF} + u_\mathrm{per}$. Loosely speaking, V_int fills the valleys of $V_\mathrm{DF} + u_\mathrm{per}$ [see Fig. 7.3(b)]. For high densities, the hard particles form a "chain" and the ultra-soft particles form a cluster which is characterised by mutual overlap. In this dense situation the contribution of V_int to $V_\mathrm{DF} + u_\mathrm{per} + V_\mathrm{int}$ can become so large that u becomes negligible. Thus, there are no hindering energy barriers any more. For both interacting systems, ultra-soft and hard particles, we actually find this case. Fig. 7.3(a) shows the hard particle case as example. The potentials plotted in Fig. 7.3(a) show that u in fact is a minor contribution to $V_\mathrm{DF} + u_\mathrm{per} + V_\mathrm{int}$. We continue the discussion of parameter variations with focus on the mobility in Sec. 7.3.2.

Similar to the single-particle case, we find oscillatory solutions in the range of intermediate to large η. For a representative system ($N = 4$ hard particles), Fig. 7.4 summarises different characteristics of the oscillations in terms of width $W(t)$, velocity $v(t)$, and plots of the density for four times during one oscillation period. The oscillation period is of the order of τ_B which is much shorter than the oscillation periods of several $10^3\tau_\mathrm{B}$ we observed in

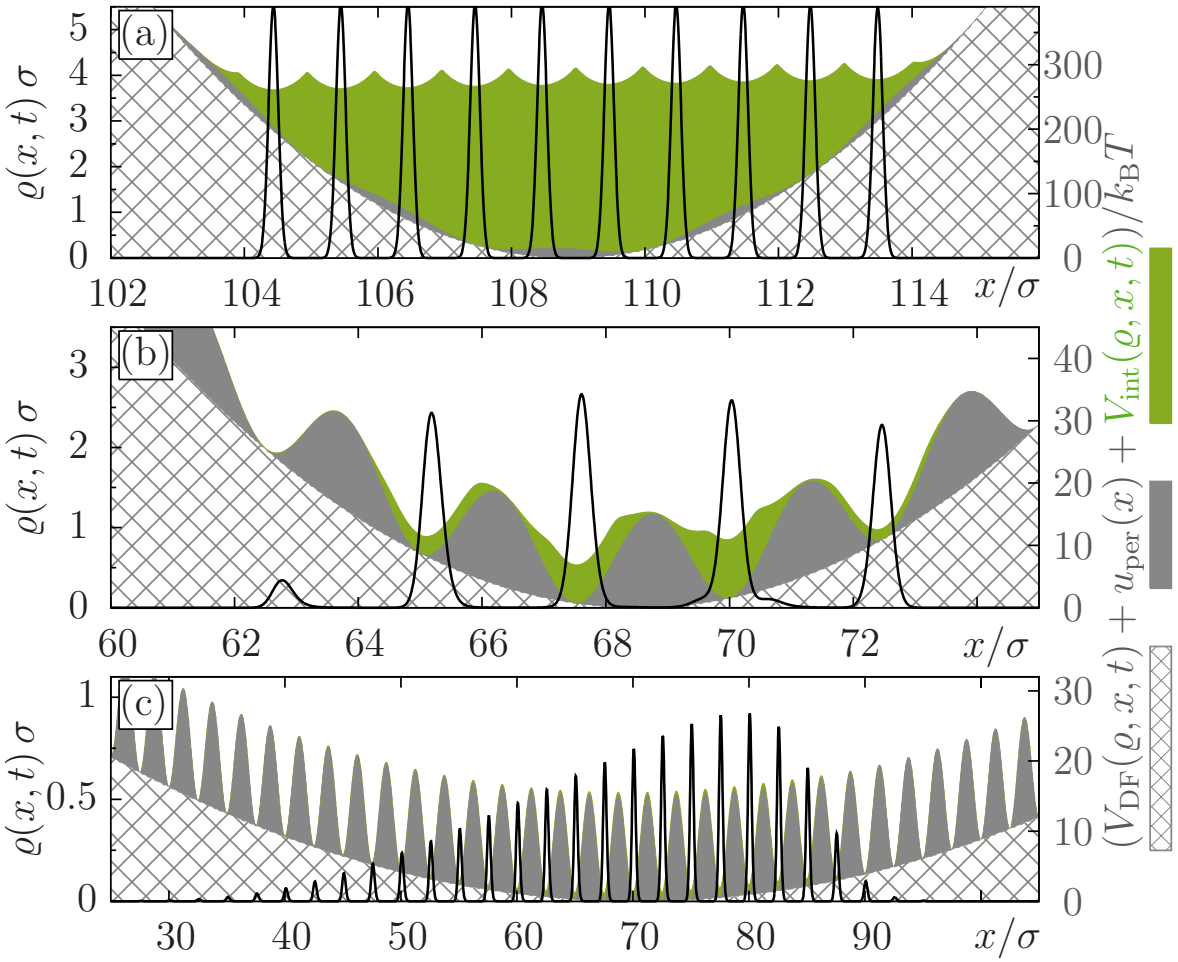

Fig. 7.3: One-particle density $\varrho(x,t)$ on the left axis (black lines) and the potentials V_{DF}, u, and V_{int} on the right axis. The parameters show (a) the case where u is suppressed, (b) the decrease of barrier height by interaction, and (c) the low-η/low-N regime. In detail, (a) shows $N = 10$ hard particles forming a chain in a narrow trap ($\eta = 10 k_{\mathrm{B}}T\sigma^{-2}, a = 2.5\sigma$) at $t = 28.9\tau_{\mathrm{B}}$, (b) $N = 4$ hard particles forming a loose chain in an moderately narrow trap ($\eta = 0.7 k_{\mathrm{B}}T\sigma^{-2}, a = 2.5\sigma$) at $t = 985\tau_{\mathrm{B}}$, and (c) $N = 4$ ultra-soft particles in a wide trap ($\eta = 10^{-2} k_{\mathrm{B}}T\sigma^{-2}, a = 2.5\sigma$) at $t = 10^5\tau_{\mathrm{B}}$.

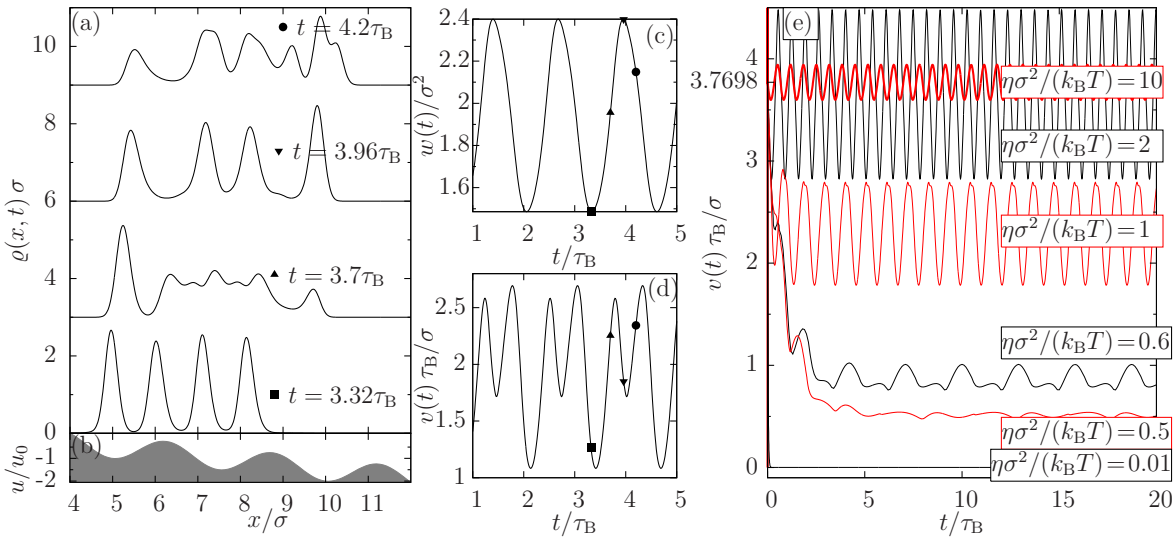

Fig. 7.4: (a) One-particle density $\varrho(x,t)$ for $N = 4$ hard particles at $\eta = 3k_BT\sigma^{-2}, a = 2.5\sigma$ for four times. For clarity the curves are shifted vertically. Each time is labelled with a symbol, reappearing in (c) and (d) which show the width $W(t)$ and the velocity $v(t)$ over time, respectively. (b) External potential $u(x)$. (e) Velocity $v(t)$ for $N = 10$ hard particles at $a = 2.5\sigma$ for several η. The velocity $3.7698\sigma/\tau_B = F/\gamma$ corresponds to the velocity of free motion under the force F. This value is reached at large η. Oscillations occur for $\eta \geq 0.03k_BT\sigma^{-2}$.

the single-particle case (see Fig. 7.1(g)). From Fig. 7.4 we see that these oscillations are intimately related to configurational changes while the particle chain moves over a distance of about one wavelength a. Studying $v(t)$ for different η, see Fig. 7.4(d), we find that a couple of different oscillation patterns emerge. Moreover, the oscillations' frequency rises with the mean of the velocity itself. This can be explained with the observation that the particles move one wavelength a during one period. Note that the maximal amplitude of oscillation neither coincides with largest η nor largest mean velocity.

7.3.2 Mobility

We now turn to the mobility, as a measure of the efficiency of feedback control. We define the mobility μ in the same way as in the single-particle case via Eq. (7.20). Figures 7.5(a) and (b) show μ in dependence of η for ultra-soft and hard particles, respectively.

For $a > \sigma$ we observe an extreme growth of μ with η and N over several orders of magnitude for both particle species. We explain this behaviour with the corresponding decrease of the height of the energy barriers in $V_{DF} + u_{per} + V_{int}$, which results in a larger diffusion rate and a faster transport. The same effect was observed in a study of the transport of super-paramagnetic colloids [396]. For certain η and N, μ increases even up to the maximal possible value $\mu = 1/\gamma$, the mobility of free motion. An example for this large mobility is the case of $N = 10$ hard particles at $\eta = 10k_BT\sigma^{-2}$, shown in Fig. 7.3(a). In this case, there are no hindering energy barriers (as we have analysed in Sec. 7.3.1) which then results in the high mobility. To achieve this suppression of u the well created by the trap potential must be

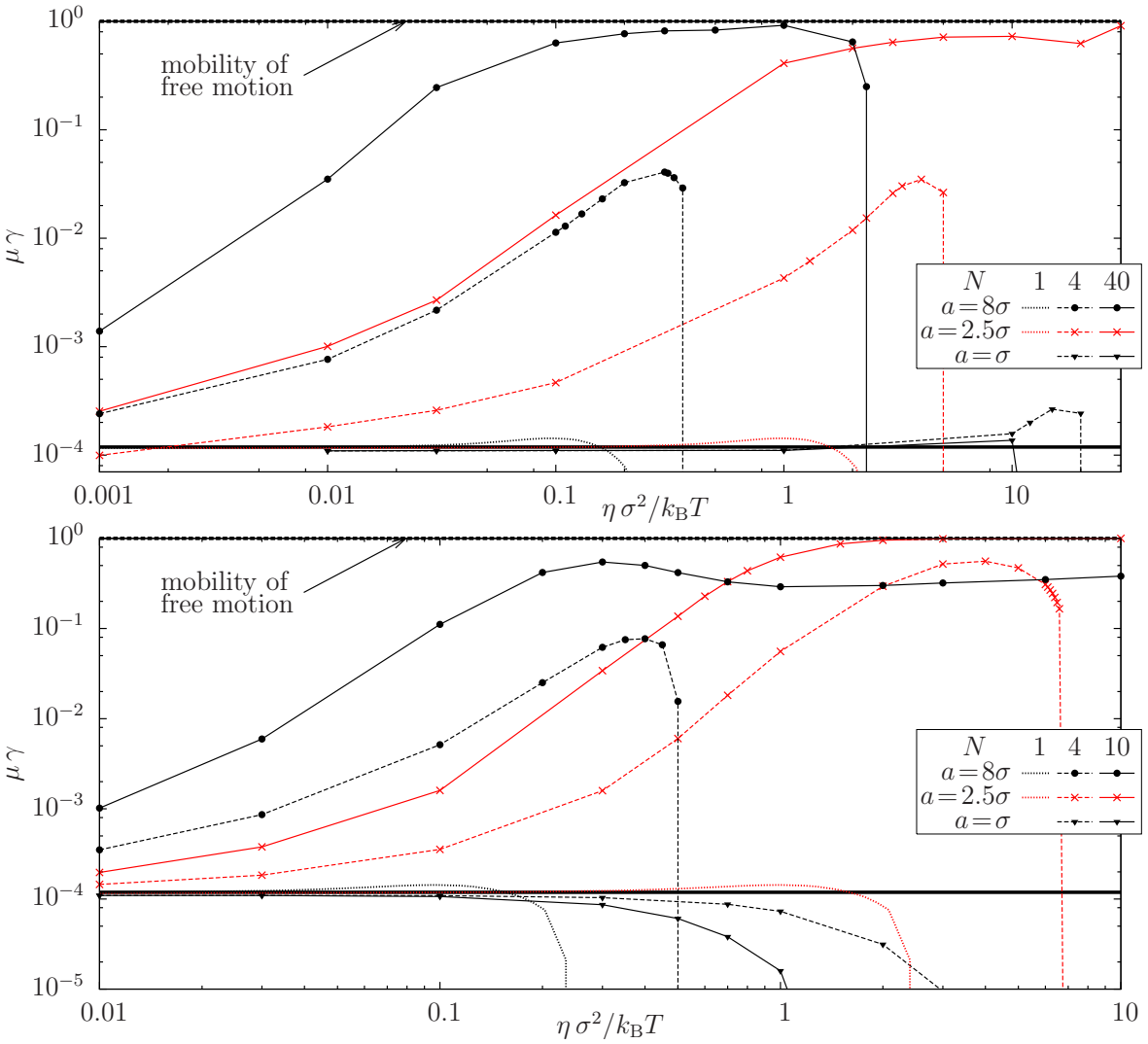

Fig. 7.5: Mobility μ for (a) ultra-soft particles and (b) hard particles in dependence of η. The mobility reaches $1/\gamma$, the mobility of free motion, if enough particles contribute. The thick line indicates the mobility in the uncontrolled case. Results from Fig. 7.2(a) are included with the notation $N=1$.

very deep, i.e. $300k_BT$ for the exemplary case shown in Fig. 7.3(a). This value exceeds those in typical experiments with light fields [81,91]. However, the transport of $N=40$ ultra-soft particles at the mobility $\mu = 1/\gamma$ at $a = 8\sigma$ needs a trap which is only $40k_BT$ deep.

Further, we see from Fig. 7.5 that our feedback control does not lead to a significant speed up for $a=\sigma$. By analysing the potential landscape for $a = \sigma$ for a series of η and N (not shown) we find that the effective potential V_{int} develops peaks *between* the minima of $V_{\text{DF}} + u_{\text{per}}$. This means that the effective potential barrier encountered by a moving particle *increases* when η or N is enlarged. This is in contrast to the case $a > \sigma$ where the peaks of V_{int} are found *at* the minima of $V_{\text{DF}} + u_{\text{per}}$ [see Fig. 7.3(b)]. Our interpretation for the case $a = \sigma$ therefore is that the particles "pin" each other to the potential minima of $u(x)$.

We now consider the behaviour of $\mu(\eta)$ for large η (Fig. 7.5). For small N we observe a breakdown of motion, similar to the one observed in the single-particle case (see Fig. 7.2(a)). However, this breakdown is shifted towards larger values of η. We recall that an increase of N at fixed η (Sec. 7.3.1) leads to a decrease of the barriers of the potential $V_{\text{DF}} + u_{\text{per}} + V_{\text{int}}$. This enhances the mobility (relative to that at $N = 1$) in the first place. However, upon increase of η (at fixed N) there can be a situation where the diffusion rate is not sufficient any more to populate the next local minimum of the potential $V_{\text{DF}} + u_{\text{per}}$. This is where transport breaks down. The combination of these two effects leads to the observed shift of the breakdown of mobility. Upon further increase of N and η, there comes a point where the large energy scales of V_{DF} and V_{int} suppress any influence from u. Therefore, we expect that the transport for high N exists for arbitrarily large η.

In Fig. 7.5(b) we see that the increase of a at constant η and N leads to an enhancement of mobility (as long as there is transport at all). This can be explained with the potential $V_{\text{DF}} + u_{\text{per}}$, whose valleys become broader the larger a. In a broader valley more particles accumulate which strengthens the role of interaction for the barrier crossing. However, this effect is limited by N: The particle number must be large enough to fill at least one valley with particles, otherwise the transport breaks down.

7.3.3 Time delay

In a realistic set up with feedback control, a finite time is required to perform the measurement required to define the control (In the present case, this measurement process concerns the average particle position). Hence, there is a certain *time delay* τ_{Delay}. To explore the sensitivity of our results towards τ_{Delay} we change the control potential given in Eq. (7.6) into the expression

$$V_{\text{DF}}^{\text{delay}}(x, \varrho) = \eta \left(x - \langle x \rangle (t - \tau_{\text{Delay}})\right)^2 . \tag{7.22}$$

We now consider two special cases involving hard particles, where the non-delayed feedback control leads to a particularly high mobility (see Fig. 7.5(b)). Numerical results are shown in Fig. 7.6. The delay causes a pronounced decrease of mobility which appears to be linear in τ_{Delay} for small delay times. Realistically, feedback mechanisms can be implemented at the time scale of 10 ms [91,240,390] whereas τ_{B}, the timescale of Brownian motion, is for μm-sized particles in the order of seconds (cf. table 2.1). Hence, we expect that the ratio $\tau_{\text{Delay}}/\tau_{\text{B}}$ is rather small, that is, of the order 10^{-1}. For such situations, our results in Fig. 7.6 predict only a small decrease of μ relative to the non-delayed case. However, even for large delays

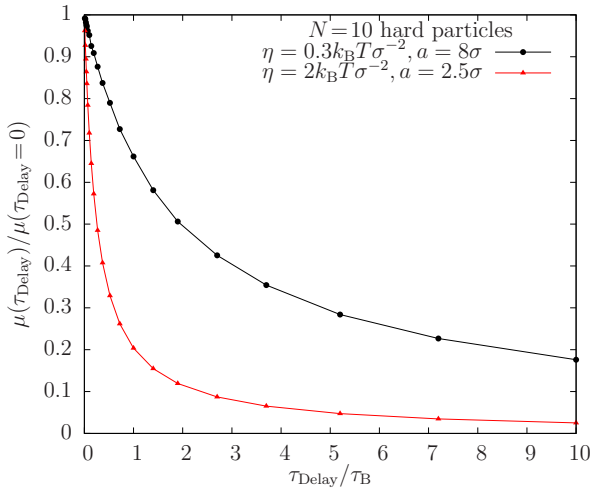

Fig. 7.6: Effect of time delay on mobility μ for hard particles. Even for very long delays the mobility is only reduced by one order of magnitude.

the mobility only decreases about one order of magnitude. This implies that even the time delayed feedback control can enhance the mobility by more than two orders of magnitude with respect to the uncontrolled case.

7.4 Conclusion

Inspired by feedback control mechanisms for the trapping of single colloids, we have proposed a feedback control strategy for the collective transport of interacting colloids through a corrugated potential landscape. Our main goal was the theoretical demonstration of the working principle for a well-defined model system. To this end we have considered the one-dimensional, overdamped motion of colloids with either hard or soft repulsive interactions in a tilted washboard potential. The feedback control enters into the equation of motion, which is a SE where the particle interactions are treated with DDFT, via a harmonic potential centred at the mean particle position. Thus, contrary to other studies [225, 246], the present feedback control cannot induce motion on its own.

The main result of our study is that the interplay of the feedback control and particle interactions can generate a drastic increase of the average mobility by several orders of magnitude relative to the uncontrolled, single-particle reference case. The largest mobilities occur for rather stiff traps and high densities (i.e., large N) inside the trap. Therein, the particles arrange themselves into chain or clusters. Here, the mobility rises up to its limiting value defined by the mobility of a freely moving, overdamped particle. Interestingly, this giant increase does not occur for a single particle under the same feedback control. This shows that the observed mobility enhancement is indeed an interaction effect. The enhancement can be explained by the fact that, in presence of particle interactions, these dominate the force acting on an individual particle, while the impact of the external potential barriers vanishes. Thus, particles "help each other" to overcome the external barriers. The same effect led to larger MSDs in chapter 6. Another new feature is the emergence of *oscillatory* behaviour of the mean velocity (and the width of the density distribution) due to the feedback-controlled

trap. Note that these oscillations are not induced by a time delay but are due to the directed motion over a washboard potential. The latter effect occurs for both, single and interacting particles, with the period of oscillations being close to the inverse of Kramers' escape rate.

From an application point of view it is interesting that, due to its coupling to the mean position, the feedback-controlled trap implies a small risk to "lose" particles. Indeed, the width of the distribution stays constant on time-average, reflecting a "dynamical freezing". This is different from externally moved, "open-loop" traps, where an inappropriate choice of the trap velocity easily lead to a broadening of the density distribution, and thus, a spreading of particles out of the trap (see discussion in section 7.2.2). Another experimentally relevant issue concerns the impact of time delay(s). Here we have shown that time delay does indeed reduce the mobility, similar to what has been observed in ratchet systems [236]. However, for realistic time delays the remaining mobility is still enhanced by two orders of magnitude.

Concerning the methodology, we note that the DDFT scheme employed here implies an "adiabatic" approximation of the time-dependent two-particle correlations (cf. section 2.3.1). It is well established [257, 268, 294] that this approximation may generate artefacts especially for densely packed particles, e.g., during the expansion of a cluster (such as in section 6.2.3). Since the transport in our systems is determined by the time the particles need to cross an effective energy barrier we expect positional correlations to play a minor role and, hence, we expect our results to be precise.

The control target $\langle x \rangle$ of our feedback control is an ensemble averaged and particle averaged quantity. In an experimental realisation only the mean $m_N(t) = N^{-1} \sum_i x_i(t)$ of N particle positions is available. It should be investigated which error is made by exchanging $\langle x \rangle$ and m_N. In BD simulations of feedback controlled systems [236, 360] it was found that the correlations between m_N and the x_i decay rapidly with rising N. Hence, we expect that our ensemble averaged control target comprises the smaller errors the larger N. Still, it would be very interesting and important to test our predictions against explicit BD simulations.

Finally, we would like to point out that the concept behind dynamical freezing is not restricted to one-dimensional washboard potentials. Indeed, the present feedback control can easily be formulated in two or three spatial dimensions. Further, the external potential hindering the motion does not have to be static or even periodic which enriches possible applications. An interesting question is how well the present control strategy works for other types of colloidal interactions, particularly attractive ones.

8. CONCLUSION AND OUTLOOK

8.1 Summary and Conclusion

In this thesis we developed new understanding in the field of transport and diffusion of colloids in one-dimensional periodic potentials. We analysed the short time behaviour of a single Brownian particle in a tilted washboard potential, which is a paradigm model for colloidal transport. We took two complementary points of view. We address cumulants of position with a model which is based on a few characteristic properties of the system and which yields analytic results. We address the time the particle needs to cross an energy barrier with our generalisation of the waiting time distribution. With these approaches we achieved an understanding of the short time behaviour. We turned to more applied research by considering feedback control and particle interaction. We proposed a time delayed feedback protocol for a single Brownian particle in an asymmetric periodic potential which operates like a rocking ratchet but can generate a higher current than a standard rocking ratchet. We implement the feedback control on the level of the Fokker-Planck equation which allows ensemble-averaged results and is well applicable to systems with many particles. Coming back to short time diffusion, we identified the influence of particle interaction, namely ultra-soft particle interaction and hard sphere repulsion, to the cumulants of position. Finally, we combined feedback control and particle interaction and presented a feedback control protocol which establishes collective localised transport in a moving trap. We show that particle interactions are essential for fast transport.

8.1.1 A single Brownian particle in a tilted washboard

In chapters 3 and 4 we considered the motion of a single Brownian particle in a tilted washboard potential, which is a model with numerous applications in theory and experiment (cf. section 1.5). In chapter 3, we analysed the cumulants of positions, such as the MSD and the non-Gaussian parameter. We focused on the "deep well" case where the local minima of the washboard potential are deeper than $k_{\mathrm{B}}T$. In experiments it is often the deep well case which is relevant [161,397–399]. Using our new 2S/W model we could drastically simplify the prediction of the cumulants of position while maintaining high accuracy. Further, the 2S/W model yields analytic expressions. This is possible because the parameters of the model represent important physical properties of the system. Therefore, our 2S/W model constitutes a formalism for the understanding of the dynamics of the single Brownian particle in a tilted washboard potential. This deeper understanding can directly be applied to systems which employ the single Brownian particle as a model. Examples include dilute suspensions of colloids in laser fields [82], the current through Josephson junctions [183], and the escape of particles from optical traps [391] or transient cages [116].

In chapter 4, we introduced a definition for the WTD for this continuous system, by generalising the established WTDs for discrete stochastic systems. We present a recipe to calculate the WTDs from a SE. By comparing to the established FPTD, we find that the WTDs we obtain via our SE constitute a splitting of the FPTD into direction-dependent parts. We verify our approaches by numerically evaluating the WTDs for the single Brownian particle in a tilted washboard potential. The results from the SE-approach and the BD-approach fully agree with each other. Further, the 2S/W model yields analytic results for intermediate and long times. The motion is characterised by waiting and jumping. Additionally to measuring the waiting times with a WTD, we characterise the duration of the jumping with a "jump duration distribution". We show the versatility of our definition of the WTD by calculating the jump duration distribution. Our generalisation of the WTD to continuous systems provides a systematic method to estimate the error one makes by discretising the dynamics of a system. Further, we enable a microscopically based input for coarse-grained models such as continuous time random walk [128, 129, 348, 400] which has high relevance for the relaxation in supercooled liquids and glasses [164, 327, 401, 402] and the diffusion of particles on interfaces [67].

8.1.2 Feedback controlled rocking ratchet

In chapter 5 we proposed a time delayed feedback control for the driving of a single particle in a periodic system with an asymmetric potential. With this time delayed feedback control we could generate a ratchet effect that allows us to induce larger currents than with corresponding open-loop ratchets. The particle current in ratchet systems is important for various systems and experiments, as discussed in section 1.5.2.

On a fundamental level, we gain new insight into stochastic thermodynamics of this feedback controlled rocking ratchet by studying the entropy production in this system. We find peaks in the total entropy production that clearly correspond to the switching events that occur in our system. These peaks indicate that the system is further away from the stationary state after switching than otherwise.

Further, our feedback control implementation presents an expansion of the current methodology, because our feedback control is included directly into the SE. Previous feedback control mechanisms are based on individual particles, whereas our feedback control is based on an ensemble averaged control target which constitutes a new approach to feedback control. Using BD simulations, we have shown that our ensemble averaged approach is a good approximation for particle-based controls with many particles. The SE based approach allows us to study much larger systems and longer times than would be feasible with BD simulations.

8.1.3 Effects of particle interaction

In chapter 6 we investigate the transformation of a dense cluster of ultra-soft particles into a dilute suspension by diffusion in tilted washboard potential. We focus on the influence of the particle interaction and the constant driving force on the short time diffusion, in particular the MSD. We extend the results of [124] for this system by considering longer times and by varying the driving force and the number of particles. We find new effects such as a long subdiffusive regime for driving forces F smaller than the critical driving force F_c. Further, for $F \approx F_c$ and $F > F_c$ we observe a giant enhancement of the diffusion coefficient D where D is

even larger than in the single particle giant diffusion effect [185]. We show that this method is particularly useful for the computational investigation of the motion of interacting colloids, because the computation time does not depend on the number of particles (in contrast to BD).

In chapter 7 we propose a feedback control for the collective transport of repulsively interacting particles through a tilted washboard potential. Previously proposed feedback controls mainly consider single particles and dilute colloidal suspensions. Our control yields a collective transport where the particle interaction plays a crucial role. The feedback control consists of a harmonic trap which is centred around the mean particle position. We achieve an enhancement of the mobility of the particle cluster about several orders of magnitude. The more particles are in the trap the larger is the mobility. For a certain regime of stiffnesses of the trap the feedback control completely suppresses the hindering effect of the washboard potential. We model the motion with an extended SE, employing the DDFT for the particle interactions. Modern experiments with feedback controls show that the inevitable time delay in feedback controls can be made short in comparison to the time scale at which colloids move. We assume instantaneous feedback for our main results and additionally show that our feedback control is robust against small and intermediate time delays. The mechanism of our control is very simple because it consists of a single optical trap (optical tweezers) and imposes low requirements on the speed of the feedback loop. Further, it does not need single particle resolution in the measurement step because it relies only on the mean particle position. This control could improve transport in various applications involving optical tweezers [403], magnetic traps [96, 394], or other confinements [231].

8.2 Outlook

8.2.1 Dimensionality

A straightforward generalisation of the effects studied in this thesis is the consideration of two degrees of freedom for the motion e.g. in two spatial dimensions. We expect similar observations in two-dimensional motion systems compared to our one-dimensional systems.

The simplest periodic two-dimensional potential has a striped geometry. Due to the symmetry of the potential, two-dimensional generalisations of our single particles systems (chapters 3, 4, and 5) can be effectively reduced to one-dimensional systems. We base this expectation on the relation derived in appendix 9.2. For the diffusion of several interacting particles (generalising chapter 6), we expect a quantitative and qualitative change of the behaviour, already for the striped potential.

More interesting effects we expect in more complicated periodic two-dimensional potentials, such as a quadratic lattice. The direction of transport induced by a constant force in that lattice is in general neither parallel to the force nor to the directions of the lattice [153, 209]. Further, the matrix of diffusion coefficients in a time-periodic driven lattice possesses a non-trivial dependence on the system directions [404]. The exploitation of these observations yields a much larger freedom to transport particles. For example, varying the amplitude of the driving force alone changes the mean direction of transport. Under a time-dependent protocol the particle could be navigated along an arbitrary path. Our techniques, such as the 2S/W model and the analysis using WTDs (chapters 3, 4) would lead to a fundamental understanding of these phenomenons. Based on this understanding one could

develop fast and efficient calculation methods and make general predictions for the transport in two-dimensional periodic potentials.

8.2.2 Particle interactions and positional correlations

The analysis of the transport of (several) interacting particles using WTDs can lead to better understanding of collective transport in periodic potentials. This understanding could be used to set up effective models which use the WTDs as input, such as in continuous time random walk [67] or kinetic Monte Carlo [405]. Thus, a rigorous microscopic base could be provided for the modelling of single particles or single clusters on large scales of time and space.

In the chapters 6 and 7 we modelled the effects of particle interaction with classical DDFT which involves an adiabatic approximation for the positional correlations. In section 6.2.3 this led to qualitative results, only. We expect that the time dependence of positional correlations are more precisely given by the non-equilibrium Ornstein-Zernike equation [406]. This has a strong impact on the short and long time diffusion of particles with strongly repulsive interaction potentials, such as charged colloids, magnetic colloids, or hard spheres. This is relevant for mixing and demixing in colloidal systems [407,408] and gelation [138,144]. In such systems a reliable ensemble averaged description is still missing for short time observables and transport in general.

8.2.3 Feedback control

The feedback control protocol we presented in chapter 7 works for two (or more) spatial dimensions after a straightforward generalisation. Further, it is not restricted to periodic potentials. This techniques enables the collective transport of a cluster of particles along an arbitrary prescribed path through any potential. This is particularly interesting for medical and biological applications [403], the assembly of complex structures [409, 410], and particle sorting.

A further interesting question would arise from the generalisation of the feedback control we proposed for ratchet systems towards several particles. Our approach could be used to optimise transport. For dimer particles in a periodic potential the particle interaction produces a giant diffusion effect and an absolute negative mobility [395]. Based on that finding, we expect that a feedback control can exploit the properties of the particle interaction specifically to optimise the transport.

Feedback control of non-interacting particles can induce effective particle interactions [360]. This effect is not yet fully understood but could be connected to fundamental physical understanding about correlations. The methods we used to study many-particle dynamics (chapters 6 and 7) could provide a basis for the investigations of this effect. These effective interactions are observed with feedback controls of finitely many particles. As we are interested in ensemble averaged properties, an extension of our methods is necessary because we expect a sensitive dependence on the number of particles.

9. APPENDIX

9.1 Integration of the SE

We calculate the integration of the N-particle SE (2.9) over $N-1$ particle coordinates assuming the pairwise structure of the potential energy given in Eq. (2.27). By making a couple of assumptions we arrive at Eq. (2.28).

We apply ∂_t to Eq. (2.23) for $n=1$. The integration over the positions and ∂_t can be exchanged and we insert the SE (2.9) for $\partial_t P$:

$$\partial_t \varrho^{(1)}(\mathbf{r}_1,t) = N\int \mathrm{d}\mathbf{r}_2\ldots\mathrm{d}\mathbf{r}_N \frac{1}{\gamma}\sum_{i=1}^{N}\boldsymbol{\nabla}_i\cdot\left(k_\mathrm{B}T\boldsymbol{\nabla}_i P + P\,\boldsymbol{\nabla}_i V\right), \tag{9.1}$$

where $P = P(\mathbf{r}_1,\ldots,\mathbf{r}_N,t)$. First, we calculate the gradient of the potential

$$\begin{aligned}\boldsymbol{\nabla}_i V(\mathbf{r}_1,\ldots,\mathbf{r}_N,t) &= \boldsymbol{\nabla}_i V_\mathrm{ext}(\mathbf{r}_i,t) + \frac{1}{2}\sum_{j,k,k\neq j}\left(\delta_{ij}\boldsymbol{\nabla}_j v_\mathrm{int}(\mathbf{r}_j,\mathbf{r}_k) + \delta_{ik}\boldsymbol{\nabla}_k v_\mathrm{int}(\mathbf{r}_j,\mathbf{r}_k)\right)\\ &= \boldsymbol{\nabla}_i V_\mathrm{ext}(\mathbf{r}_i,t) + \frac{1}{2}\sum_{k\neq i}\boldsymbol{\nabla}_i v_\mathrm{int}(\mathbf{r}_i,\mathbf{r}_k) + \frac{1}{2}\sum_{j\neq i}\boldsymbol{\nabla}_i v_\mathrm{int}(\mathbf{r}_j,\mathbf{r}_i)\,.\end{aligned} \tag{9.2}$$

We *assume* that $v_\mathrm{int}(\mathbf{r}_i,\mathbf{r}_j) = v_\mathrm{int}(\mathbf{r}_j,\mathbf{r}_i)$ which yields

$$\boldsymbol{\nabla}_i V = \boldsymbol{\nabla}_i V_\mathrm{ext}(\mathbf{r}_i,t) + \sum_{j\neq i}\boldsymbol{\nabla}_i v_\mathrm{int}(\mathbf{r}_i,\mathbf{r}_j)\,. \tag{9.3}$$

We split Eq. (9.1) into three terms

$$\partial_t \varrho^{(1)}(\mathbf{r}_1,t) = T^\mathrm{diff} + T^\mathrm{ext} + T^\mathrm{int}\,, \tag{9.4}$$

where each term is further decomposed to the terms of the sum in Eq. (9.1) for $i=1$ and $i>1$. We begin with the diffusive terms

$$\begin{aligned}T^\mathrm{diff}_{i=1} &= N\frac{k_\mathrm{B}T}{\gamma}\boldsymbol{\nabla}_1\cdot\boldsymbol{\nabla}_1\int \mathrm{d}\mathbf{r}_2\ldots\mathrm{d}\mathbf{r}_N\,P\\ &= D_0\boldsymbol{\nabla}_1^2\varrho^{(1)}(\mathbf{r}_1,t)\end{aligned} \tag{9.5}$$

$$\begin{aligned}T^\mathrm{diff}_{i>1} &= ND_0\sum_{i=2}^{N}\int \mathrm{d}\mathbf{r}_2\ldots\mathrm{d}\mathbf{r}_N\boldsymbol{\nabla}_i\cdot\boldsymbol{\nabla}_i P\\ &= ND_0\sum_{i=2}^{N}\int \mathrm{d}\mathbf{r}_2\ldots\mathrm{d}\mathbf{r}_{i-1}\mathrm{d}\mathbf{r}_{i+1}\ldots\mathrm{d}\mathbf{r}_N\oint \mathbf{dA}(\mathbf{r}_i)\cdot\boldsymbol{\nabla}_i P\,.\end{aligned} \tag{9.6}$$

In the last equation Gauss' theorem was used. The integration with the surface element $\mathbf{dA}$ runs over the boundary of the domain on which P is defined, which was not specified yet. However, it makes sense to *assume* that the boundary integrals vanish for every i:

$$\oint \mathbf{dA}(\mathbf{r}_i) \cdot \boldsymbol{\nabla}_i P = 0 \quad \text{and} \quad \oint \mathbf{dA}(\mathbf{r}_i) \cdot P \boldsymbol{\nabla}_i V = 0\,. \tag{9.7}$$

Periodic boundary conditions fulfil Eq. (9.7) and natural boundary conditions ($P = 0$ and $\boldsymbol{\nabla}_i P = 0$ at the boundary) fulfil Eq. (9.7), too. Using the boundary conditions Eq. (9.7) in Eq. (9.6) yields

$$T^{\text{diff}}_{i>1} = 0\,. \tag{9.8}$$

We now consider the external terms

$$\begin{aligned} T^{\text{ext}}_{i=1} &= \frac{N}{\gamma} \boldsymbol{\nabla}_1 \cdot \int \mathrm{d}\mathbf{r}_2 \ldots \mathrm{d}\mathbf{r}_N \, P \, \boldsymbol{\nabla}_1 V_{\text{ext}}(\mathbf{r}_1, t) \\ &= \frac{1}{\gamma} \boldsymbol{\nabla}_1 \cdot \left(\varrho^{(1)}(\mathbf{r}_1, t) \boldsymbol{\nabla}_1 V_{\text{ext}}(\mathbf{r}_1, t) \right) \end{aligned} \tag{9.9}$$

$$\begin{aligned} T^{\text{ext}}_{i>1} &= \frac{N}{\gamma} \int \mathrm{d}\mathbf{r}_2 \ldots \mathrm{d}\mathbf{r}_N \sum_{i=2}^{N} \boldsymbol{\nabla}_i \cdot (P \boldsymbol{\nabla}_i V_{\text{ext}}(\mathbf{r}_i, t)) \\ &= N D_0 \sum_{i=2}^{N} \int \mathrm{d}\mathbf{r}_2 \ldots \mathrm{d}\mathbf{r}_{i-1} \mathrm{d}\mathbf{r}_{i+1} \ldots \mathrm{d}\mathbf{r}_N \oint \mathbf{dA}(\mathbf{r}_i) \cdot P \boldsymbol{\nabla}_i V_{\text{ext}}(\mathbf{r}_i, t) \\ &= 0\,. \end{aligned} \tag{9.10}$$

We now turn to the interaction terms

$$T^{\text{int}}_{i=1} = \frac{N}{\gamma} \boldsymbol{\nabla}_1 \cdot \int \mathrm{d}\mathbf{r}_2 \ldots \mathrm{d}\mathbf{r}_N \sum_{j=2}^{N} P \, \boldsymbol{\nabla}_1 v_{\text{int}}(\mathbf{r}_1, \mathbf{r}_j) \tag{9.11}$$

$$\begin{aligned} T^{\text{int}}_{i>1} &= \frac{N}{\gamma} \int \mathrm{d}\mathbf{r}_2 \ldots \mathrm{d}\mathbf{r}_N \sum_{i=2}^{N} \boldsymbol{\nabla}_i \cdot \left(P \sum_{j \neq i} \boldsymbol{\nabla}_i v_{\text{int}}(\mathbf{r}_i, \mathbf{r}_j) \right) \\ &= \frac{N}{\gamma} \sum_{i=2}^{N} \int \mathrm{d}\mathbf{r}_2 \ldots \mathrm{d}\mathbf{r}_{i-1} \mathrm{d}\mathbf{r}_{i+1} \ldots \mathrm{d}\mathbf{r}_N \oint \mathbf{dA}(\mathbf{r}_i) \cdot \left(P \sum_{j \neq i} \boldsymbol{\nabla}_i v_{\text{int}}(\mathbf{r}_i, \mathbf{r}_j) \right) \\ &= 0\,. \end{aligned} \tag{9.12}$$

In Eq. (9.11) we swap sum and integration and rename the integration variables such that $\mathbf{r}_2$ and $\mathbf{r}_j$ are swapped. Under the *assumption* that $\mathbf{r}_i$ and $\mathbf{r}_j$ can be swapped in P, i.e.

$$\begin{aligned} &P(\mathbf{r}_1, \ldots, \mathbf{r}_{i-1}, \mathbf{r}_i, \mathbf{r}_{i+1}, \ldots, \mathbf{r}_{j-1}, \mathbf{r}_j, \mathbf{r}_{j+1}, \ldots, \mathbf{r}_N, t) \\ =&P(\mathbf{r}_1, \ldots, \mathbf{r}_{i-1}, \mathbf{r}_j, \mathbf{r}_{i+1}, \ldots, \mathbf{r}_{j-1}, \mathbf{r}_i, \mathbf{r}_{j+1}, \ldots, \mathbf{r}_N, t)\,, \end{aligned} \tag{9.13}$$

we arrive at

$$\begin{aligned} T^{\text{int}}_{i=1} &= \frac{N}{\gamma} \boldsymbol{\nabla}_1 \cdot \sum_{j=2}^{N} \int \mathrm{d}\mathbf{r}_2 \boldsymbol{\nabla}_1 v_{\text{int}}(\mathbf{r}_1, \mathbf{r}_2) \int \mathrm{d}\mathbf{r}_3 \ldots \mathrm{d}\mathbf{r}_N \, P(\mathbf{r}_1, \mathbf{r}_2, \mathbf{r}_3, \ldots, \mathbf{r}_N, t) \\ &= \frac{1}{\gamma} \boldsymbol{\nabla}_1 \cdot \int \mathrm{d}\mathbf{r}_2 \, \boldsymbol{\nabla}_1 v_{\text{int}}(\mathbf{r}_1, \mathbf{r}_2) \, \varrho^{(2)}(\mathbf{r}_1, \mathbf{r}_2, t)\,. \end{aligned} \tag{9.14}$$

Gathering the terms together, we see that all $i > 1$ terms are zero and that the $i = 1$ contributions to Eq. (9.4) yield Eq. (2.28).

9.2 Separation of the 2D Smoluchowski equation

We consider the SE (2.9) in two dimensions where the force is a gradient of a potential of the form

$$V(x, y) = u(x) + w(y)\,, \tag{9.15}$$

where u and w are arbitrary potentials. The SE reads

$$\partial_t P(x, y, t) = D_0 \partial_{xx} P + D_0 \partial_{yy} P + \partial_x (P u')/\gamma + \partial_y (P w')/\gamma\,. \tag{9.16}$$

We introduce the operators $\mathcal{L}_x$ and $\mathcal{L}_y$ which operate on a 1D probability density

$$\mathcal{L}_\alpha p(\alpha) = D_0 \partial_{\alpha\alpha} p - \partial_\alpha (p f_\alpha)/\gamma\,. \tag{9.17}$$

The force f_α is set to $f_x(x) = -u'(x)$ and $f_y(y) = -w'(y)$. Using the operator notation, the SE reads

$$\partial_t P(x, y, t) = \mathcal{L}_x P + \mathcal{L}_y P\,. \tag{9.18}$$

The solution of Eq. (9.18) is given by

$$P(x, y, t) = \exp(t(\mathcal{L}_x + \mathcal{L}_y)) P(x, y, 0)\,, \tag{9.19}$$

where the exponential function of an operator is defined as the series

$$\exp(A) = \sum_{i=0}^{\infty} \frac{A^n}{n!}\,. \tag{9.20}$$

The solution can be verified by inserting Eq. (9.19) into Eq. (9.18). By applying the Baker-Campbell-Hausdorff formula we can transform Eq. (9.19) into

$$P(x, y, t) = \exp(t\mathcal{L}_x) \exp(t\mathcal{L}_y) P(x, y, 0)\,, \tag{9.21}$$

because $\mathcal{L}_x$ and $\mathcal{L}_y$ commute. We now assume that the probability density is separable at $t = 0$, i.e. functions $\xi(x, 0)$ and $\psi(y, 0)$ exist such that

$$P(x, y, 0) = \xi(x, 0)\psi(y, 0)\,. \tag{9.22}$$

It follows that the probability density is separable at all times:

$$\begin{aligned} P(x, y, t) &= \exp(t\mathcal{L}_x) \exp(t\mathcal{L}_y) \xi(x, 0)\psi(y, 0) = \exp(t\mathcal{L}_x)\xi(x, 0) \exp(t\mathcal{L}_y)\psi(y, 0) \\ &= \xi(x, t)\psi(y, t)\,, \end{aligned} \tag{9.23}$$

where $\xi(x, t) = \exp(t\mathcal{L}_x)\xi(x, 0)$ and $\psi(y, t) = \exp(t\mathcal{L}_y)\psi(y, 0)$ are solutions of 1D SEs.

BIBLIOGRAPHY

[1] Z. Li and T. Ngai: "Microgel particles at the fluid-fluid interfaces" Nanoscale **5**, 1399 (2013).

[2] A. B. Kolomeisky: "Motor proteins and molecular motors: how to operate machines at the nanoscale" J. Phys.: Cond. Mat. **25**, 463101 (2013).

[3] U. Raviv, S. Giasson, N. Kampf, J.-F. Gohy, R. Jérôme, and J. Klein: "Lubrication by charged polymers" Nature **425**, 163 (2003).

[4] R. W. Baker: "Membrane technology and applications" Wiley (2004).

[5] G. L. Hunter and E. R. Weeks: "The physics of the colloidal glass transition" Rep Prog Phys **75**, 066501 (2012).

[6] R. C. Spero, L. Vicci, J. Cribb, D. Bober, V. Swaminathan, E. T. O'brien, S. L. Rogers, and R. Superfine: "High throughput system for magnetic manipulation of cells, polymers, and biomaterials" Rev. Sci. Instrum. **79**, 083707 (2008).

[7] F. Marchesoni and P. Hänggi: "Artificial Brownian motors: Controlling transport on the nanoscale" Rev. Mod. Phys. **81**, 387 (2009).

[8] P. S. Burada, P. Hänggi, F. Marchesoni, G. Schmid, and P. Talkner: "Diffusion in Confined Geometries" Chemphyschem **10**, 45 (2009).

[9] P. Reimann: "Brownian motors: noisy transport far from equilibrium" Phys. Rep. **361**, 57 (2002).

[10] H. Risken: "The Fokker-Planck Equation" Springer, (1984).

[11] P. Hänggi, P. Talkner, and M. Borkovec: "Reaction-rate theory: fifty years after Kramers" Rev. Mod. Phys. **62**, 251 (1990).

[12] T. Tadros: "Emulsion science and technology" Wiley (2009).

[13] L. L. Schramm: "Emulsions, Foams, and Suspensions: Fundamentals and Applications" Wiley (2006).

[14] R. Mezzenga, P. Schurtenberger, A. Burbidge, and M. Michel: "Understanding foods as soft materials" Nature Materials **4**, 729 (2005).

[15] A. Otto, J. D. Plessis, and J. W. Wiechers: "Formulation effects of topical emulsions on transdermal and dermal delivery" International Journal Of Cosmetic Science **31**, 1 (2009).

[16] T. F. Tadros: "Colloids in Paints" Wiley, Weinheim (2010).

[17] D. F. Evans and H. Wennerström: "The colloidal domain – where physics, chemistry, biology, and technology meet" VCH New York, Weinheim, Cambridge (1994).

[18] W. B. Russel, D. A. Saville, and W. R. Showalter: "Colloidal Dispersions" Cambridge University Press (1989).

[19] S. Friberg, K. Larsson, and J. Sjöblom: "Food emulsions" Marcel Dekker, New York, Basel (2004).

[20] J. E. Norton and I. T. Norton: "Designer colloids – towards healthy everyday foods?" Soft Matter **6**, 3735 (2010).

[21] C. J. Brinker and G. W. Scherer: "Sol-gel science – The physics and chemistry of sol-gel processing" Academic Press Elsevier (1990).

[22] H. Löwen: "Introduction to colloidal dispersions in external fields" Eur. Phys. J. Spec. Top. **222**, 2727 (2013).

[23] M. Hecht, J. Harting, T. Ihle, and H. J. Herrmann: "Simulation of claylike colloids" Phys. Rev. E **72**, 011408 (2005).

[24] C. Rodriguez-Navarro, E. Ruiz-Agudo, M. Ortega-Huertas, and E. Hansen: "Nanostructure and Irreversible Colloidal Behavior of Ca(OH)2: Implications in Cultural Heritage Conservation" Langmuir **21**, 10948 (2005).

[25] M. Takeda, T. Matsunaga, T. Nishida, H. Endo, T. Takahashi, and M. Shibayama: "Rheo-SANS Studies on Shear Thickening in Clay-Poly(ethylene oxide) Mixed Solutions" Macromolecules **43**, 7793 (2010).

[26] S. Papatzani, K. Paine, and J. Calabria-Holley: "A comprehensive review of the models on the nanostructure of calcium silicate hydrates" Construction And Building Materials **74**, 219 (2015).

[27] F. M. Fernandes, T. Coradin, and C. Aimé: "Self-Assembly in Biosilicification and Biotemplated Silica Materials" Nanomaterials **4**, 792 (2014).

[28] J. Perez-Vilar and R. L. Hill: "The Structure and Assembly of Secreted Mucins" J Biol Chem **274**, 31751 (1991).

[29] Y. Cu and W. M. Saltzman: "Mathematical modeling of molecular diffusion through mucus" Adv Drug Deliv Rev **61**, 101 (2009).

[30] I. Hamley: "Introduction to Soft Matter: Synthetic and Biological Self-Assembling Materials" Wiley (2007).

[31] P.-G. de Gennes: "Soft matter: more than words" Soft Matter **1**, 16 (2005).

[32] E. Zaccarelli: "Colloidal gels: equilibrium and non-equilibrium routes" J Phys: Cond Mat **19**, 323101 (2007).

[33] H. Schmidle: "Computer simulations of complex fluids in two dimensions" PhD thesis, urn:nbn:de:kobv:83-opus-35267 (2012).

[34] P. J. Lu and D. A. Weitz: "Colloidal Particles: Crystals, Glasses, and Gels" Ann Rev Cond Mat Phys **4**, 217 (2013).

[35] E. del Gado and W. Kob: "Length-Scale-Dependent Relaxation in Colloidal Gels" Phys. Rev. Lett. **98**, 028303 (2007).

[36] D. Briedis, M. F. Moutrie, and R. T. Balmer: "A study of the shear viscosity of human whole saliva" Rheol Acta **19**, 365 (1980).

[37] O. K. Baskurt and H. J. Meiselman: "Blood Rheology and Hemodynamics" Semin Thromb Hemost **29**, 435 (2003).

[38] N. J. Wagner and J. F. Brady: "Shear thickening in colloidal dispersions" Physics Today, October, p27 (2009).

[39] A. Majumdar, B. S. Butola, and A. Srivastava: "Optimal designing of soft body armour materials using shear thickening fluid" Materials And Design **46**, 191 (2013).

[40] X. Gong, Y. Xu, W. Zhu, S. Xuan, W. Jiang, and W. Jiang: "Study of the knife stab and puncture-resistant performance for shear thickening fluid enhanced fabric" J Composite Mater **48**, 641 (2014).

[41] J. K. G. Dhont: "An introduction to dynamics of colloids" Elsevier, Amsterdam (2003).

[42] R. Taylor, S. Coulombe, T. Otanicar, P. Phelan, A. Gunawan, W. Lv, G. Rosengarten, R. Prasher, and H. Tyagi: "Small particles, big impacts: A review of the diverse applications of nanofluids" J Appl Phys **113**, 011301 (2013).

[43] X. Z. Fan, E. Pomerantseva, M. Gnerlich, A. Brown, K. Gerasopoulos, M. McCarthy, J. Culver, and R. Ghodssi: "Tobacco mosaic virus: A biological building block for micro/nano/biosystems" J. Vac. Sci. Technol. A **31**, 050815 (2013).

[44] A. J. Archer, M. J. Robbins, and U. Thiele: "Dynamical density functional theory for the dewetting of evaporating thin films of nanoparticle suspensions exhibiting pattern formation" Phys. Rev. E **81**, 021602 (2010).

[45] C. P. Royall and S. R. Williams: "C60: The First One-Component Gel?" J. Phys. Chem. B **115**, 7288 (2011).

[46] H. M. Jaeger: "Celebrating Soft Matter's 10th Anniversary: Toward jamming by design" Soft Matter **11**, 12 (2015).

[47] R. P. Behringer, K. E. Daniels, T. S. Majmudar, and M. Sperl: "Fluctuations, correlations and transitions in granular materials: statistical mechanics for a non-conventional system" Phil. Trans. R. Soc. A **366**, 493 (2008).

[48] N. Singh, J. Singh, L. Kaur, N. S. Sodhi, and B. S. Gill: "Morphological, thermal and rheological properties of starches from different botanical sources" Food Chemistry **81**, 219 (2003).

[49] H. Freundlich and F. Juliusburger: "Quicksand as a thixotropic system" Trans. Faraday Soc. **31**, 769 (1935).

[50] A. Khaldoun, E. Eiser, G. H. Wegdam, and D. Bonn: "Rheology: Liquefaction of quicksand under stress" Nature **437**, 635 (2005).

[51] R. Wayne: "Light and Video microscopy" Academic Press, Elsevier (2014).

[52] J. C. Crocker and D. G. Grier: "Methods of Digital Video Microscopy for Colloidal Studies" J Coll Inter Sci **179**, 298 (1996).

[53] R. M. Velasco, L. S. García-Colín, and F. J. Uribe: "Entropy Production: Its Role in Non-Equilibrium Thermodynamics" Entropy **13**, 82 (2011).

[54] C. N. Likos: "Colloidal interactions: From effective potentials to structure" Rivista del nouvo cimento **37**, 125 (2014).

[55] U. Seifert: "Stochastic thermodynamics, fluctuation theorems and molecular machines, entropy, fluctuation dissipation theorem" Rep. Prog. Phys. **75**, 126001 (2012).

[56] R. Roth: "Fundamental measure theories for hard-sphere mixtures: a Review" J. Phys.: Cond. Mat. **22**, 063102 (2010).

[57] P. Olmsted: "Perspectives on shear banding in complex fluids" Rheol. Acta **47**, 283 (2008).

[58] J. C. Mauro and M. M. Smedskjaer: "Statistical mechanics of glass" J. Non-Cryst. Solids **396**, 41 (2014).

[59] J.-P. Hansen and I. R. McDonald: "Theory of simple liquids" Elsevier (2006).

[60] B. Alberts: "Molecular biology of the cell" Wiley, Weinhein, 4th edition (2004).

[61] M.-J. Huang, R. Kapral, A. S. Mikhailov, and H.-Y. Chen: "Coarse-grain simulations of active molecular machines in lipid bilayers" J. Chem. Phys. **138**, 195101 (2013).

[62] R. Lipowsky and S. Klumpp: "'Life is motion': multiscale motility of molecular motors" Physica A **352**, 53 (2005).

[63] R. Ganapathy, M. R. Buckley, S. J. Gerbode, and I. Cohen: "Direct Measurements of Island Growth and Step-Edge Barriers in Colliodal Epitaxy" Science **22**, 445 (2010).

[64] S. Bommel, N. Kleppmann, C. Weber, H. Spranger, P. Schafer, J. Novak, S. V. Roth, F. Schreiber, S. H. L. Klapp, and S. Kowarik: "Unravelling the multilayer growth of the fullerene C60 in real time" Nat. Commun. **5**, 5388 (2014).

[65] P. Tierno, F. Sagues, T. H. Johansen, and T. M. Fischer: "Colloidal transport on magnetic garnet films" Phys. Chem. Chem. Phys. **11**, 9615 (2009).

[66] K. Palczynski and J. Dzubiella: "Anisotropic Electrostatic Friction of para-Sexiphenyl on the ZnO (1010) Surface" J Phys Chem C **118**, 26368 (2014).

[67] M. J. Skaug, J. Mabry, and D. K. Schwartz: "Intermittent Molecular Hopping at the Solid-Liquid Interface" Phys. Rev. Lett. **110**, 256101 (2013).

[68] Q. Xu, L. Feng, R. Sha, N. C. Seeman, , and P. M. Chaikin: "Subdiffusion of a Sticky Particle on a Surface" Phys. Rev. Lett. **106**, 228102 (2011).

[69] T. M. Squires and S. R. Quake: "Microfluidics: Fluid physics at the nanoliter scale" Rev. Mod. Phys. **77**, 977 (2005).

[70] L. Bogunovic, R. Eichhorn, J. Regtmeier, D. Anselmetti, and P. Reimann: "Particle sorting by a structured microfluidic ratchet device with tunable selectivity: theory and experiment" Soft Matter **8**, 3900 (2012).

[71] L. Gorre-Talini, S. Jeanjean, and P. Silberzan: "Sorting of Brownian particles by the pulsed application of an asymmetric potential" Phys. Rev. E **56**, 2025 (1997).

[72] H. Wei, B.-H. Chueh, H. Wu, E. W. Hall, C.-W. Li, R. Schirhagl, J.-M. Lin, and R. N. Zare: "Particle sorting using a porous membrane in a microfluidic device" Lab Chip **11**, 238 (2011).

[73] A. B. Theberge, F. Courtois, Y. Schaerli, M. Fischlechner, C. Abell, F. Hollfelder, and W. T. S. Huck: "Microdroplets in Microfluidics: An Evolving Platform for Discoveries in Chemistry and Biology" Angew. Chem. Int. Ed. **49**, 5846 (2010).

[74] M. Yamada and M. Seki: "Hydrodynamic filtration for on-chip particle concentration and classification utilizing microfluidics" Lab On A Chip **5**, 1233 (2005).

[75] P. Tierno, S. V. Reddy, M. G. Roper, T. H. Johansen, and T. M. Fischer: "Transport and Separation of Biomolecular Cargo on Paramagnetic Colloidal Particles in a Magnetic Ratchet" J Phys Chem B **112**, 3833 (2008).

[76] C. Marquet, A. Buguin, L. Talini, and P. Silberzan: "Rectified Motion of Colloids in Asymmetrically Structured Channels" Phys. Rev. Lett. **88**, 168301 (2002).

[77] L. Gao, M. A. Tahir, L. N. Virgin, and B. B. Yellen: "Multiplexing superparamagnetic beads driven by multi-frequency ratchets" Lab Chip **11**, 4214 (2011).

[78] M. C. Jenkins and S. U. Egelhaaf: "Colloidal suspensions in modulated light fields" J. Phys.: Cond. Mat. **20**, 404220 (2008).

[79] M. Wördemann: "Application in Optical Trapping, Manipulation, and Organisation: Structured Light Fields" Springer (2012).

[80] H. Löwen: "Colloidal soft matter under external control" J. Phys.: Cond. Mat. **13**, R415 (2001).

[81] M. P. N. Juniper, R. Besseling, D. G. A. L. Aarts, and R. P. A. Dullens: "Acousto-optically generated potential energy landscapes: Potential mapping using colloids under flow" Optics Express **20**, 28707 (2012).

[82] C. Dalle-Ferrier, M. Krüger, R. D. L. Hanes, S. Walta, M. C. Jenkins, and S. U. Egelhaaf: "Dynamics of dilute colloidal suspensions in modulated potentials" Soft Matter **7**, 2064 (2011).

[83] F. Evers, R. D. L. Hanes, C. Zunke, R. F. Capellmann, J. Bewerunge, C. Dalle-Ferrier, M. C. Jenkins, I. Ladadwa, A. Heuer, R. Castaneda-Priego, and S. U. Egelhaaf: "Colloids in light fields: particle dynamics in random and periodic energy landscapes" Eur. Phys. J. Spec. Top. **222**, 2995 (2013); arxiv:1308.5632 [cond-mat.soft] (2013).

[84] V. Blickle, T. Speck, L. Helden, U. Seifert, and C. Bechinger: "Thermodynamics of a Colloidal Particle in a Time-Dependent Nonharmonic Potential" Phys. Rev. Lett. **96**, 070603 (2006).

[85] J. Mikhael, G. Gera, T. Bohlein, and C. Bechinger: "Phase behavior of colloidal monolayers in quasiperiodic light fields" Soft Matter **7**, 1352 (2011).

[86] A. V. Arzola, K. Volke-Sepulveda, and J. L. Mateos: "Experimental Control of Transport and Current Reversals in a Deterministic Optical Rocking Ratchet" Phys. Rev. Lett. **106**, 168104 (2011).

[87] R. D. L. Hanes, C. Dalle-Ferrier, M. Schmiedeberg, M. C. Jenkins, and S. U. Egelhaaf: "Colloids in one dimensional random energy landscapes" Soft Matter **8**, 2714 (2012).

[88] S. Bleil, P. Reimann, and C. Bechinger: "Directing Brownian motion by oscillating barriers" Phys. Rev. E **75**, 031117 (2007).

[89] M. Evstigneev, O. Zvyagolskaya, S. Bleil, R. Eichhorn, C. Bechinger, and P. Reimann: "Diffusion of colloidal particles in a tilted periodic potential: Theory versus experiment" Phys. Rev. E **77**, 041107 (2008).

[90] T. Bohlein, J. Mikhael, and C. Bechinger: "Observation of kinks and antikinks in colloidal monolayers driven across ordered surfaces" Nature Materials **11**, 126 (2012).

[91] B. J. Lopez, N. J. Kuwada, E. M. Craig, B. R. Long, and H. Linke: "Realization of a Feedback Controlled Flashing Ratchet" Phys. Rev. Lett. **101**, 220601 (2008).

[92] S.-H. Lee and D. G. Grier: "Giant Colloidal Diffusivity on Corrugated Optical Vortices" Phys. Rev. Lett. **96**, 190601 (2006).

[93] J. Fisher, J. Cummings, K. Desai, L. Vicci, B. Wilde, K. Keller, C. Weigle, G. Bishop, R. Taylor, and C. Davis: "Three-dimensional force microscope: A nanometric optical tracking and magnetic manipulation system for the biomedical sciences" Rev. Sci. Instrum. **76**, 053711 (2005).

[94] M. A. Tahir, L. Gao, L. N. Virgin, and B. B. Yellen: "Transport of superparamagnetic beads through a two-dimensional potential energy landscape" Phys. Rev. E **84**, 011403 (2011).

[95] U. Häfeli: "Magnetically modulated therapeutic systems" International J. Pharmaceutics **277**, 19 (2004).

[96] I. de Vlaminck and C. Dekker: "Recent Advances in Magnetic Tweezers" Annual Review Of Biophysics **41**, 453 (2012).

[97] E. Mirowski, J. Moreland, A. Zhang, S. E. Russek, and M. J. Donahue: "Manipulation and sorting of magnetic particles by a magnetic force microscope on a microfluidic magnetic trap platform" Appl. Phys. Lett. **86**, 243901 (2005).

[98] S. Aliaskarisohi, T. H. Johansen, and T. M. Fischer: "Using Symmetry Breaking for Directed Transport of Paramagnetic Colloids on Garnet Films" J Phys Chem B **115**, 2243 (2011).

[99] A. Ros, R. Eichhorn, J. Regtmeier, T. T. Duong, P. Reimann, and D. Anselmetti: "Brownian motion: Absolute negative particle mobility" Nature **436**, 928 (2005).

[100] Y. Jun, M. Gavrilov, and J. Bechhoefer: "High-Precision Test of Landauer's Principle in a Feedback Trap" Phys. Rev. Lett. **113**, 190601 (2014).

[101] G. Johnson: "Kinesin protein with cargo" ValeLab,https://valelab.ucsf.edu/external/images/res-kinesin-new/KinesinCargoArt.jpg (last access 25th Mar 2015).

[102] N. Kleppmann: "Simulation of growth and self-assembly of complex molecules on surfaces" PhD thesis, TU Berlin (2015).

[103] D. Reguera, A. Luque, P. S. Burada, G. Schmid, J. M. Rubi, and P. Hänggi: "Entropic Splitter for Particle Separation" Phys. Rev. Lett. **108**, 020604 (2012).

[104] M. Venturolia, M. M. Sperotto, M. Kranenburg, and B. Smit: "Mesoscopic models of biological membranes" Physics Reports **437**, 1 (2006).

[105] P. Vidossich, M. Cascella, and P. Carloni: "Dynamics and Energetics of Water Permeation Through the Aquaporin Channel" Proteins **55**, 924 (2004).

[106] K. Siva and R. Elber: "Ion permeation through the gramicidin channel: Atomically detailed modeling by the Stochastic Difference Equation" Proteins: Structure, Function, And Genetics **50**, 63 (2003).

[107] D. Bemporad, J. W. Essex, and C. Luttmann: "Permeation of Small Molecules through a Lipid Bilayer: A Computer Simulation Study" J. Phys. Chem. B **108**, 4875 (2004).

[108] K. Hahn, J. Kärger, and V. Kukla: "Single-File Diffusion Observation" Phys. Rev. Lett. **76**, 2762 (1996).

[109] P. K. Ghosh, P. Hanggi, F. Marchesoni, F. Nori, and G. Schmid: "Detectable inertial effects on Brownian transport through narrow pores" EPL **98**, 50002 (2012).

[110] E. Beerdsen, D. Dubbeldam, and B. Smit: "Molecular Understanding of Diffusion in Confinement" Phys. Rev. Lett. **95**, 164505 (2005).

[111] D. A. Nield and A. Bejan: "Convection in Porous Media" Springer (2006).

[112] A. Manthiram, Y. Fu, S.-H. Chung, C. Zu, and Y.-S. Su: "Rechargeable Lithium-Sulfur Batteries" Chem. Rev. **114**, 11751 (2014).

[113] G. Zhao, Y. Niu, L. Zhang, and K. Sun: "Ruthenium oxide modified titanium dioxide nanotube arrays as carbon and binder free lithium-air battery cathode catalyst" Journal Of Power Sources **270**, 386 (2014).

[114] S. Kubo, R. Demir-Cakan, L. Zhao, R. White, and M.-M. Titirici: "Porous Carbohydrate-Based Materials via Hard Templating" Chemsuschem **3**, 188 (2010).

[115] J. Chmiola, G. Yushin, Y. Gogotsi, C. Portet, P. Simon, and P. L. Taberna: "Anomalous Increase in Carbon Capacitance at Pore Sizes Less Than 1 Nanometer" Science **313**, 1760 (2006).

[116] E. R. Weeks and D. A. Weitz: "Subdiffusion and the cage effect studied near the colloidal glass transition" Chem Phys **284**, 361 (2002).

[117] P. Pal, C. S. O'hern, J. Blawzdziewicz, E. R. Dufresne, and R. Stinchcombe: "Minimal model for kinetic arrest" Phys. Rev. E **78**, 011111 (2008).

[118] W. Kob, J.-L. Barrat, F. Sciortino, and P. Tartaglia: "Aging in a simple glass former" J. Phys.: Cond. Mat. **12**, 6385 (2000).

[119] B. Vorselaars, A. V. Lyulin, K. Karatasos, and M. A. J. Michels: "Non-Gaussian nature of glassy dynamics by cage to cage motion" Phys. Rev. E **75**, 011504 (2007).

[120] K. Schweizer: "Derivation of a microscopic theory of barriers and activated hopping transport in glassy liquids and suspensions" J. Chem. Phys. **123**, 244501 (2005).

[121] A. Heuer, B. Doliwa, and A. Saksaengwijit: "Potential-energy landscape of a supercooled liquid and its resemblance to a collection of traps" Phys. Rev. E **72**, 021503 (2005).

[122] M. Bestehorn: "Hydrodynamik und Strukturbildung" Springer (2006).

[123] A. J. Archer, P. Hopkins, and M. Schmidt: "Dynamics in inhomogeneous liquids and glasses via the test particle limit" Phys. Rev. E **75**, 040501 (2007).

[124] K. Lichtner and S. H. L. Klapp: "Feedback-controlled transport in an interacting colloidal system" EPL **92**, 40007 (2010).

[125] P. Reimann, C. van den Broeck, H. Linke, P. Hänggi, J. M. Rubi, and A. Perez-Madrid: "Diffusion in tilted periodic potentials: Enhancement, universality, and scaling" Phys. Rev. E **65**, 031104 (2002).

[126] A. Einstein: "Über die von der molekularkinetischen Theorie der Wärme geforderte Bewegung von in ruhenden Flüssigkeiten suspendierten Teilchen" Annalen Der Physik **17**, 549 (1905).

[127] H. A. Kramers: "Brownian motion in a field of force and the diffusion model of chemical reactions" Physica **7**, 284 (1940).

[128] E. W. Montroll and G. H. Weiss: "Random Walks on Lattices. II" J Math Phys **6**, 167 (1965).

[129] J. W. Haus and K. W. Kehr: "Diffusion in regular and disordered lattices" Phys. Rep. **150**, 263 (1987).

[130] F. Höfling and T. Franosch: "Anomalous transport in the crowded world of biological cells" Rep Prog Phys **76**, 046602 (2013).

[131] R. Metzler and J. Klafter: "The random walk's guide to anomalous diffusion: a fractional dynamics approach" Phys. Rep. **339**, 1 (2000).

[132] R. Metzler and J. Klafter: "The restaurant at the end of the random walk: recent developments in the description of anomalous transport by fractional dynamics" J. Phys. A: Math. Gen. **37**, R161 (2004).

[133] M. J. Saxton: "Anomalous Diffusion Due to Obstacles: A Monte Carlo Study" Biophys. J. **66**, 394 (1994).

[134] S. Havlin and D. Ben-Avraham: "Diffusion in disordered media" Adv Phys **36**, 695 (1987).

[135] W. Gotze and L. Sjogren: "Relaxation processes in supercooled liquids" Rep. Prog. Phys. **55**, 241 (1992).

[136] D. Winter, J. Horbach, P. Virnau, and K. Binder: "Active Nonlinear Microrheology in a Glass-Forming Yukawa Fluid" Phys. Rev. Lett. **108**, 028303 (2012).

[137] T. A. Vezirov and S. H. L. Klapp: "Non-equilibrium dynamics of a confined colloidal bilayer in planar shear flow" Phys. Rev. E **88**, 052307 (2013); arxiv:1305.7371 [cond-mat.soft] (2013).

[138] H. Schmidle, S. Jäger, C. K. Hall, O. D. Velev, and S. H. L. Klapp: "Two-dimensional colloidal networks induced by a uni-axial external field" Soft Matter **9**, 2518 (2013).

[139] M. Bier, R. van Roij, M. Dijkstra, and P. V. D. Schoot: "Self-Diffusion of Particles in Complex Fluids: Temporary Cages and Permanent Barriers" Phys. Rev. Lett. **101**, 215901 (2008).

[140] N. Kleppmann and S. H. L. Klapp: "Particle-resolved dynamics during multilayer growth of C60" Phys Rev B **91**, 045436 (2015); arxiv:1410.8763 [cond-mat.mes-hall] (2014).

[141] E. Zaccarelli, C. Valeriani, E. Sanz, W. C. K. Poon, M. E. Cates, and P. N. Pusey: "Crystallization of Hard-Sphere Glasses" Phys. Rev. Lett. **103**, 135704 (2009).

[142] J. Jordanovic, S. Jäger, and S. H. L. Klapp: "Crossover from Normal to Anomalous Diffusion in Systems of Field-Aligned Dipolar Particles" Phys. Rev. Lett. **106**, 038301 (2011).

[143] M. J. Saxton: "A Biological Interpretation of Transient Anomalous Subdiffusion. I. Qualitative Model" Biophys. J. **92**, 1178 (2007).

[144] Y. Gao and M. L. Kilfoil: "Intermittent and spatially heterogeneous single-particle dynamics close to colloidal gelation" Phys. Rev. E **79**, 051406 (2009).

[145] D. G. Levitt: "Dynamics of a Single-File Pore: Non-Fickian Behavior" Phys. Rev. A **8**, 3050 (1973).

[146] D. Lucena, D. V. Tkachenko, K. Nelissen, V. R. Misko, W. P. Ferreira, G. A. Farias, and F. M. Peeters: "Transition from single-file to two-dimensional diffusion of interacting particles in a quasi-one-dimensional channel" Phys. Rev. E **85**, 031147 (2012).

[147] S. Herrera-Velarde and R. Castañeda-Priego: "Structure and dynamics of interacting Brownian particles in one-dimensional periodic substrates" J. Phys.: Cond. Mat. **19**, 226215 (2007).

[148] A. Taloni and F. Marchesoni: "Single-File Diffusion on a Periodic Substrate" Phys. Rev. Lett. **96**, 020601 (2006).

[149] M. Evstigneev, S. von Gehlen, and P. Reimann: "Interaction-controlled Brownian motion in a tilted periodic potential" Phys. Rev. E **79**, 011116 (2009).

[150] R. L. Stratonovich: "The synchronization of a self-oscillator in the presence of noise" Radiotekh. Elektron. **3**, 497 (1958).

[151] For an english translation of [150] see [152]. The velocity formula can be found in [10,125], too..

[152] P. I. Kuznetsov, R. L. Stratonovich, and V. I. Tikhonov: "Non-Linear Transformations of Stochastic Processes" Oxford , Pergamon (1965).

[153] J. M. Sancho and A. M. Lacasta: "The rich phenomenology of Brownian particles in nonlinear potential landscapes" Eur. Phys. J. Spec. Top. **187**, 49 (2010).

[154] C. W. Gardiner: "Handbook of Stochastic Methods" Springer, Berlin, Heidelberg, New York (1985).

[155] P. Reimann, G. J. Schmid, and P. Hänggi: "Universal equivalence of mean-first passage time and Kramers rate" Phys. Rev. E **60**, R1 (1999).

[156] S. Redner: "A Guide to First-Passage Processes" Cambridge Univ. Press (2007).

[157] D. R. Cox: "Renewal theory" Wiley, New York todo:check publisher (1962).

[158] V. Tejedor, R. Voituriez, and O. Benichou: "Optimizing Persistent Random Searches" Phys. Rev. Lett. **108**, 088103 (2012).

[159] T. Verechtchaguina, I. M. Sokolov, and L. Schimansky-Geier: "First passage time densities in resonate-and-fire models" Phys. Rev. E **73**, 031108 (2006).

[160] M. N. Shadlen and W. T. Newsome: "The Variable Discharge of Cortical Neurons: Implications for Connectivity, Computation, and Information Coding" J Neuro Sci **18**, 3870 (1998).

[161] M. Siler and P. Zemánek: "Particle jumps between optical traps in a one-dimensional (1D) optical lattice" New J. Phys. **12**, 083001 (2010).

[162] B. Dybiec: "Escape from the potential well: Competition between long jumps and long waiting times" J. Chem. Phys. **133**, 244114 (2010).

[163] D. Mondal and D. S. Ray: "Diffusion over an entropic barrier: Non-Arrhenius behavior" Phys. Rev. E **82**, 032103 (2010).

[164] O. Benichou, A. Bodrova, D. Chakraborty, P. Illien, A. Law, C. Mejía-Monasterio, G. Oshanin, and R. Voituriez: "Geometry-Induced Superdiffusion in Driven Crowded Systems" Phys. Rev. Lett. **111**, 260601 (2013).

[165] M. von Smoluchowski: "Experimentall nachweisbare, der üblichen Thermodynamik widersprechende Molekularphänomene" Physik. Zeitschr. **13**, 1069 (1912).

[166] M. Jacobs: "Diffusion processes" Springer, New York (1967).

[167] S. Martens, G. Schmid, L. Schimansky-Geier, and P. Hänggi: "Entropic particle transport: Higher-order corrections to the Fick-Jacobs diffusion equation" Phys. Rev. E **83**, 051135 (2011).

[168] S. Martens, G. Schmid, L. Schimansky-Geier, and P. Hänggi: "Biased Brownian motion in extremely corrugated tubes" Chaos **21**, 047518 (2011).

[169] S. Martens, G. Schmid, A. V. Straube, L. Schimansky-Geier, and P. Hänggi: "How entropy and hydrodynamics cooperate in rectifying particle transport" Eur. Phys. J. Spec. Top. **222**, 2453 (2013); arxiv:1304.4438v1 [cond-mat.stat-mech] (2013).

[170] P. Kalinay: "When is the next extending of Fick-Jacobs equation necessary?" J. Chem. Phys. **139**, 054116 (2013).

[171] B.-Q. Ai, Y.-F. He, F.-G. Li, and W.-R. Zhong: "Hydrodynamically enforced entropic Brownian pump" J. Chem. Phys. **138**, 154107 (2013).

[172] U. M. B. Marconi, S. Melchionna, and I. Pagonabarraga: "Effective electrodiffusion equation for non-uniform nanochannels" J. Chem. Phys. **138**, 244107 (2013).

[173] S. Martens: "Transport of Brownian particles in confined geometries – steps beyond the Fick-Jacobs approach" PhD thesis, HU Berlin, urn:nbn:de:kobv:11-100210715 (2013).

[174] J. A. Greenberg, B. L. Schmittberger, and D. J. Gauthier: "Bunching-induced optical nonlinearity and instability in cold atoms" Optics Express **19**, 22535 (2011).

[175] J. A. Greenberg: "Collective Light-matter Interactions via Emergent Order in Cold Atoms" PhD thesis, Duke University, http://dukespace.lib.duke.edu/dspace/handle/10161/5595 (2012).

[176] O. M. Braun and Y. S. Kivshar: "Nonlinear dynamics of the Frenkel–Kontorova model" Phys. Rep. **306**, 1 (1998).

[177] C. Noguera and J. Goniakowski: "Structural phase diagrams of supported oxide nanowires from extended Frenkel-Kontorova models of diatomic chains" J. Chem. Phys. **139**, 084703 (2013).

[178] C. Reichhardt, C. Bairnsfather, and C. J. O. Reichhardt: "Positive and negative drag, dynamic phases, and commensurability in coupled one-dimensional channels of particles with Yukawa interactions" Phys. Rev. E **83**, 061404 (2011).

[179] C. Bairnsfather, C. J. O. Reichhardt, and C. Reichhardt: "The effect of pinning on drag in coupled one-dimensional channels of particles" EPL **94**, 18001 (2011).

[180] R. Bustos-Marún, G. Refael, and F. von Oppen: "Adiabatic Quantum Motors" Phys. Rev. Lett. **111**, 060802 (2013).

[181] G. Augello, D. Valenti, and B. Spagnolo: "Non-Gaussian noise effects in the dynamics of a short overdamped Josephson junction" Eur. Phys. J B **78**, 225 (2010).

[182] V. I. Mel'Nikov: "The Kramers problem: Fifty years of development" Phys. Rep. **209**, 1 (1991).

[183] D. Vion, M. Götz, P. Joyez, D. Esteve, and M. H. Devoret: "Thermal Activation above a Dissipation Barrier: Switching of a Small Josephson Junction" Phys. Rev. Lett. **77**, 3435 (1996).

[184] S. D. Goldt and E. M. Terentjev: "Role of the potential landscape on the single-file diffusion through channels" J. Chem. Phys. **141**, 224901 (2014).

[185] P. Reimann, C. van den Broeck, H. Linke, P. Hänggi, J. M. Rubi, and A. Pérez-Madrid: "Giant Acceleration of Free Diffusion by Use of Tilted Periodic Potentials" Phys. Rev. Lett. **87**, 010602 (2001).

[186] P. Tierno, P. Reimann, T. H. Johansen, and F. Sagués: "Giant Transversal Particle Diffusion in a Longitudinal Magnetic Ratchet" Phys. Rev. Lett. **105**, 230602 (2010).

[187] E. Heinsalu, T. Örd, and R. Tammelo: "Peculiarities of Brownian motion depending on the structure of the periodic potentials" Acta Physica Polonica B **36**, 1613 (2004).

[188] M. J. Kim and K. S. Breuer: "Use of Bacterial Carpets to Enhance Mixing in Microfluidic Systems" J. Fluids Eng. **129**, 319 (2006).

[189] M. Schreier, P. Reimann, P. Hänggi, and E. Pollak: "Giant enhancement of diffusion and particle selection in rocked periodic potentials" Europhys. Lett. **44**, 416 (1998).

[190] P. Romanczuk, F. Müller, and L. Schimansky-Geier: "Quasideterministic transport of Brownian particles in an oscillating periodic potential" Phys. Rev. E **81**, 061120 (2010).

[191] E. Munoz-Gutiérrez, J. Alvarez-Ramirez, L. Dagdug, and G. Espinosa-Paredes: "Diffusion in one-dimensional channels with zero-mean time-periodic tilting forces" J. Chem. Phys. **136**, 114103 (2012).

[192] M. Borromeo and F. Marchesoni: "Resonant transport in pulsated devices: Mobility oscillations and diffusion peaks" Phys. Rev. E **78**, 051125 (2008).

[193] W. C. Germs, E. M. Roeling, L. J. van Ijzendoorn, R. A. J. Janssen, and M. Kemerink: "Diffusion enhancement in on/off ratchets" Appl. Phys. Lett. **102**, 073104 (2013).

[194] D. K. C. MacDonald: "Thermoelectricity" New York, Wiley (1962).

[195] E. R. Kay, D. A. Leigh, and F. Zerbetto: "Synthetic Molecular Motors and Mechanical Machines" Angew. Chem. Int. Ed. **46**, 72 (2007).

[196] C. S. Niman, M. J. Zuckermann, M. Balaz, J. O. Tegenfeldt, P. M. G. Curmi, N. R. Forde, and H. Linke: "Fluidic switching in nanochannels for the control of Inchworm: a synthetic biomolecular motor with a power stroke" Nanoscale **6**, 15008 (2014).

[197] E. Lundh and M. Wallin: "Ratchet Effect for Cold Atoms in an Optical Lattice" Phys. Rev. Lett. **94**, 110603 (2005).

[198] A. Wickenbrock, D. Cubero, N. A. A. Wahab, P. Phoonthong, and F. Renzoni: "Current reversals in a rocking ratchet: The frequency domain" Phys. Rev. E **84**, 021127 (2011).

[199] J. M. Kivioja, T. E. Nieminen, J. Claudon, O. Buisson, F. W. J. Hekking, and J. P. Pekola: "Observation of Transition from Escape Dynamics to Underdamped Phase Diffusion in a Josephson Junction" Phys. Rev. Lett. **94**, 247002 (2005).

[200] I. Zapata, R. Bartussek, F. Sols, and P. Hänggi: "Voltage Rectification by a SQUID Ratchet" Phys. Rev. Lett. **77**, 2292 (1996).

[201] M. A. Shahzamanian, M. Eatesami, and H. Yavary: "Analytical results of the Fokker-Planck equation derived for one superconducting nanowire quantum interference device and for DC SQUID: symmetric devices" Supercond. Sci. Technol. **20**, 640 (2007).

[202] S. Leibler: "moving forward noisily" Nature **370**, 412 (1994).

[203] T. R. Kelly, I. Tellitu, and J. P. Sestelo: "In Search of molecular ratchets" Angew. Chem. Int. Ed. Engl. **36**, 1866 (1997).

[204] S. H. Lee and D. G. Grier: "One-dimensional optical thermal ratchets" J. Phys.: Condens. Matt. **17**, S3685 (2005).

[205] A. Ehresmann, D. Lengemann, T. Weis, A. Albrecht, J. Langfahl-Klabes, F. Göllner, and D. Engel: "Asymmetric Magnetization Reversal of Stripe-Patterned Exchange Bias Layer Systems for Controlled Magnetic Particle Transport" Advanced Materials **23**, 5568 (2011).

[206] P. Tierno, S. V. Reddy, T. H. Johansen, and T. M. Fischer: "Rupture and healing of one-dimensional chains in a parametric magnetic ratchet potential" Phys. Rev. E **75**, 041404 (2007).

[207] C. Kettner, P. Reimann, P. Hänggi, and F. Müller: "Drift ratchet" Phys. Rev. E **61**, 312 (2000).

[208] R. Eichhorn, J. Regtmeier, D. Anselmetti, and P. Reimann: "Negative mobility and sorting of colloidal particles" Soft Matter **6**, 1858 (2010).

[209] K. Xiao and D. G. Grier: "Sorting colloidal particles into multiple channels with optical forces: Prismatic optical fractionation" Phys. Rev. E **82**, 051407 (2010).

[210] B. Spagnolo and A. Dubkov: "Diffusion in flashing periodic potentials" Eur. Phys. J. B **50**, 299 (2006).

[211] R. Bartussek, P. Hänggi, and J. G. Kissner: "Periodically Rocked Thermal Ratchets" EPL **28**, 459 (1994).

[212] P. Kalinay: "Rectification of confined diffusion driven by a sinusoidal force" Phys. Rev. E **89**, 042123 (2014).

[213] C. L. Phillips and J. M. Parr: "Feedback control systems" Pearson (2011).

[214] P. R. Belanger: "Control engineering: a modern approach" New York (2011).

[215] J. Löber and H. Engel: "Controlling the Position of Traveling Waves in Reaction-Diffusion Systems" Phys. Rev. Lett. **112**, 148305 (2014).

[216] J. Löber, S. Martens, and H. Engel: "Shaping wave patterns in reaction-diffusion systems" Phys. Rev. E **90**, 062911 (2014); arxiv:1405.4321 [nlin.ps] (2014).

[217] C. Sayrin, I. Dotsenko, X. Zhou, B. Peaudecerf, T. Rybarczyk, S. Gleyzes, P. Rouchon, M. Mirrahimi, H. Amini, M. Brune, J.-M. Raimond, and S. Haroche: "Real-time quantum feedback prepares and stabilizes photon number states" Nature **477**, 73 (2011).

[218] T. Brandes: "Feedback Control of Quantum Transport" Phys. Rev. Lett. **105**, 060602 (2010).

[219] D. A. Strehober, E. Schöll, and S. H. L. Klapp: "Feedback control of flow alignment in sheared liquid crystals" Phys. Rev. E **88**, 062509 (2013).

[220] T. Dahms, V. Flunkert, F. Henneberger, P. Hövel, S. Schikora, E. Schöll, and H. J. Wünsche: "Noninvasive optical control of complex semiconductor laser dynamics" Eur. Phys. J. Spec. Top. **191**, 71 (2010).

[221] C. Masoller, M. C. Torrent, and J. García-Ojalvo: "Interplay of subthreshold activity, time-delayed feedback, and noise on neuronal firing patterns" Phys. Rev. E **78**, 041907 (2008).

[222] J. Lehnert, T. Dahms, P. Hövel, and E. Schöll: "Loss of synchronization in complex neural networks with delay" EPL **96**, 60013 (2011).

[223] E. Schöll: "Neural control: Chaos control sets the pace" Nature Physics **6**, 161 (2010).

[224] S. Toyabe, T. Sagawa, M. Ueda, E. Muneyuki, and M. Sano: "Experimental demonstration of information-to-energy conversion and validation of the generalized Jarzynski equality" Nature Physics **6**, 988 (2010); arxiv:1009.5287 [cond-mat.stat-mech] (2010).

[225] D. Abreu and U. Seifert: "Extracting work from a single heat bath through feedback" EPL **94**, 10001 (2011).

[226] E. M. Craig, N. J. Kuwada, B. J. Lopez, and H. Linke: "Feedback control in flashing ratchets" Ann. Phys. (Berlin) **17**, 115 (2008).

[227] J. J. Juarez and M. A. Bevan: "Feedback Controlled Colloidal Self-Assembly" Adv. Func. Mater. **22**, 3833 (2012).

[228] T. A. Vezirov, S. Gerloff, and S. H. L. Klapp: "Manipulating shear-induced non-equilibrium transitions by feedback control" Soft Matter **11**, 406 (2015); arxiv:1403.6994v2 [cond-mat.soft] (2014).

[229] C. Prohm and H. Stark: "Feedback control of inertial microfluidics using axial control forces" Lab Chip **14**, 2115 (2014).

[230] A. Balijepalli, J. J. Gorman, S. K. Gupta, and T. W. Lebrun: "Significantly Improved Trapping Lifetime of Nanoparticles in an Optical Trap using Feedback Control" Nano Lett. **12**, 2347 (2012).

[231] B. Qian, D. Montiel, A. Bregulla, F. Cichos, and H. Yang: "Harnessing thermal fluctuations for purposeful activities: the manipulation of single micro-swimmers by adaptive photon nudging" Chem. Sci. **4**, 1420 (2013).

[232] P. J. Lu, E. Zaccarelli, F. Ciulla, A. B. Schofield, F. Sciortino, and D. A. Weitz: "Gelation of particles with short-range attraction" Nature **453**, 499 (2008).

[233] P. Chaudhuri, Y. Gao, L. Berthier, M. Kilfoil, and W. Kob: "A random walk description of the heterogeneous glassy dynamics of attracting colloids" J. Phys.: Cond. Mat. **20**, 244126 (2008).

[234] M. Selmke, A. Heber, M. Braun, and F. Cichos: "Photothermal single particle microscopy using a single laser beam" Appl. Phys. Lett. **105**, 013511 (2014).

[235] M. Feito and F. J. Cao: "Time-delayed feedback control of a flashing ratchet" Phys. Rev. E **76**, 061113 (2007).

[236] E. M. Craig, B. R. Long, J. M. R. Parrondo, and H. Linke: "Effect of time delay on feedback control of a flashing ratchet" EPL **81**, 10002 (2008).

[237] C. Emary: "Delayed feedback control in quantum transport" Phil. Trans. R. Soc. A **371**, 20120468 (2013).

[238] T. Munakata and M. L. Rosinberg: "Entropy production and fluctuation theorems for Langevin processes under continuous non-Markovian feedback control" Phys. Rev. Lett. **112**, 180601 (2014); arxiv:1401.0771v1 [cond-mat.stat-mech] (2014).

[239] K. Pyragas: "Continuous control of chaos by self-controlling feedback" Phys. Lett. A **170**, 421 (1992).

[240] A. E. Cohen and W. E. Moerner: "Suppressing Brownian motion of individual biomolecules in solution" PNAS **103**, 4362 (2006).

[241] C. Jarzynski: "Nonequilibrium Equality for Free Energy Differences" Phys. Rev. Lett. **78**, 2690 (1997).

[242] T. Sagawa and M. Ueda: "Role of mutual information in entropy production under information exchanges" New J. Phys. **15**, 125012 (2013).

[243] H. Jiang, T. Xiao, and Z. Hou: "Stochastic thermodynamics for delayed Langevin systems" Phys. Rev. E **83**, 061144 (2011).

[244] P. Strasberg, G. Schaller, T. Brandes, and M. Esposito: "Thermodynamics of quantum-jump-conditioned feedback control" Phys. Rev. E **88**, 062107 (2013).

[245] P. Strasberg, G. Schaller, T. Brandes, and C. Jarzynski: "Second laws for an information driven current through a spin valve" Phys. Rev. E **90**, 062107 (2014).

[246] M. Bauer, D. Abreu, and U. Seifert: "Efficiency of a Brownian information machine" J. Phys. A: Math. Theor. **45**, 162001 (2012).

[247] J. V. Koski, V. F. Maisi, J. P. Pekola, and D. V. Averin: "Experimental realization of a Szilard engine with a single electron" PNAS **111**, 13786 (2014).

[248] P. E. Kloeden and E. Platen: "Numerical solution of stochastic differential equations" Springer, Berlin (1992).

[249] T. Verechtchaguina, L. Schimansky-Geier, and I. M. Sokolov: "Spectra and waiting-time densities in firing resonant and nonresonant neurons" Phys. Rev. E **70**, 031916 (2004).

[250] L. R. Nie and D. C. Mei: "Noise and time delay: Suppressed population explosion of the mutualism system" EPL **79**, 20005 (2007).

[251] D. A. Kessler and E. Barkai: "Theory of Fractional Levy Kinetics for Cold Atoms Diffusing in Optical Lattices" Phys. Rev. Lett. **108**, 230602 (2012).

[252] D. Derks, Y. L. Wu, A. van Blaaderen, and A. Imhof: "Dynamics of colloidal crystals in shear flow" Soft Matter **5**, 1060 (2009).

[253] R. Gommers, V. Lebedev, M. Brown, and F. Renzoni: "Gating Ratchet for Cold Atoms" Phys. Rev. Lett. **100**, 040603 (2008).

[254] K. Lindenberg, J. M. Sancho, A. M. Lacasta, and I. M. Sokolov: "Dispersionless Transport in a Washboard Potential" Phys. Rev. Lett. **98**, 020602 (2007).

[255] G. Costantini and F. Marchesoni: "Threshold diffusion in a tilted washboard potential" Europhys. Lett. **48**, 491 (1999).

[256] E. Pollak: "Theory of activated rate processes: A new derivation of Kramers' expression" J. Chem. Phys. **85**, 865 (1986).

[257] U. M. B. Marconi and P. Tarazona: "Dynamic density functional theory of fluids" J. Chem. Phys. **110**, 8032 (1999).

[258] R. Zwanzig: "Memory effects in irreversible thermodynamics" Phys. Rev. **124**, 983 (1961).

[259] P. Espanol and H. Löwen: "Derivation of dynamical density functional theory using the projection operator technique" J. Chem. Phys. **131**, 244101 (2009).

[260] A. J. Archer and R. Evans: "Dynamical density functional theory and its application to spinodal decomposition" J. Chem. Phys. **121**, 4246 (2004).

[261] P. Tarazona, J. A. Cuesta, and Y. Martinez-Raton: "Density Functional Theories of Hard Particle Systems" Lect Notes Phys **753**, 247 (2008).

[262] Y. Singh: "density-functional theory of freezing and properties of the ordered phase" Phys. Rep. **207**, 351 (1991).

[263] P. Hohenberg and W. Kohn: "Inhomogeneous electron gas" Phys. Rev. **136**, B864 (1964).

[264] W. Kohn and L. J. Sham: "Self-Consistent Equations Including Exchange and Correlation Effects" Phys. Rev. **140**, A1133 (1965).

[265] R. Evans: "The nature of the liquid-vapour interface and other topics in the statistical mechanics of non-uniform, classical fluids" Adv Phys **28**, 143 (1979).

[266] T. de Vos and M. Baus: "A density functional study of a twisted nematic cell and its relation to the Frank–Oseen theory" J. Chem. Phys. **128**, 194903 (2008).

[267] A. J. Archer: "Dynamical density functional theory for molecular and colloidal fluids: a microscopic approach to fluid mechanics" J. Chem. Phys. **130**, 014509 (2009).

[268] A. Fortini, D. de las Heras, J. M. Brader, and M. Schmidt: "Superadiabatic Forces in Brownian Many-Body Dynamics" Phys. Rev. Lett. **113**, 167801 (2014).

[269] F. Penna, J. Dzubiella, and P. Tarazona: "Dynamic density functional study of a driven colloidal particle in polymer solutions" Phys. Rev. E **68**, 061407 (2003).

[270] M. Rex, C. N. Likos, J. Dzubiella, and H. Löwen: "Ultrasoft colloids in cavities of oscillating size or sharpness" Molecular Physics **104**, 527 (2006).

[271] M. Rex and H. Löwen: "Dynamical Density Functional Theory with Hydrodynamic Interactions and Colloids in Unstable Traps" Phys. Rev. Lett. **101**, 148302 (2008).

[272] A. Pototsky, A. J. Archer, M. Bestehorn, D. Merkt, S. Savel'ev, and F. Marchesoni: "Collective shuttling of attracting particles in asymmetric narrow channels" Phys. Rev. E **82**, 030401 (2010).

[273] J. Bleibel, S. Dietrich, A. Dominguez, and M. Oettel: "Shock Waves in Capillary Collapse of Colloids: A Model System for Two-Dimensional Screened Newtonian Gravity" Phys. Rev. Lett. **107**, 128302 (2011).

[274] S. Jäger, H. Stark, and S. H. L. Klapp: "Dynamics of cluster formation in driven dipolar colloids dispersed on a monolayer" J. Phys.: Cond. Mat. **25**, 195104 (2013); arxiv:1212.1338 [cond-mat.soft] (2012).

[275] L. Almenar and M. Rauscher: "Dynamics of colloids in confined geometries" J Phys: Condens Matt **23**, 184115 (2011).

[276] H. Löwen: "Particle-resolved instabilities in colloidal dispersions" Soft Matter **6**, 3133 (2010).

[277] E. C. Euan-Diaz, V. R. Misko, F. M. Peeters, S. Herrera-Velarde, and R. Castaneda-Priego: "Single-file diffusion in periodic energy landscapes: The role of hydrodynamic interactions" Phys. Rev. E **86**, 031123 (2012).

[278] G. K.-L. Chan and R. Finken: "Time-Dependent Density Functional Theory of Classical Fluids" Phys. Rev. Lett. **94**, 183001 (2005).

[279] B. D. Goddard, A. Nold, N. Savva, P. Yatsyshin, and S. Kalliadasis: "Unification of dynamic density functional theory for colloidal fluids to include inertia and hydrodynamic interactions: derivation and numerical experiments" J Phys Condens Matter **25**, 035101 (2013).

[280] U. M. B. Marconi and S. Melchionna: "Charge Transport in Nanochannels: A Molecular Theory" Langmuir **28**, 13727 (2012).

[281] U. M. B. Marconi, P. Tarazona, F. Cecconi, and S. Melchionna: "Beyond dynamic density functional theory: the role of inertia" J Phys Condens Matter **20**, 494233 (2008).

[282] A. J. Archer: "Dynamical density functional theory for dense atomic liquids" J Phys: Condens Matter **18**, 5617 (2006).

[283] S. Heidenreich, S. Hess, and S. H. L. Klapp: "Shear-Induced Dynamic Polarization and Mesoscopic Structure in Suspensions of Polar Nanorods" Phys. Rev. Lett. **102**, 028301 (2009).

[284] J. Reinhardt, A. Scacchi, and J. M. Brader: "Microrheology close to an equilibrium phase transition" J. Chem. Phys. **140**, 144901 (2014).

[285] F. Goujon, A. Ghoufi, P. Malfreyt, and D. J. Tildesley: "The kinetic friction coefficient of neutral and charged polymer brushes" Soft Matter **9**, 2966 (2013).

[286] R. Messina and H. Löwen: "Confined colloidal bilayers under shear: Steady state and relaxation back to equilibrium" Phys. Rev. E **73**, 011405 (2006).

[287] S. Gerloff, T. A. Vezirov, and S. H. L. Klapp: "Dynamics of density excitations in shear-driven, confined binary mixtures" in preparation.

[288] J. M. Brader and M. Krüger: "Density profiles of a colloidal liquid at a wall under shear flow" Mol. Phys. **109**, 1029 (2011).

[289] J. M. Brader and M. Schmidt: "Dynamic correlations in Brownian many-body systems" J. Chem. Phys. **140**, 034104 (2014).

[290] J. Reinhardt, F. Weysser, and J. M. Brader: "Density functional approach to nonlinear rheology" EPL **102**, 28011 (2013).

[291] A. A. Aerov and M. Krüger: "Driven colloidal suspensions in confinement and density functional theory: Microstructure and wall-slip" J. Chem. Phys. **140**, 094701 (2014); arxiv:1402.1628 [cond-mat.stat-mech] (2014).

[292] F. Penna and P. Tarazona: "Dynamical correlations in Brownian hard rods" J. Chem. Phys. **124**, 164903 (2006).

[293] M. Schmidt and J. M. Brader: "Power functional theory for Brownian dynamics" J. Chem. Phys. **138**, 214101 (2013).

[294] J. Reinhardt and J. M. Brader: "Dynamics of localized particles from density functional theory" Phys. Rev. E **85**, 011404 (2012).

[295] Q. H. Wei, C. Bechinger, and P. Leiderer: "Single-File Diffusion of Colloids in One-Dimensional Channels" Science **287**, 625 (2000).

[296] J. K. Percus: "Equilibrium state of a classical fluid of hard rods in an external field" J. Stat. Phys. **15**, 505 (1976).

[297] D. Schirok: "Transport getriebener Kolloide in einer Dimension" Master thesis,Masterarbeit in Physik an der Technischen Universität Berlin, AG Klapp (2013).

[298] Y. Rosenfeld: "Free-energy model for the inhomogeneous hard-sphere fluid mixture and density-functional theory of freezing" Phys. Rev. Lett. **63**, 980 (1989).

[299] C. N. Likos: "Effective interactions in soft condensed matter physics" Phys. Rep. **348**, 267 (2001).

[300] F. Sciortino and P. Tartaglia: "Glassy colloidal systems" Advances In Physics **54**, 471 (2005).

[301] A. Fortini and M. Schmidt: "Computer simulations of colloidal transport on a patterned magnetic substrate" Phys. Rev. E **83**, 041411 (2011).

[302] A. J. Archer and A. Malijevskí: "On the interplay between sedimentation and phase separation phenomena in two-dimensional colloidal fluids" Mol. Phys. **109**, 1087 (2011).

[303] J. Bergenholtz, W. C. K. Poon, and M. Fuchs: "Gelation in Model Colloid-Polymer Mixtures" Langmuir **19**, 4493 (2003).

[304] C. Caccamo: "Integral equation theory description of phase equilibria in classical fluids" Phys. Rep. **274**, 1 (1996).

[305] L. van Hove: "Correlations in Space and Time and Born Approximation Scattering in Systems of Interacting Particles" Phys. Rev. **95**, 249 (1954).

[306] A. Rahman: "Correlations in the motion of atoms in liquid argon" Phys. Rev. **136**, A405 (1964).

[307] K. Lichtner: "Colloids in non-equilibrium : from one-dimensional transport to pattern formation at surfaces" PhD thesis, urn:nbn:de:kobv:83-opus4-60668 (2014).

[308] P. Hopkins, A. Fortini, A. J. Archer, and M. Schmidt: "The van Hove distribution function for Brownian hard spheres: Dynamical test particle theory and computer simulations for bulk dynamics" J. Chem. Phys. **133**, 224505 (2010).

[309] A. J. Archer: "Dynamical density functional theory: binary phase-separating colloidal fluid in a cavity" J. Phys.: Cond. Mat. **17**, 1405 (2005).

[310] K. Sekimoto: "Langevin Equation and Thermodynamics" Prog Theor Phys Suppl **130**, 17 (1998).

[311] U. Seifert: "Entropy Production along a Stochastic Trajectory and an Integral Fluctuation Theorem" Phys. Rev. Lett. **95**, 040602 (2005).

[312] T. Sagawa and M. Ueda: "Nonequilibrium thermodynamics of feedback control" Phys. Rev. E **85**, 021104 (2012).

[313] C. A. J. Fletcher: "Computational techniques for Fluid Dynamics, Volume 1" 2nd edition, Springer (1991).

[314] M. Frigo and S. G. Johnson: "The website of FFTW" http://www.fftw.org/ (last access 6th Feb 2004).

[315] M. Frigo and S. G. Johnson: "The Design and Implementation of FFTW3" Proc. Ieee **93**, 216 (2005).

[316] D. L. Ermak: "A computer simulation of charged particles in solution. I. Technique and equilibrium properties" J. Chem. Phys. **62**, 4189 (1975).

[317] M. Matsumoto and T. Nishimura: "Mersenne Twister: A 623-Dimensionally Equidistributed Uniform Pseudo-Random Number Generator; C++ port by Jasper Bedaux: http://www.bedaux.net/mtrand/ (2003)" Acm Tran. Mod. Comp. Sim. **8**, 3 (1998).

[318] C. Emary, R. Gernert, and S. H. L. Klapp: "A minimal model for short-time diffusion in periodic potentials" Phys. Rev. E **86**, 061135 (2012).

[319] E. Heinsalu, M. Patriarca, I. Goychuk, and P. Hänggi: "Fractional diffusion in periodic potentials" J. Phys.: Cond. Mat. **19**, 065114 (2007).

[320] X.-T. Zheng, J.-C. Wu, B.-Q. Ai, and F.-G. Li: "Brownian pump induced by the phase difference between the potential and the entropic barrier" Eur. Phys. J. B **86**, 479 (2013).

[321] D. Speer, R. Eichhorn, and P. Reimann: "Directing Brownian Motion on a Periodic Surface" Phys. Rev. Lett. **102**, 124101 (2009).

[322] B. Wang, J. Kuo, S. C. Bae, and S. Granick: "When Brownian diffusion is not Gaussian" Nat. Mater. **11**, 481 (2012).

[323] T. Odagaki and Y. Hiwatari: "Stochastic model for the glass transition of simple classical liquids" Phys. Rev. A **41**, 929 (1990).

[324] B. Doliwa and A. Heuer: "Hopping in a supercooled Lennard-Jones liquid: Metabasins, waiting time distribution, and diffusion" Phys. Rev. E **67**, 030501R (2003).

[325] J. Qian, Y. Lin, H. Jiang, and H. Yao: "Bond formation of surface-tethered receptor-ligand pairs in relative separation" Appl. Phys. Lett. **103**, 223702 (2013).

[326] H. Schmidle, C. K. Hall, O. D. Velev, and S. H. L. Klapp: "Phase diagram of two-dimensional systems of dipole-like colloids" Soft Matter **8**, 1521 (2012).

[327] O. Rubner and A. Heuer: "From elementary steps to structural relaxation: A continuous-time random-walk analysis of a supercooled liquid" Phys. Rev. E **78**, 011504 (2008).

[328] D. Bedeaux, K. Lakatos-Lindenberg, and K. E. Shuler: "On the Relation between Master Equations and Random Walks and Their Solutions" J. Math. Phys. **12**, 2116 (1971).

[329] V. M. Kenkre, E. W. Montroll, and M. F. Shlesinger: "Generalized master equations for continuous-time random walks" J. Stat. Phys. **9**, 45 (1973).

[330] B. R. Martin: "Statistics for Physicists" Academic Press, London, New York (1971).

[331] R. Gernert, C. Emary, and S. H. L. Klapp: "Waiting time distribution for continuous stochastic systems" Phys. Rev. E **90**, 062115 (2014); arxiv:1407.1675 [cond-mat.stat-mech] (2014).

[332] H. Scher and M. Lax: "Stochastic Transport in a Disordered Solid. I. Theory" Phys Rev B **7**, 4491 (1973).

[333] A. K. Erlang: "Calculus of probability applied to the design of antomatic telephone exchanges" Elektrotechnische Zeitschrift Etz **39**, 504 (1918).

[334] E. R. Higgins, H. Schmidle, and M. Falcke: "Waiting time distributions for clusters of IP3 receptors" J. Theo. Bio. **259**, 338 (2009).

[335] S. Saha, A. Sinha, and A. Dua: "Single-molecule enzyme kinetics in the presence of inhibitors" J. Chem. Phys. **137**, 045102 (2012).

[336] B. P. English, W. Min, A. M. van Oijen, K. T. Lee, G. Luo, H. Sun, B. J. Cherayil, S. C. Kou, and X. S. Xie: "Ever-fluctuating single enzyme molecules: Michaelis-Menten equation revisited" Nature Chemical Biology **2**, 87 (2006).

[337] F. Mainardi, M. Raberto, R. Gorenflo, and E. Scalas: "Fractional calculus and continuous-time finance II: the waiting-time distribution" Physica A **287**, 468 (2000).

[338] T. Prager and L. Schimansky-Geier: "Drift and Diffusion in Periodically Driven Renewal Processes" J. Stat. Phys. **123**, 391 (2006).

[339] C. Hartmann, R. Banisch, M. Sarich, T. Badowski, and C. Schütte: "Characterization of Rare Events in Molecular Dynamics" Entropy **16**, 350 (2014).

[340] R. Thul and M. Falcke: "Waiting time distributions for clusters of complex molecules" EPL **79**, 38008 (2007).

[341] Y. Jung, J. P. Garrahan, and D. Chandler: "Dynamical exchanges in facilitated models of supercooled liquids" J. Chem. Phys. **123**, 084509 (2005).

[342] J. W. Ahn, B. Falahee, C. del Piccolo, M. Vogel, and D. Bingemann: "Are rare, long waiting times between rearrangement events responsible for the slowdown of the dynamics at the glass transition?" J. Chem. Phys. **138**, 12A527 (2013).

[343] T. Brandes: "Waiting times and noise in single particle transport" Ann. Phys. (Berlin) **17**, 477 (2008).

[344] L. Rajabi, C. Pöltl, and M. Governale: "Waiting Time Distributions for the Transport through a Quantum-Dot Tunnel Coupled to One Normal and One Superconducting Lead" Phys. Rev. Lett. **111**, 067002 (2013).

[345] M. Albert, C. Flindt, and M. Büttiker: "Distributions of Waiting Times of Dynamic Single-Electron Emitters" Phys. Rev. Lett. **107**, 086805 (2011).

[346] C. Flindt, C. Fricke, F. Hohls, T. Novotny, K. Netocny, T. Brandes, and R. J. Haug: "Universal oscillations in counting statistics" PNAS **106**, 10116 (2009).

[347] P. E. Goa, H. Hauglin, M. Baziljevich, E. Il'yashenko, P. L. Gammel, and T. H. Johansen: "Real-time magneto-optical imaging of vortices in superconducting NbSe2" Supercond. Sci. Technol. **14**, 729 (2001).

[348] A. I. Shushin: "Non-Markovian stochastic Liouville equation and its Markovian representation: Extensions of the continuous-time random-walk approach" Phys. Rev. E **77**, 031130 (2008).

[349] L. Sacerdote, O. Telve, and C. Zucca: "Joint densities of first hitting times of a diffusion process through two time-dependent boundaries" Adv. In Appl. Probab. **46**, 186 (2014).

[350] D. J. Navarro and I. G. Fuss: "Fast and accurate calculations for first-passage times in Wiener diffusion models" Journal Of Mathematical Psychology **53**, 222 (2009).

[351] J. Xing, H. Wang, and G. Oster: "From Continuum Fokker-Planck Models to Discrete Kinetic Models" Biophys. J. **89**, 1551 (2005).

[352] E. Barkai, E. Aghion, and D. Kessler: "From the Area under the Bessel Excursion to Anomalous Diffusion of Cold Atoms" Phys. Rev. X **4**, 021036 (2014).

[353] G. Bandyopadhyay, W. Gosnold, and M. Mann: "Analytical and semi-analytical solutions for short-time transient response of ground heat exchangers" Energy And Buildings **40**, 1816 (2008).

[354] S. Guillouzic, I. L'heureux, and A. Longtin: "Small delay approximation of stochastic delay differential equations" Phys. Rev. E **59**, 3970 (1999).

[355] K. Lichtner, A. Pototsky, and S. H. L. Klapp: "Feedback-induced oscillations in one-dimensional colloidal transport" Phys. Rev. E **86**, 051405 (2012).

[356] G. Gang and Q. Xiaogang: "First passage time distributions of anomalous biased diffusion with double absorbing barriers" Physica A **411**, 80 (2014).

[357] T. Verechtchaguina, I. M. Sokolov, and L. Schimansky-Geier: "First passage time densities in non-Markovian models with subthreshold oscillations" Europhys. Lett. **73**, 691 (2006).

[358] M. Albert, G. Haack, C. Flindt, and M. Büttiker: "Electron Waiting Times in Mesoscopic Conductors" Phys. Rev. Lett. **108**, 186806 (2012).

[359] S. A. M. Loos, R. Gernert, and S. H. L. Klapp: "Delay-induced transport in a rocking ratchet under feedback control" Phys. Rev. E **89**, 052136 (2014); arxiv:1403.5905 [cond-mat.stat-mech] (2014).

[360] F. J. Cao, L. Dinis, and J. M. R. Parrondo: "Feedback Control in a Collective Flashing Ratchet" Phys. Rev. Lett. **93**, 040603 (2004).

[361] M. Feito and F. J. Cao: "Threshold feedback control for a collective flashing ratchet: Threshold dependence" Phys. Rev. E **74**, 041109 (2006).

[362] E. Schöll and H. G. Schuster: "Handbook of Chaos Control" Wiley, 2nd edition (2008).

[363] J. Garcia-Ojalvo and R. Roy: "Noise amplification in a stochastic Ikeda model" Phys. Lett. A **224**, 51 (1996).

[364] M. Xiao and J. Cao: "Delayed feedback-based bifurcation control in an Internet congestion model" J. Math. Anal. Appl. **332**, 1010 (2007).

[365] M. Kantner and S. Yanchuk: "Bifurcation analysis of delay-induced patterns in a ring of Hodgkin-Huxley neurons" Phil. Trans. R. Soc. A **371**, 20120470 (2013).

[366] D. Hennig, L. Schimansky-Geier, and P. Hänggi: "Directed transport of an inertial particle in a washboard potential induced by delayed feedback" Phys. Rev. E **79**, 041117 (2009).

[367] S. V. Gurevich and R. Friedrich: "Instabilities of Localized Structures in Dissipative Systems with Delayed Feedback" Phys. Rev. Lett. **110**, 014101 (2013).

[368] F. M. Atay: "Complex Time-Delay Systems" Springer (2010).

[369] M. O. Magnasco: "Forced thermal ratchets" Phys. Rev. Lett. **71**, 1477 (1993).

[370] T. D. Frank, P. J. Beek, and R. Friedrich: "Fokker-Planck perspective on stochastic delay systems: Exact solutions and data analysis" Phys. Rev. E **68**, 021912 (2003).

[371] C. Zeng and H. Wang: "Noise-and delay-induced phase transitions of the dimer-monomer surface reaction model" Chem. Phys. **402**, 1 (2012).

[372] H. Kamegawa, T. Hondou, and F. Takagi: "Energetics of a Forced Thermal Ratchet" Phys. Rev. Lett. **80**, 5251 (1998).

[373] O. D'Huys, T. Jüngling, and W. Kinzel: "Stochastic switching in delay-coupled oscillators" Phys. Rev. E **90**, 032918 (2014).

[374] M. Feito, J. P. Baltanas, and F. J. Cao: "Rocking feedback-controlled ratchets" Phys. Rev. E **80**, 031128 (2009).

[375] D. Cubero, J. Casado-Pascual, A. Alvarez, M. Morillo, and P. Hänggi: "Overdamped Deterministic Ratchets Driven by Multifrequency Forces" Acta Physica Polonica B **37**, 1467 (2006).

[376] M. Braun, A. Würger, and F. Cichos: "Trapping of single nano-objects in dynamic temperature fields" Phys Chem Chem Phys **16**, 15207 (2014).

[377] D. Speer, R. Eichhorn, and P. Reimann: "Anisotropic diffusion in square lattice potentials: Giant enhancement and control" EPL **97**, 60004 (2012).

[378] F. H. Stillinger: "Phase transitions in the Gaussian core system" J. Chem. Phys. **65**, 3968 (1976).

[379] A. A. Louis, P. G. Bolhuis, J. P. Hansen, and E. J. Meijer: "Can Polymer Coils Be Modeled as "Soft Colloids"?" Phys. Rev. Lett. **85**, 2522 (2000).

[380] A. Pototsky, A. J. Archer, S. E. Savel'ev, U. Thiele, and F. Marchesoni: "Ratcheting of driven attracting colloidal particles: Temporal density oscillations and current multiplicity" Phys. Rev. E **83**, 061401 (2011).

[381] I. O. Götze, A. J. Archer, and C. N. Likos: "Structure, phase behavior, and inhomogeneous fluid properties of binary dendrimer" J. Chem. Phys. **124**, 084901 (2006).

[382] L. Mederos and G. Navascues: "Phase diagram of the hard-sphere/attractive-Yukawa system" J. Chem. Phys. **101**, 9841 (1994).

[383] M. Dijkstra: "Phase behavior of hard spheres with a short-range Yukawa attraction" Phys. Rev. E **66**, 021402 (2002).

[384] M. H. J. Hagen and D. Frenkel: "Determination of phase diagrams for the hardcore attractive Yukawa system" J. Chem. Phys. **101**, 4093 (1994).

[385] M. E. Leunissen, C. G. Christova, A.-P. Hynninen, C. P. Royall, A. I. Campbell, A. Imhof, M. Dijkstra, R. van Roij, and A. van Blaaderen: "Ionic colloidal crystals of oppositely charged particles" Nature **437**, 235 (2005).

[386] R. Roth, K. Mecke, and M. Oettel: "Communication: Fundamental measure theory for hard disks: Fluid and solid" J. Chem. Phys. **136**, 081101 (2012).

[387] J. Dzubiella and C. N. Likos: "Mean-field dynamical density functional theory" J. Phys.: Cond. Mat. **15**, L147 (2003).

[388] U. M. B. Marconi and P. Tarazona: "Dynamic density functional theory of fluids" J. Phys.: Cond. Mat. **12**, A413 (2000).

[389] R. Gernert and S. H. L. Klapp: "Enhancement of mobility in an interacting colloidal system under feedback control" Phys. Rev. E **92**, 022132 (2015); arxiv:1506.01846 [cond-mat.soft] (2015).

[390] A. P. Bregulla, H. Yang, and F. Cichos: "Stochastic Localization of Microswimmers by Photon Nudging" Acs Nano **8**, 6542 (2014).

[391] D. G. Cole and J. G. Pickel: "Nonlinear Proportional Plus Integral Control of Optical Traps for Exogenous Force Estimation" J Dyn Syst Meas Control **134**, 011020 (2012).

[392] C. Pöltl, C. Emary, and T. Brandes: "Feedback stabilization of pure states in quantum transport" Phys. Rev. B **84**, 085302 (2011).

[393] E. L. Florin, A. Pralle, E. H. K. Stelzer, and J. K. H. Hörber: "Photonic force microscope calibration by thermal noise analysis" Appl. Phys. A **66**, 75 (1998).

[394] H. Lee, A. M. Purdon, and R. M. Westervelt: "Manipulation of biological cells using a microelectromagnet matrix" Appl. Phys. Lett. **85**, 1063 (2004).

[395] D. Speer, R. Eichhorn, M. Evstigneev, and P. Reimann: "Dimer motion on a periodic substrate: Spontaneous symmetry breaking and absolute negative mobility" Phys. Rev. E **85**, 061132 (2012).

[396] C. Kreuter, U. Siems, P. Nielaba, P. Leiderer, and A. Erbe: "Transport phenomena and dynamics of externally and self-propelled colloids in confined geometry" Eur. Phys. J. Spec. Top. **222**, 2923 (2013).

[397] A. V. Straube and P. Tierno: "Tunable interactions between paramagnetic colloidal particles driven in a modulated ratchet potential" Soft Matter **10**, 3915 (2014).

[398] Y. Makoudi, E. Arras, N. Kepcija, W. Krenner, S. Klyatskaya, F. Klappenberger, M. Ruben, A. P. Seitsonen, and J. V. Barth: "Hierarchically Organized Bimolecular Ladder Network Exhibiting Guided One-Dimensional Diffusion" Acsnano **6**, 549 (2012).

[399] U. Siems and P. Nielaba: "Transport and diffusion properties of interacting colloidal particles in two-dimensional microchannels with a periodic potential" Phys. Rev. E **91**, 022313 (2015).

[400] A. Kaminska and T. Srokowski: "Mean first passage time for a Markovian jumping process" Acta Physica Polonica B **38**, 3119 (2007).

[401] C. F. E. Schroer and A. Heuer: "Anomalous Diffusion of Driven Particles in Supercooled Liquids" Phys. Rev. Lett. **110**, 067801 (2013).

[402] O. Bénichou and R. Voituriez: "From first-passage times of random walks in confinement to geometry-controlled kinetics" Phys. Rep. **539**, 225 (2014).

[403] M. Woerdemann, C. Alpmann, M. Esseling, and C. Denz: "Advanced optical trapping by complex beam shaping" Laser Photon Rev **7**, 839 (2013).

[404] M. Khoury, J. P. Gleeson, J. M. Sancho, A. M. Lacasta, and K. Lindenberg: "Diffusion coefficient in periodic and random potentials" Phys. Rev. E **80**, 021123 (2009).

[405] N. Kleppmann and S. H. L. Klapp: "A scale-bridging modeling approach for anisotropic organic molecules at patterned semiconductor surfaces" J. Chem. Phys. **142**, 064701 (2015); arxiv:1407.6265 [cond-mat.mtrl-sci] (2015).

[406] J. M. Brader and M. Schmidt: "Nonequilibrium Ornstein-Zernike relation for Brownian dynamics" J. Chem. Phys. **139**, 104108 (2013).

[407] G. M. Range and S. H. L. Klapp: "Demixing in simple dipolar mixtures: Integral equation versus density functional results" Phys. Rev. E **70**, 031201 (2004).

[408] D. de las Heras and M. Schmidt: "Bulk fluid phase behaviour of colloidal platelet-sphere and platelet-polymer mixtures" Phil. Trans. R. Soc. A **371**, 20120259 (2012); arxiv:1210.2551v1 [cond-mat.soft] (2012).

[409] S. C. Glotzer and M. J. Solomon: "Anisotropy of building blocks and their assembly into complex structures" Nature Materials **6**, 557 (2007).

[410] D. L. J. Vossen, J. P. Hoogenboom, K. Overgaag, and A. van Blaaderen: "Building Two and Three-dimensional Structures of Colloidal Particles on Surfaces using Optical Tweezers and Critical Point Drying" Mat. Res. Soc. Symp. Proc. **705**, Y6.8.1 (2002).